

Doctoral Thesis

---

**Automation of electroweak NLO  
corrections in general models**

---

Dissertation zur Erlangung  
des naturwissenschaftlichen Doktorgrades  
der Julius-Maximilians-Universität Würzburg



Vorgelegt von  
Jean-Nicolas Olivier Lang  
aus  
Schwäbisch Gmünd  
Würzburg 2017

Eingereicht am 23. Juni 2017  
bei der Fakultät für Physik und Astronomie

1. Gutachter: Prof. Dr. Ansgar Denner
2. Gutachter: Prof. Dr. Werner Porod
3. Gutachter:

Vorsitzende(r): \_\_\_\_\_

1. Prüfer: Prof. Dr. Ansgar Denner
2. Prüfer: Prof. Dr. Werner Porod
3. Prüfer:

im Promotionskolloquium

Tag des Promotionskolloquiums: \_\_\_\_\_

Doktorurkunde ausgehändigt am: \_\_\_\_\_

*I dedicate this thesis to my parents and my sister.*



# Publications

1. A. Denner, J.-N. Lang, and S. Uccirati, *NLO electroweak corrections in extended Higgs Sectors with RECOLA2*, [arXiv:1705.06053](#).
2. A. Denner, J.-N. Lang, M. Pellen, and S. Uccirati, *Higgs production in association with off-shell top-antitop pairs at NLO EW and QCD at the LHC*, *JHEP* **02** (2017) 053, [[arXiv:1612.07138](#)].
3. A. Denner, L. Jenniches, J.-N. Lang, and C. Sturm, *Gauge-independent  $\overline{MS}$  renormalization in the 2HDM*, *JHEP* **09** (2016) 115, [[arXiv:1607.07352](#)].
4. S. Actis, A. Denner, L. Hofer, J.-N. Lang, A. Scharf, and S. Uccirati, *RECOLA: REcursive Computation of One-Loop Amplitudes*, *Comput. Phys. Commun.* **214** (2017) 140–173, [[arXiv:1605.01090](#)].
5. A. Denner and J.-N. Lang, *The Complex-Mass Scheme and Unitarity in perturbative Quantum Field Theory*, *Eur. Phys. J.* **C75** (2015), no. 8 377, [[arXiv:1406.6280](#)].
6. B. Chokouf  Nejad, T. Hahn, J.-N. Lang, and E. Mirabella, *FormCalc 8: Better Algebra and Vectorization*, *J. Phys. Conf. Ser.* **523** (2014) 012050, [[arXiv:1310.0274](#)].
7. B. Chokouf  Nejad, T. Hahn, J.-N. Lang, and E. Mirabella, *FormCalc 8: Better Algebra and Vectorization*, *Acta Phys. Polon.* **B44** (2013), no. 11 2231–2239.



# Abstract

The thesis deals with the automated generation and efficient evaluation of scattering amplitudes in general relativistic quantum field theories at one-loop order in perturbation theory. At the present time we lack signals beyond the Standard Model which, in the past, have guided the high-energy physics community, and ultimately led to the discovery of new physics phenomena. In the future, precision tests could acquire this guiding role by systematically probing the Standard Model and constraining Beyond the Standard Model theories. As current experimental constraints strongly favour Standard Model-like theories, only small deviations with respect to the Standard Model are expected which need to be studied in detail. The required precision demands one-loop corrections in all future analyses, ideally in a fully automated way, allowing to test a variety of observables in different models and in an effective field theory approach.

In the process of achieving this goal we have developed an enhanced version of the tool RECOLA and on this basis the generalization RECOLA2. These tools represent fully automated tree- and one-loop-amplitude providers for the Standard Model, or in the case of RECOLA2 for general models. Concerning the algorithm, we use a purely numerical and fully recursive approach allowing for extreme calculations of yet unmatched complexity. RECOLA has led to the first computation involving 9-point functions.

Beyond the Standard Model theories and Effective Field theories are integrated into the RECOLA2 framework as model files. Renormalized model files are produced with the newly developed tool REPTIL, which can perform the renormalization in a fully automated way, starting from nothing but Feynman rules. In view of validation, we have extended RECOLA2 to new gauges such as the Background-Field Method and the class of  $R_\xi$  gauges. In particular, the Background-Field Method formulation for new theories serves as an automated validation, and is very useful in practical calculations and the formulation of renormalization conditions. We have applied the system to produce the first results for Higgs-boson production in Higgs strahlung and vector-boson fusion in the Two-Higgs-Doublet Model and the Higgs-Singlet Extension of the Standard Model. All in all, we have laid the foundation for an automated generation and computation of one-loop amplitudes within a large class of phenomenologically interesting theories. Furthermore, we enable the use of our system via a very flexible and dynamic control which does not require any intermediate intervention.

# Kurzzusammenfassung

In dieser Arbeit behandeln wir die automatisierte Generierung und effiziente Auswertung von Streuamplituden in allgemeinen relativistischen Quantenfeldtheorien auf Einschleifen-Niveau. Gegenwärtig gibt es keine konkreten Hinweise auf Physik jenseits des Standard Models und daher auch keine Möglichkeit, gezielt nach neuer Physik in Teilchenbeschleuniger-Experimenten zu suchen. In der Zukunft könnten Präzisionstests eine richtungsweisende Rolle übernehmen und Aufschluss über Abweichungen zum Standard Model geben, und dabei möglicherweise erlauben, indirekt auf neue Physik zu schließen. Nach dem derzeitigen experimentellen Stand werden Standard-Model-artige Theorien deutlich bevorzugt. Infolgedessen werden nur kleine Abweichungen zum Standard Model erwartet, die mit hoher Präzision untersucht werden müssen. Auf der theoretischen Seite erfordert die nötige Präzision die Berechnung von Einschleifen-Korrekturen in allen zukünftigen Analysen, die, idealerweise, vollautomatisiert durchgeführt werden, um alle grundsätzlich zugänglichen Observablen in verschiedensten Theorien testen zu können.

Um dieses Ziel schrittweise zu erreichen, haben wir das Programm RECOLA weiterentwickelt, und auf dieser Basis die Verallgemeinerung RECOLA2 entwickelt. Die Programme erlauben eine vollautomatisierte Erzeugung und Auswertung von Baumgraphen- und Einschleifen-Amplituden für das Standard Model, beziehungsweise, im Falle von RECOLA2, für allgemeine Theorien. Der zugrundeliegende numerische Algorithmus arbeitet vollständig rekursiv und erlaubt die Berechnung von Prozessen mit bislang unerreichter Komplexität. Beispielsweise hat RECOLA zur ersten Berechnung mit 9-Punkt Funktionen geführt.

In RECOLA2 werden neue Theorien durch spezifische RECOLA2 Modelfiles in das System integriert. Die Renormierung wird mit dem neu entwickelten Programm REPT1L vollautomatisch durchgeführt, wobei lediglich die Feynman Regeln als externe Abhängigkeit benötigt werden. Zur Validierung des Systems wurden zum einen Vergleiche mit unabhängigen Rechnungen durchgeführt, und zum anderen RECOLA2 soweit verallgemeinert, dass dessen Konsistenz in verschiedenen Eichungen getestet werden kann. Besonders die Background-Field Formulierung erlaubt es neue Theorien automatisch zu validieren und ist darüberhinaus sehr nützlich für praktische Rechnungen, sowie für die Formulierung von Renormierungsbedingungen. Mit diesem System haben wir die ersten Berechnungen zur Higgs-Boson-Produktion in Higgs-Strahlung und Vektor-Boson-Fusion im Zwei-Higgs-Doublet Model und der Higgs-Singlet Erweiterung des Standard Models durchgeführt. Alles in allem wurden die Voraussetzungen geschaffen, Einschleifen-Amplituden in einer großen Klasse von phänomenologisch interessanten Theorien automatisiert erzeugen zu können. Darüberhinaus ermöglichen wir die Nutzung für andere durch eine sehr flexible und dynamische Bedienung, die keinerlei Zwischenschritte benötigt.



# Contents

<b>1</b>	<b>Introduction</b>	<b>1</b>
<b>2</b>	<b>Probing Beyond Standard Model theories with precision</b>	<b>5</b>
2.1	Beyond Standard Model theories and the necessity for precision . . . . .	5
2.2	Aspects of the Standard Model . . . . .	7
2.2.1	Overview . . . . .	7
2.2.2	Kinetic terms for gauge bosons . . . . .	8
2.2.3	Kinetic terms for fermions . . . . .	8
2.2.4	Brout-Englert-Higgs mechanism . . . . .	9
2.3	Two-Higgs-Doublet Model and the Higgs-Singlet extension of the Standard Model	11
2.3.1	Fields and potential in the symmetric basis . . . . .	11
2.3.2	Parameters in the physical basis . . . . .	12
2.3.3	Yukawa Interactions . . . . .	14
<b>3</b>	<b>Matrix elements for generic theories with RECOLA2</b>	<b>17</b>
3.1	Berends-Giele recursion relation . . . . .	18
3.2	Tree skeletons for general theories . . . . .	20
3.3	Extension to one-loop level . . . . .	24
3.4	Off-shell currents for general theories . . . . .	26
<b>4</b>	<b>Computational framework for one-loop corrections</b>	<b>31</b>
4.1	Regularization and computation of rational terms . . . . .	32
4.1.1	Computation of $R_1$ . . . . .	33
4.1.2	Computation of $R_2$ . . . . .	33
4.1.3	Treatment of $\gamma_5$ . . . . .	34
4.2	Tadpole counterterm schemes . . . . .	35
4.2.1	The FJ Tadpole Scheme for a general Higgs sector . . . . .	35
4.2.2	The FJ Tadpole Scheme in the SM . . . . .	40
4.2.3	Interplay of tadpoles with $\overline{\text{MS}}$ subtraction . . . . .	45
4.2.4	Automation of the FJ Tadpole Scheme . . . . .	47
4.3	Renormalization conditions for physical particles . . . . .	48
4.3.1	Mass and field renormalization counterterms . . . . .	49
4.3.2	Renormalization conditions for mixing and self-energies . . . . .	49
4.3.3	IR rational terms in self-energies . . . . .	52
4.4	Treatment of unstable particles . . . . .	53
4.4.1	Complex-Mass Scheme at one-loop order . . . . .	53
4.4.2	Aspects of automation for general theories . . . . .	55

4.5	Renormalization of couplings in the SM and extended Higgs sector . . . . .	56
4.5.1	Renormalization of $\alpha$ . . . . .	56
4.5.2	Renormalization of $\alpha_s$ . . . . .	58
4.5.3	Renormalization of $M_{sb}$ in the THDM . . . . .	59
4.6	Renormalization of mixing angles . . . . .	60
4.6.1	Mixing angle $\alpha$ . . . . .	61
4.6.2	Mixing angle $\beta$ . . . . .	62
4.6.3	Conceptual problems in the $\overline{\text{MS}}$ scheme . . . . .	63
<b>5</b>	<b>Automated generation of renormalized model files in REPT1L</b>	<b>66</b>
5.1	Model-file generation with REPT1L . . . . .	67
5.1.1	Model-file generation flow . . . . .	67
5.1.2	Colour-flow computation . . . . .	68
5.1.3	Off-shell current basis . . . . .	69
5.2	Counterterm expansion, renormalization and computation of $R_2$ terms . . . . .	70
5.2.1	Counterterm expansion . . . . .	70
5.2.2	Renormalization conditions . . . . .	71
5.2.3	Computation of $R_2$ terms . . . . .	72
<b>6</b>	<b>Validation methods</b>	<b>73</b>
6.1	Background-Field Method . . . . .	73
6.1.1	The background-field effective action . . . . .	74
6.1.2	Background and quantum fields in extended Higgs sectors . . . . .	75
6.1.3	Background-field gauge-invariant gauge-fixing function . . . . .	75
6.1.4	Construction of the ghost function . . . . .	77
6.1.5	Renormalization and implementation details . . . . .	78
6.2	$R_\xi$ gauge for massive vector bosons . . . . .	80
6.2.1	Gauge-fixing function . . . . .	80
6.2.2	Implementation details of the $R_\xi$ gauge . . . . .	81
6.3	Automated testing suite . . . . .	82
<b>7</b>	<b>Phenomenology in the HSESM and THDM</b>	<b>84</b>
7.1	Interface to HAWK 2.0 . . . . .	84
7.1.1	Process generation with RECOLA2 . . . . .	85
7.1.2	Infrared divergences . . . . .	86
7.2	Setup and benchmark points . . . . .	86
7.2.1	Input parameters . . . . .	86
7.2.2	Cut setup . . . . .	86
7.3	Renormalization conditions for mixing angles . . . . .	88
7.4	Numerical results for total cross sections . . . . .	91
<b>8</b>	<b>Conclusion and outlook</b>	<b>97</b>

<b>Appendices</b>	<b>99</b>
A Tensor integrals . . . . .	101
A.1 Tensor-integral conventions . . . . .	101
A.2 Selected PV reduction results . . . . .	101
B The FJ Tadpole Scheme applied to the THDM and HSESM . . . . .	104
B.1 Results for tadpoles in the THDM . . . . .	105
B.2 Results for 2-point tadpole counterterms in the FJ Tadpole Scheme in the THDM . . . . .	106
B.3 Results for tadpoles in the HSESM . . . . .	107
C Alternative tadpole counterterm schemes . . . . .	108
C.1 Gauge dependence of the mixing angle $\alpha$ in popular tadpole schemes . . .	110
C.2 Gauge dependence of the mixing angle $\beta$ in popular tadpole schemes . . .	115
C.3 Feynman rules in the $\xi_\beta$ gauge . . . . .	120
D Two-loop Higgs-boson self-energy in the FJ Tadpole Scheme . . . . .	122
E Distributions for Higgs strahlung and VBF in Higgs-boson production . . . . .	124
<b>Bibliography</b>	<b>138</b>



# Introduction

The Standard Model (**SM**) is undoubtedly one of the most successful fundamental theories of our time due to its vast predictive power allowing for precision tests which are in almost perfect agreement with current experiments. Despite its success, the **SM** is not the final fundamental theory and at energies beyond the Large Hadron Collider (**LHC**)'s current reach the **SM** will fail as it does not include the gravitational force. The compatibility with gravity, however, is only one of many other aspects the **SM** cannot account for in its current form. For instance, the **SM** does not have a proper dark matter candidate as required by cosmological observations, nor does it explain dark energy. The matter-antimatter asymmetry induced by CP violation is too small to account for our matter-dominated world. In its minimal form the **SM** does not explain neutrino oscillations. Then, there is the long-standing issue with the anomalous magnetic moment of the muon showing a significant discrepancy to the **SM**, though it is not clear yet if the discrepancy is caused by new physics or if we do not control the uncertainties well enough. Finally, some people also argue that the **SM** lacks naturalness which is disputable. There is still space left for extensions of the **SM**, and Beyond Standard Model (**BSM**) theories can account for many of the **SM** shortcomings. Relevant **BSM** theories include the **SM** in one way or the other. For instance, they can be built on top of the **SM** by either enlarging the space-time symmetry group as done in Supersymmetry (**SUSY**), e.g. the Minimal Supersymmetric Standard Model (**MSSM**), or by extending the internal symmetries, e.g. additional  $U(1)$  gauge boson(s), or keeping the symmetry structure, but extending the field content, e.g. extended Higgs models. Alternatively, effects on new theories can be studied in a model-independent way keeping the **SM** symmetry and adding higher dimensional operators in order to capture new physics at higher energy scales.

Since the discovery of a Higgs boson at the **LHC** [1, 2] the community is moving forward focusing on precision which serves as the new guiding principle for new physics searches. Precision is the key to probe the **SM** and **BSM** physics and potentially allows, together with automation, to disprove the **SM** or single out new models. Progress in this direction requires the best possible measurements as they are provided by the **LHC**, upcoming upgrades and future experiments, as well as accurate theoretical predictions with small uncertainties. On the theoretical side higher precision is achieved by including loops in calculations, which are much more complex to compute. One of the many reasons is that the number of contributions grows rapidly with the number of particle multiplicities and loops, pushing even modern computers to their limits of memory and CPU workload. Further, numerical instabilities become apparent and need to be treated with care. Besides the technical problems, the procedure of renormalization, rendering theories valid beyond leading order (**LO**), and making the results ready for practical application still raises many questions in view of **BSM** models, even though from a conceptual point of view,

the renormalization procedure is well understood.

In the last decades huge effort was made in the automation of next-to-leading order (NLO) corrections. Originally, the progress was initiated by the so-called NLO revolution and driven by the unitarity techniques [3, 4, 5, 6, 7, 8]. The resulting tools could overcome many of the drawbacks of the traditional Feynman-diagrammatic approach, allowing for the first time fully automated computations at NLO Quantum Chromodynamics (QCD). A distinct feature of these new approaches was the fact that amplitudes could be written directly in terms of scalar integrals, thus, bypassing the necessity for costly tensor reduction methods, but at the price of having to address numerical instabilities with higher precision. The reduction techniques nowadays have evolved and circumvent the need for higher numerical precision by performing the reduction with suitable phase-space dependent methods which avoid spurious singularities. Despite the fact that the Feynman-diagrammatic approach can be improved via a factorized treatment of colour and further posterior algebraic simplifications, it is still not suited for high particle multiplicities. A few years ago the Feynman-diagrammatic approach has been combined with recursive techniques succeeding in the efficient computation of QCD corrections for general processes. The arisen tools [9, 10] have now become standard tools for phenomenological studies at colliders. As a result, the calculation of NLO QCD corrections is considered as a solved problem and with the need of higher precision, the focus shifts to the calculation of QCD corrections of next-to-next-to-leading order (NNLO) and of NLO Electroweak (EW) corrections. EW corrections are important for many observables at the LHC. Typically they are of the order of NNLO QCD corrections, i.e. of several percent. However, they can be enhanced for various reasons, e.g. Sudakov logarithms. For BSM models EW corrections are as important as QCD corrections and can easily reach 50%. The reason being large parameter choices in the Higgs-potential, i.e.  $\lambda = \mathcal{O}(10)$  which are still allowed and only constrained by tree-level perturbativity, but not yet by searches.

SM EW corrections became available recently in various approaches, e.g. OPENLOOPS [11], MADGRAPH5\_AMC@NLO [12], GOSAM [13, 14], FEYNARTS/FORMCALC [15, 16]. As an alternative to these pure or semi Feynman-diagrammatic approaches, with recursive elements, the method in Ref. [17] has been proposed for evaluating one-loop gluonic amplitudes. It relies on the representation of the amplitude in terms of tensor integrals, whose coefficients are computed recursively [18] without resorting to Feynman diagrams at any stage. Thus, the algorithm benefits from the stable and universal reduction methods for tensor integrals and recursive techniques which tame the vast number of contributions to one-loop amplitudes. This is the basis for the fully recursive approach in RECOLA [19, 20], in combination with the tensor-integral library COLLIER [21]. RECOLA has been successfully used in many NLO QCD and EW computations. The first computations were carried out for various lepton-pair-production channels in association with two hard jets [22, 23]. In a new series of publications the NLO QCD and EW off-shell vector-boson-pair-production channels were investigated [24, 25, 26]. Yet in another series the  $\bar{t}t$  and  $\bar{t}t\gamma$  fully off-shell final states were computed at NLO QCD and EW [27, 28, 29, 30]. Finally, the first fully off-shell prediction of vector-boson scattering has been computed in Ref. [31] at NLO EW. In all of the calculations RECOLA has been used with in-house Monte Carlo integrators. However, in order to make contact with experimental data the integration of matrix

elements is only the beginning of a proper theoretical prediction. In this respect it is advantageous to combine amplitude providers, such as RECOLA, with advanced event generators, which go beyond the standard Monte Carlo integration, in the sense that besides the simulation of the hard process via matrix elements, also soft processes via parton shower algorithms and hadronization processes are taken into account. This requires flexible and user friendly amplitude providers which can be used as a black box working in a fully automated way. RECOLA perfectly meets these requirements and has been interfaced to the general purpose event generator SHERPA [32, 33] which has been made publicly accessible [30]. Soon also WHIZARD [34, 35] will have an official support [36].

Amplitude providers are confronted with the needs of the future, namely the ability to calculate NLO QCD and EW corrections in general weakly interacting theories, similarly to the existing automated tools for the calculation of QCD corrections. However, the automation for one-loop BSM physics is more involved and requires the following three ingredients: First, new models need to be defined, typically in form of a Lagrangian and followed by the computation of the Feynman rules. For this kind of task FEYNRULES [37] and SARAH [38] are established tools. Then, a systematic and yet flexible approach to renormalization and computation of further ingredients is required to deal with generic models. Finally, the renormalized models need to be interfaced to a generic one-loop matrix element generator. As for the automation of renormalization, there has been progress in the FEYNRULES/FEYNARTS approach [39]. In this thesis a fully automated procedure to renormalization and computation of amplitudes in general models has been developed, thus, combining the second and third step. Our approach makes use of bare Universal FeynRules Output (UFO) model files [40] and results in renormalized one-loop model files for RECOLA2, a generalized version of RECOLA, allowing anyone, in principle, to compute any process in the underlying theory at the one-loop level. Much effort has been spent in the validation of the system which resulted in the support for additional gauges such as the Background-Field Method or the  $R_\xi$  gauges, and a systematic treatment of the tadpole renormalization. As an application of the system, we focused on two BSM Higgs-production processes at the LHC, namely Higgs production in association with a vector boson and Higgs production in association with two jets, in the Two-Higgs-Doublet Model (THDM) and the Higgs-Singlet extension of the SM (HSESM). Those processes are particularly interesting for an extended Higgs sector, as they represent the next-to-most-dominant Higgs-production mechanisms at the LHC.

The outline of the thesis is as follows

- In Chapter 2 we motivate BSM physics and give a brief description of the key aspects of the SM. We introduce the THDM and the HSESM, and derive the physical parameter basis which is used throughout the thesis.
- In Chapter 3 we introduce RECOLA2, focussing on the generalization with respect to RECOLA. The generalization is two-fold and concerns the dynamic process generation and the computation of processes.
- In Chapter 4 we discuss our framework for one-loop renormalized BSM theories, which

consists of the regularization scheme, the renormalization of 1-point functions (tadpoles), two-point functions (self- and mixing energies) and higher-point functions (couplings). We discuss the application of the Complex-Mass Scheme (CMS) with a focus on automation. Further, basic commonly used renormalization schemes in the SM are extended to BSM theories.

- In Chapter 5 we introduce the computer program REPT1L and describe our approach to a fully automated renormalization procedure, covering the model-file generation in a format suited for RECOLA2, the counterterm expansion, the formulation of renormalization conditions and the computation of  $R_2$  rational terms.
- In Chapter 6 the main validation tools are presented. In particular we apply the Background-Field Method (BFM) to extended Higgs sectors and highlight differences with regard to the renormalization.
- In Chapter 7 we present our numerical analysis for Higgs-production processes in the THDM and HSESM. We study various renormalization schemes and investigate genuine effects from the underlying models.

The thesis is supplemented by analytic calculations and results in the appendices which are referred to whenever suited. In App. A the reader finds our conventions for scalar and tensor integrals. In App. B we give the effective prescriptions for the *FJ Tadpole Scheme* and explicit tadpole expressions in the THDM and HSESM. In App. C we discuss the gauge dependence of the mixing-angle renormalization in the THDM and its implication on the gauge dependence of the  $S$ -matrix. In App. D we investigate the *FJ Tadpole Scheme* at two-loop order at the example of a scalar self-energy. Finally, in App. E we discuss shape-distortion effects on selected distributions in the considered processes of Chapter 7.



# Probing Beyond Standard Model theories with precision

Despite of all the successes of the **SM** it remains an incomplete theory with many shortcomings which demand explanation. Some of these questions can be addressed by simple extension, e.g. extended Higgs sectors as discussed in this chapter. In Section 2.1 we argue in favour for **BSM** theories and the necessity for precision in future investigations. In Section 2.2 we review the **SM**, focusing on the aspects relevant for the later discussion. Finally, we discuss simple, but yet viable extensions of the **SM** Higgs sector in Section 2.3, namely the **THDM** and **HSESM**. These models are then subject to the automated renormalization discussed in Chapter 5.

## 2.1 Beyond Standard Model theories and the necessity for precision

The overall agreement of observables predicted by the **SM** and measured by particle colliders such as the **LHC**, does not show, at the time of writing, any deviation larger than  $3\sigma$ . Nevertheless, the **SM** is clearly not the final answer to nature as many questions remain unanswered. Among the fundamental ones is the compatibility with the theory of gravity, namely General Relativity (**GR**). **GR** is a well-established theory and has been confirmed recently once again by the discovery of the gravitational waves at **LIGO** [41], which, in its importance, is comparable to the discovery of the Higgs boson. Yet, both **GR** and the **SM** are expected to break down at very high energies, namely at the Planck scale, where they should be replaced by a unified quantum version. The idea of unification is most appealing and is deeply rooted in our understanding of nature via simple principles as encountered in gauge theories and **GR**. Besides, unification is nothing new and has already successfully lead to the unification of **EW** theory. Therefore, there are good reason to believe in a unification, but there is no guarantee that we are able to see it, if it happens at all. The new physics scale might be separated by a large gap from the electroweak scale and we would not be able to see anything, at least not with human-build machines like the **LHC**. However, astrophysical observations make hope for new physics which may very well reside within our grasp. For instance, neither the **SM** nor **GR** are able to describe the preponderance of matter over antimatter as seen in our universe, or the existence of dark matter as nowadays accepted to explain the rotational velocity curves, or dark energy which is responsible for the acceleration of the universe [42, 43]. All of these phenomena can be addressed and explained by non-gravitational interactions which should leave an imprint at particle colliders. Besides the astrophysical observations the **SM** arguably suffers from aesthetic deficiencies which demand an

explanation. This concerns e.g. the fermionic mass hierarchies or the true nature of neutrinos which is yet to be discovered. The **SM** is not restricted to its current form and allows for various simple extensions. In particular, there is no reason why the Higgs-sector should be composed of just a single Higgs doublet. In fact, non-minimal extensions of the scalar sector can account for astrophysical observations concerning matter antimatter asymmetry, or dark matter. For instance, the **THDM** is (still) viable for a successful baryogenesis [44]. All in all there is enough motivation to believe that the **SM** is not complete up to the Planck scale and new physics might yet show up, even if there is a large gap between the **EW** scale and new physics.

With this in mind two strategies can be pursued in investigating new physics. On the one hand, we can study concrete new models, and the relevant ones should behave **SM** like, at least at low energy, otherwise we would have seen something at the **LHC**. On the other hand, we can consider decoupling scenarios which are based on the assumption that new physics scale is much higher compared to, e.g. the Higgs-boson mass. Decoupling scenarios are not excluded by any means and a systematic approach without considering concrete models is possible via Effective Field Theory (**EFT**). The quest is to search for small deviations in both approaches, and finding evidence for **BSM** indirectly.

There are several ways to constrain the parameter space of theories with precision. For instance, in the days of LEP the oblique parameters S, T and U were computed to study universal corrections [45]. The closely related  $\rho$  parameter, defined as [43]

$$\rho = \frac{M_W^2}{c_w^2 M_Z^2}, \quad (2.1)$$

equals exactly one in the **SM** at tree level. The experimental value, currently given by [43]

$$\rho = 1.00040 \pm 0.00024, \quad (2.2)$$

strongly favours theories which fulfil  $\rho = 1$  at tree-level. In the **THDM** and **HSESM** discussed in Section 2.3 this requirement is fulfilled without fine-tuning, yet, radiative corrections to (2.1) differ from the **SM** and can be used as a testing ground for **BSM** benchmark points. In extended Higgs sectors the oblique parameters can be studied in a systematic way, as done e.g. in Ref. [46] for theories with additional  $SU(2)_w$  doublets and singlets. Further, the tools **HIGGSBOUNDS** [47] and **HIGGSIGNALS** [48] incorporate these and other precision tests, including the comparison to measured Higgs rates, automatically. In the **THDM** this has been automated via an interface to the dedicated tool **2HDMC** [49]. Finally, to ultimately test models one has to confront them directly with experimental data, which requires accurate predictions for realistic final states. This is where **RECOLA2** comes into play.

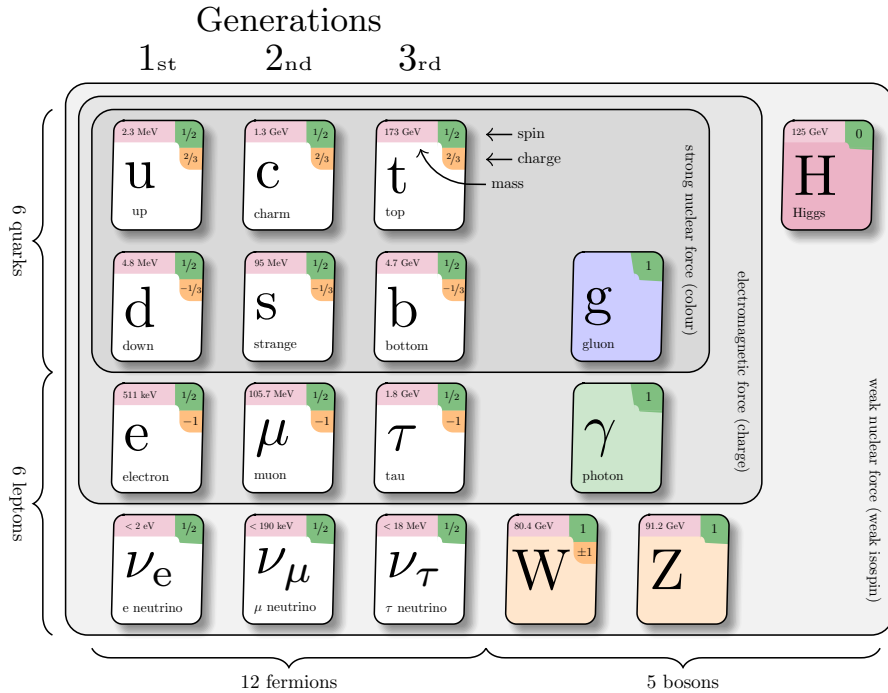


Figure 2.1: The particle content of the SM. The innermost region unifies strongly interacting particles. The next to innermost region describes the QED interactions with the photon. The outermost region represents the weak force mediated by the massive gauge bosons, which includes interactions with neutrinos. The Higgs boson interacts with all massive particles.<sup>1</sup>

## 2.2 Aspects of the Standard Model

### 2.2.1 Overview

The SM is a relativistic Quantum Field Theory (QFT) based on the postulation of matter fields in specific representations of the Poincaré and gauge groups, compatible with nature. More precisely, the SM gauge group is

$$SU(3)_c \times SU(2)_w \times U(1)_Y, \quad (2.3)$$

composed of the QCD ( $SU(3)_c$ ) and EW ( $SU(2)_w \times U(1)_Y$ ) components. Interactions between fields are introduced by promoting the invariance under (2.3) to a local gauge invariance, i.e. making this particular symmetry transformation space–time dependent. As a consequence, new dynamic fields emerge, mediating gauge interactions. The strong force is mediated by the gluon, which solely interacts with colour-charged particles, namely the quarks in the SM. The EW force is mediated by the photon and the massive gauge bosons Z, W, which interact with quarks and leptons. Together with the Higgs boson, which couples to all massive particles in the SM, the complete SM particle content is depicted in Fig. 2.1.

<sup>1</sup>Modified template source code from <http://www.texample.net/tikz/examples/model-physics/>

Field	Representation	Dimension	Gauge coupling
$G^a$	$\mathbf{8} \times \mathbf{1} \times \mathbf{1}(0)$	8	$g_s$
$W^i$	$\mathbf{1} \times \mathbf{3} \times \mathbf{1}(0)$	3	$g$
$B$	$\mathbf{1} \times \mathbf{1} \times \mathbf{1}(0)$	1	$g'$

Table 2.1: Gauge-boson fields and associated gauge couplings in the SM.  $\mathbf{8}$  stands for octet,  $\mathbf{3}$  for triplet and  $\mathbf{1}$  for singlet representations. The value in the parenthesis denotes the hypercharge.

### 2.2.2 Kinetic terms for gauge bosons

Vector bosons are defined in the adjoint representation of the gauge group (2.3) as given in Table 2.1. In this classification the fields are in the so-called gauge eigenbasis allowing for a straightforward gauge-invariant definition of the Yang-Mills Lagrangian in terms of the field-strength tensors  $G_{\mu\nu}^a, W_{\mu\nu}^i, B_{\mu\nu}$  as follows

$$\mathcal{L}_{\text{YM}} = -\frac{1}{4} \sum_{a=1}^8 G_{\mu\nu}^a G^{a,\mu\nu} - \frac{1}{4} \sum_{i=1}^3 W_{\mu\nu}^i W^{i,\mu\nu} - \frac{1}{4} B_{\mu\nu} B^{\mu\nu}. \quad (2.4)$$

The field-strength tensors are constructed from the commutator of covariant derivatives in the adjoint representation with the following result

$$\begin{aligned} G_{\mu\nu}^a &= \partial_\mu G_\nu^a - \partial_\nu G_\mu^a + \sum_{b,c=1}^8 g_s f^{abc} G_\mu^b G_\nu^c, \\ W_{\mu\nu}^i &= \partial_\mu W_\nu^i - \partial_\nu W_\mu^i + \sum_{j,k=1}^3 g \epsilon^{ijk} W_\mu^j W_\nu^k, \\ B_{\mu\nu} &= \partial_\mu B_\nu - \partial_\nu B_\mu, \end{aligned} \quad (2.5)$$

where  $f^{abc}$  and  $\epsilon^{ijk}$  are the structure constants of  $\text{SU}(3)_c$  and  $\text{SU}(2)_w$ , respectively.

### 2.2.3 Kinetic terms for fermions

The fermions can be decomposed into left- and right-handed components which in the SM transform under different representations. The left-handed ones form an  $\text{SU}(2)_w$  doublet, whereas the right-handed ones are defined as singlet fields,

$$Q_L = \begin{pmatrix} u_L \\ d_L \end{pmatrix}, \quad L_L = \begin{pmatrix} \nu_L \\ l_L \end{pmatrix}, \quad u_R, \quad d_R, \quad l_R, \quad (2.6)$$

with  $u, d, l$  and  $\nu$  generically denoting up-type quark, down-type quark, charged lepton and neutrino, respectively. Notice that the minimal SM does not anticipate right-handed neutrinos. Table 2.2 summarizes the fermion-field representations. The fermions come in three different generations which can be thought of as two additional copies of (2.6). Denoting the generation

Field	Representation	Dimension
$Q_L$	$\mathbf{3} \times \mathbf{2} \times \mathbf{1} \left( \frac{1}{3} \right)$	6
$L_L$	$\mathbf{1} \times \mathbf{2} \times \mathbf{1} \left( -1 \right)$	2
$u_R$	$\mathbf{3} \times \mathbf{1} \times \mathbf{1} \left( \frac{2}{3} \right)$	3
$d_R$	$\mathbf{3} \times \mathbf{1} \times \mathbf{1} \left( -\frac{1}{3} \right)$	3
$l_R$	$\mathbf{1} \times \mathbf{1} \times \mathbf{1} \left( -2 \right)$	1

Table 2.2: Fermion-field representations of (2.3) in the SM.  $\mathbf{3}$  stands for triplet,  $\mathbf{2}$  for doublet and  $\mathbf{1}$  for singlet representations. The value in the parenthesis denotes the hypercharge  $Y$ .

index by  $i$ , the complete kinetic term reads

$$\mathcal{L}_{\text{Dirac}} = \sum_{i=1}^3 \left( i\bar{Q}_L^i \not{D} Q_L^i + i\bar{L}_L^i \not{D} L_L^i + i\bar{u}_R^i \not{D} u_R^i + i\bar{d}_R^i \not{D} d_R^i + i\bar{l}_R^i \not{D} l_R^i \right), \quad (2.7)$$

with  $\not{D} = \gamma_\mu D^\mu$  denoting the covariant derivative contracted with the Dirac gamma matrices. The covariant derivative is defined as

$$D_\mu = \partial_\mu - \sum_{a=1}^8 ig_s t^a G_\mu^a - \sum_{i=1}^3 igt^i W_\mu^i - ig' t B_\mu, \quad (2.8)$$

with  $t^a, t^i, t$  being the generators in appropriate representation when acting on the fields. For quarks one chooses the Gell-Mann matrices  $\lambda^a$  as  $t^a = \lambda^a/2$ . For the left-handed isospin doublets the generator  $t^i = \sigma^i/2$  is given by the Pauli matrices  $\sigma^i$ , and weak hypercharge generator  $t = -Y/2$  is just the value for the weak hypercharge as given in Table 2.2.

### 2.2.4 Brout-Englert-Higgs mechanism

The SM is a chiral theory and the naive mass terms for fermions

$$-m_f (\bar{\psi}_L \psi_R + \bar{\psi}_R \psi_L) \quad (2.9)$$

are forbidden by the requirement of gauge invariance, since left- and right-handed fermions transform differently under the gauge group (2.3). The Brout-Englert-Higgs (BEH) mechanism circumvents this apparent problem by generating masses dynamically in a gauge-invariant way, at the cost of introducing new dynamic fields and interactions. The precondition for the mechanism is a suited scalar potential exhibiting Spontaneous Symmetry Breaking (SSB). In the SM one chooses

$$V_{\text{SM}} = \frac{\lambda}{4} \left( \Phi^\dagger \Phi \right)^2 - \mu^2 \Phi^\dagger \Phi, \quad (2.10)$$

Field	Representation	Dimension
$\Phi$	$\mathbf{1} \times \mathbf{2} \times \mathbf{1}(1)$	2

Table 2.3: SM Higgs doublet field representations.  $\mathbf{2}$  stands for doublet and  $\mathbf{1}$  for singlet representations. The value in the parenthesis denotes the hypercharge  $Y$ . Since the Higgs doublet is chosen to be complex, it comes with 4 dof instead of 2.

with the parameters  $\lambda$  and  $\mu$  chosen to be real and positive. The field  $\Phi$  is a complex  $SU(2)_w$  doublet defined in components as follows

$$\Phi = \begin{pmatrix} \phi^+ \\ \frac{1}{\sqrt{2}} [v_h + h + i\chi] \end{pmatrix}. \quad (2.11)$$

The linear combination  $v_h + h$  represents the neutral component of  $\Phi$ . Note that the vacuum expectation value (**vev**)  $v_h$  is not a parameter of the theory, but merely a convenient field parametrization. The scalar potential is minimized by imposing the condition

$$\left. \frac{\partial V}{\partial \Phi} \right|_{\Phi=(0, v_h/\sqrt{2})^T} = 0, \quad (2.12)$$

which yields the solutions for the **vev**  $v_h$

$$v_h^2 = \frac{4\mu^2}{\lambda}. \quad (2.13)$$

The Higgs Lagrangian is composed of the potential (2.10) and the standard scalar kinetic term, augmented by covariant derivatives as follows

$$\mathcal{L}_H = (D_\mu \Phi)^\dagger (D^\mu \Phi) - V_{SM}. \quad (2.14)$$

The kinetic term couples the Higgs doublet field to gauge bosons, which gives rise to the gauge-boson masses<sup>2</sup>

$$M_W = \frac{gv_h}{2}, \quad M_Z = \frac{\sqrt{g^2 + g'^2}v_h}{2}, \quad M_\gamma = 0. \quad (2.15)$$

For the fermions additional Yukawa interactions are postulated as follows

$$\mathcal{L}_{\text{Yukawa}} = - \sum_{i,j=1}^3 \left( \Gamma_d^{ij} \bar{Q}_L^i \Phi d_R^j + \Gamma_u^{ij} \bar{Q}_L^i \tilde{\Phi} u_R^j + \Gamma_l^{ij} \bar{L}_L^i \Phi l_R^j + \text{h.c.} \right), \quad (2.16)$$

where  $\tilde{\Phi} = i\sigma^2 \Phi$  is the charge-conjugated Higgs doublet, and h.c. denotes the inclusion of the hermitian conjugate terms in order to make (2.16) hermitian. With this we conclude the review of the SM.

<sup>2</sup>The identification of  $M_Z$  requires to diagonalize the neutral gauge-boson sector. See e.g. Ref. [50].

## 2.3 Two-Higgs-Doublet Model and the Higgs-Singlet extension of the Standard Model

In this section we give an introduction to the **THDM** and the **HSESM** which are simple extensions of the **SM** Higgs sector. Parts were taken from Refs. [51, 52] and extended in order to be self-contained. We start with the definition of the fields and the scalar potential in Section 2.3.1. In the second part in Section 2.3.2 we translate the potential to the mass eigenbasis, identifying suitable physical parameters. Finally, in Section 2.3.3 the Yukawa Lagrangian of the **THDM** is discussed, which for the **HSESM** coincides with the one of the **SM** (2.16). All models are given with the restriction of a CP-conserving  $Z_2$  symmetric scalar potential, which in the case of the **THDM** is allowed to be softly broken. For the **THDM** we stick to the conventions of Refs. [53, 54]. For the **HSESM** we follow Refs. [55, 56, 57, 58] which are based on the original literature [59, 60, 61]. The **HSESM** conventions are adapted to the ones used in the **THDM**. The models were incorporated in RECOLA2 as model files allowing for an automated computation of any process, with the only limitations being internal memory and CPU power. The renormalization is performed as generically described in Chapter 4. The generation of the renormalized model file is presented in Chapter 5.

### 2.3.1 Fields and potential in the symmetric basis

Both models are simple extensions of the **SM**, only affecting the form and fields entering the scalar potential and for the **THDM** also the Yukawa interactions. In the case of the **THDM** we have two Higgs doublets with hypercharge  $Y = 1$ , generically denoted as  $\Phi_i$  with  $i = 1, 2$  and defined component-wise by

$$\Phi_i = \begin{pmatrix} \phi_i^+ \\ \frac{1}{\sqrt{2}}(v_i + \rho_i + i\eta_i) \end{pmatrix}, \quad (2.17)$$

with  $v_i$  denoting the **vevs**. Under the constraint of CP conservation plus the  $Z_2$  symmetry ( $\Phi_1 \rightarrow -\Phi_1, \Phi_2 \rightarrow \Phi_2$ ), the most general renormalizable potential reads [53]

$$\begin{aligned} V_{\text{THDM}} = & m_1^2 \Phi_1^\dagger \Phi_1 + m_2^2 \Phi_2^\dagger \Phi_2 - m_{12}^2 (\Phi_1^\dagger \Phi_2 + \Phi_2^\dagger \Phi_1) \\ & + \frac{\lambda_1}{2} (\Phi_1^\dagger \Phi_1)^2 + \frac{\lambda_2}{2} (\Phi_2^\dagger \Phi_2)^2 + \lambda_3 (\Phi_1^\dagger \Phi_1) (\Phi_2^\dagger \Phi_2) + \lambda_4 (\Phi_1^\dagger \Phi_2) (\Phi_2^\dagger \Phi_1) \\ & + \frac{\lambda_5}{2} \left[ (\Phi_1^\dagger \Phi_2)^2 + (\Phi_2^\dagger \Phi_1)^2 \right], \end{aligned} \quad (2.18)$$

with five real couplings  $\lambda_1 \dots \lambda_5$ , two real mass parameters  $m_1^2$  and  $m_2^2$ , and the soft  $Z_2$ -breaking parameter  $m_{12}^2$ .

The **HSESM** scalar potential involves one Higgs doublet  $\Phi$  with  $Y = 1$  and a singlet field  $S$  with  $Y = 0$  defined as

$$\Phi = \begin{pmatrix} \phi^+ \\ \frac{1}{\sqrt{2}}(v + \rho_1 + i\eta) \end{pmatrix}, \quad S = \frac{v_s + \rho_2}{\sqrt{2}}. \quad (2.19)$$

Note that  $\rho_1, \rho_2$  are intentionally identified with the same symbols appearing in the Higgs doublets of the **THDM** (2.17) which allows for a treatment on equal footing in the mass diagonalization and renormalization of mixing angles for both models. Under the same constraints, the most general potential reads

$$V_{\text{HSESM}} = m_1^2 \Phi^\dagger \Phi + m_2^2 S^2 + \frac{\lambda_1}{2} (\Phi^\dagger \Phi)^2 + \frac{\lambda_2}{2} S^4 + \lambda_3 \Phi^\dagger \Phi S^2, \quad (2.20)$$

with all parameters being real.

### 2.3.2 Parameters in the physical basis

Both potentials are subject to **SSB** which requires a rotation of fields to the mass eigenstates in order to identify the physical degrees of freedom. For the **THDM** there are five physical Higgs bosons  $H_1, H_h, H_a, H^\pm$  and in the **HSESM** there are two physical Higgs bosons  $H_1$  and  $H_h$ , intentionally identified with the same symbols as in the **THDM**. Besides the physical Higgs bosons, there are the three would-be Goldstone bosons  $G_0$  and  $G^\pm$  in the 't Hooft–Feynman gauge. The mass eigenstates for the neutral Higgs-boson fields are obtained in both models by the transformation

$$\begin{pmatrix} \rho_1 \\ \rho_2 \end{pmatrix} = R(\alpha) \begin{pmatrix} H_h \\ H_1 \end{pmatrix}, \quad \text{with} \quad R(\alpha) = \begin{pmatrix} \cos \alpha & -\sin \alpha \\ \sin \alpha & \cos \alpha \end{pmatrix}, \quad (2.21)$$

with  $\alpha$  being fixed such that the mass matrix

$$M_{ij} := \left. \frac{\partial^2 V}{\partial \rho_i \partial \rho_j} \right|_{\varphi=0} \quad (2.22)$$

is diagonalized via  $R(-\alpha)MR(\alpha)$ , with the potential  $V$  being either (2.18) or (2.20). The solution to (2.22) for symmetric  $2 \times 2$  matrices is generically given by (see Ref. [53])

$$\sin 2\alpha = \frac{2M_{12}}{\sqrt{(M_{11} - M_{22})^2 + 4M_{12}^2}}. \quad (2.23)$$

In the **THDM** there are additional mixings between charged and pseudo-scalar bosons and Goldstone bosons, which are diagonalized as follows

$$\begin{pmatrix} \phi_1^\pm \\ \phi_2^\pm \end{pmatrix} = R(\beta) \begin{pmatrix} G^\pm \\ H^\pm \end{pmatrix}, \quad \begin{pmatrix} \eta_1 \\ \eta_2 \end{pmatrix} = R(\beta) \begin{pmatrix} G_0 \\ H_a \end{pmatrix}, \quad (2.24)$$

with

$$R(\beta) = \begin{pmatrix} \cos \beta & -\sin \beta \\ \sin \beta & \cos \beta \end{pmatrix}. \quad (2.25)$$

The angle  $\beta$  is related to the vevs according to  $t_\beta \equiv \tan \beta = v_2/v_1$  in the **THDM**. For the **HSESM** we define  $t_\beta \equiv \tan \beta = v_s/v$ . The Higgs sector is minimally coupled to the gauge bosons. Collecting quadratic terms and identifying the masses one obtains the well-known tree-



level relations

$$M_W = \frac{1}{2}gv, \quad M_Z = \frac{1}{2}\sqrt{g^2 + g'^2} v, \quad (2.26)$$

where  $g$  and  $g'$  denote the weak isospin and hypercharge gauge couplings, and  $M_W$  and  $M_Z$  the W- and Z-boson masses, respectively. For the **THDM** we identify  $v = \sqrt{v_1^2 + v_2^2}$ . Then, one employs the minimum conditions for the scalar potential which, in both models, read

$$\langle \rho_i \rangle = 0, \quad (2.27)$$

and obtains solutions for  $m_1^2$  and  $m_2^2$ . Finally, physical mass parameters are identified as the quadratic terms in the Lagrangian after **SSB** and after diagonalization. The physical mass parameters are identified with the Higgs-boson masses,  $M_{H_1}$  (light Higgs boson),  $M_{H_h}$  (heavy Higgs boson),  $M_{H_a}$  (pseudoscalar Higgs boson),  $M_{H^\pm}$  (charged Higgs boson), the two mixing angles  $\alpha$  and  $\beta$ , the soft- $Z_2$ -breaking scale  $M_{\text{sb}}$ , and the vacuum expectation value  $v$ . Whereas for the **HSESM** we have  $M_{H_1}$  (light Higgs boson),  $M_{H_h}$  (heavy Higgs boson), and the two mixing angles  $\alpha$  and  $\beta$ .

The mass parameters are obtained in terms of the  $\lambda_i$  parameters which are given separately for the **THDM** and **HSESM** in the following:

**THDM:** The solutions to (2.27) read

$$\begin{aligned} m_1^2 &= M_{\text{sb}}^2 \sin^2 \beta - \frac{2M_W^2}{g^2} \left[ \lambda_1 \cos^2 \beta + (\lambda_3 + \lambda_4 + \lambda_5) \sin^2 \beta \right], \\ m_2^2 &= M_{\text{sb}}^2 \cos^2 \beta - \frac{2M_W^2}{g^2} \left[ \lambda_2 \sin^2 \beta + (\lambda_3 + \lambda_4 + \lambda_5) \cos^2 \beta \right], \end{aligned} \quad (2.28)$$

where we have defined the soft-breaking scale  $M_{\text{sb}}$  as

$$M_{\text{sb}}^2 = \frac{m_{12}^2}{\cos \beta \sin \beta}. \quad (2.29)$$

and the **vev**  $v$  has been substituted using Eq. (2.26). The  $\lambda_i$  parameters are expressed by the physical Higgs-boson masses  $M_{H_1}$ ,  $M_{H_h}$ ,  $M_{H_a}$ ,  $M_{H^\pm}$  and the soft-breaking scale  $M_{\text{sb}}$  as follows

$$\begin{aligned} \lambda_1 &= \frac{g^2}{4M_W^2 \cos^2 \beta} \left[ \cos^2 \alpha M_{H_h}^2 + \sin^2 \alpha M_{H_1}^2 - \sin^2 \beta M_{\text{sb}}^2 \right], \\ \lambda_2 &= \frac{g^2}{4M_W^2 \sin^2 \beta} \left[ \sin^2 \alpha M_{H_h}^2 + \cos^2 \alpha M_{H_1}^2 - \cos^2 \beta M_{\text{sb}}^2 \right], \\ \lambda_3 &= \frac{g^2}{4M_W^2} \left[ \frac{\cos \alpha \sin \alpha}{\cos \beta \sin \beta} (M_{H_h}^2 - M_{H_1}^2) + 2M_{H^\pm}^2 - M_{\text{sb}}^2 \right], \\ \lambda_4 &= \frac{g^2}{4M_W^2} (M_{H_a}^2 - 2M_{H^\pm}^2 + M_{\text{sb}}^2), \\ \lambda_5 &= \frac{g^2}{4M_W^2} (M_{\text{sb}}^2 - M_{H_a}^2). \end{aligned} \quad (2.30)$$

Using the identities

$$\begin{aligned}\cos \beta &= \frac{1}{\sqrt{1+t_\beta^2}}, & \sin \beta &= \frac{t_\beta}{\sqrt{1+t_\beta^2}}, \\ \cos \alpha &= \frac{c_{\alpha\beta} - s_{\alpha\beta}t_\beta}{\sqrt{1+t_\beta^2}}, & \sin \alpha &= \frac{s_{\alpha\beta} + c_{\alpha\beta}t_\beta}{\sqrt{1+t_\beta^2}},\end{aligned}\quad (2.31)$$

the angles can be converted to the basis [53]

$$\alpha, \beta \quad \rightarrow \quad c_{\alpha\beta} := \cos(\alpha - \beta), \quad t_\beta := \tan \beta, \quad (2.32)$$

which is a natural choice for studying (almost) aligned scenarios. The angle  $\alpha$  is defined in the window  $[-\pi/2, \pi/2]$ , whereas the angle  $\beta$  is defined in the window  $[0, \pi/2]$ . This implies  $\cos \alpha = \sqrt{1 - \sin^2 \alpha}$ ,  $\cos \beta = \sqrt{1 - \sin^2 \beta}$  and  $t_\beta > 0$ . The solutions are valid only for  $M_{H_h} > M_{H_1}$ .

**HSESM:** The stability conditions for the potential (2.27) yield

$$\begin{aligned}m_1^2 &= -\frac{2M_W^2}{g^2} [\lambda_1 + \lambda_3 t_\beta^2], \\ m_2^2 &= -\frac{2M_W^2}{g^2} [\lambda_2 t_\beta^2 + \lambda_3].\end{aligned}\quad (2.33)$$

The solutions to the  $\lambda_i$  parameters expressed by the physical Higgs-boson masses  $M_{H_1}$  and  $M_{H_h}$  read

$$\begin{aligned}\lambda_1 &= \frac{g^2}{4M_W^2} [\cos^2 \alpha M_{H_h}^2 + \sin^2 \alpha M_{H_1}^2], \\ \lambda_2 &= \frac{g^2}{4M_W^2 t_\beta^2} [\sin^2 \alpha M_{H_h}^2 + \cos^2 \alpha M_{H_1}^2], \\ \lambda_3 &= \frac{g^2}{4M_W^2 t_\beta} [\cos \alpha \sin \alpha (M_{H_h}^2 - M_{H_1}^2)].\end{aligned}\quad (2.34)$$

The mixing angle  $\alpha$  is defined in the window  $[-\pi/2, \pi/2]$ , which implies  $\cos \alpha = \sqrt{1 - \sin^2 \alpha}$ . Further  $t_\beta$  is taken positive  $t_\beta > 0$ , and the solutions are valid only for  $M_{H_h} > M_{H_1}$ .

In Table 2.4 we summarize the independent parameters related to the Higgs potential in both Models.

### 2.3.3 Yukawa Interactions

The fermionic sector in the HSESM is the same as in the SM, whereas the THDM allows for a richer structure. In the general case of the THDM, fermions can couple to both  $\Phi_1$  and  $\Phi_2$ , leading to flavour-changing neutral currents (FCNC) already at tree level. Since FCNC processes are extremely rare in nature they highly constrain BSM models. In order to prevent tree-level

	$V_{\text{2HDM}}$	$\mathcal{L}_{\text{Gauge}}$
Before <b>SSB</b>	$m_1, m_2, m_{12}, \lambda_1, \lambda_2, \lambda_3, \lambda_4, \lambda_5$	$g, g'$
After <b>SSB</b> (choice)	$M_{H_1}, M_{H_h}, M_{H_a}, M_{H^\pm}, c_{\alpha\beta}, t_\beta, M_{\text{sb}}, M_{\text{W}}$	$e, s_{\text{W}}$
	$V_{\text{HSESM}}$	$\mathcal{L}_{\text{Gauge}}$
Before <b>SSB</b>	$m_1, m_2, \lambda_1, \lambda_2, \lambda_3$	$g, g'$
After <b>SSB</b> (choice)	$M_{H_1}, M_{H_h}, s_\alpha, t_\beta, M_{\text{W}}$	$e, s_{\text{W}}$

Table 2.4: Independent parameters in the gauge and mass eigenbasis of the **THDM** and **HSESM**. The **EW** gauge couplings need to be considered in order to properly identify the independent parameters in the mass eigenbasis after **SSB**. Note that there are no additional independent parameters, and we intentionally did not list **vev** or tadpole parameters.

FCNC, one imposes the  $Z_2$  symmetry

$$Z_2 : \quad \Phi_1 \rightarrow -\Phi_1, \quad \Phi_2 \rightarrow \Phi_2, \quad (2.35)$$

as already introduced in the Higgs potential in Section 2.3.2. This  $Z_2$  symmetry is motivated by the Glashow–Weinberg–Paschos theorem in Refs. [62, 63], which states that for an arbitrary number of Higgs doublets, if all right-handed fermions couple to exactly one of the Higgs doublets, FCNCs are absent at tree level. This can be realized by imposing, in addition to (2.35), a parity for right-handed fermions under  $Z_2$  symmetry. One obtains four distinct **THDM** Yukawa terms which are given by:

**Type I:** By requiring for all fermions an even parity under  $Z_2$ , all have to couple to the second Higgs doublet  $\Phi_2$ . The corresponding Yukawa Lagrangian reads

$$\mathcal{L}_Y = -\Gamma_{\text{d}} \bar{Q}_L \Phi_2 d_R - \Gamma_{\text{u}} \bar{Q}_L \tilde{\Phi}_2 u_R - \Gamma_1 \bar{L}_L \Phi_2 l_R + \text{h.c.}, \quad (2.36)$$

where  $\tilde{\Phi}_2$  is the charge-conjugated Higgs doublet of  $\Phi_2$ . Neglecting flavour mixing, the coefficients are directly expressed by the fermion masses  $m_{\text{d}}$ ,  $m_{\text{u}}$  and  $m_l$ , and the mixing angle  $\beta$ ,

$$\Gamma_{\text{d}} = \frac{g m_{\text{d}}}{\sqrt{2} M_{\text{W}} \sin \beta}, \quad \Gamma_{\text{u}} = \frac{g m_{\text{u}}}{\sqrt{2} M_{\text{W}} \sin \beta}, \quad \Gamma_1 = \frac{g m_l}{\sqrt{2} M_{\text{W}} \sin \beta}. \quad (2.37)$$

Again, the vev  $v$  has been substituted using Eq. (2.26).

**Type II:** This is the **MSSM**-like scenario obtained by requiring odd parity for down-type quarks and leptons:  $d_R \rightarrow -d_R$ ,  $l_R \rightarrow -l_R$  and even parity for up-type quarks. It follows that the down-type quarks and leptons couple to  $\Phi_1$ , while up-type quarks couple to  $\Phi_2$ . The corresponding Yukawa Lagrangian reads

$$\mathcal{L}_Y = -\Gamma_{\text{d}} \bar{Q}_L \Phi_1 d_R - \Gamma_{\text{u}} \bar{Q}_L \tilde{\Phi}_2 u_R - \Gamma_1 \bar{L}_L \Phi_1 l_R + \text{h.c.}. \quad (2.38)$$

Again, neglecting flavour mixing, the coefficients are expressed by the fermion masses  $m_{\text{d}}$ ,

$m_u$  and  $m_l$ , and the mixing angle  $\beta$ ,

$$\Gamma_d = \frac{g m_d}{\sqrt{2} M_W \cos \beta}, \quad \Gamma_u = \frac{g m_u}{\sqrt{2} M_W \sin \beta}, \quad \Gamma_l = \frac{g m_l}{\sqrt{2} M_W \cos \beta}. \quad (2.39)$$

**Type Y:** This type, also referred to as *lepton-specific*, is obtained by requiring odd parity only for leptons:  $l_R \rightarrow -l_R$ .

**Type X:** This type, also referred to as *flipped*, is obtained by requiring odd parity only for down-type quarks:  $d_R \rightarrow -d_R$ .

In the numerical analysis in Chapter 7 we focus on Type II, which is the most popular and most constrained type due to the connection to the [MSSM](#) scalar potential, which is also of type II. There is, however, a difference to the [THDM](#), namely the  $\lambda_i$ s are constrained by gauge symmetry in the [MSSM](#). Further, in Chapter 7 we consider all fermions as massless except for the top quark which makes Type I equivalent to Type II. This restriction only applies to the numerical analysis and not to the model file derivation and renormalization which we kept fully general. In particular, we note that the [THDM RECOLA2](#) model file can handle all Yukawa types, and switching between different Yukawa types is done by a simple function call. To this end, the Lagrangian has been defined as the sum of all possible combinations of Fermion doublets coupling with  $\Phi_1$  and  $\Phi_2$ , and additional parameters enforcing a specific potential type.

# Matrix elements for generic theories with RECOLA2

RECOLA2 is a tree and one-loop matrix-element provider for general models involving scalars, fermions and vector particles. It is based on its predecessor RECOLA [19, 20], which uses Dyson-Schwinger (DS) equations [64, 65, 66] to compute matrix elements in a fully numerical and recursive approach. The implementation at tree-level follows the strategy developed in Ref. [67], supplemented by a special treatment of the colour algebra. The one-loop extension, inspired by Ref. [17], relies on the decomposition of one-loop amplitudes as linear combination of tensor integrals and tensor coefficients. The former are evaluated by means of the library COLLIER [21], while the latter can be computed by making use of similar recursion relations as for tree amplitudes. The key task of RECOLA2 is the construction of the proper tensor structure of the coefficients at each step of the recursive procedure, which has been implemented in RECOLA relying on the fact that in the Standard Model in the 't Hooft–Feynman gauge the combination (vertex) $\times$ (propagator) is at most linear in the momenta. RECOLA2 circumvents these and other limitations of RECOLA and allows, in particular, to deal with different gauges, such as  $R_\xi$  gauge or BFM, and more generic structures as well as higher  $n$ -point vertices as encountered in SM EFT.<sup>1</sup> RECOLA2 is written in pure FORTRAN95 and depends, besides the COLLIER library, on RECOLA2 specific model files.

In the following Section 3.1 we give a short overview of the core algorithm, and derive some aspects from first principles. The RECOLA2 algorithm operates in two stages which we discuss separately. The first stage concerns the dynamic process generation where the so-called tree skeletons are constructed, dictating the order in which the off-shell currents are computed in the process-computation stage, i.e. the second stage. In Section 3.2 we discuss implementation details of the skeleton construction, focusing on parts which have been extended in order to support general QFT. In Section 3.3 we discuss the extension to the one-loop order. Several of the building blocks used in RECOLA in the process-computation stage now need be provided by the model file as they are no longer part of RECOLA2. This concerns, in particular, the rules for computing outgoing off-shell currents in terms of incoming ones at the tree and one-loop level. Since they are closely linked to the RECOLA2 algorithm we discuss their structure in this chapter in Section 3.4, again with a focus on generalizations.

---

<sup>1</sup>For instance, RECOLA2 supports the operators encountered in Higgs SM EFT of Refs. [68], [69].

### 3.1 Berends-Giele recursion relation

The principle behind the Berends-Giele recursion (**BGR**) is the **DS** equation which is derived from the generating functional and using vanishing boundary terms in the path integral, i.e.

$$\int \mathbb{D}\phi \frac{\partial}{\partial \phi(x)} e^{i(S[\phi] + \int d^4y \phi(y)j(y))} = 0, \quad (3.1)$$

with  $\mathbb{D}\phi$  being the path-integral measure. Performing the differentiation on the exponential of the generating functional yields a relation between the action  $S$  and its sources  $j$  as a quantum mechanical expectation value as follows

$$0 \stackrel{(3.1)}{=} \int \mathbb{D}\phi \left( \frac{\delta S[\phi]}{\delta \phi(x)} + j(x) \right) e^{i(S[\phi] + \int d^4y \phi(y)j(y))} \equiv \left\langle \frac{\delta S[\phi]}{\delta \phi(x)} + j(x) \right\rangle. \quad (3.2)$$

In order to make the recursive structure explicit we exemplify the implications of (3.2) for a generic scalar theory  $S$  with  $n$ -point interactions. Omitting any space–time dependence, we have

$$\frac{\delta S[\phi]}{\delta \phi} = -\Delta^{-1}\phi - \frac{\lambda_3}{2!}\phi^2 - \frac{\lambda_4}{3!}\phi^3 - \frac{\lambda_5}{4!}\phi^4 + \dots, \quad (3.3)$$

where  $\Delta^{-1} = \square + m^2$  is the Klein-Gordon differential operator. Multiplying the **DS** Equation (Eq. (3.2)) with the Feynman propagator  $\Delta$ , performing an integration over space–time and using  $\Delta_y^{-1}\Delta(x, y) = \delta^4(x - y)$ , permits to solve (3.2) for the single field  $\phi$  in (3.3). By replacing each  $\phi$  with functional derivatives with respect to (**wrt**) the corresponding sources  $j$ , the integrand (3.2) can be pulled out and one obtains the *chain rule* for the functional derivative of this theory as

$$\frac{\delta}{i\delta j(x)} = \int d^4y \Delta(x, y) \left[ j(y) - \frac{\lambda_3}{2!} \left( \frac{\delta}{i\delta j(y)} \right)^2 - \frac{\lambda_4}{3!} \left( \frac{\delta}{i\delta j(y)} \right)^3 - \frac{\lambda_5}{4!} \left( \frac{\delta}{i\delta j(y)} \right)^4 + \dots \right], \quad (3.4)$$

where we left out the  $\langle \dots \rangle$ , keeping in mind that the action of this operator is defined on expectation values. Eq. (3.4) allows to compute general Green's functions by computing multiple derivatives

$$\frac{\delta}{\delta j(x_1)} \cdots \frac{\delta}{\delta j(x_n)}, \quad (3.5)$$

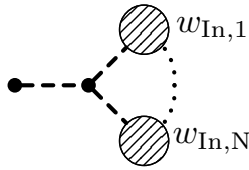
without the need to resort to Feynman diagrams. The perturbative expansion is performed by the recursion of (3.4) up to certain powers of  $\lambda_i$ . For instance, consider the computation of a 4-point function via

$$\frac{\delta}{\delta j(x_1)} \frac{\delta}{\delta j(x_2)} \frac{\delta}{\delta j(x_3)} \frac{\delta}{\delta j(x_4)} = \left( \frac{\delta}{\delta j(x_1)} \frac{\delta}{\delta j(x_2)} \frac{\delta}{\delta j(x_3)} \right) \frac{\delta}{\delta j(x_4)}, \quad (3.6)$$

where on the right-hand side (**rhs**) one of the derivatives is singled out, predestined for the expansion. Next, we iteratively expand the derivative with Eq. (3.4) to the order of  $\mathcal{O}(\lambda_3^2, \lambda_4^1)$

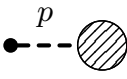


to the construction of the current on the left-hand side, referred to as outgoing current. The contribution to the outgoing current generated in each term of equation (3.10), can be formally seen as the result of the action of the **BGR** operator defined by:

$$\text{BGR}(w_{\text{In},1}, \dots, w_{\text{In},N}) := \text{Diagram} \Rightarrow w_{\text{Out}} = \sum_{(3.10)} \text{BGR}(w_{\text{In},1}, \dots, w_{\text{In},N}), \quad (3.11)$$


with  $N$  being the number of incoming currents and the sum running over all contributions on the rhs of (3.10). The explicit form of the **BGR** operator depends on the underlying theory and is discussed in Section 3.4.

In the process-generation phase RECOLA2 derives the graphs of processes based on the recursion (3.10), which we call the tree skeletons. This is done by iteratively inserting the right-hand side of (3.10) into itself, resulting in all possible graphs differing from one another by different independent momentum combinations, as indicated in (3.8). The recursion stops for a desired final state which respects four-momentum conservation. The skeleton construction is implemented in a model-independent way, treating all currents on equal footing, i.e. independent of their particle nature.<sup>2</sup> Finally,  $S$ -matrix elements at tree-level are computed by taking the last current in the recursion and putting it on-shell via

$$i\mathcal{M}_0 = \lim_{p^2 \rightarrow m^2} \text{Diagram} ( \text{Diagram} )^{-1}, \quad (3.12)$$


with  $m$  being the mass of the external field. With this we conclude the computation of the **BGR** at tree level. In the next section we discuss the implementation details of the skeleton construction which is the basis for the computation of **BGR** in general theories at tree level and one-loop order.

## 3.2 Tree skeletons for general theories

The iterative recursion of (3.10) results in all possible graphs which respect momentum conservation, the so-called skeletons. A systematic approach to their generation is possible in the binary representation of momenta [70] which is defined as follows. For a given process of  $n$  external particles we assign each particle  $i$  ( $i = 1, \dots, n$ ) a momentum  $p_{k_i}$ , with the momentum integer  $k_i := 2^{i-1}$ . The set of independent external momentum integers is denoted by  $P_{\text{ext}} = \{k_i | i \in [1, \dots, n-1]\}$ , and restricted to, in total,  $n-1$  independent momenta due to momentum conservation. Defining the momentum flow for all momenta as incoming, except for the last one, momentum conservation reads

$$\sum_{k \in P_{\text{ext}}} p_k = p_{k_n}. \quad (3.13)$$

<sup>2</sup>We use model file information to omit contributions which are zero due to conservation laws or because of vanishing couplings.



In order to define linear combinations in the binary representation, we consider a set  $A$  of distinct momentum integers  $k$  with  $k \in A$ . The sum of momenta in  $A$  is denoted as  $P_A$ . The binary representation of  $P_A$ , denoted as  $B_{P_A}$ , is defined as the sum of the corresponding momentum integers as follows

$$P_A := \sum_{k \in A} p_k \quad \Rightarrow \quad B_{P_A} = \sum_{k \in A} k. \quad (3.14)$$

For example, the binary representation of the sum of the first and third particle momentum is given by

$$p_{k_1} + p_{k_3} \Rightarrow k_1 + k_3 = 1 + 4 = 5 = B_{p_{k_1} + p_{k_3}}. \quad (3.15)$$

The requirement for distinct momentum combinations in this basis is realized by requiring that the sum of two momenta is forbidden if their binary representations have a non-zero bitwise overlap. For instance, the sum of the numbers 21 and 12 is forbidden because  $21 \wedge 12 = 4 \neq 0$ , with  $\wedge$  being the bitwise AND operation. The number 4 stands for the momentum  $p_{k_3}$ , which is included in both 21 and 12. This can be seen by mapping back from binary representation to momentum sums

$$\begin{aligned} 21 &= 1 + \underline{4} + 16 \Leftrightarrow p_{21} = p_{k_1} + \underline{p_{k_3}} + p_{k_5}, \\ 12 &= \underline{4} + 8 \quad \Leftrightarrow p_{12} = \underline{p_{k_3}} + p_{k_4}. \end{aligned} \quad (3.16)$$

Momentum conservation (3.13) implies that  $B_{P_{\text{ext}}}$  needs to be identified with  $B_{p_n}$

$$B_{p_n} \sim B_{P_{\text{ext}}} \quad \Leftrightarrow \quad 2^{n-1} \sim \sum_{i=1}^{n-1} 2^{i-1} = 2^{n-1} - 1. \quad (3.17)$$

The number  $B_{P_{\text{ext}}} = 2^{n-1} - 1$  is an integer number with all bits set to one up to the bit position  $n - 1$ . This number plays the role of the recursion stop in the **BGR**, signalling that no further independent momentum combinations exist. Finally, we can define the set of *all* distinct momentum combinations in the binary representation

$$\text{INV}(n) = \{k | 1 \leq k < B_{p_n}\}. \quad (3.18)$$

The proof follows directly from the fact that each integer in  $\text{INV}(n)$  has a unique decomposition in bits and since every number is distinct we have all possible combinations. The distinct momenta can be classified by their number of bits in the binary representation. For instance, the set of external momenta is a subset of  $\text{INV}(n)$  with exactly one bit set

$$P_{\text{ext}} = \{k | k \in \text{INV}(n), \text{bits}(k) = 1\}. \quad (3.19)$$

Current	Momentum	Binary
$w(1) := 1$	$p_{k_1}$	000 <b>1</b>
$w(2) := 1$	$p_{k_2}$	00 <b>1</b> 0
$w(4) := 1$	$p_{k_3}$	0 <b>1</b> 00
$w(3) = (w(2), w(1))$	$p_{k_1} + p_{k_2}$	00 <b>11</b>
$w(5) = (w(4), w(1))$	$p_{k_1} + p_{k_3}$	0 <b>1</b> 0 <b>1</b>
$w(6) = (w(4), w(2))$	$p_{k_2} + p_{k_3}$	0 <b>11</b> 0
$w(7) = (w(6), w(1)) + (w(5), w(2)) + (w(4), w(3))$ $+ (w(4), w(2), w(1))$	$p_{k_1} + p_{k_2} + p_{k_3}$	0 <b>111</b> = <b>1</b> 000

Table 3.1: Recursive computation of a 4-particle process using BGR ordered in increasing number of bits. The external currents are set to one, treating them as scalars. Note that the computation order in RECOLA2 is slightly different.

External momenta can be identified in various ways, for instance, the following conditions are equivalent

$$\text{bits}(k) = 1 \quad \Leftrightarrow \quad \exists i \Rightarrow k = 2^i \quad \Leftrightarrow \quad k \wedge (k - 1) = 0, \quad (3.20)$$

with the last version being used in RECOLA2 to test whether a momentum is external.<sup>3</sup> In general, counting the number of bits is more involved. For not too large numbers<sup>4</sup> the most efficient method are lookup tables, which is used in RECOLA2.

The numbers in  $\text{INV}(n)$  represent all possible off-shell currents which need to be computed in a process with  $n$  particles. In order to account for dependencies among off-shell currents their computation needs to be performed in the ascending order defined by their momentum integers starting from the smallest number one. In each step, the evaluation of the BGR consists in the construction of all contributions on the rhs of (3.10). For an off-shell current with momentum integer  $i$  the contributions are identified as the *ordered and distinct integer partitions* of  $i$  with *no bitwise overlap among partition elements*. In the following we exemplify the construction and computation of the rhs of the (3.10) for the 4-particle process (3.8) (see overview Table 3.1), making use of the BGR operator defined in (3.11) and abbreviated as

$$\text{BGR}(\dots) = (\dots). \quad (3.21)$$

We have  $B_{P_{\text{ext}}} = 7$  and thus  $\text{INV}(n) = \{1, 2, 3, 4, 5, 6, 7\}$ . RECOLA2 proceeds as follows:

(1,2): The first two numbers 1 and 2 represent external fields due to (3.20). Their corresponding currents  $w(1)$  and  $w(2)$  are identified with polarization vectors.

(3): The number 3 decomposes into  $2 + 1$ . Thus, the corresponding current is given by

$$- w(3) = (w(2), w(1)).$$

(4): The current associated to 4 is identified with a polarization vector due to (3.20).

<sup>3</sup>Since for  $p \in P_{\text{ext}}$  only one bit is set in  $B_p$ , subtracting the number 1 from  $B_p$  results in a binary number where all bits are set to one up to the position of the original bit. Thus,  $B_p$  and  $B_p - 1$  have no bitwise overlap.

<sup>4</sup>We typically consider processes with less than 12 external particles. The number  $2^{12}$  is not large in that respect.

(5,6): These numbers decompose as  $5 = 4+1$  and  $6 = 4+2$ . Therefore, the currents are computed via

$$\begin{aligned} - w(5) &= (w(4), w(1)), \\ - w(6) &= (w(4), w(2)). \end{aligned}$$

(7): The number 7 decomposes into multiple valid partitions, namely  $6 + 1$ ,  $5 + 2$ ,  $4 + 3$  and  $4 + 2 + 1$ . Thus, we obtain

$$- w(7) = (w(6), w(1)) + (w(5), w(2)) + (w(3), w(4)) + (w(4), w(2), w(1)).$$

The steps 1, 2 and 4 are initial conditions and depend on the choice of external particles and their polarization. The steps 3, 5 and 6 correspond to the computation of the subamplitudes. In the final step 7 four different currents are computed. Performing the recursion and inserting the expressions in one another results in a sum of contributions which can be identified with the sum of Feynman diagrams in (3.8).

In this last part we discuss the generalization for generic theories. The key ingredient for the skeleton construction is the (efficient) generation of integer partitions. More precisely, we are interested in partitions of the integer  $i$  with the following properties:

I True partition:  $i = i_1 + i_2 + \dots + i_n$

II Ordering:  $i_k > i_{k+1} \quad \forall k$

III No bitwise overlap :  $i_k \wedge i_l = 0 \quad \text{for} \quad \forall k, l \quad \text{with} \quad k \neq l.$

IV Max  $n$ -point:  $n < N$

Certainly, the partitions can be computed iteratively by a simple brute force approach starting from the hypercubus

$$(i_1, i_2, \dots, i_n) \in D_i^n := \underbrace{[1, \dots, i-1] \times \dots \times [1, \dots, i-1]}_n, \quad (3.22)$$

and deriving the subset of vectors in  $D_i^n$  which fulfil the conditions I-IV. However, the efficiency of the partition generation has a significant impact on the speed of the dynamic process generation. In particular for higher  $n$  point vertices naive brute force approaches or precomputed linked lists of the partitions are slow, and an efficient algorithm is desirable. In Algorithm 1 we sketch our recursive algorithm for arbitrary partition size  $n$  as used in RECOLA2.<sup>5</sup> Note that even though the algorithm is general, in RECOLA2 only up to 8-point interactions are supported due to internal optimizations. The procedure expects five arguments, but only  $i$  and  $n$  are chosen freely. The argument  $i$  is an integer which is subject to being decomposed into integer partitions of size  $n$ . The arguments  $\{i_q\}$ ,  $k$  and  $u$  are auxiliary variables which are set automatically in the recursion. The argument  $\{i_q\}$  represents an integer array of size  $k-1$  filled recursively and fulfilling condition II-IV in every intermediate step. The integer  $k$  represents the level of recursion. Each level  $k$  deals with the construction of the  $k$ -th element  $i_k$ . The argument  $u$  is

<sup>5</sup>For better readability we left out details on the implementation of condition IV in Algorithm 1.

**Algorithm 1** Recursive Binary Partitioning

---

```

1: procedure PARTITION( $i, n, \{i_q\}, u, k$ )
2:   for  $i_k = u, 1, -1$  do
3:     if  $\{i_k \wedge i_q \neq 0 \ \forall q, q < k\}$  then ▷ Condition III
4:       continue 2
5:     end if
6:     if  $n == k + 1$  then
7:        $i_{k+1} = i - \sum_{q < k+1} i_q$  ▷ Condition I
8:       if  $\{i_{k+1} > i_k\}$  or  $\{i_{k+1} \wedge i_q \neq 0 \ \forall q, q < k + 1\}$  then ▷ Condition II,III
9:         continue 2
10:      end if
11:      yield  $(i_1, \dots, i_k)$  ▷ Valid partition
12:    else
13:      PARTITION( $i, n, \{i_q\}, \text{Min}[i_k - 1, i - \sum_{q < k} i_q - 1], k + 1$ )
14:    end if
15:  end for
16: end procedure

```

---

the highest possible value for  $i_k$  compatible with the conditions I-IV. The recursion is properly initiated with  $\{i_q\} = \{\}$ ,  $k = 1$ ,  $u = i - 1$ , and  $i, n$  chosen freely. In line 2 the algorithm performs a loop over possibly allowed values for  $i_k$  in descending order which is natural due to condition II and the increase in  $k$  with each additional level of recursion. A test for bitwise overlap is performed in line 3 to make sure that the value is not in conflict with previous elements in  $\{i_q\}$ . In line 6 the algorithm verifies if a partition of size  $n$  can be finalized which requires precisely  $n = k + 1$  recursion steps. If this condition is not yet satisfied a recursion step  $k$  to  $k + 1$  is performed in line 13. In each recursion step an appropriate highest value  $u$  for the next element in the partition is computed based on previous elements in the partition. Finally, in line 7 the condition I is used to construct the last element  $i_n$ , and in line 8 it is verified that the last element respects the conditions II and III. Anything passing line 8 represents a valid partition of  $i$  of size  $n$ . With this we conclude the generation of tree skeletons for processes with arbitrary  $n$ -point interactions, which represent the basis for the dynamic generation of tree- and one-loop amplitudes in RECOLA2.

### 3.3 Extension to one-loop level

The extension of the BGR to one-loop amplitudes in RECOLA2 follows the implementation in RECOLA in Refs. [19, 20] which has been inspired by the algorithm in Ref. [17], originally proposed for one-loop QCD amplitudes. In contrast to the evaluation of tree-level  $S$ -matrix elements (3.12), one-loop amplitudes cannot be computed directly by the same recursion techniques due to the presence of tensor integrals. In general, a one-loop amplitude  $\mathcal{M}_1$  can be cast into the form

$$i\mathcal{M}_1 = \sum_k c_{k, \mu_1 \mu_2 \dots} T_k^{\mu_1 \mu_2 \dots}, \quad (3.23)$$





Using (3.10) and (3.28) the BGR operator is given by

$$\begin{aligned}
 w_1^{\mu_1}(p_1) &= \text{Diagram} = \frac{-ig_{\mu}^{\mu_1}}{p_1^2 - m_1^2} L_{\mu_2}^{\mu}(p_1, p_2) w_2^{\mu_2}(p_2) w_3(p_3) \\
 &= (w_2^{\mu_1}(p_2) (C_1 + C_2 p_1 \cdot p_2) + p_1^{\mu_1} C_3 p_2 \cdot w_2(p_2) + p_2^{\mu_1} C_4 p_1 \cdot w_2(p_2)) w_3(p_3) \frac{-i}{p_1^2 - m_1^2}, \quad (3.29)
 \end{aligned}$$

where we assumed the 't Hooft–Feynman gauge for simplicity. For an efficient evaluation on modern CPUs it is essential to write expressions like (3.29) in vectorized form, which is done in REPT1L by default whenever possible. In addition, REPT1L supports identifying similar structures and subsequent replacement by smaller expressions, which is known as Common Subexpression Elimination (CSE). This feature is essential in one-loop computations for preventing unnecessary repetitive computation as will be demonstrated below.

The computation of the loop BGR (3.27) is more involved as different powers of loop momenta need to be isolated. Note that the loop line is not fixed a priori, and, in general, we have to consider all possible loop lines attached to the outgoing current. In this example we only consider the loop line flow from  $V_2$  to  $V_1$ . Then, the vertex structure corresponding to (3.28) is given by

$$\begin{aligned}
 L^{\mu_1 \mu_2}(p_1 + q, p_2 + q) &= C_1 g^{\mu_1 \mu_2} + C_2 (p_1 + q) \cdot (p_2 + q) g^{\mu_1 \mu_2} \\
 &\quad + C_3 (p_1 + q)^{\mu_1} (p_2 + q)^{\mu_2} + C_4 (p_1 + q)^{\mu_2} (p_2 + q)^{\mu_1} \quad (3.30)
 \end{aligned}$$

with  $q$  being the loop momentum. Note that the shift in the momenta is consistent with momentum conservation. The off-shell current is derived using (3.27), which yields

$$\begin{aligned}
 c_1^{\mu_1}(p_1, q) &= \text{Diagram} = -ig_{\mu}^{\mu_1} L_{\mu_2}^{\mu}(p_1 + q, p_2 + q) c_2^{\mu_2}(p_2, q) w_3(p_3), \quad (3.31)
 \end{aligned}$$

where, again, we assumed the 't Hooft–Feynman gauge for simplicity. Note that the propagator denominator is included in the tensor integrals, and thus left out in (3.31). First, we discuss the case  $C_1 \neq 0$ , and  $C_2 = C_3 = C_4 = 0$ , which corresponds to a vertex in a renormalizable theory. For renormalizable theories in the 't Hooft–Feynman gauge the rank<sup>6</sup> can be increased only by one in the BGR (3.27). The outgoing tensor coefficient  $c_1$  is proportional to the incoming one  $c_2$  according to

$$c_1^{\mu_1}(q, p_1) = -ic_2^{\mu_1}(q, p_2) C_1 w_3(p_3). \quad (3.32)$$

To make this more explicit, we decompose tensor coefficients according to different ranks as

<sup>6</sup>The rank corresponds to the power of loop-momenta  $q$ . The precise definition for the rank of a tensor integral is given in App. A.1

follows

$$c_i^\mu(q, p) = c_{i,0}^\mu(p) + q_\nu c_{i,1}^{\mu,\nu}(p) + q_\nu q_\rho c_{i,2}^{\mu,\nu\rho}(p) + \dots \quad (3.33)$$

The index  $\mu$  is intentionally separated from the other indices  $\nu, \rho, \dots$  as it is related to the particle nature of  $V_1$ , and not (necessarily) to the rank. Performing the rank classification (3.33) on both sides of Eq. (3.32) we obtain

$$\begin{aligned} c_{1,0}^\mu(p_1) &= -i c_{2,0}^\mu(p_2) C_1 w_3(p_3), \\ c_{1,1}^{\mu,\nu}(p_1) &= -i c_{2,1}^{\mu,\nu}(p_2) C_1 w_3(p_3), \\ c_{1,2}^{\mu,\nu\rho}(p_1) &= -i c_{2,2}^{\mu,\nu\rho}(p_2) C_1 w_3(p_3), \\ &\dots \end{aligned} \quad (3.34)$$

Therefore, the proportionality (3.32) holds on the level of components of tensor coefficients. For  $C_2 \neq 0$  the outgoing tensor coefficient  $c_1$  is no longer proportional to  $c_2$  and needs to be reordered according to the rank. The solution for  $c_1$  changes in the following way

$$\begin{aligned} c_{1,0}^\mu(p_1) &= -i \left[ c_{2,0}^\mu(p_2) (C_1 + C_2 p_1 \cdot p_2) \right] w_3(p_3), \\ c_{1,1}^{\mu,\nu}(p_1) &= -i \left[ c_{2,1}^{\mu,\nu}(p_2) (C_1 + C_2 p_1 \cdot p_2) + c_{2,0}^\mu(p_2) C_2 (p_1 + p_2)^\nu \right] w_3(p_3), \\ c_{1,2}^{\mu,\nu\rho}(p_1) &= -i \left[ c_{2,2}^{\mu,\nu\rho}(p_2) (C_1 + C_2 p_1 \cdot p_2) + c_{2,1}^{\mu,\nu}(p_2) C_2 (p_1 + p_2)^\rho + c_{2,0}^\mu(p_2) C_2 g^{\nu\rho} \right] w_3(p_3), \\ &\dots \end{aligned} \quad (3.35)$$

The computation of these rules and the classification according to the rank has been automated in REPT1L. In fact, a large part of REPT1L is devoted to the computation of tree and one-loop BGR relations and exporting the results to FORTRAN95. One could argue, that not too many different operators are required, at least for renormalizable theories, which could have been hard-coded, as it is done in RECOLA. However, in view of different conventions, different gauges and non-renormalizable theories, we decided for a flexible system which is essential for a full automation. Our implementation is kept fully general concerning the Feynman rules, i.e. it is possible to derive the BGR in the form of (3.35) starting from any Feynman rule, with the result (optionally) exported to FORTRAN95. For instance, for the one-loop BGR (3.31) REPT1L calls<sup>7</sup>

$$\text{write\_loop\_current}(C_1 g^{\mu_1 \mu_2} + C_2 p_1 \cdot p_2 g^{\mu_1 \mu_2}), \quad (3.36)$$

with the argument being the (tree-level) vertex structure (3.28) with two generic couplings  $C_1$  and  $C_2$ . In this case the open index  $\mu_1$  is considered as the outgoing one, which also defines the propagator type, whereas all other open indices are considered as incoming ones. The loop momentum shift is performed automatically assuming the loop line going from  $V_2$  to  $V_1$ . The

<sup>7</sup>The argument form has been slightly altered. In REPT1L all structures have to be given in the UFO syntax as strings.



---

**Algorithm 2** BGR of (3.31) for tensor coefficients as computed by REPT1L.

---

```

1: procedure BGR_VVS( $c_1, c_2, w_3, C_1, C_2, r_i^{\max}, r^{\max}$ )
2:   ! Metric(1,2)*C1
3:   ! Metric(1,2)*P(-1,1)*P(-1,2)*C2
4:   for  $ri = r_i^{\max}, 0, -1$  do
5:      $x_0(:) = -iC_2 w_3 c_2(:, ri)$ 
6:      $c_1(:, ri) = p_1 \cdot p_2 x_0(:) - iC_1 w_3 c_2(:, ri)$ 
7:     if  $r^{\max} < 1$  continue
8:     for  $\mu = 0, 3$  do
9:        $ri_{\text{out}} = \text{Inc}(\mu, ri)$ 
10:       $c_1(:, ri_{\text{out}})+ = x_0(:) (p_1(\mu) + p_2(\mu))$ 
11:      if  $r^{\max} < 2$  continue
12:       $ri_{\text{out}} = \text{Inc}(\mu, \text{Inc}(\mu, ri))$ 
13:       $c_1(:, ri_{\text{out}})+ = g^{\mu\mu} x_0(:)$ 
14:    end for
15:  end for
16: end procedure

```

---

result of this call is the FORTRAN95 subroutine given in Algorithm 2. The generated code has been translated to pseudo code and adapted to the conventions used here. The structure has not been modified and is kept as generated by REPT1L. In order to make the transition from (3.35) to the algorithm, a few ingredients need to be explained:

$ri$ :  $ri$  is a multi index grouping symmetrized Lorentz indices and the rank of tensors. For instance, the first  $ri$  can be identified with the components of the usual tensor integrals as follows

rank	$T^{\mu\nu\rho\dots}$	ri
0	$T$	0
1	$T^0, T^1, T^2, T^3$	(1, 2, 3, 4)
2	$T^{00}, T^{01}, T^{02}, T^{03}, T^{11}, T^{12}, T^{13}, T^{22}, T^{23}, T^{33}$	(5, ..., 15)

$\text{Inc}(\mu, ri)$ : The mapping  $\text{Inc}(\mu, ri)$  combines a symmetrized index  $ri$  with the Lorentz index  $\mu$  and creates a new combined symmetrized index. The mapping is used to increase the rank of symmetrized tensors as follows

$$T^{ri'} = g^{\mu\mu} T^{ri}, \quad \text{with } ri' = \text{Inc}(\mu, ri). \quad (3.37)$$

$c_i(\mu, ri)$ : Tensor coefficients carry an explicit dependence on the combined symmetrized index  $ri$ . The index  $\mu$  refers to the field nature. In this example for both  $c_1, c_2$  the associated index  $\mu$  is a Lorentz index since the loop line connects  $V_1$  and  $V_2$  which are vector-bosons.

$r^{\max}$ :  $r^{\max}$  is the highest rank increase for the BGR. The rank increase may occasionally decrease when couplings are zero. In our example this is the case for  $C_2 = 0$  and the rank increase drops from  $r^{\max} = 2$  to  $r^{\max} = 0$ .

$ri^{\max}$ :  $ri^{\max}$  is the highest value for the combined symmetrized index of the incoming tensor coefficient  $c_2$ .

$x_0^\mu$ : REPT1L introduces auxiliary variables when applying the CSE. These variables can be scalar-, vector- or even tensor-valued and may depend on the combined symmetrized index  $ri$ .

The algorithm starts with a loop in line 4 running over all incoming symmetrized indices. First consider the case  $C_2 = 0$  with no rank increase. The only calculation occurs in line 6 (colour code blue) and corresponds to (3.34) handling all cases at once. For  $C_2 \neq 0$  the algorithm is allowed to continue on line 7, entering a Lorentz index loop. A new combined symmetrized index  $ri_{\text{out}}$  is computed in line 9, and in line 10 the rank is increased by one corresponding to the terms proportional to  $c_{2,0}^\mu$  in the second and to  $c_{2,1}^{\mu,\nu}$  in the third line in (3.35) (colour code red). Finally, the rank increase by two, corresponding to the term proportional to  $c_{2,0}^\mu$  in the third line in (3.35) (colour code green), is computed in the lines 12 and 13, but without an additional Lorentz index sum. This is possible because the rank is increased by the symmetric product  $q^2 = q^\mu q_\mu$  and can be handled within the same  $\mu$  loop. For  $C_3 \neq 0$ ,  $C_4 \neq 0$  this is no longer the case and one has to extend the procedure by an additional loop over a free Lorentz index, say  $\nu$ . In this situation REPT1L can optimize the loop by symmetrization of the current which allows to restrict the additional loop to the domain  $\nu < \mu$ .

With this we conclude the discussion of the generalization of the BGR to general theories. Further aspects related to the model-file generation and renormalization are discussed in Chapter 5.

# Calculational framework for one-loop corrections

Canonically formulated QFT is known to suffer from divergences in loop amplitudes which are cured by a reinterpretation via the renormalization procedure. In this formulation [71] every theory is considered as an effective one, being valid up to a certain energy scale. In practice, this picture is enforced by cutting theories at a given energy scale, and imposing renormalization group equations (RGE) invariance, which guarantees that the theory's prediction are unaffected by the precise cut-off.<sup>1</sup> Among potential fundamental theories are the so-called renormalizable theories, e.g. in this work the SM, HSESM or THDM, which differ from non-renormalizable ones by the fact that the cut-off can be shifted to infinity, making them, in principle, valid up to arbitrary high energies. Nowadays non-renormalizable theories are not less attractive. On the contrary, a lot of effort has gone into the study of EFTs which allow for a systematic parametrization of deviations wrt e.g. the SM,<sup>2</sup> and being well-defined at higher order<sup>3</sup> as opposed to the usual  $\kappa$  framework.

The cut off procedure, also known as the regularization, can be shown to have no physical meaning, and a favoured scheme can be chosen. Over the years many elegant and mathematically rigorous regularization methods have emerged, but for computational purposes dimensional regularization (DREG) [75] and variants thereof have the distinction of respecting most symmetries while allowing for straightforward analytic computations of loop integrals in QFT. The basics of this regularization method are discussed in Section 4.1. There, we present the analytic computation of rational terms of type  $R_1$  and  $R_2$  and the treatment of  $\gamma_5$  in combination with DREG.

Besides the regularization, theories need to be renormalized permitting to connect parameters of the theory, with a priori no physical meaning, to actually measurable quantities like couplings or masses. In the renormalization procedure one considers a set of relevant Green's functions, imposing conditions which fix their values in given subtraction schemes. For renormalizable theories it is enough to consider a finite set of Green's functions to render all others finite and uniquely fix their values. This fact is exploited in the automated renormalization procedure in Chapter 5 for renormalizable theories. In the following we discuss the renormalization of a standard set of Green's functions consisting of the tadpoles, i.e. the one-point functions, in Section 4.2, and the two-point functions in Section 4.3. In the presence of unstable particles,

<sup>1</sup>A scale dependence remains when theories are truncated to finite order.

<sup>2</sup>For instance, see the EFT program for vector-boson pair production [72, 73] of Higgs related anomalous couplings [74].

<sup>3</sup>See e.g. precision calculations in Higgs EFT at NLO [68, 69].

the renormalization of two-point functions is extended and handled in the **CMS** as described in Section 4.4. Concerning the renormalization of couplings we consider the standard renormalization conditions for gauge and other couplings in Section 4.5. In the theories with extended Higgs sector (see Chapter 2.3) independent mixing-angle parameters make their appearance. Their renormalization requires special attention and will be discussed in the  $\overline{\text{MS}}$  scheme in Section 4.6. Alternative renormalization schemes concerning the mixing angles are presented in Chapter 7.

## 4.1 Regularization and computation of rational terms

As mentioned in the introduction we use **DREG** [75] for the regularization of tensor integrals in the conventions given in App. A.1. In order to preserve symmetries which manifest themselves in form of Slavnov-Taylor Identities (**STI**) as a consequence of Becchi, Rouet, Stora and Tyutin (**BRST**) invariance [76, 77, 78], the space-time algebra needs to be handled appropriately. As long as non-supersymmetric theories are concerned, as it is the case in this work, **DREG** is an appropriate choice. In order to preserve supersymmetry **DREG** can to be replaced by e.g. dimensional reduction (**DRED**) [79].

In **DREG** all fields, momenta, momentum integrals, and  $\gamma$ -matrices are analytically continued to  $D$  dimensions. From a practical point of view this requires to replace the metric with its  $D$  dimensional analogue, which fulfils

$$g_{\mu}^{\mu} = 4 \rightarrow g_{\mu}^{\mu} = D. \quad (4.1)$$

Similar identities result for  $\gamma$ -matrices as e.g.

$$\gamma^{\mu}\gamma_{\mu} = \frac{1}{2} \{\gamma^{\mu}, \gamma_{\mu}\} = g_{\mu}^{\mu} \mathbb{1}_{4 \times 4} = D \mathbb{1}_{4 \times 4}, \quad (4.2)$$

where we used the anticommutation relation for  $\gamma$ -matrices and (4.1).<sup>4</sup> The analytic continuation to  $D$  dimensions gives rise to so-called rational terms, which emerge from products of  $D$ -dimensional objects and divergent terms for  $D \rightarrow 4$ , e.g.

$$\left[ \alpha + (D - 4)\beta + \mathcal{O}\left((D - 4)^2\right) \right] \times \frac{1}{D - 4} = \frac{\alpha}{D - 4} + \beta + \mathcal{O}(D - 4). \quad (4.3)$$

The  $\alpha$  term leads to a divergence when taking the limit  $D \rightarrow 4$  and requires renormalization, whereas  $\beta$  remains finite and is not necessarily subtracted in the renormalization procedure, e.g. in  $\overline{\text{MS}}$  subtraction. The  $\beta$  term defines the notion of a rational term, namely a finite non-zero remnant of products like (4.3). Rational terms are classified according to their origin, as discussed in the following sections.

---

<sup>4</sup>In **DRED** (4.2) is purely 4-dimensional  $\gamma^{\mu}\gamma_{\mu} = 4\mathbb{1}_{4 \times 4} \neq D\mathbb{1}_{4 \times 4}$ .

### 4.1.1 Computation of $R_1$

The rational terms of type  $R_1$  emerge in the tensor-integral reduction as a consequence of a Lorentz-covariant decomposition and the identity (4.1). For instance, the Passarino-Veltman Reduction (PVR) of the 1-point tensor integral of rank 2

$$A^{\mu\nu}(m_0) = g^{\mu\nu} A_{00}(m_0), \quad (4.4)$$

can be contracted with a metric tensor which then relates  $A_{00}$  with the standard scalar integral  $A_0$  (A.4). Using the integral representation (A.4) and (4.1) yields

$$A^\mu{}_\mu(m_0) = m_0^2 A_0(m_0) = D A_{00}. \quad (4.5)$$

Solving for  $A_{00}$  and expanding to 4 dimensions gives

$$\begin{aligned} A_{00}(m_0) &= \frac{m_0^2}{D} A_0(m_0) = \frac{m_0^2}{4} \left( 1 - \frac{D-4}{4} + \mathcal{O}\left((D-4)^2\right) \right) A_0(m_0) \\ &= \frac{m_0^2}{4} \left( A_0(m_0) + \frac{m_0^2}{2} \right) + \mathcal{O}(D-4), \end{aligned} \quad (4.6)$$

where we used

$$\lim_{D \rightarrow 4} (D-4) A_0(m_0) = -2m_0^2. \quad (4.7)$$

Thus, we see an additional term in the reduction which would not be present if we had not used (4.1). We have derived further PVR expressions for 1- and 2-point functions up to rank 6 given in App. A.2. The PVR can be employed in REPT1L when deriving counterterms, but is disabled by default.

### 4.1.2 Computation of $R_2$

The rational terms of type  $R_2$  originate as remnants of products of tensor coefficients and tensor integrals. Consider the one-loop part of a vertex function  $\Gamma_s$  with definite external state  $s$ , expressed in terms of tensor coefficients and tensor integrals as follows

$$\Gamma_s = \sum_{c \in C_s} c_{\mu_1 \dots \mu_p} T^{N_c, \mu_1 \dots \mu_p}, \quad (4.8)$$

with  $N_c$  and  $p$  denoting an  $N_c$ -point integral with rank  $p$ . The set  $C_s$  of tensor coefficients defines the vertex  $\Gamma_s$  and is constructed according to the Feynman rules of the underlying model. The tensor coefficients can be expanded around  $D = 4$  as follows

$$c_{\mu_1 \dots \mu_p} = c_{\mu_1 \dots \mu_p}^0 + (D-4) c_{\mu_1 \dots \mu_p}^1 + \mathcal{O}\left((D-4)^2\right). \quad (4.9)$$

Regarding the  $R_2$  terms only the pole parts of tensor integrals are relevant. Defining the pole part as

$$\text{PP} [T^{N,\mu_1\dots\mu_P}] = \lim_{D \rightarrow 4} (D - 4) T^{N,\mu_1\dots\mu_P}, \quad (4.10)$$

the rational term of type  $R_2$  associated to the vertex  $\Gamma_s$  is given by

$$\Gamma_s^{R_2} = \sum_{c \in C_s} c_{\mu_1\dots\mu_P}^1 \text{PP} [T_c^{N,\mu_1\dots\mu_P}]. \quad (4.11)$$

Again, this kind of rational term arises from products like (4.3). In purely numerical approaches with only  $c^0$  (4.9) being computed, the additional terms (4.11) need to be included in the computation. The actual computation of (4.11) requires two ingredients. The analytic computation of tensor coefficients in  $D$  dimensions is done with RECOLA2 for generic models and arbitrary vertex functions which is described in Chapter 5. The computation of pole parts follows the standard methods in Ref. [80]. Fortunately, the results need to be derived only once in analytic form as they are model independent. To this end, one can start from a generic Lorentz-covariant decomposition Ref. [80]

$$T^{N,\mu_1\dots\mu_P} = \sum_{n=0}^{\lfloor P/2 \rfloor} \sum_{i_{2n+1}, \dots, i_P=1}^{N-1} \underbrace{\{g \dots g p \dots p\}}_{2n}^{\mu_1 \dots \mu_P} T_{i_{2n+1} \dots i_P}^{0 \dots 0}_{2n}, \quad (4.12)$$

The term  $\lfloor P/2 \rfloor$  is the rounded integer number smaller or equal to  $P/2$ . The index  $i$  labels different momentum indices. For  $N$  point functions there are  $N - 1$  independent momentum combinations. The curly bracket denotes the symmetrization `wrt` to Lorentz indices only. With (4.12) the computation of pole parts is a matter of computing pole parts of scalar integrals. Finally, one can make use of the Feynman parameter representation to extract the pole part. In fact, a closed algebraic expression has been derived for the generic scalar integrals  $T_{0 \dots 0 i_{2n+1} \dots i_P}$  in Ref. [81].

### 4.1.3 Treatment of $\gamma_5$

Chiral theories face the problem of a consistent treatment of  $\gamma_5$  in  $D$  dimensions, which is non-trivial since the standard Dirac algebra is incompatible with arbitrary dimensions. Yet, there are solutions to describe anomalies in theories within DREG correctly, and we refer to a summary of popular methods collected in Ref. [82]. As our focus is on anomaly-free theories, we use the naive Dirac algebra in 4 dimensions with an anti-commuting  $\gamma_5$  matrix. Note that potential anomalies can only appear in the  $R_2$  terms, and REPT1L explicitly checks that the anomaly terms drop out. This naive treatment has to be done with care and requires an additional ad-hoc prescription, which dictates that each closed fermion loop has to start from the very same Lorentz index, e.g. by selecting a specific vector boson as the starting point. Since this prescription is based on the Feynman-diagram representation it cannot be used in RECOLA. Instead, the cyclic property of the Dirac trace is used on the final result to bring all closed fermion loops in a specific order compatible with the ad-hoc prescription, before applying any further algebraic identities. To

see how the anomaly terms cancel, consider the vertex  $\Gamma_{\gamma_1\gamma_2 Z}$  with two photons  $\gamma_1, \gamma_2$  and a  $Z$  boson. REPT1L obtains for the rational term  $R_2$

$$\Gamma_{\gamma_1\gamma_2 Z}^{R_2} = -\frac{ie^3(N_c - 3)}{24\pi^2 c_w s_w} (p_{\gamma_1} - p_{\gamma_2})^\nu \epsilon_\nu^{\mu\gamma_1\mu\gamma_2\mu Z}, \quad (4.13)$$

which is zero for  $N_c = 3$ , i.e. for three quark families, thus, consistent with the SM being anomaly free.

## 4.2 Tadpole counterterm schemes

This section deals with various aspects of tadpoles and tadpole renormalization schemes encountered in the literature. The arguments are all given in the perspective that we have developed in Ref. [51]. This work is essential for a consistent renormalization in general weakly interacting theories, in particular, when working with  $\overline{\text{MS}}$  renormalization schemes, discussed in Section 4.6. The *FJ Tadpole Scheme* clarifies common misunderstandings concerning the gauge (in-)dependence of counterterm parameters and the  $S$ -matrix and helps to understand the origin of large contributions in the presence of mixing angles as discussed in Section 7.4.

In Section 4.2.1 we give an introduction to the *FJ Tadpole Scheme*, a consistent tadpole counterterm scheme for arbitrary theories. The scheme is applied to the SM in Section 4.2.2, followed by a discussion on gauge dependence related to tadpoles. The corresponding results for the HSESM and THDM are given in App. B. The importance of the *FJ Tadpole Scheme* in combination with physical renormalization schemes is discussed in Section 4.2.3, where we point out misunderstandings in the literature related to tadpoles and their renormalization. Several arguments concerning the gauge dependence are reinforced by explicit calculations presented in App. C.1 and App. C.2, and are referred to whenever suited. Finally, we discuss the automation of the *FJ Tadpole Scheme* on the level of Feynman rules in Section 4.2.4.

### 4.2.1 The FJ Tadpole Scheme for a general Higgs sector

Among all tadpole counterterm schemes the *FJ Tadpole Scheme* is the most complicated one in terms of numbers of contributions which may be the reason why it has been ignored so far in BSM theories. The original idea in Ref. [83] has been presented for the SM. The generalization to BSM theories is straightforward and is given in the following, focussing on the renormalization of tadpoles in two-point functions. We stress that any of these results concerning the tadpoles directly translate to  $n$ -point (vertex) functions.

We start with the bare Higgs Lagrangian given in terms of bare fields  $\Phi_{i,B}$  and the theory-defining bare parameters  $c_{j,B}$ , being defined in the unbroken phase and being by definition gauge independent, as follows

$$\mathcal{L}_{H,B}(\Phi_{1,B}, \dots, \Phi_{l,B}; c_{1,B}, \dots, c_{k,B}; \dots), \quad (4.14)$$

with  $i = 1, \dots, l$  and  $j = 1, \dots, k$ . After spontaneous symmetry breaking, the neutral scalar components  $\varphi_{i,B}$  of the Higgs multiplets obtain vevs  $v_{i,B} + \Delta v_i$ , and the Lagrangian can be

written as

$$\mathcal{L}_{\text{H,B}}(\varphi_{1,\text{B}} + v_{1,\text{B}} + \Delta v_1, \dots, \varphi_{l,\text{B}} + v_{l,\text{B}} + \Delta v_l; \dots; c_{1,\text{B}}, \dots, c_{k,\text{B}}; \dots), \quad (4.15)$$

where the shifts of the **vevs**  $\Delta v_i$  are introduced for later convenience. The  $v_{i,\text{B}}$  are chosen in such a way that the **vevs** of the shifted fields  $\varphi_{i,\text{B}}$

$$\langle \varphi_{i,\text{B}} \rangle = 0 + t_i(\Delta v_1, \dots, \Delta v_l) + \text{higher-order corrections}, \quad (4.16)$$

vanish at tree level, where  $\Delta v = 0$ . Here,  $\Delta v = 0$  is the short notation for  $\Delta v_1 = 0, \dots, \Delta v_l = 0$ . Note that the  $\Delta v_i$  are introduced as shifts to **vevs** for reasons of sticking to the original formulation. It is, however, safer to think of  $\Delta v_i$  as shifts of the bare fields  $\varphi_{i,\text{B}}$ , because, from a technical point of view, shifting the **vevs** has to be done prior to solving (4.16), but a field redefinition can be done after any manipulation of the Lagrangian. Since the  $v_{i,\text{B}}$  are thus defined to minimize the bare scalar potential, they are directly given in terms of the bare (theory-defining) parameters of the Lagrangian [see (4.42) for the SM].

The tadpole counterterms are defined as the  $\Delta v_i$ -dependent terms in the Lagrangian, where at  $L$ -loop order terms up to the power  $(\Delta v_i)^L$  need to be kept. All tadpole counterterms in the theory are contained in the Lagrangian  $\Delta \mathcal{L}$  in the *FJ Tadpole Scheme*, which is defined as

$$\Delta \mathcal{L} := \mathcal{L} - \mathcal{L}|_{\Delta v=0}. \quad (4.17)$$

The tadpole counterterm  $t_i$  is obtained by taking the derivative of  $\Delta \mathcal{L}$  with respect to the field  $\varphi_i$ , and setting all fields to zero

$$t_i(\Delta v_1, \dots, \Delta v_l) \equiv \Delta \mathcal{L}_i(\Delta v_1, \dots, \Delta v_l; \dots) \quad \text{with} \quad \Delta \mathcal{L}_i := \left. \frac{\partial \Delta \mathcal{L}}{\partial \varphi_i} \right|_{\varphi=0}, \quad (4.18)$$

where the field  $\varphi_i$  can be any scalar in the theory. The tadpole counterterms to two-point functions are given by derivatives of (4.17) with respect to  $\varphi_i$  and  $\varphi_j$ , i.e.

$$t_{ij}(\Delta v_1, \dots, \Delta v_l) \equiv \Delta \mathcal{L}_{ij}(\Delta v_1, \dots, \Delta v_l; \dots) \quad \text{with} \quad \Delta \mathcal{L}_{ij} := \left. \frac{\partial^2 \Delta \mathcal{L}}{\partial \varphi_i \partial \varphi_j} \right|_{\varphi=0}, \quad (4.19)$$

where the fields  $\varphi_i$  and  $\varphi_j$  can be scalars, vector bosons or fermions. Analogously, the tadpole counterterms to the interactions of three fields is obtained via

$$t_{ijk}(\Delta v_1, \dots, \Delta v_l) \equiv \Delta \mathcal{L}_{ijk}(\Delta v_1, \dots, \Delta v_l; \dots) \quad \text{with} \quad \Delta \mathcal{L}_{ijk} := \left. \frac{\partial^3 \Delta \mathcal{L}}{\partial \varphi_i \partial \varphi_j \partial \varphi_k} \right|_{\varphi=0}, \quad (4.20)$$

where the fields  $\varphi_i$ ,  $\varphi_j$  and  $\varphi_k$  can only be scalars or vector bosons in renormalizable quantum field theories. Tadpole counterterms to scalars arise from the Higgs potential, while the tadpole counterterms involving vector bosons and fermions originate from the kinetic terms and the Yukawa terms, respectively, of the Lagrangian of the theory.

Moving towards the tadpole renormalization, the one-particle irreducible (1PI) tadpole loop



corrections are generically denoted as  $T_i$ , which should not be confused with the tadpole counterterms  $t_i$ . The **1PI** tadpole loop corrections are graphically given by

$$T_i = 0 + \underbrace{\text{---}\overset{\textcircled{1}}{\bullet}\text{---}}_{T_i^{(1)}} \varphi_i + \underbrace{\text{---}\overset{\textcircled{2}}{\bullet}\text{---}}_{T_i^{(2)}} \varphi_i + \dots =: \text{---}\overset{\text{hatched}}{\bullet}\text{---} \varphi_i, \quad (4.21)$$

with the contributions at tree level (0), one loop ( $T_i^{(1)}$ ), two loops ( $T_i^{(2)}$ ), and the hatched graph denoting the sum of all **1PI** tadpole graphs.<sup>5</sup> Choosing the shifts of the vevs as  $\Delta v = 0$  implies that all tadpole counterterms  $t_i$  vanish ( $\Delta\mathcal{L} = 0$ ), and  $\langle\varphi_{i,B}\rangle = 0$  holds at tree level. At the one-loop order, the bare fields receive a non-vanishing vev due to the tadpole loop corrections in (4.21).

With this we move on to the renormalization of tadpoles in full self-energies. The self-energy  $\Sigma_{ii}(q^2)$  of a field  $i$  is defined as the higher-order (beyond tree-level) contributions to the inverse connected two-point function, and the corresponding **1PI** contributions are denoted by  $\Sigma_{ii}^{\text{1PI}}$ . Renormalized objects are indicated by a hat. The renormalized self-energy at one-loop order can be written in terms of **1PI** graphs as follows

$$\hat{\Sigma}_{ii}^{(1)}(q^2) = \underbrace{\text{---}\overset{\textcircled{1}}{\bullet}\text{---}}_{\hat{\Sigma}_{ii}^{(1),\text{1PI}}} + \underbrace{\text{---}\times\text{---}}_{\hat{T}_{ii}^{(1)}} + \sum_n \left( \text{---}\overset{\textcircled{1}}{\bullet}\varphi_n + \text{---}\overset{\times}{\bullet}\varphi_n \right) \quad (4.22)$$

$$= \text{---}\overset{\textcircled{1R}}{\bullet}\text{---} + \sum_n \text{---}\overset{\textcircled{1R}}{\bullet}\varphi_n, \quad (4.23)$$

where the subscript R indicates renormalized **1PI** graphs. At two-loop order the two-loop contributions are

$$\begin{aligned} \hat{\Sigma}_{ii}^{(2)}(q^2) = & \text{---}\overset{\textcircled{2R}}{\bullet}\text{---} + \text{---}\overset{\textcircled{2R}}{\bullet}\text{---} + \text{---}\overset{\textcircled{1R}}{\bullet}\overset{\textcircled{1R}}{\bullet}\text{---} + \text{---}\overset{\textcircled{1R}}{\bullet}\overset{\textcircled{1R}}{\bullet}\text{---} \\ & + \text{---}\overset{\textcircled{1R}}{\bullet}\overset{\textcircled{1R}}{\bullet}\text{---} + \text{---}\overset{\textcircled{1R}}{\bullet}\overset{\textcircled{1R}}{\bullet}\text{---}, \end{aligned} \quad (4.24)$$

where the summation over tadpoles of different fields is suppressed for simplicity. In the *FJ Tadpole Scheme* the counterterm corresponding to the two-point irreducible part reads

$$\text{---}\times\text{---} = t_{ii}(\Delta v_1, \dots, \Delta v_l) - \delta m_i^2 + (p^2 - m_i^2) \delta Z_i, \quad (4.25)$$

<sup>5</sup>Note that when tadpoles are renormalized order by order, the **1PI** tadpole graphs  $T_i^{(N)}$  contain  $(N-1)$ -loop counterterm contributions cancelling subdivergencies. See (D.135) in App. D for an explicit two-loop example.

with the tadpole counterterm  $t_{ii}$  being defined in (4.19),  $\delta m_i^2$  being the mass counterterm, and  $\delta Z_i$  being the field-renormalization counterterm.

Both,  $t_i$  and  $t_{ii}$  vanish for  $\Delta v = 0$ , therefore, the non-renormalized sum of the tadpole diagrams  $T_{ii}$ , i.e. the third contribution in (4.22), has to be taken into account. To avoid calculating these contributions, one can use the freedom of choosing  $\Delta v \neq 0$  in (4.15) and relate  $\Delta v$  to the loop tadpole corrections. More precisely, the shift  $\Delta v$  is chosen such that the fields  $\varphi$  do not develop a **vev** to any order in perturbation theory, which is equivalent to setting all renormalized tadpole contributions  $\hat{T}_i$  of the theory to zero. The shifts  $\Delta v$  are thus determined by solving the non-linear equations

$$-T_i = t_i(\Delta v_1, \dots, \Delta v_l), \quad (4.26)$$

with  $t_i$  defined in (4.18). This equation is solved order by order in perturbation theory upon using the perturbative expansion of  $\Delta v$ ,

$$\Delta v_i = \Delta v_i^{(1)} + \Delta v_i^{(2)} + \dots, \quad (4.27)$$

and the perturbative expansion of the tadpole contributions (4.21).

As an important consequence of the consistent inclusion of tadpole contributions, as in (4.23) and (4.24), connected Green's functions do not depend on a particular choice of  $\Delta v$ . To proof this, consider the generating functional of Green's functions  $Z[j]$  defined using the Lagrangian (4.15) with  $\Delta v = 0$  and the generating functional  $Z'[j]$  based on (4.15) with an arbitrary  $\Delta v \neq 0$ . Restricting for simplicity to the case with only one Higgs field  $\varphi$ , the two functionals can be related by a field redefinition  $\varphi \rightarrow \varphi - \Delta v$  in  $Z'[j]$  using the invariance of the path integral measure under a constant shift. The corresponding generating functionals of connected Green's functions  $W[j] = \log Z[j]$  and  $W'[j] = \log Z'[j]$  are related by

$$W'[j] = W[j] - i\Delta v \int d^4x j(x). \quad (4.28)$$

Consequently, it follows for the connected Green's functions

$$\left. \frac{\delta^n W'}{i\delta j(x_1) \dots i\delta j(x_n)} \right|_{j=0} = \left. \frac{\delta^n W}{i\delta j(x_1) \dots i\delta j(x_n)} \right|_{j=0}, \quad \text{for } n > 1, \quad (4.29)$$

$$\left. \frac{\delta W'}{i\delta j(x_1)} \right|_{j=0} = \left. \frac{\delta W}{i\delta j(x_1)} \right|_{j=0} - \Delta v. \quad (4.30)$$

Note that this does not imply that the vertex functions are the same. The connection between the vertex functions in both formulations is given by

$$\Gamma'[\bar{\varphi}'(j)] = \Gamma[\bar{\varphi}(j)] \quad \text{with} \quad \bar{\varphi}(j(x)) := \frac{\delta W}{i\delta j(x)} \quad \text{and} \quad \bar{\varphi}' = \bar{\varphi} - \Delta v. \quad (4.31)$$

Eq. (4.29) states that the tadpole counterterm dependence originating from  $\Gamma^\Delta$  cancels in connected Green's functions with more than one external leg.

According to (4.29) the tadpole renormalization condition  $\hat{T}_i = 0$  does not modify connected Green's functions in the *FJ Tadpole Scheme* since  $\Delta v$  can be freely chosen, in particular, such that the tadpole equations (4.26) are fulfilled. This has interesting consequences for the interpretation of the tadpole counterterms. For example, using that the expression (4.22) is independent of  $\Delta v$ , the one-loop two-point tadpole counterterm derived from (4.17) obeys

$$\text{---} \overset{\times}{\text{---}} \underset{t_{ij}}{\text{---}} = - \sum_n \text{---} \overset{\times}{\uparrow} \underset{\varphi_n}{\bullet} \text{---}, \quad (4.32)$$

independently of the nature of the external particle(s). This can also be seen directly at one-loop order by computing the two-point tadpole contribution  $t_{ij}$ . To this end, assume a typical scalar potential  $V$  in the Lagrangian (4.14) without derivative interactions. Expanding  $t_{ij}$  to first order in  $\Delta v$  and using that  $\Delta v$  acts as a field shift, one obtain

$$\begin{aligned} \text{---} \overset{\times}{\text{---}} \underset{t_{ij}}{\text{---}} &= \text{F.T.} \sum_n \Delta v_n \left. \frac{\partial \delta^2 S}{\partial \Delta v_n \delta \varphi_i \delta \varphi_j} \right|_{\varphi=0, \Delta v=0} + \mathcal{O}((\Delta v)^2), \\ &= \text{F.T.} \sum_n \Delta v_n \left. \frac{\delta^3 S}{\delta \varphi_n \delta \varphi_i \delta \varphi_j} \right|_{\varphi=0, \Delta v=0} + \mathcal{O}((\Delta v)^2), \end{aligned} \quad (4.33)$$

where we used that  $\Gamma$  is given by the action  $S$  at tree-level<sup>6</sup> and F.T. denotes the Fourier transform that translates Green's functions from configuration space to momentum space. Defining the mass squared matrix of the scalar fields as

$$(M^2)_{ij} := \left. \frac{\partial^2 V}{\partial \varphi_i \partial \varphi_j} \right|_{\varphi=0, \Delta v=0}, \quad (4.34)$$

the explicit tadpole counterterm to the two-point function reads

$$\sum_n \text{---} \overset{\times}{\uparrow} \underset{\varphi_n}{\bullet} \text{---} = \sum_{n,k} \left( \text{F.T.} \left. \frac{\delta^3 S}{\delta \varphi_n \delta \varphi_i \delta \varphi_j} \right|_{\varphi=0, \Delta v=0} \right) (M^2)_{nk}^{-1} t_k. \quad (4.35)$$

For the tadpole counterterm, one finds

$$\begin{aligned} t_i &= \left. \frac{\partial \Delta \mathcal{L}}{\partial \varphi_i} \right|_{\varphi=0} = \sum_n \left. \frac{\partial^2 \mathcal{L}}{\partial \varphi_i \partial \Delta v_n} \right|_{\varphi=0, \Delta v=0} \Delta v_n + \mathcal{O}((\Delta v)^2) \\ &= - \sum_n \left. \frac{\partial^2 V}{\partial \varphi_i \partial \varphi_n} \right|_{\varphi=0, \Delta v=0} \Delta v_n + \mathcal{O}((\Delta v)^2) = - \sum_n (M^2)_{in} \Delta v_n + \mathcal{O}((\Delta v)^2). \end{aligned} \quad (4.36)$$

Inserting this into (4.35), yields

$$\sum_n \text{---} \overset{\times}{\uparrow} \underset{\varphi_n}{\bullet} \text{---} = \sum_{n,k,l} \text{F.T.} \left. \frac{\delta^3 S}{\delta \varphi_n \delta \varphi_i \delta \varphi_j} \right|_{\varphi=0, \Delta v=0} (M^2)_{nk}^{-1} \left[ - (M^2)_{kl} \Delta v_l \right] + \mathcal{O}((\Delta v)^2)$$

<sup>6</sup>The contribution (4.33) is a higher-order contribution because  $\Delta v$  is identified with a higher-order correction.

$$= -\text{F.T.} \sum_n \frac{\delta^3 S}{\delta\varphi_n \delta\varphi_i \delta\varphi_j} \Big|_{\varphi=0, \Delta v=0} \Delta v_n + \mathcal{O}((\Delta v)^2). \quad (4.37)$$

Combining this result with (4.33), Eq. (4.32) is explicitly verified at one-loop order.

Using the tadpole renormalization condition (4.26), the one-loop two-point tadpole counterterm can be expressed as

$$\text{---} \times \text{---} \underset{t_{ij}}{\quad} = - \sum_n \text{---} \overset{\times}{\uparrow} \varphi_n = \sum_n \text{---} \overset{\textcircled{1}}{\uparrow} \varphi_n, \quad \text{if } t_n = -T_n \quad \forall n. \quad (4.38)$$

Therefore, the tadpole counterterms mimic the contribution of tadpole diagrams  $T_i$ , once  $T_i$  is identified with  $-t_i$ .

We conclude that the *FJ Tadpole Scheme* is equivalent to not renormalize tadpoles at all, which corresponds to setting  $\Delta v$  to zero in (4.15) and computing all tadpole diagrams explicitly. The consistent use of the *FJ Tadpole Scheme* defined in (4.15) and (4.18)–(4.20) guarantees the independence of the chosen tadpole renormalization, meaning that the value for any physical quantity is independent of the value of  $t_i$  and thus  $\hat{T}_i$ . The  $\Delta v_i$  can be used to solve the tadpole equation (4.26) order by order in perturbation theory, and relating them to the tadpole counterterms  $t_i$ , which is consistent within the freedom of field reparametrization invariance of QFT. After spontaneous symmetry breaking, the bare physical parameters like particle masses can be expressed through the theory defining parameters, i.e. the coupling constants in the Higgs potential before spontaneous symmetry breaking.

## 4.2.2 The FJ Tadpole Scheme in the SM

### Derivation of the FJ Tadpole Scheme in the SM

In this section, we derive the *FJ Tadpole Scheme* in the SM at two-loop order and apply the results to the renormalized self-energy at one-loop order. An explicit two-loop example for the Higgs self-energy is given in App. D. The starting point is the bare Lagrangian for the Higgs field  $\Phi_B$  defined in (4.14), which is identified with the SM Higgs Lagrangian (2.14) and the Higgs doublet  $\Phi$  being replaced by the bare Higgs doublet  $\Phi_B$  parametrized as follows

$$\Phi_B = \begin{pmatrix} \phi_B^+ \\ \frac{1}{\sqrt{2}} [v_B + \Delta v + h_B + i\chi_B] \end{pmatrix}. \quad (4.39)$$

Collecting the terms linear,  $V_B^1$ , and quadratic,  $V_B^2$ , in the bare, neutral, scalar Higgs field  $h_B$ , yields

$$\begin{aligned} V(\Phi_B) &\supset (v_B + \Delta v) \left( \frac{\lambda_B}{4} (v_B + \Delta v)^2 - \mu_B^2 \right) h_B + \left( \frac{3\lambda_B}{8} (v_B + \Delta v)^2 - \frac{1}{2} \mu_B^2 \right) h_B^2 \\ &\equiv V^1(\Delta v, h_B) + V^2(\Delta v, h_B). \end{aligned} \quad (4.40)$$

The relation between  $\Delta v$  and the tadpole counterterm  $t_h$  is determined according to (4.18),

$$t_h h_B = -V^1. \quad (4.41)$$

Using the tree-level condition,  $\Delta v = 0 \Leftrightarrow t_h = 0$ , gives the relations between the bare parameters

$$\lambda_B = \frac{4\mu_B^2}{v_B^2}, \quad \mu_B^2 = \frac{M_{h,B}^2}{2}, \quad v_B = \frac{2M_{W,B}}{g_B}, \quad (4.42)$$

where the last relation defines the bare W-boson mass. The exact form of the shift  $\Delta v$  in terms of the tadpole counterterm  $t_h$  can be obtained from (4.18), which requires the knowledge of the linear term of the Higgs potential (4.40) for  $\Delta v \neq 0$ ,

$$\begin{aligned} V^1(\Delta v, h_B) &= (v_B + \Delta v) \left( \frac{\lambda_B}{4} (v_B + \Delta v)^2 - \mu_B^2 \right) h_B \\ &= \frac{M_{h,B}^2 \Delta v}{8M_{W,B}^2} (2M_{W,B} + g_B \Delta v) (4M_{W,B} + g_B \Delta v) h_B, \\ &\stackrel{!}{=} -t_h h_B. \end{aligned} \quad (4.43)$$

Eq. (4.43) is used to relate  $\Delta v$  to the tadpole counterterms  $t_h$  at every order in perturbation theory. With the ansatz  $\Delta v = \Delta v^{(1)} + \Delta v^{(2)} + \dots$  and  $t_h^{(L)}$  being the  $L$ -loop tadpole counterterm corresponding to the SM Higgs boson, one obtains

$$\Delta v^{(1)} = -\frac{t_h^{(1)}}{M_{h,B}^2} \quad (4.44)$$

at one-loop order and

$$\Delta v^{(2)} = -\frac{t_h^{(2)}}{M_{h,B}^2} - \frac{3g_B (\Delta v^{(1)})^2}{4M_{W,B}} \quad (4.45)$$

at two loops. The tadpole counterterm to the two-point function of the SM Higgs boson is derived from (4.19)

$$\begin{aligned} V^2(\Delta v, h_B) &= \left( \frac{3\lambda_B}{4} (v_B + \Delta v)^2 - \mu_B^2 \right) \frac{h_B^2}{2} \\ &\stackrel{!}{=} \frac{M_{h,B}^2 - t_{hh}}{2} h_B^2, \end{aligned} \quad (4.46)$$

where  $\lambda_B$ ,  $\mu_B^2$ , and  $v_B$  are replaced according to (4.42) as before. This yields

$$t_{hh} h_B^2 = - \left( \frac{3g_B M_{h,B}^2 \Delta v}{2M_{W,B}} + \frac{3g_B M_{h,B}^2 (\Delta v)^2}{8M_{W,B}^2} \right) h_B^2, \quad (4.47)$$

which is valid to all orders. At one-loop order the bare parameters in (4.47) can be replaced by renormalized ones. Omitting anything beyond one loop, the two-point tadpole counterterm is

given by

$$t_{hh}^{(1)} = \frac{3gt_h^{(1)}}{2M_W}. \quad (4.48)$$

Using the on-shell condition  $q^2 = M_{h,R}^2$ , where  $M_{h,R}$  denotes the renormalized Higgs-boson mass, and the tadpole renormalization condition  $\hat{T}_h = 0$ , the renormalized on-shell two-point function of the Higgs boson reads

$$\hat{\Sigma}_{hh}^{(1)}(M_{h,R}^2) = \Sigma_{hh}^{(1),1PI}(M_{h,R}^2) - \frac{3gT_h^{(1)}}{2M_W} - (\delta M_h^2)^{(1)}. \quad (4.49)$$

This expression can be used to determine the counterterm of the Higgs-boson mass  $\delta M_h^2$ , as discussed in Section 4.3.2. The on-shell renormalization is a gauge-independent renormalization condition, and since the bare parameters are defined in a gauge-independent way in the *FJ Tadpole Scheme*, the mass counterterm is necessarily gauge independent. We stress that the renormalized self-energy (4.49) is independent of the choice of  $\Delta v$ . Beyond one-loop order there is a mixing of the usual counterterms and the tadpole counterterm (4.44) contributing to the same loop order, which can be seen from (4.47) and expanding the bare parameters and  $\Delta v$  up to e.g. two-loop order.

We showed how to derive the *FJ Tadpole Scheme* in the SM at the example of the SM Higgs-boson self-energy. Yet, the work is not complete and many additional tadpole counterterms need to be derived for two- and three-point functions involving scalars, vector bosons and fermions. Tadpole counterterms for two- and three-point functions involving vector bosons originate from the kinetic terms of the SM Higgs sector, while tadpole counterterms to fermion self-energies result from the Yukawa terms of the SM Lagrangian.

### Gauge independence of physical parameters in the SM

In this section, we use the SM to demonstrate potential problems with gauge dependence in tadpole counterterm schemes commonly used in the literature. However, it is pointed out that no problems emerge for  $S$ -matrix elements computed in the SM as typically on-shell renormalization conditions are employed for all parameters emerging through SSB. In this case, gauge dependencies introduced by careless treatments of tadpoles cancel in all renormalized physical quantities. Nevertheless, a conceptual problem is present in the SM, which would, in case  $\overline{\text{MS}}$  renormalization schemes were employed, lead to a gauge-dependent  $S$ -matrix unless the *FJ Tadpole Scheme* is used. In order to illustrate the effect of different tadpole renormalization schemes on the gauge dependence of the counterterms of physical parameters, we compare the gauge dependence of the Higgs-boson mass counterterm  $\delta M_h^2$  in the scheme described in Ref. [84] and the  $\beta_h$  scheme from Ref. [85] to the *FJ Tadpole Scheme*.

The scheme described in Ref. [84] requires the vev of the bare Higgs-boson field to vanish at one-loop order

$$\langle h_B \rangle = 0, \quad (4.50)$$

such that  $t_h$  is fixed via (4.26). At the same time, the bare Higgs-boson mass  $M_{h,B}^2$  is defined as the coefficient of the quadratic term in the Higgs field. As a consequence, no tadpole counterterm  $t_{hh}$  appears in the two-point function. However, the so-defined bare Higgs-boson mass, e.g. at one loop

$$M_{h,B}^2 = 2\mu_B^2 - t_{hh} = 2\mu_B^2 - \frac{3g_B t_h}{2M_{W,B}}, \quad (4.51)$$

depends on the tadpole counterterm  $t_h$  and thus becomes gauge dependent as well. If the tadpoles are not renormalized, then  $t_h = t_{hh} = 0$  and the scheme is equivalent to the *FJ Tadpole Scheme*. In the original reference of this scheme in Ref. [84] the tadpoles are included in the definition of bare parameters (4.51). This mismatch can be resolved by comparing to e.g. (4.46).

The mass counterterm of the Higgs boson, defined as the difference between the bare mass squared  $M_{h,B}^2$  and the renormalized Higgs-boson mass squared  $M_{h,R}^2$ ,

$$M_{h,B}^2 \equiv M_{h,R}^2 + \delta M_h^2, \quad (4.52)$$

is determined by requiring that the renormalized self-energy (4.22) vanishes on-shell, i.e. for  $q^2 = M_{h,R}^2$ . Since the renormalized tadpole contribution  $\hat{T}_h^{(1)}$  vanishes [according to Eq. (4.50)], the Higgs-boson mass counterterm is given by the **1PI** contribution

$$\hat{\Sigma}_{hh}^{1\text{PI}}(M_{h,R}^2) = \Sigma_{hh}^{1\text{PI}}(M_{h,R}^2) - \delta M_h^2 \stackrel{!}{=} 0. \quad (4.53)$$

The gauge dependence of  $\Sigma_{hh}^{1\text{PI}}(M_{h,R}^2)$ , which results in a gauge-dependent mass counterterm  $\delta M_h^2$ , can be shown by means of an explicit calculation as in Ref. [86]. In the scheme of Ref. [84] the gauge-dependence of bare masses is not restricted to the Higgs-boson mass, but applies to all massive fields acquiring their mass through **SSB**, since they are defined using the shifted **vev** ( $v_B + \Delta v$ ). For instance, the bare W-boson mass is given by

$$M_{W,B} = \frac{1}{2}g_B(v_B + \Delta v) = \frac{1}{2}g_B \left( v_B - \frac{t_h}{M_{h,B}^2} \right) \quad (4.54)$$

at one-loop order.

The gauge dependence of the Higgs-boson mass counterterm can also be understood from its definition (4.52). As the renormalized mass parameter is identified with the physical mass in the on-shell scheme, which has to be gauge independent, the gauge dependence of a bare parameter must be compensated by the gauge dependence of the counterterm. Using the shorthand notation  $\partial_\xi$  for  $\partial/\partial\xi$ , (4.52) leads to

$$\partial_\xi M_{h,B}^2 = \partial_\xi M_{h,R}^2 + \partial_\xi \delta M_h^2, \quad (4.55)$$

with  $\xi$  denoting the gauge parametrization of a generic gauge choice. As  $\partial_\xi M_{h,R}^2 = 0$ , the gauge dependence of  $M_{h,B}^2$  is directly related to the gauge dependence of  $\delta M_h^2$ . From the gauge independence of the mass counterterm in the *FJ Tadpole Scheme* and Eq. (4.49) it follows using

(4.53)

$$\partial_\xi \delta M_h^2 \stackrel{(4.53)}{=} \partial_\xi \Sigma_{hh}^{1\text{PI}}(M_{h,R}^2) \stackrel{(4.49)}{=} \frac{3g\partial_\xi T_h^{(1)}}{2M_W} = -\frac{3g\partial_\xi t_h^{(1)}}{2M_W}, \quad (4.56)$$

which is consistent with the bare mass definition (4.51).

A similar discussion applies to the  $\beta_h$  scheme in Ref. [85] which also requires the  $\text{vev} \langle h_B \rangle$  to vanish at higher orders and defines the bare masses using the shifted  $\text{vev}$ , e.g.

$$M_{h,B}^2 = \frac{1}{2}\lambda_B(v_B + \Delta v)^2 = \frac{1}{2}\lambda_B v_B \left( v_B - 2\frac{t_h}{M_{h,B}^2} \right) = \frac{1}{2}\lambda_B v_B^2 - \frac{g_B t_h}{M_{W,B}}, \quad (4.57)$$

$$M_{W,B} = \frac{1}{2}g_B(v_B + \Delta v) = \frac{1}{2}g_B \left( v_B - \frac{t_h}{M_{h,B}^2} \right), \quad (4.58)$$

at one-loop order. In this scheme, the parameter  $\mu_B$  is eliminated from the bare Lagrangian in favour of  $t_h$  and  $M_{h,B}^2$ , while  $\lambda_B$  is expressed in terms of  $M_{h,B}^2$ ,  $M_{W,B}^2$  and  $g_B$ . As a consequence, all tadpoles to 3-point functions are absorbed into the definition of the bare physical parameters. This has the advantage that tadpole counterterms appear exclusively in one- and two-point functions for the Higgs and would-be Goldstone bosons. However, the bare masses become gauge dependent via the dependence on the tadpole  $t_h$ . The Higgs-boson mass counterterm reads

$$\delta M_h^2 = \Sigma_{hh}^{1\text{PI}}(M_{h,R}^2) - \frac{g_B T_h^{(1)}}{2M_{W,B}}. \quad (4.59)$$

This definition differs from the one resulting from (4.49) upon imposing the on-shell mass renormalization condition  $\hat{\Sigma}_{hh}(M_{h,R}^2) = 0$  by gauge-dependent tadpole terms. In Ref. [85], the  $\beta_t$  scheme has been introduced to cure this problem. There, the bare particle masses are defined in terms of the bare  $\text{vev}$  and are therefore gauge independent. When tadpoles are renormalized requiring  $\hat{T}_h = 0$ , the *FJ Tadpole Scheme* in the **SM** is equivalent to the  $\beta_t$  scheme.

For convenience we have derived simple prescriptions to generate tadpole counterterms in different tadpole counterterm schemes from the original bare Lagrangian (4.15) or (2.14) augmented by gauge, fermion and Yukawa terms. The results for the **SM**, **THDM** and **HSESM** are given in App. C.

We conclude that the *FJ Tadpole Scheme* is a natural scheme for dealing with the tadpoles, as it prevents tadpoles from being absorbed into the definition of bare parameters. Moreover, the tadpole renormalization condition  $\hat{T} = 0$  is very useful, since no explicit tadpole loop contributions have to be computed. We stress that the presented tadpole renormalization procedure is general and not restricted to the **SM**, **THDM** or **HSESM**, and can be automated as described in Section 4.2.4.



### 4.2.3 Interplay of tadpoles with $\overline{\text{MS}}$ subtraction

In this section, we come back to the original motivation for the *FJ Tadpole Scheme*, namely a consistent  $\overline{\text{MS}}$  subtraction in the presence of **SSB**. For every new **BSM** model the question of renormalization conditions arise for new physical parameters. As there is no guiding principle for yet unmeasured parameters, one usually relies on the  $\overline{\text{MS}}$  scheme which is simple, universal, and allows for estimations of higher-order corrections via scale variations. Thus, the  $\overline{\text{MS}}$  scheme should always be favoured, unless serious problems with perturbativity are encountered.<sup>7</sup>

Even though the  $\overline{\text{MS}}$  scheme is straightforward to apply, there are subtleties in the **EW** theory in the presence of **SSB**. The difficulties are mainly caused by a confusing and inconsistent treatment of tadpoles and tadpole counterterms in the literature, which, we think, is caused by two common misbeliefs. The first one is related to the definition of vertex functions as being **1PI**. The vertex functional yields **1PI** graphs for fields  $\bar{\varphi}'$  fulfilling the stationary condition

$$\left. \frac{\delta W[j]}{\delta j} \right|_{j=0} = \bar{\varphi}'(0) = 0 \quad \Leftrightarrow \quad \left. \frac{\delta \Gamma'[\varphi]}{\delta \varphi} \right|_{\varphi=\bar{\varphi}'(0)=0} = j(0) = 0 \quad (4.60)$$

to all orders. This is exactly the situation in the *FJ Tadpole Scheme* if the tadpoles are renormalized via the tadpole condition (4.26), i.e. with a suited choice for the shift  $\Delta v$  the field  $\bar{\varphi}'$  fulfils (4.60). However, by cancelling all explicit tadpoles, new  $n$ -point counterterms make their appearance through (4.17) in vertex-functions. We have shown that these counterterms behave precisely like explicit tadpole graphs [see (4.38)], which is a necessity of the independence of Green's functions of the  $\Delta v$  shifts. This is perfectly compatible with the connection between vertex and connected Green's functions via Legendre transformation. For instance, from the definition of the two-point function one obtains

$$\begin{aligned} iG(x, x') &= \left. \frac{\delta^2 W[j]}{i\delta j(x)i\delta j(x')} \right|_{j=0} = \left. \frac{\delta \bar{\varphi}'(j)}{i\delta j} \right|_{j=0} (x, x') = - \left. \left( \frac{\delta j(\varphi)}{i\delta \varphi} \right)^{-1} \right|_{\varphi=\bar{\varphi}'(0)} (x, x') \\ &= - \left. \left( \frac{\delta^2 \Gamma'[\varphi]}{\delta \varphi \delta \varphi} \right)^{-1} \right|_{\varphi=\bar{\varphi}'(0)=0} (x, x') := - \left( \Gamma'^{(2)}(0) \right)^{-1} (x, x') \end{aligned} \quad (4.61)$$

with  $\Gamma'^{(2)}$  being **1PI**. However, if one chooses not to renormalize the tadpoles ( $\Delta v = 0$ ) Eq. (4.61) raises the question whether vertex functions remain **1PI**, since explicit tadpole graphs show up on the **lhs** in the two-point Green's function. The difference between the vertex functional with the tadpoles renormalized, denoted as  $\Gamma'$ , and the vertex functional without tadpole renormalization, denoted as  $\Gamma$ , can be derived using the *FJ Tadpole Scheme*. The solution for the two-point function at one-loop order<sup>8</sup> reads

$$\Gamma^{(2)}(0) = \Gamma'^{(2)}(0) - t_{\varphi\varphi}, \quad (4.62)$$

<sup>7</sup>This is the case for the renormalization of mixing angles. See Section 4.6.

<sup>8</sup>The argument can be extended to all orders. However, for beyond one-loop order the difference between the two vertex functionals involves mixing terms including tadpole counterterms, normal counterterms and bare loop parts. One can work out the difference based on the discussion in App. D.

i.e.  $\Gamma^{(2)}(0)$  is 1PI and free of tadpoles or tadpole counterterms. But since  $\Gamma^{(2)}(0)$  is 1PI it cannot fulfil (4.61). This is because in (4.61)  $\varphi'(0) = 0$  is assumed as the stationary point, and the apparent contradiction can be resolved by again making use of the *FJ Tadpole Scheme* which interpolates between  $\Gamma'$  and  $\Gamma$ . Eq. (4.31) implies

$$\Gamma^{(n)}(\varphi(0)) = \Gamma^{(n)}(\Delta v) \stackrel{(4.31)}{=} \Gamma'^{(n)}(0) = \Gamma'^{(n)}(\varphi'(0)), \quad (4.63)$$

with  $(n)$  denoting the  $n$ -fold differentiation wrt  $\varphi$ , and  $\Delta v$  determined from (4.26). For the case  $n = 1$  the condition (4.60) together with (4.63) imply

$$\Gamma'^{(1)}(0) = 0 \quad \Rightarrow \quad \Gamma^{(1)}(\Delta v) = 0, \quad (4.64)$$

which determines the stationary point for  $\Gamma$ . Therefore, Eq. (4.63) states that independent of the tadpole renormalization *all vertex functions are precisely the same if evaluated at the stationary points* which is essential when comparing to Green's functions as they are defined for  $j = 0$ . We conclude that  $\Gamma^{(2)}(\Delta v)$  contains tadpole contributions which make their way through the field expansion via [compare with (4.37) and (4.62)]

$$\Gamma^{(2)}(\Delta v) = \Gamma^{(2)}(0) + \Delta v \Gamma^{(3)}(0) + \mathcal{O}(\Delta v^2), \quad (4.65)$$

and there is no contradiction with (4.61) when tadpoles are not renormalized.

The other confusion concerns alternative tadpole counterterm schemes in combination with the tadpole condition  $\hat{T}_{H_i} = 0$ , which is very useful because it allows to omit graphs with explicit tadpoles everywhere. However, in the literature the tadpole condition is realized by tadpole counterterms which are not based on the freedom of field reparametrization, which, unfortunately, is never mentioned. Since there is no other freedom for an independent tadpole parameter this inevitably leads to inconsistencies which manifest themselves in tadpoles being absorbed into the definition of bare parameters, as exemplified in the previous Section 4.2.2.<sup>9</sup> The problem with the dof can be seen already at the example of the SM (see Section 2.2). The parameters of the Higgs potential  $\lambda$  and  $\mu$  can be traded for physical parameters in the following way

	$V_{\text{SM}}$	$\mathcal{L}_{\text{Gauge}}$
Before SSB	$\mu, \lambda$	$g, g'$
After SSB (choice)	$M_h, M_W$	$e, s_w$

with the vev not being an independent parameter, but determined after SSB by minimizing the scalar potential. Therefore, in the Higgs sector there are only two dof which can be used to define, e.g. the renormalized Higgs-boson mass  $M_h$  and the renormalized W-boson mass  $M_W$ .<sup>10</sup> *There is no freedom for an independent tadpole counterterm parameter based on the freedom of parameter choice.*

<sup>9</sup>This is also evident from the effective prescriptions given in App. C

<sup>10</sup>The counterterm to  $M_Z$  can be traded for the counterterm of the gauge coupling  $g'$  and is thus independent of  $M_W$ .

We come back to  $\overline{\text{MS}}$  subtraction and to the question when a rigorous renormalization of tadpoles is required. In tadpole counterterm schemes other than the *FJ Tadpole Scheme*, the bare parameters absorb tadpole contributions, which can ultimately lead to a gauge-dependent  $S$ -matrix due to the gauge dependence of the tadpoles. Yet, as a matter of fact, tadpoles always cancel for on-shell schemes or momentum-subtraction schemes. The reason is that within those subtraction schemes any renormalized vertex can be written as a difference of the bare vertex and the subtraction part corresponding to the vertex evaluated at a specific kinematic point. Since tadpoles have no momentum dependence they drop out in this difference. This implies that in the **SM** the standard renormalization schemes used in Ref. [84] and Ref. [85] yield physical amplitudes independent of the tadpole renormalization, since all renormalization conditions are based on complete subtraction of the relevant vertex functions. Once  $\overline{\text{MS}}$  schemes are used this no longer has to be true. However, if one chooses to renormalize the bare theory-defining parameters, e.g. the  $\lambda_i$ , then **BRST** invariance guarantees the gauge independence of  $S$ -matrix elements [87]. The only situation where the gauge independence of the  $S$ -matrix is spoiled in an  $\overline{\text{MS}}$  scheme is when  $\overline{\text{MS}}$  subtraction is applied to gauge-dependent bare parameters, e.g. parameters in the physical basis in combination with alternative tadpole counterterm schemes. This is precisely the case in the **THDM**, **HSESM** or **MSSM** with the definition of mixing angles in an  $\overline{\text{MS}}$  scheme.<sup>11</sup> In the **THDM**, we prove the gauge dependence of the  $S$ -matrix at one-loop order resulting from a careless tadpole treatment in the  $R_\xi$  gauge for the renormalization of the mixing angle  $\alpha$  in the  $\overline{\text{MS}}$  scheme in App. C.1. A similar proof can be given for  $\beta$  at one-loop order in  $\overline{\text{MS}}$  schemes which is more involved and requires mixing propagators propagating the gauge dependence. In App. C.2, we prove the gauge dependence for the pole part of  $\delta\beta$  in the **THDM** which can be used to prove the gauge dependence of the  $S$ -matrix.

Finally, we conclude that dealing with tadpoles is always a delicate issue, since a careless treatment can easily lead to a gauge-dependent  $S$ -matrix. The situation is aggravated by the fact that the treatment of tadpoles for practical calculations in the literature is confusing, and, as a consequence, no preferred scheme has emerged. From the point of view of applicability, automation and gauge independence, the *FJ Tadpole Scheme* is the only reliable scheme, which can be employed for arbitrary theories [51] and is easily automated as presented in the next section.

#### 4.2.4 Automation of the FJ Tadpole Scheme

The *FJ Tadpole Scheme* presented in the previous sections is based on the freedom of field reparametrization. Under the general assumption that the theory under consideration is expressed in the physical basis without tree-level mixings and restricting to the one-loop case, the solutions to the tadpole equations (4.18) can be translated to a field redefinition as follows

$$H_i \rightarrow H_i + \Delta v_i := H_i - \frac{\delta t_{H_i}}{m_{H_i}^2}, \quad (4.66)$$

---

<sup>11</sup>Note the same applies to a definition of masses in the  $\overline{\text{MS}}$  scheme, but in **EW** theory they are usually defined in the on-shell scheme.

which is performed for every physical field  $H_i$  developing a **vev**, and  $\delta t_{H_i}$  being the associated tadpole counterterm. By fixing  $t_{H_i}$  to the tadpole graphs  $T_{H_i}$  via

$$t_{H_i} = -T_{H_i}, \quad (4.67)$$

explicit tadpoles are cancelled and only tadpole counterterms to 1PI graphs remain. In REPT1L the tadpole counterterms in the *FJ Tadpole Scheme* can be derived automatically, which is done on the level of the Feynman rules as REPT1L does not have access to the Lagrangian nor can it derive Feynman rules. Here, one has to be careful with combinatorial factors. For instance, consider a vertex with two equal flavour Higgs bosons  $H_i$  and several other particles not developing a **vev**. We denote the vertex as  $V_{\dots, H_i, H_i}$  and the associated coupling as  $c_{\dots, H_i, H_i}$ . Then, at the one-loop level  $V_{\dots, H_i, H_i}$  gives rise to a tadpole counterterm vertex  $V_{\dots, H_i}$  with a coupling proportional to  $\Delta v_i$ . The Feynman rule is derived by applying the shift (4.66) on the term in the Lagrangian corresponding to  $V_{\dots, H_i, H_i}$ , and mapping back to the Feynman rule with one less leg as follows

$$V_{\dots, H_i, H_i} \equiv V_{\dots} \frac{\delta^2}{\delta H_i \delta H_i} \frac{H_i^2}{2!} \xrightarrow{(4.66)} V_{\dots} \frac{\delta}{\delta H_i} \frac{2\Delta v_i H_i}{2!} \equiv \Delta v_i V_{\dots, H_i}, \quad (4.68)$$

with the functional derivatives symbolising the derivation of the Feynman rules from the Lagrangian. Thus, the tadpole counterterm coupling is  $c_{\dots, H_i, H_i} \Delta v_i$ .

This rule is generalized in the presence of various Higgs flavours by taking one representative for each Higgs flavour in a Feynman rule and performing the shift (4.66) for every different Higgs flavour once, i.e. without including any combinatorial factors. For instance, the Feynman rule for  $V_{\dots, H_i, H_i, H_j, H_k}$  gives rise to the three different tadpole counterterms

$$V_{\dots, H_i, H_i, H_j, H_k} \xrightarrow{(4.66)} \Delta v_i V_{\dots, H_i, H_j, H_k}, \quad \Delta v_j V_{\dots, H_i, H_i, H_k}, \quad \Delta v_k V_{\dots, H_i, H_i, H_j}, \quad (4.69)$$

Finally, we note that different vertices can contribute to the same tadpole counterterm vertex. In this case the couplings originating from different vertices are merged to one counterterm coupling.

### 4.3 Renormalization conditions for physical particles

In this section we apply the standard on-shell renormalization conditions imposed on two-point functions associated to physical fields and translate them to conditions for mixing and self-energies following Ref. [84]. The restriction to physical fields is not mandatory and REPT1L can renormalize two-point functions involving unphysical fields, which, however, is not necessary for a finite  $S$ -matrix. We start by introducing mass and field renormalization counterterms associated to physical fields in Section 4.3.1. The same conventions are used by REPT1L in the default counterterm expansion. We proceed with generic on-shell conditions for mixing and self-energies in Section 4.3.2, and we conclude with subtleties concerning rational terms in self-energies in Section 4.3.3.

### 4.3.1 Mass and field renormalization counterterms

We split the bare masses in the Lagrangian into renormalized masses and mass counterterms. Our convention for the splitting depends on the spin of the associated field and differs for scalars (S), vector bosons (V) and fermions (f) in the following way

$$M_{V,B}^2 = M_V^2 + \delta M_V^2, \quad M_{S,B}^2 = M_S^2 + \delta M_S^2, \quad m_{f,B} = m_f + \delta m_f. \quad (4.70)$$

Bosonic fields  $\varphi_i$  are renormalized uniformly according to

$$\varphi_{i,B} = \sum_j Z_{ij}^{\frac{1}{2}} \varphi_j, \quad (4.71)$$

where  $j$  runs over all of fields having the same quantum numbers as the field  $i$ . The field renormalization constant  $Z_{ij}$  is expanded around the unit matrix as follows

$$Z_{ij} = \begin{cases} 1 + \delta Z_{ii} & i = j \\ \delta Z_{ij} & i \neq j \end{cases}. \quad (4.72)$$

For instance, for the SM gauge-fields we obtain

$$W_B^\pm = \left(1 + \frac{1}{2}\delta Z_{WW}\right) W^\pm, \quad \begin{pmatrix} Z_B \\ A_B \end{pmatrix} = \begin{pmatrix} 1 + \frac{1}{2}\delta Z_{ZZ} & \frac{1}{2}\delta Z_{ZA} \\ \frac{1}{2}\delta Z_{AZ} & 1 + \frac{1}{2}\delta Z_{AA} \end{pmatrix} \begin{pmatrix} Z \\ A \end{pmatrix}. \quad (4.73)$$

Any other possible mixing in the scalar sector is defined in the same way. Note that, in general, we include off-diagonal field renormalization constants for the mixings between physical Higgs and Goldstone bosons, e.g. in the THDM for the mixings  $H_a$ ,  $G_0$  and  $H^\pm$ ,  $G^\pm$ . For fermionic fields  $\psi$  the left-handed (L) and right-handed (R) components are renormalized independently, i.e. with different field renormalization constants, via

$$\psi_{f,B}^L = \left(1 + \frac{1}{2}\delta Z_{f,L}\right) \psi_f^L, \quad \psi_{f,B}^R = \left(1 + \frac{1}{2}\delta Z_{f,R}\right) \psi_f^R, \quad (4.74)$$

for each fermion flavour  $f$ . We do not consider a possible mixing between different fermions which, in general, requires the renormalization of the Cabibbo Kobayashi Maskawa (CKM) matrix. Note there is no obstacle and REPT1L can deal with the CKM renormalization and mixing in the fermion sector.

### 4.3.2 Renormalization conditions for mixing and self-energies

The mass and field renormalization counterterms are fixed by imposing conditions on full two-point functions, generically denoted as  $\hat{G}_{ij}^{\alpha_i\beta_j}$ , with the hat indicating renormalized functions. The indices  $i$  and  $j$  specify the external flavour, and the associated indices  $\alpha_i$  and  $\beta_j$  are the indices related to the spin of the corresponding particle flavour. The generic on-shell renormal-

ization conditions read

$$\epsilon_{\alpha_i}(q) \hat{G}_{ij}^{-1, \alpha_i \beta_j}(q^2) \Big|_{q^2=M_i^2} = 0, \quad \forall i, j, \quad (4.75)$$

$$\lim_{q^2 \rightarrow M_i^2} \epsilon_{\alpha_i}(q) \frac{\hat{G}_{ii}^{-1, \alpha_i \beta_i}(q^2)}{q^2 - M_i^2} = 1, \quad \forall i \quad (4.76)$$

with  $\epsilon_{\alpha_i}$  being a physical polarization vector associated to flavour  $i$ , and the masses being, in general, complex-valued.<sup>12</sup> For  $i = j$  (4.75) corresponds to the usual on-shell renormalization condition with the mass  $M_i$  being identified as the physical mass. Further, for  $i \neq j$  the condition (4.75) prevents a mixing from the flavour  $j$  to on-shell  $i$ , with  $j$  not necessarily being a physical field. The off-diagonal condition (4.75) for  $i \neq j$  and the residue condition (4.76) can be left out, however, for a properly normalized  $S$ -matrix according to the **LSZ** theorem they should be included whenever possible. Otherwise it is necessary to include additional **LSZ** factors in  $S$ -matrix computations.

The renormalization conditions can be translated to conditions for mixing and self-energies which can be solved subsequently in terms of coefficients of Lorentz covariants. The decomposition into covariants depends on the spin representations and conventions for the projections which are defined in the following. We assume the tadpole renormalization condition  $\hat{T}_i = 0$  [see Eq. (4.26)] which makes the mixing and self-energies strictly **1PI**. Nevertheless, certain tadpole counterterms may still be present which depend on the actual counterterm scheme.

**Spin 0:** The connection between the renormalized diagonal scalar two-point function  $\hat{G}$  and the renormalized scalar self-energy  $\hat{\Sigma}$  is given by

$$i\hat{G}^{-1}(q^2) = q^2 - M_S^2 + \hat{\Sigma}(q^2). \quad (4.77)$$

With the expansion rules for masses (4.70) and fields (4.71), we obtain the renormalized self-energy components as

$$\hat{\Sigma}_{SS}(q^2) = \Sigma_{SS}^{1\text{PI}}(q^2) + (q^2 - M_S^2) \delta Z_{SS} - \delta M_S^2 + t_{SS}. \quad (4.78)$$

$\Sigma_{SS}^{1\text{PI}}$  denotes the pure scalar **1PI** bare-loop contribution and  $\delta Z_{SS}, \delta M_S, t_{SS}$  denote the scalar diagonal field renormalization constant, mass and tadpole counterterm, respectively. The tadpole counterterm  $t_{SS}$  is defined implicitly and stands for all tadpole counterterms to the self-energy. The scalar mixing energy is defined in analogy to (4.77), (4.78), and is given by

$$\hat{\Sigma}_{SS'}(q^2) = \Sigma_{SS'}^{1\text{PI}}(q^2) + \frac{1}{2}(q^2 - M_S^2) \delta Z_{SS'} + \frac{1}{2}(q^2 - M_{S'}^2) \delta Z_{S'S} + t_{SS'}. \quad (4.79)$$

**Spin 1:** Within the 't Hooft–Feynman gauge the connection between the diagonal two-point

<sup>12</sup>Details on the treatment of complex momenta in the **CMS** are given in Section 4.4.

function and the self-energy for vector bosons is given by

$$i\hat{G}_{VV}^{-1,\mu\nu}(q) = -g^{\mu\nu}(q^2 - M_V^2) - \hat{\Sigma}_{VV}^{\mu\nu}(q). \quad (4.80)$$

The decomposition for the renormalized vector-boson self-energy is defined as

$$\hat{\Sigma}_{VV}^{\mu\nu}(q) = \hat{\Sigma}_{VV}^T(q^2) \left( g^{\mu\nu} - \frac{q^\mu q^\nu}{q^2} \right) + \hat{\Sigma}_{VV}^L(q^2) \left( \frac{q^\mu q^\nu}{q^2} \right), \quad (4.81)$$

with the transverse component given by

$$\hat{\Sigma}_{VV}^T(q^2) = \Sigma_{VV}^{1PI,T}(q^2) + (q^2 - M_V^2) \delta Z_{VV} - \delta M_V^2 - t_{VV}. \quad (4.82)$$

Notice the different sign convention for the tadpole counterterm  $t_{VV}$  compared to the scalar case. Similar to the diagonal case the mixing vector energies read

$$\hat{\Sigma}_{VV'}^T(q^2) = \Sigma_{VV'}^{1PI,T}(q^2) + \frac{1}{2}(q^2 - M_{V'}^2) \delta Z_{VV'} + \frac{1}{2}(q^2 - M_V^2) \delta Z_{VV'} - t_{VV'}. \quad (4.83)$$

Note for the **SM** gauge group the only possible mixing is between the photon and the Z boson. Further, for all tadpole counterterm schemes under considerations we have  $t_{\gamma Z} = 0$ .

**Spin 1/2:** The fermionic self-energy is related to the diagonal two-point function via

$$i\hat{G}_{ff}^{-1}(q) = \not{q} - m_R + \hat{\Sigma}_{ff}(q), \quad (4.84)$$

with  $\not{q} = q_\mu \gamma^\mu$ . The decomposition for the renormalized fermionic self-energy is defined as

$$\hat{\Sigma}_{ff}(q) = \not{q} \frac{1 - \gamma_5}{2} \hat{\Sigma}_{ff}^L(q^2) + \not{q} \frac{1 + \gamma_5}{2} \hat{\Sigma}_{ff}^R(q^2) + \hat{\Sigma}_{ff}^S(q^2), \quad (4.85)$$

with the coefficients given by

$$\begin{aligned} \hat{\Sigma}_{ff}^L(q^2) &= \Sigma_{ff}^{1PI,L}(q^2) + \delta Z_{f,L}, \\ \hat{\Sigma}_{ff}^R(q^2) &= \Sigma_{ff}^{1PI,R}(q^2) + \delta Z_{f,R}, \\ \hat{\Sigma}_{ff}^S(q^2) &= \Sigma_{ff}^{1PI,S}(q^2) - \frac{1}{2} m_f (\delta Z_{f,L} + \delta Z_{f,R}) - \delta m_f + t_{ff}. \end{aligned} \quad (4.86)$$

With this the renormalization conditions (4.75), (4.76) can be expressed in terms of renormalized mixing and self-energy form factors. For the diagonal bosonic parts one can derive the following conditions for the transverse renormalized self-energies

$$\begin{aligned} \hat{\Sigma}_{VV}^T(M_V^2) = 0, \quad \left. \frac{\partial \hat{\Sigma}_{VV}^T(q^2)}{\partial q^2} \right|_{q^2=M_V^2} &= 0, \\ \hat{\Sigma}_{SS}(M_S^2) = 0, \quad \left. \frac{\partial \hat{\Sigma}_{SS}(q^2)}{\partial q^2} \right|_{q^2=M_S^2} &= 0. \end{aligned} \quad (4.87)$$

The off-diagonal renormalization conditions impose the following conditions on the scalar and vector mixing energies

$$\begin{aligned}\hat{\Sigma}_{VV'}^T(M_{V'}^2) &= 0, & \hat{\Sigma}_{VV'}^T(M_V^2) &= 0, \\ \hat{\Sigma}_{SS'}(M_S^2) &= 0, & \hat{\Sigma}_{SS'}(M_{S'}^2) &= 0.\end{aligned}\quad (4.88)$$

As for the fermionic self-energies the renormalization conditions read

$$\begin{aligned}m_f \hat{\Sigma}_{ff}^L(m_f^2) + \hat{\Sigma}_{ff}^S(m_f^2) &= m_f \hat{\Sigma}_{ff}^R(m_f^2) + \hat{\Sigma}_{ff}^S(m_f^2) = 0, \\ \hat{\Sigma}_{ff}^R(m_f^2) + \hat{\Sigma}_{ff}^L(m_f^2) + 2 \frac{\partial}{\partial q^2} \left[ m_f^2 \left( \hat{\Sigma}_{ff}^R(q^2) + \hat{\Sigma}_{ff}^L(q^2) \right) + 2m_f \hat{\Sigma}_{ff}^S(q^2) \right] \Big|_{q^2=m_f^2} &= 0.\end{aligned}\quad (4.89)$$

Inserting the expressions (4.78), (4.79), (4.82), (4.83), (4.86) into the renormalization conditions (4.87)–(4.89), we obtain the mass and field renormalization constants in terms of the 1PI mixing and self-energies and tadpole counterterm contributions. We note that REPT1L follows precisely this procedure, but none of the scalar form factors (4.78), (4.79), (4.82), (4.83), (4.86) are hard-coded. Instead the projections are computed explicitly which guarantees the independence of the precise counterterm expansion.

### 4.3.3 IR rational terms in self-energies

As any vertex function, self-energies give rise to rational terms which need to be included as explained in Section 4.1.2 for the rational terms of type  $R_2$ . In the on-shell renormalization there is a subtlety concerning the reduction to four dimensions. Since the self-energies are evaluated at exceptional kinematic points they can give rise to  $R_2$  terms originating from IR divergences. To see this, consider the  $B_0$  function which gives rise to the following UV rational term

$$\lim_{D \rightarrow 4} (D - 4) B_0(0, m, m) = -2, \quad (4.90)$$

with  $m$  denoting a non-zero mass. If we decide to regularize the mass in dimensional regularization, the expression (4.90) turns dimensionless and the result has to vanish

$$\lim_{D \rightarrow 4} (D - 4) B_0(0, 0, 0) = 0, \quad (4.91)$$

which, as already mentioned, is due to a IR rational term cancelling the UV one. This situation is encountered in theories with massless gauge bosons and fermions whose masses are treated in dimensional regularization. As RECOLA2 supports dimensional and mass regularization for fermions, model files need to provide counterterms in the corresponding regularization schemes. To this end, a particle can be assigned a *light particle* attribute in the UFO format which tells REPT1L to regularize this particle in dimensional and mass regularization as well as keeping the full mass dependence. In Ref. [88] it has been shown that IR rational terms cancel in all truncated unrenormalized amplitudes, and may enter in renormalized amplitudes only via external self-energy corrections. This allows to compute the IR rational terms only for field



renormalization constants which is what is done in REPT1L.

## 4.4 Treatment of unstable particles

The majority of the known fundamental particles are unstable and their study at particle colliders is of utmost interest. As the short lifetime of the heavier particles does not allow for a direct detection, a discovery of unstable particles requires the study of so-called signal- and background-processes. From a field-theoretic point of view signal processes can be defined as a (gauge-invariant) collection of initial and final states and the occurrence of one or more specific resonant (unstable) particles. Typically, signal processes are approximated with the assumption that the intermediate resonance can be considered as stable, i.e. as an asymptotic state in QFT.<sup>13</sup> For instance, the Higgs-boson fulfils this requirements as it has a tiny width over mass ratio, and the so-called narrow-width approximations can be applied. However, in many other cases this LO approximation breaks down. An alternative approximation is given by the pole scheme [90, 91, 92] which is well-defined, allowing for the inclusion of higher orders. RECOLA2 supports the pole approximation which is automated for the so-called factorisable corrections. Yet, the pole approximation does not capture all the physics (see e.g. the distributions in Ref. [30]) and exact results are highly desirable. RECOLA2 has the ability to compute many particle final states at NLO exactly, i.e. including all of the production and decay, but one-loop computations with intermediate resonances require a proper treatment of finite-width effects in a gauge-independent way which is problematic [93, 94, 95]. A possible solution to this problem is given by the CMS [96, 97, 98] which is the natural choice due to its gauge-independence, validity in all phase-space and applicability to higher-orders [99, 100]. In Section 4.4.1 we give a short introduction to the CMS at the one-loop order. Then, in Section 4.4.2, we discuss implementation details.

### 4.4.1 Complex-Mass Scheme at one-loop order

The CMS prescription is straightforward to apply and the underlying idea is just an analytic continuation of real-valued masses to complex-valued ones. At tree-level this merely implies the use of complex valued masses  $\mu$  defined in the following way

$$\mu^2 = M^2 - i\Gamma M, \quad (4.92)$$

with  $M$  and  $\Gamma$  being the real mass and width of the unstable particle, respectively. In the case of the EW theory implicit dependencies on the masses have to be resolved. For instance, the cosine of the weak mixing angle  $c_w$ , which is defined via the mass ratio of W and Z bosons, necessarily becomes complex. In general, for a proper application of the CMS all the parameters of the theory need to be expressed in terms of an independent set of parameters which has to include the masses of the unstable particles. In cases where this is not possible new solutions must first be developed.

---

<sup>13</sup> From a conceptual point of view, unstable particles need to be excluded from asymptotic states to make the  $S$ -matrix unitary [89].

The generalization to one-loop order in combination with on-shell renormalization conditions requires an analytic continuation of 2-point scalar integrals to complex momenta. For instance, in the **CMS** the W-boson on-shell renormalization conditions read

$$\hat{\Sigma}_{WW}^T(p^2)\Big|_{p^2=\mu_W^2} = 0, \quad \frac{\partial \hat{\Sigma}_{WW}^T(p^2)}{\partial p^2}\Big|_{p^2=\mu_W^2} = 0. \quad (4.93)$$

The mass counterterm is defined as  $\delta\mu_W^2 = M_{W,B}^2 - \mu_W^2$ , with  $M_{W,B}$  and  $\mu_W$  being the bare and renormalized (complex) W-boson mass, respectively. The first condition in (4.93) determines the mass counterterm as follows

$$\delta\mu_W^2 = \Sigma_{WW}^{1PI,T}(p^2)\Big|_{p^2=\mu_W^2}. \quad (4.94)$$

Therefore, the self-energy needs to be evaluated at the complex pole of the two-point function which can be shown to be gauge independent. Since the bare masses of the theory are real-valued the width has to fulfil the consistency equation

$$\Gamma_W M_W = -\text{Im}[\mu_W^2] = \text{Im}[\delta\mu_W^2] = \text{Im}\left[\Sigma_{WW}^{1PI,T}(p^2)\Big|_{p^2=\mu_W^2}\right], \quad (4.95)$$

which can be shown to be consistent with the unitarity of the  $S$ -matrix [101]. In practice, the evaluation of scalar integrals of the form (4.94), (4.95) is done via an expansion around the real mass since the analytic continuation of the two-point function to complex momentum arguments is not available for all necessary cases. The proper expansion can be motivated using the one-loop corrected self-energy denoted as  $f(k^2)$  (see Ref. [97])

$$f(k^2) = \frac{\Sigma(k^2) - \delta\mu_P^2}{k^2 - \mu_P^2} + \delta Z_P, \quad (4.96)$$

with  $\delta\mu_P$  and  $\delta Z_P$  being the mass and field renormalization counterterm for a particle  $P$ . As approximated solutions to the **CMS** on-shell renormalization conditions we choose

$$\begin{aligned} \delta\mu_P^2 &= \Sigma(M_P^2) - iM_P\Gamma_P\Sigma'(M_P^2) + \mathcal{O}(\alpha^4), \\ \delta Z_P &= -\Sigma'(M_P^2) + \mathcal{O}(\alpha^2). \end{aligned} \quad (4.97)$$

Note that the field renormalization constant is kept at one-loop order, but the mass counterterm includes specific higher order terms of the order  $\alpha^2$ , i.e. formally of two-loop order. Using (4.96) yields

$$f(k^2) = \frac{\Sigma(k^2) - \Sigma(M_P^2) - (k^2 - M_P^2)\Sigma'(M_P^2) + \mathcal{O}(\alpha^2)}{k^2 - \mu_P^2}. \quad (4.98)$$

which represents a strict one-loop expansion  $\mathcal{O}(\alpha)$  of the numerator of two-point functions, justifying the ansatz (4.97).

### 4.4.2 Aspects of automation for general theories

In REPT1L the approximated on-shell renormalization conditions within the CMS are implemented as conditions without performing the expansion (4.97) explicitly as required by (4.98). In fact, the expansion is circumvented since it is equivalent to require that the one-loop corrected CMS two-point function (4.96) vanishes exactly on the real mass squared value  $f(M_P^2) \stackrel{!}{=} 0$ .

The truncation (4.97) comes at the cost of several problems. One is that gauge-dependent terms make their way in the mass counterterm. The gauge-dependence can be seen directly by comparing to the BFM which is discussed in Section 6.1.5. Another complication is that the expansion is not always applicable due to terms not being Taylor expandable. From a physical point of view the reason is the exchange of massless particles which lead to resonant contributions known as non-factorisable corrections.<sup>14</sup> To correct for the false expansion a term can be added to self-energies as given for the individual cases [84]. In REPT1L a general solution is implemented which can be applied independent of the precise model or physics. To this end, we have related the origin of the non-analytic terms to the scalar function  $B_0$  which, in combination with the PVR, can be used to handle all cases. The relevant cases are the ones with the following on-shell configurations

$$\begin{aligned} B_0(\mu_P^2, \mu_P, 0) &= \Delta_{\text{UV}} + 2 - \log \frac{\mu_P^2}{\mu_{\text{UV}}^2} \\ B_0(M_P^2, \mu_P, 0) &= B_0(\mu_P^2, \mu_P, 0) - \frac{M_P^2 - \mu_P^2}{\mu_P^2} \log \frac{\mu_P^2 - M_P^2}{\mu^2} \\ B'_0(M_P^2, \mu_P, 0) &= -\frac{1}{M_P^2} - \frac{\mu_P^2}{M_P^4} \log \frac{\mu_P^2 - M_P^2}{\mu_P^2}. \end{aligned} \quad (4.99)$$

Computing the expansion of  $B_0(\mu_P^2, \mu_P, 0)$  around the real mass and subtracting the exact result yields

$$B_0(M_P^2, \mu_P, 0) + (\mu_P^2 - M_P^2) B'_0(M_P^2, \mu_P, 0) - B_0(\mu_P^2, \mu_P, 0) = i \frac{\Gamma_P}{M_P} + \mathcal{O}\left(\frac{\Gamma_P^2}{M_P^2} \log \frac{\Gamma_P}{M_P}\right), \quad (4.100)$$

with the expansion parameter being defined as

$$\frac{\Gamma_P}{M_P} := \frac{M_P^2 - \mu_P^2}{iM_P^2}. \quad (4.101)$$

Note that the order  $\mathcal{O}(\Gamma_P/M_P \log(\Gamma_P/M_P))$  cancels, but the term of order  $\mathcal{O}(\Gamma_P/M_P)$  remains. The leading term on the rhs of (4.100) can be incorporated, after solving the approximated on-shell conditions in the CMS, by shifting specific derivatives of scalar integrals in the mass counterterm. The shifts have been determined for all scalar functions up to rank two and the only non-vanishing cases read

$$B'_0(M_P^2, \mu_P, 0) \rightarrow B'_0(M_P^2, \mu_P, 0) + \frac{1}{M_P^2},$$

<sup>14</sup>The technical reason is that in the expansion a branch cut is crossed.

$$\begin{aligned}
B'_0(M_P^2, 0, \mu_P) &\rightarrow B'_0(M_P^2, 0, \mu_P) + \frac{1}{M_P^2}, \\
B'_1(M_P^2, \mu_P, 0) &\rightarrow B'_1(M_P^2, \mu_P, 0) - \frac{1}{M_P^2}, \\
B'_{11}(M_P^2, \mu_P, 0) &\rightarrow B'_{11}(M_P^2, \mu_P, 0) + \frac{1}{M_P^2}.
\end{aligned} \tag{4.102}$$

These rules depend on the conventions of the tensor reduction which are listed in App. A.1. In addition to the shift, REPT1L makes sure that no higher-order terms are introduced via couplings. For instance, if a coupling  $c(\mu)$  (with a width dependence) is multiplied with  $B'_0(M_P^2, \mu_P, 0)$ , then the correction term will be included as

$$c(\mu_P) B'_0(M_P^2, \mu_P, 0) \rightarrow c(\mu_P) B'_0(M_P^2, \mu_P, 0) + \frac{c(M_P)}{M_P^2}, \tag{4.103}$$

and note the different arguments of the coupling on the `rhs`.

## 4.5 Renormalization of couplings in the SM and extended Higgs sector

In this section we discuss standard renormalization conditions concerning the SM gauge couplings and the parameter  $M_{\text{sb}}$  in the THDM. The renormalization of couplings can only be automatized to some extent since in new theories new physical situations are encountered which require alternative renormalization conditions. Nevertheless, our approach can be considered as automatized since we provide a simple framework for implementing custom renormalization conditions. Further, we provide standard renormalization conditions for SM gauge couplings which have been implemented in a model-independent way, being valid for each of the models in Chapter 2. Yet, for each new model it is necessary to verify whether the schemes are applicable. In any case, the  $\overline{\text{MS}}$  schemes can always be employed which is fully automated.

In Section 4.5.1 we discuss the renormalization of  $\alpha$ , which is related to the electric charge  $e$ . The renormalization of  $\alpha_s$  is covered in Section 4.5.2, representing the QCD sector of the SM. Finally, we deal with the renormalization of  $M_{\text{sb}}$  in the THDM in Section 4.5.3.

### 4.5.1 Renormalization of $\alpha$

#### Thomson limit

The Thomson-Limit (TL) defines a non-relativistic kinematic configuration which can be used to identify the renormalized electric charge  $e$  with the electric charge measured in low-energy experiments. More precisely, the renormalized electric charge  $e$  in the TL is defined via a

fermion–fermion–photon vertex  $\Gamma_\mu^{\gamma\bar{f}f}$  at vanishing photon momentum as follows

$$\begin{array}{c}
 \begin{array}{c}
 \text{---} \gamma, k, \epsilon \text{---} \\
 \text{---} \bar{f}, p', \bar{u} \text{---} \\
 \text{---} f, p, u \text{---}
 \end{array}
 \begin{array}{c}
 \text{---} \\
 \text{---} \\
 \text{---}
 \end{array}
 \left. \begin{array}{c}
 \text{---} \\
 \text{---} \\
 \text{---}
 \end{array} \right|_{k=0, p^2=p'^2=m_f^2}
 \end{array}
 \stackrel{\dagger}{=}
 -iQ_f e \bar{u}(p') \not{k} \gamma_\mu u(p), \quad (4.104)$$

with  $\epsilon$ ,  $\bar{u}$  and  $u$  being the polarization vectors/spinors of the photon, anti-fermion and fermion, respectively.  $Q_f$  represents a multiplicity of the electric charge associated to the fermion flavour  $f$  which can be a rational number if  $f$  is a quark.<sup>15</sup> The renormalization of the charge is universal and simultaneously fulfilled for all fermions. The universality is guaranteed by the **STI**, which, in the case of **QED**, takes the simple form of a Ward identity (**WI**) relating the vertex to the fermionic self-energies as follows (see e.g. [102])

$$k^\mu \Gamma_\mu^{\gamma\bar{f}f}(k, p, p') = -eQ_f \left[ \Gamma^{\bar{f}f}(p) - \Gamma^{\bar{f}f}(p') \right]. \quad (4.105)$$

Requiring (4.105) for the renormalized vertex yields the well-known one-loop relation

$$\delta Z_e = -\frac{1}{2} \delta Z_A, \quad (4.106)$$

which is consistent with the **TL** if the photon is renormalized on shell. Yet, this relation is not valid in the **EW SM** sector and needs to be extended as follows [102]

$$\delta Z_e = -\frac{1}{2} \delta Z_A - \frac{s_w}{2c_w} \delta Z_{Z_A}, \quad (4.107)$$

which is compatible with the conventions for field renormalization constants (4.73) and on-shell renormalization conditions (4.87).

### The Fermi scheme

For **LHC** phenomenology the **TL** does not provide an appropriate renormalization due to the difference of the scale in the underlying processes. One possibility is to run the coupling to a more suited scale, e.g. the Z-mass scale. Another possibility is to use a different renormalization condition. A popular choice is the  $G_F$  scheme [84, 103, 104] which can be defined via the muon decay. To this end, the renormalized electric charge is related to the experimentally measured value for the Fermi constant  $G_F$  in an **EFT** approach. The scale of the process is taken to be smaller than the W-mass  $M_W$  which implies that the process is effectively mediated by the 4-point interaction involving a muon, a muon-neutrino, an electron and an electron-anti-neutrino. The full computation in the **SM**, excluding pure **QED** corrections, can be expanded in the limit  $\frac{s}{M_W^2}, \frac{t}{M_W^2}, \frac{u}{M_W^2} \ll 1$ , resulting in simple functions. The final result is solved for the renormalized electric charge and higher order corrections are shifted in  $\delta Z_e$ . This defines  $\Delta r$

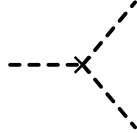
$$\delta Z_e^{G_F} = \delta Z_e^{\text{TL}} - \frac{\Delta r}{2}, \quad (4.108)$$

<sup>15</sup>For electrons the sign of the charge is  $Q_f = -1$ .





The dependence of this vertex on  $\delta M_{\text{sb}}$  reads



$$= \frac{e}{M_W s_w} \left[ (\dots) + \left( -2c_{\alpha\beta} + 3c_{\alpha\beta}^3 + \frac{3}{2}s_{\alpha\beta}c_{\alpha\beta}^2 \left( \frac{1}{t_\beta} - t_\beta \right) \right) \delta M_{\text{sb}}^2 \right] + t_{H_1 H_1 H_1},$$

where (...) stands for other counterterms and  $t_{H_1 H_1 H_1}$  is the tadpole counterterm. As an alternative, we can trade  $M_{\text{sb}}$  for other parameters and renormalize those in the  $\overline{\text{MS}}$  scheme instead. For instance, in Ref. [111]  $m_{12}$  is renormalized, and in Ref. [112] the renormalization of  $\lambda_5$  is proposed. It is possible to employ alternative  $\overline{\text{MS}}$  renormalization schemes while keeping  $M_{\text{sb}}$  as an external parameter. To this end, the counterterm for  $M_{\text{sb}}$  can be shifted by finite parts. In the case of  $m_{12}$  being renormalized  $\overline{\text{MS}}$  we obtain

$$\begin{aligned} \delta M_{\text{sb}}^2 m_{12}^{\overline{\text{MS}}} &:= \frac{\delta m_{12}^2 \overline{\text{MS}}}{\cos \beta \sin \beta} + M_{\text{sb}}^2 \frac{\sin^2 \beta - \cos^2 \beta}{\cos \beta \sin \beta} \delta \beta \\ &= \frac{\delta m_{12}^2 \overline{\text{MS}}}{\cos \beta \sin \beta} + M_{\text{sb}}^2 \frac{\sin^2 \beta - \cos^2 \beta}{\cos \beta \sin \beta} \left( \delta \beta^{\overline{\text{MS}}} + \delta \beta^{\text{fin}} \right) \\ &= \delta M_{\text{sb}}^2 \overline{\text{MS}} + M_{\text{sb}}^2 \frac{\sin^2 \beta - \cos^2 \beta}{\cos \beta \sin \beta} \delta \beta^{\text{fin}}. \end{aligned} \quad (4.116)$$

From the second to the third line in (4.116) we combined the pole parts allowing to identify  $\delta M_{\text{sb}}^2 \overline{\text{MS}}$ . After this step finite parts, denoted as “fin”, remain which depend on the precise renormalization of the mixing angle  $\beta$ .

## 4.6 Renormalization of mixing angles

Mixing phenomena emerge for particles which carry the same conserved quantum numbers. In the **SM**, mixings are encountered between the photon and the Z boson which is parametrized by the weak mixing angle and between fermions when allowing for non-diagonal entries in the **CKM** matrix. For every independent mixing angle the question of a proper renormalization condition arises. In the **SM** the mixing of the neutral gauge bosons is governed by gauge symmetry which relates the weak mixing angle to the gauge-boson masses. Thus, the renormalization does not pose any problems since the Z and W boson can be renormalized in the on-shell scheme which fixes the renormalized weak mixing angle in a physical way. In the **MSSM** a similar gauge mechanism is observed for neutral Higgs-boson mixings, but for e.g. squark mixings the renormalization needs to be addressed. As for the **SM** the renormalization of the **CKM** has been approached many times. The first proposal was a simple on-shell renormalization via mixing field renormalization constants [113], which has also been applied to inter-family mixing of Dirac and Majorana fermions [114]. Later it has been observed that these on-shell schemes are gauge-dependent [115], which has led to a new series of alternative proposals [116, 117, 118, 119, 120, 121]. Yet, all of them are not satisfying due to arising complications or lack of generality. Simpler prescriptions were proposed [122, 123, 124] which successfully extract the gauge-dependence in the class of  $R_\xi$  gauges at one-loop order, but cannot be applied to other





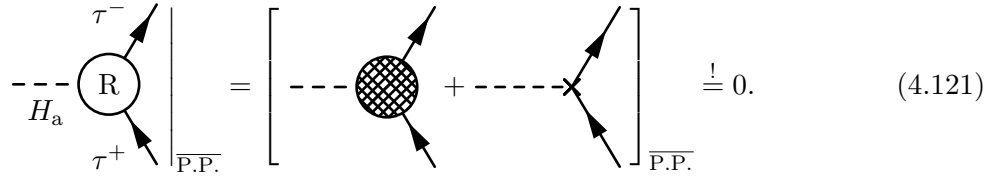
performing the  $\overline{\text{MS}}$  renormalization at a vertex (4.117), one can use the following identity

$$\delta\alpha^{\overline{\text{MS}}} = \frac{\delta Z_{H_h H_1}^{\overline{\text{MS}}} - \delta Z_{H_1 H_h}^{\overline{\text{MS}}}}{4}, \quad (4.120)$$

which has been remarked before (e.g. Refs. [128, 129]). Note that (4.120) depends on the conventions for the field renormalization constants (4.71) and the definition of the mixing angle  $\alpha$  (2.21). The identity (4.120) holds to all orders and is a simple consequence of the renormalizability within a minimal (diagonal) renormalization in the interaction basis  $\rho_{i,B} = \delta Z_i \rho_i$ , with  $\rho_i$  being one of the Higgs doublets or Higgs singlet fields in the THDM (2.17) and HSESM (2.19).<sup>19</sup> The  $\overline{\text{MS}}$  scheme is gauge-independent only in the *FJ Tadpole Scheme*, which is explicitly shown for different tadpole counterterm schemes in general  $R_\xi$  gauge in App. C.1.

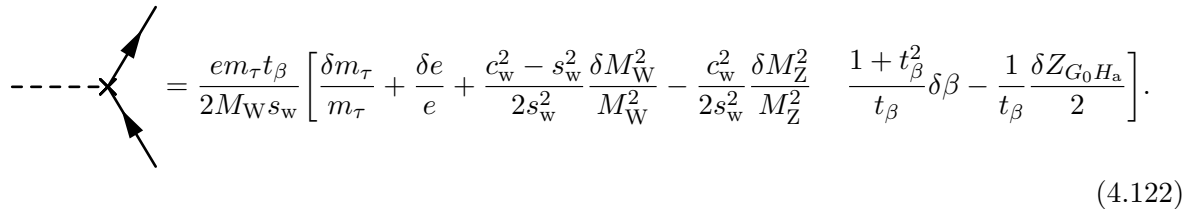
### 4.6.2 Mixing angle $\beta$

In the THDM  $\beta$  enters the Lagrangian as an additional mixing angle (see Eq. (2.24)) and can be renormalized in the  $\overline{\text{MS}}$  scheme following the same steps as for  $\alpha$ . For instance, the process  $H_a \rightarrow \tau^- \tau^+$  is suited for the renormalization:



$$\text{---} H_a \text{---} \bigcirc \text{---} \begin{matrix} \tau^- \\ \tau^+ \end{matrix} \Big|_{\text{P.P.}} = \left[ \text{---} \bigcirc \text{---} \begin{matrix} \tau^- \\ \tau^+ \end{matrix} + \text{---} \times \text{---} \begin{matrix} \tau^- \\ \tau^+ \end{matrix} \right] \Big|_{\text{P.P.}} \stackrel{!}{=} 0. \quad (4.121)$$

The corresponding counterterm in the THDM reads



$$\text{---} \times \text{---} \begin{matrix} \tau^- \\ \tau^+ \end{matrix} = \frac{em_\tau t_\beta}{2M_W s_w} \left[ \frac{\delta m_\tau}{m_\tau} + \frac{\delta e}{e} + \frac{c_w^2 - s_w^2}{2s_w^2} \frac{\delta M_W^2}{M_W^2} - \frac{c_w^2}{2s_w^2} \frac{\delta M_Z^2}{M_Z^2} - \frac{1 + t_\beta^2}{t_\beta} \delta\beta - \frac{1}{t_\beta} \frac{\delta Z_{G_0 H_a}}{2} \right]. \quad (4.122)$$

Again, there is no tadpole counterterms for this vertex in the *FJ Tadpole Scheme*, and  $\delta\beta$  is gauge independent only in the *FJ Tadpole Scheme*, but gauge dependent in popular tadpole counterterm schemes already at one-loop order as shown in App. C.2. The proof is more involved as no gauge-dependence can be seen in the class of  $R_\xi$  gauges at the one-loop level as argued in App. C.2. The renormalizability of the model with a symmetric field renormalization allows to derive the following UV identities for  $\delta\beta$

$$\delta\beta^{\overline{\text{MS}}} = \frac{\delta Z_{G_0 H_a}^{\overline{\text{MS}}} - \delta Z_{H_a G_0}^{\overline{\text{MS}}}}{4}, \quad \delta\beta^{\overline{\text{MS}}} = \frac{\delta Z_{G^\pm H^\mp}^{\overline{\text{MS}}} - \delta Z_{H^\pm G^\mp}^{\overline{\text{MS}}}}{4}, \quad (4.123)$$

which can be used instead of performing renormalization at the vertex. In the HSESM  $\beta$  is not a mixing angle and appears only in the Higgs potential. In this case the  $\overline{\text{MS}}$  renormalization can be performed e.g. on the vertex  $H_h H_1 H_1$ . In the HSESM as well as THDM  $\beta$  can be expressed in

<sup>19</sup>See e.g. [112] for the derivation of (4.120) and other UV identities.

terms of the ratio of **vevs** (see Section 2.3.2), which allows to deduce further pole part identities<sup>20</sup>

$$\delta\beta = \frac{\sin\beta\cos\beta}{2(\sin^2\alpha - \cos^2\alpha)} \left( \delta Z_{H_h H_h}^{\overline{\text{MS}}} - \delta Z_{H_1 H_1}^{\overline{\text{MS}}} \right) + \frac{g}{2M_W} \left( \sin\beta\Delta v_1^{\overline{\text{MS}}} - \cos\beta\Delta v_2^{\overline{\text{MS}}} \right), \quad (4.124)$$

$$\delta\beta = \frac{\sin\beta\cos\beta}{4\sin\alpha\cos\alpha} \left( \delta Z_{H_h H_1}^{\overline{\text{MS}}} + \delta Z_{H_1 H_h}^{\overline{\text{MS}}} \right) + \frac{g}{2M_W} \left( \sin\beta\Delta v_1^{\overline{\text{MS}}} - \cos\beta\Delta v_2^{\overline{\text{MS}}} \right), \quad (4.125)$$

with the solutions for  $\Delta v_1, \Delta v_2$  given in (B.31). In the case of the **THDM** the following additional relations are obtained

$$\delta\beta = \frac{1}{4} \left( \delta Z_{H_a G_0}^{\overline{\text{MS}}} + \delta Z_{G_0 H_a}^{\overline{\text{MS}}} \right) + \frac{g}{2M_W} \left( \sin\beta\Delta v_1^{\overline{\text{MS}}} - \cos\beta\Delta v_2^{\overline{\text{MS}}} \right), \quad (4.126)$$

$$\delta\beta = \frac{1}{4} \left( \delta Z_{H^\pm G^\mp}^{\overline{\text{MS}}} + \delta Z_{G^\pm H^\mp}^{\overline{\text{MS}}} \right) + \frac{g}{2M_W} \left( \sin\beta\Delta v_1^{\overline{\text{MS}}} - \cos\beta\Delta v_2^{\overline{\text{MS}}} \right). \quad (4.127)$$

### 4.6.3 Conceptual problems in the $\overline{\text{MS}}$ scheme

Moving towards  $S$ -matrix elements it becomes apparent that  $\overline{\text{MS}}$  schemes for the mixing angles suffer from conceptual problems. The most striking one is that the  $S$ -matrix does not have a continuous limit in the degenerate mass scenario i.e.  $M_{H_1} \rightarrow M_{H_h}$ . This behaviour can be traced back to the off-diagonal **LSZ** factors which in our framework are included in the solutions to the mixing field renormalization constants. For instance,  $\delta Z_{H_h H_1}$  is given by

$$\delta Z_{H_h H_1} = \frac{\Sigma_{H_1 H_h}^{\text{1PI,BFM}}(M_{H_1}^2) + t_{H_1 H_h}}{2(M_{H_h}^2 - M_{H_1}^2)}, \quad (4.128)$$

which is divergent in the degenerate limit

$$\lim_{M_{H_1} \rightarrow M_{H_h}} |\delta Z_{H_h H_1}| = \infty, \quad (4.129)$$

because the self-energy is non-zero in that limit. The  $S$ -matrix is also divergent since the **LSZ** theorem requires to include those finite terms of  $\delta Z_{H_h H_1}$ . When it comes to the counterterm of the mixing angle  $\alpha$ , one observes that it always appears in vertices as a combination of the following terms

$$\delta\alpha - \frac{\delta Z_{H_h H_1}}{2}, \quad \delta\alpha + \frac{\delta Z_{H_1 H_h}}{2}, \quad (M_{H_1}^2 - M_{H_h}^2)\delta\alpha \quad (4.130)$$

The first two terms, where  $\delta\alpha$  is accompanied by the mixing field renormalization constants, originate from the counterterm expansion of the field rotation (2.21) and a subsequent mixing field renormalization. The third term emerges from the counterterm expansion of the Higgs potential parameters  $\lambda_i$ . For instance, the  $\delta\alpha$  dependence of the expansion of  $\lambda_1, \lambda_2, \lambda_3$  in the **HSESM** derived from (2.34) is given by

$$\delta\lambda_1 = \frac{g^2}{4M_W^2} (M_{H_1}^2 - M_{H_h}^2) s_\alpha c_\alpha \delta\alpha + \dots,$$

<sup>20</sup>The pole parts of the **vevs** renormalize in the same way as the corresponding fields.

$$\begin{aligned}\delta\lambda_2 &= \frac{g^2}{4M_W^2 t_\beta^2} (M_{H_h}^2 - M_{H_1}^2) s_\alpha c_\alpha \delta\alpha + \dots, \\ \delta\lambda_3 &= \frac{g^2}{4M_W^2 t_\beta^2} (\sin^2 \alpha - \cos^2 \alpha) (M_{H_h}^2 - M_{H_1}^2) \delta\alpha + \dots,\end{aligned}\tag{4.131}$$

The same follows for the **THDM** directly from the definition of  $\lambda_i$  in (2.30). From (4.130) the solution to cure the singularity introduced by the **LSZ** factors is perfectly clear, namely the divergences can be avoided by absorbing UV-finite terms in  $\delta\alpha$  which cancel the problematic terms in  $\delta Z_{H_h H_1}$ ,  $\delta Z_{H_1 H_h}$ . This is not in conflict with the third term (4.130) and the singularity is not shifted elsewhere. The divergent terms in the degenerate limit are necessarily gauge independent as the  $S$ -matrix is gauge independent in the  $\overline{\text{MS}}$  scheme. The difficulty lies in the extraction of gauge-independent parts of mixing energies in the non-degenerate mass case which to this date remains an unsolved problem. In the context of the **CKM**-matrix renormalization the momentum-independent terms in the fermionic mixing energies are expected to be gauge independent, which can be shown in the class of  $R_\xi$  gauges via e.g. extended **BRST** symmetry [115]. This has been used in Ref. [122] to construct the gauge-independent parts at the one-loop order. Unfortunately this prescription is not applicable in our case and can not be used at higher orders.

One might think that the whole problem is due to the bad choice of  $\alpha$  for the  $\overline{\text{MS}}$  renormalization. For instance, we can trade  $\alpha$  for another parameter e.g. one of the  $\lambda_i$  and perform an  $\overline{\text{MS}}$  renormalization for this parameter. This is equivalent to perform an  $\overline{\text{MS}}$  renormalization of  $\alpha$  and include finite terms which relate both parameters at **NLO**, in the same way as done for  $M_{\text{sb}}$  and  $m_{12}$  in Section 4.5.3 [see Eq. (4.116)]. In the **HSESM** this succeeds in cancelling the degenerate mass divergence in the case that  $\alpha$  is traded for

$$[v_s v \lambda_3]^{\overline{\text{MS}}} = [(M_{H_h}^2 - M_{H_1}^2) c_\alpha s_\alpha]^{\overline{\text{MS}}},\tag{4.132}$$

leading to a universal and gauge-independent finite term of the form

$$\delta\alpha = \delta\alpha^{\overline{\text{MS}}} + \frac{s_\alpha c_\alpha}{c_\alpha^2 - s_\alpha^2} \frac{1}{M_{H_h}^2 - M_{H_1}^2} (\delta M_{H_h}^2 - \delta M_{H_1}^2)^{\text{fin}}.\tag{4.133}$$

The underlying mechanism cancelling the degenerate mass singularity is the following relation between the on-shell mixing and self-energies<sup>21</sup>

$$\lim_{M_{H_1} \rightarrow M_{H_h}} \Sigma_{H_1 H_h}(M_{H_h}^2) - \frac{f_1 f_2}{f_1^2 - f_2^2} (\Sigma_{H_h}(M_{H_h}^2) - \Sigma_{H_1}(M_{H_1}^2)) = 0,\tag{4.134}$$

with suited mixing angles  $f_i$  chosen as follows

**HSESM:**  $f_1 = c_\alpha$ ,  $f_2 = -s_\alpha$ ,

**THDM:**  $f_1 = c_{\alpha\beta}$ ,  $f_2 = -s_{\alpha\beta}$ .

From (4.134) one can easily see that (4.133) cures the problem in the degenerate limit, i.e.

<sup>21</sup>This relation can be checked via explicit calculation in the considered models.

renders (4.130) finite in this limit, but merely trades it for another singularity in the limit  $f_1 \rightarrow f_2$ , which is again unsatisfying. Finally trading all critical parameters, i.e.  $\alpha, \beta$  in the HSESM and  $\alpha, \beta, M_{\text{sb}}$  in the THDM, does not solve the problem and divergences associated to degenerate scenarios remain in pure  $\overline{\text{MS}}$  schemes.

In principle, one could ignore all of this discussion since one is typically interested in non-degenerate scenarios where additional Higgs bosons are heavier than the SM-like one. However, it turns out that the momentum-independent contributions that remain in the degenerate mass limit and that are not subtracted by the  $\overline{\text{MS}}$  scheme, give rise to unnaturally large corrections which render the  $\overline{\text{MS}}$  scheme in the *FJ Tadpole Scheme* useless. Surprisingly by including the finite correction (4.133) partially succeeds in subtracting the large contributions, but benchmark scenarios can be found where it fails nevertheless. The on-shell schemes discussed later in Chapter 7 avoid the conceptual problems and yield corrections in the expected ballpark for all benchmark scenarios, but at the cost of having to fix the gauge, and without the possibility for a proper estimation of higher orders. We conclude that, at the moment, the community is unable to define an  $\overline{\text{MS}}$  or on-shell scheme for the mixing angles which is well-defined in QFT, gauge independent, and free of singularities related to the LSZ factors (4.129).

# Automated generation of renormalized model files in REPT1L

In this chapter we address the generation of renormalized model files for RECOLA2 which is based on Ref. [52]. For this purpose the new tool REPT1L (**R**ecola's **r**Enormalization **P**rocedure **T**ool at **1** **L**oop) has been developed which is a multi-purpose tool for analytic computations at the one-loop order. The necessity for an additional tool for the generation of model files is due to the inner workings of RECOLA2 which requires the Feynman rules in a very particular format as described in Section 3.4. As RECOLA has proved to be an extremely efficient tool, RECOLA2 has been designed closely to RECOLA in order to benefit from all the experience acquired in its development. The support for general models requires a flexible tool that meets RECOLA2's requirements. REPT1L has been written in PYTHON 2.7<sup>1</sup> allowing for a flexible meta programming approach which can generate source code in languages such as FORTRAN95 and FORM [130]. REPT1L depends on other tools, most notably RECOLA2 for the process generation (see Section 3.2), which is used in combination with FORM to construct analytic vertex functions, and SYMPY [131], which is a computer algebra system (CAS) for Python. REPT1L requires the Feynman rules in the UFO format [40] which can be derived via FEYNRULES [37] or SARAH [38]. There has been progress for an automated renormalization in the FEYNRULES framework [39], but we do not make use of these results. In our approach the counterterms and rational terms are automatically derived from the tree-level Feynman rules in a self-contained fashion as explained in the following.

The generation of renormalized model files is a two-pass process. In the first pass a model file is generated as described in Section 5.1. This step involves several manipulations of the Feynman rules, most notably the computation of colour flows and the transformation of these colour-ordered structures to a BGR operator basis. The model file thus obtained is linked to RECOLA2 and used by REPT1L to set up and solve renormalization conditions analytically and to compute rational terms as discussed in Section 5.2. In the second pass the renormalized model file is generated, including explicit counterterm parameters and rational terms.

---

<sup>1</sup>There is ongoing work for PYTHON 3.X compatibility.

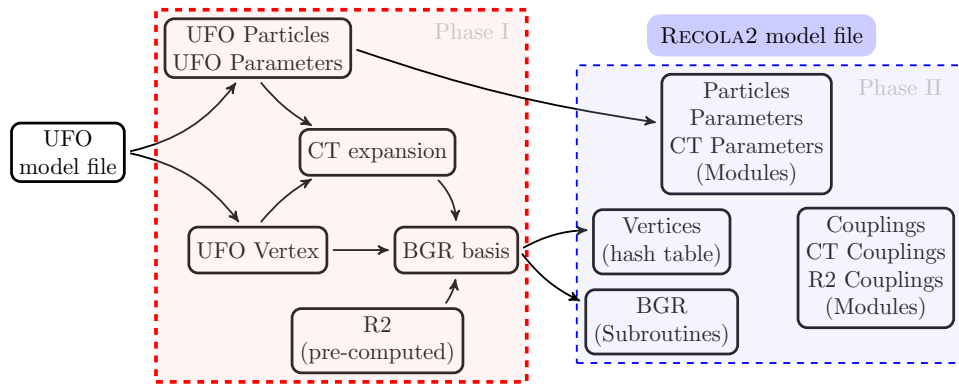


Figure 5.1: The RECOLA2 model file generation. **UFO** vertices are taken as input and each vertex is permuted and mapped to a suited **BGR** operator. Given a counterterm expansion (5.9), REPT1L can generate all counterterm vertices and include them in the **BGR**. Once the renormalization is done and the  $R_2$ -terms are computed, the model file is derived once again, including solutions to counterterm parameters and  $R_2$  terms.

## 5.1 Model-file generation with REPT1L

### 5.1.1 Model-file generation flow

The RECOLA2 model-file generation consists of two phases. In the first phase REPT1L loops over all vertices in the **UFO** model file, disassembling each one into the vertex particles, Lorentz and colour structures, and couplings. The colour structure is transformed to the colour-flow basis possibly rearranging Lorentz structures and couplings. This is discussed in more detail in Section 5.1.2. The resulting Lorentz structures are used to derive the **BGR** operators in a model-independent way. For every Feynman rule REPT1L tries to map the encountered Lorentz structure onto one of those operators. If a new structure cannot be mapped onto an existing operator a new operator is added. In an optional second pass, the existing base of operators is minimized as discussed in Section 5.1.3.

In the second phase of the model-file generation the information is exported as FORTRAN95 code in form of a model-file library, visualized in Fig. 5.1. Particle configurations are linked to the individual contributions on the right-hand side of (3.10), which differ in the underlying **BGR** (3.11), colour flow, colour factors, couplings, coupling orders or other information, via a FORTRAN95 hash table, allowing for a flexible and efficient access. The actual **BGR** are computed and exported as FORTRAN95 subroutines in different forms. For the numerical evaluation tree and loop **BGR** are used to construct tree-level and one-loop amplitudes. The tree **BGR** are a special case of the loop **BGR**, with no loop-momentum dependence. An example for a tree and loop **BGR** as used by RECOLA2 in the numerical evaluation is given in Section 3.4. As a new feature in RECOLA2, an analytic version of the **BGR** allows to generate amplitudes as FORM code,<sup>2</sup> using precisely the same code segment in RECOLA2 for the process generation. This construction guarantees that the numerical and analytic amplitudes are not independent. Finally,

<sup>2</sup>REPT1L is exporting FORTRAN95 subroutines which are able to write the analytic expression for the **BGR** in FORM.

RECOLA2 requires particle information such as the mass, spin, and colour of particles. This information is directly obtained from `UFO` particle instances and is translated to `FORTTRAN95` code.

These steps conclude the tree-level model file generation. In Section 5.1.2 we elaborate in more detail on the translation to the colour-flow basis, and in the Section 5.1.3 we exemplify the derivation of the off-shell current basis.

### 5.1.2 Colour-flow computation

In RECOLA2 the colour flow is constructed recursively. For a given off-shell current the outgoing colour configuration is determined from the incoming ones and the possible colour flows associated to the interaction vertex. As the `UFO` format does not incorporate the colour flow, we need to translate between the two representations. We implemented a dynamical system for computing the colour flow from the generators and structure constants, rather than substituting for known results. In the conventions of Ref. [20] the colour flow associated to a given colour structure

$$C_{a_1, \dots, j_1, \dots}^{i_1, \dots} \quad (5.1)$$

is obtained by multiplying (5.1) with the normalized generator  $(\Delta_{a_p})^{i_p}_{j_p}$  for each index  $a_p$  corresponding to an open index in the adjoint representation. The indices  $i_p$  and  $j_p$  refer to the colour and anti-colour indices, respectively. The generators  $\Delta_a$  and structure constants  $f_{abc}$  define the  $SU(3)$  Lie algebra<sup>3</sup>

$$[\Delta_a, \Delta_b] = i\sqrt{2}f_{abc}\Delta_c, \quad \text{Tr}\{\Delta_a\Delta_b\} = \delta_{ab}, \quad \Delta_a = \frac{\lambda_a}{\sqrt{2}}, \quad (5.2)$$

with  $\lambda_a$  being the Gell-Mann matrices. The computation then consists of eliminating the structure constants and the generators by solving (5.2) for the structure constants and using the (Fierz) completeness relation for the generators as follows

$$f_{abc} = -\frac{1}{\sqrt{2}}i\text{Tr}\{\Delta_a[\Delta_b, \Delta_c]\},$$

$$\sum_a (\Delta_a)^{i_1}_{j_1} (\Delta_a)^{i_2}_{j_2} = \delta_{j_2}^{i_1} \delta_{j_1}^{i_2} - \frac{1}{3} \delta_{j_1}^{i_1} \delta_{j_2}^{i_2}. \quad (5.3)$$

Performing all contractions yields a sum of Kronecker deltas which represent the individual colour flows. For instance, the quartic gluon vertex of the `SM` reads

$$g_s^2 \sum_k (f_{ka_1a_2} f_{ka_3a_4} L_1^{\mu_1\mu_2\mu_3\mu_4} + f_{ka_1a_3} f_{ka_2a_4} L_2^{\mu_1\mu_2\mu_3\mu_4} + f_{ka_1a_4} f_{ka_2a_3} L_3^{\mu_1\mu_2\mu_3\mu_4}), \quad (5.4)$$

<sup>3</sup>The  $\Delta_a$  generators are related to the conventional ones  $T_a$ , as used e.g. in `FEYNRULES` via  $(\Delta_a)^i_j = \sqrt{2}(T_a)^i_j$  with  $\text{Tr}\{T_a T_b\} = \delta_{ab}/2$  and  $[T_a, T_b] = if_{abc}T_c$ . Note that the structure constants  $f_{abc}$  in Ref. [20] are related to the ones in this paper via  $\tilde{f}_{abc} = \sqrt{2}f_{abc}$ .



with  $L_1, L_2, L_3$  being Lorentz structures which, for the following discussion, are left unspecified. Focusing on the colour structure  $\delta_{j_2}^{i_1} \delta_{j_3}^{i_2} \delta_{j_4}^{i_3} \delta_{j_1}^{i_4}$ , we obtain for the two relevant contributions

$$\begin{aligned} \sum_{k, a_1, a_2, a_3, a_4} (\Delta_{a_1})_{j_1}^{i_1} (\Delta_{a_2})_{j_2}^{i_2} (\Delta_{a_3})_{j_3}^{i_3} (\Delta_{a_4})_{j_4}^{i_4} f_{ka_1 a_2} f_{ka_3 a_4} &= \frac{1}{2} \left( -\delta_{j_2}^{i_1} \delta_{j_3}^{i_2} \delta_{j_4}^{i_3} \delta_{j_1}^{i_4} + \dots \right), \\ \sum_{k, a_1, a_2, a_3, a_4} (\Delta_{a_1})_{j_1}^{i_1} (\Delta_{a_2})_{j_2}^{i_2} (\Delta_{a_3})_{j_3}^{i_3} (\Delta_{a_4})_{j_4}^{i_4} f_{ka_1 a_4} f_{ka_2 a_3} &= \frac{1}{2} \left( +\delta_{j_2}^{i_1} \delta_{j_3}^{i_2} \delta_{j_4}^{i_3} \delta_{j_1}^{i_4} + \dots \right). \end{aligned} \quad (5.5)$$

Combining this result with (5.4), results in the contribution

$$\delta_{j_2}^{i_1} \delta_{j_3}^{i_2} \delta_{j_4}^{i_3} \delta_{j_1}^{i_4} \times \frac{g_s^2}{2} (L_3 - L_1). \quad (5.6)$$

Thus, diagonalizing the vertex in the colour-flow basis requires, in general, to redefine Lorentz structures and couplings.

### 5.1.3 Off-shell current basis

For a given Lorentz structure and a definite colour-flow state the **BGR** is derived from the Feynman rules by selecting one of the particles as the outgoing one, multiplying with the corresponding propagator and the incoming currents of the other particles. Since the structure of currents depends on the outgoing particle, one needs to derive the **BGR** for all distinct outgoing particles. Consider for instance the **QED** vertex  $e^+ e^- \gamma$ . REPT1L constructs three different recursion relations

$$\begin{aligned} w_\alpha &= ie \sum_{\beta, \delta, \mu} D_{\alpha\beta}^{e^-}(\gamma^\mu)_{\beta\delta} \times w_\mu \times w_\delta, \\ \bar{w}_\beta &= ie \sum_{\alpha, \delta, \mu} D_{\alpha\beta}^{e^+}(\gamma^\mu)_{\delta\alpha} \times w_\mu \times \bar{w}_\delta, \\ w_\mu &= ie \sum_{\alpha, \beta, \nu} D_{\mu\nu}^\gamma(\gamma^\nu)_{\alpha\beta} \times \bar{w}_\alpha \times w_\beta, \end{aligned} \quad (5.7)$$

with  $w_i, \bar{w}_j, w_\mu$  being either incoming or outgoing off-shell currents, depending on whether they are on the right- or left-hand side of (5.7). For many Feynman rules, the underlying **BGR** are formally the same if the couplings or masses of the particles are not further specified. Assuming that the colour flow has been factorized as explained in App. 5.1.2, all fermion–fermion–vector rules, e.g.  $Ze \rightarrow e$ ,  $\gamma e \rightarrow e$ ,  $gu \rightarrow u$ ,  $Zu \rightarrow u$ , can be mapped onto the same structures realizing that  $\gamma^\mu \omega^+$  and  $\gamma^\mu \omega^-$  form a suitable basis,

$$\begin{aligned} w_\alpha &= \sum_{\beta, \delta, \mu} D_{\alpha\beta}^f (c_1 \gamma^\mu \omega^+ + c_2 \gamma^\mu \omega^-)_{\beta\delta} \times w_\mu \times w_\delta, \\ \bar{w}_\beta &= \sum_{\alpha, \delta, \mu} D_{\alpha\beta}^{\bar{f}} (c_1 \gamma^\mu \omega^+ + c_2 \gamma^\mu \omega^-)_{\delta\alpha} \times w_\mu \times \bar{w}_\delta, \\ w_\mu &= \sum_{\alpha, \beta, \nu} D_{\mu\nu}^V (c_1 \gamma^\nu \omega^+ + c_2 \gamma^\nu \omega^-)_{\alpha\beta} \times \bar{w}_\alpha \times w_\beta, \end{aligned} \quad (5.8)$$

with  $D_{\alpha\beta}^f, D_{\alpha\beta}^{\bar{f}}, D_{\mu\nu}^V$  denoting generic propagators for fermions, anti-fermions and vector bosons, respectively. REPT1L has the ability to derive a minimal basis, dynamically, i.e. depending on the operators of the theory, without relying on the Lorentz basis in the UFO format. This is done in two steps. In the first step, all distinct BGR in the underlying theory are registered. In the next step the BGR are merged recursively until a minimal basis is obtained. The size of the BGR can be controlled by a parameter for the maximal number of allowed distinct generic couplings. If a merge yields a BGR size larger than allowed, the merging is not accepted. Finally, all vertices are mapped to the minimal basis.

## 5.2 Counterterm expansion, renormalization and computation of $R_2$ terms

REPT1L supports an automated renormalization of model files following the standard procedure (see e.g. Ref. [84]). Here we give a quick summary of all the steps, followed by details on the counterterm expansion, the renormalization conditions, and the computation of rational terms of type  $R_2$ .

The starting point is a tree-level UFO model file. In the first step an independent set of parameters is identified, followed by a counterterm expansion. The RECOLA2 model file is derived once, enabling the formal counterterm expansion in REPT1L and leaving the values for counterterm parameters unspecified. Renormalization conditions are used to solve for counterterm parameters. The rational terms of type  $R_2$  are derived from vertex functions of the underlying theory. The model file is derived once again, including the counterterm expansion and explicit results for counterterm parameters and  $R_2$  terms. This yields the desired renormalized model file, ready for computation of processes supported by the underlying theory.

### 5.2.1 Counterterm expansion

In the default setup, REPT1L defines the counterterm expansion rules of the masses  $M_V, M_S, m_f$ , associated to scalars ( $S$ ), vector bosons ( $V$ ) and fermions ( $f$ ), of the not necessarily physical bosonic ( $\phi$ ) and fermionic fields ( $\psi$ ), and of a set of external couplings  $g_k$ , according to (see also Section 4.3.1)

$$\begin{aligned}
 M_V^2 &\rightarrow M_V^2 + \delta M_V^2, & M_S^2 &\rightarrow M_S^2 + \delta M_S^2, & m_f &\rightarrow m_f + \delta m_f, \\
 \phi_j &\rightarrow \sum_l \left( \delta_{jl} + \frac{1}{2} \delta Z_{jl} \right) \phi_l, & \psi_i^L &\rightarrow \left( 1 + \frac{1}{2} \delta Z_{L,i} \right) \psi^{L,i}, & \psi_i^R &\rightarrow \left( 1 + \frac{1}{2} \delta Z_{R,i} \right) \psi^{R,i}, \\
 g_k &\rightarrow g_k + \delta g_k,
 \end{aligned} \tag{5.9}$$

with  $\delta Z_{jl}$  being, in general, a non-diagonal matrix and L, R denoting the left- and right-handed components of fermionic fields, which, by default, are assumed to be diagonal. REPT1L automatically deals with counterterm dependencies if the parameters, being assigned a counterterm expansion, are declared as external parameters in the UFO format. Here, an external parameter is an independent parameter, whereas internal parameters depend on external ones and

their counterterm expansion can be determined by the chain rule. Once all parameters have a counterterm expansion, the most efficient way to generate counterterm vertices of the theory is through an expansion of the bare vertices via (5.9). It is possible to add counterterm vertices by hand, or, as a third alternative, to induce counterterm vertices from bare ones, which are not included in the model, via counterterm expansion rules. The latter is used to handle 2-point counterterms and counterterms originating from the gauge-fixing function since both of these types have no corresponding tree-level Feynman rules.

### 5.2.2 Renormalization conditions

The standard set of renormalization conditions given in Chapter 4 are implemented in REPT1L as conditions, rather than solutions to conditions, which are solved upon request. As an advantage of solving equations, the form of vertex functions or conventions can change without breaking the system. We assume standard renormalization of the physical fields and masses from the complex poles of Dyson-resummed propagators and their residues (see Section 4.3.2), while we allow for several choices of renormalization conditions for the gauge-fixing function and for unphysical fields. If the normalization condition is not fulfilled because e.g. the theory does not allow to employ the on-shell conditions, the LSZ factors need to be included by hand.<sup>4</sup> For the renormalization of couplings we support all the general schemes introduced in Section 4.5 and special schemes concerning the mixing angles in the THDM and HSESM, later given in Section 7.3. Note that REPT1L is not restricted to these renormalization conditions and custom ones can be implemented in PYTHON. Setting up renormalization conditions requires a RECOLA2 model file including counterterms.

The model-file derivation is done as discussed in the previous section with enabled vertex-counterterm expansion (see Fig. 5.1) and leaving the counterterm parameter unspecified. The renormalization conditions are derived analytically. To this end, REPT1L uses RECOLA2 to generate all the process skeletons required by the renormalization conditions. The results are written to a FORM file and evaluated, yielding vertex functions, which are parsed to Python and processed with SYMPY. The procedure is visualized in Fig. 5.2. REPT1L supports the renormalization of the same parameters in different schemes. All schemes are exported to the RECOLA2 model file and for a given parameter a specific scheme can be selected before the process generation phase. For instance, this system can be used to allow the user to choose between different QCD and EW renormalization schemes within the same model file. The same system is used for dealing with light fermions. In general, particles can be tagged as light particles, which, when a particle is subject to on-shell renormalization, makes REPT1L to renormalize the associated diagonal two-point function in three different setups, namely dimensional regularization, mass regularization and keeping the full mass dependence. In a RECOLA2 session a suited renormalization scheme for light particles is set automatically, depending on the choice of the mass value, unless a particle is explicitly required in a specific scheme. In the case of unstable particles, i.e. massive particles with finite widths, REPT1L applies, by default, the CMS as discussed in Section 4.4.

---

<sup>4</sup>The LSZ factors can be computed with REPT1L.

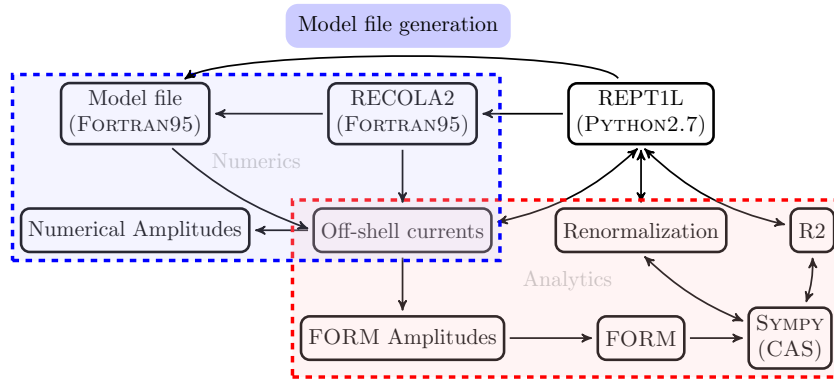


Figure 5.2: The REPT1L–RECOLA2 tool chain. REPT1L can generate tree-level model files which can then be used in combination with the RECOLA2 library to generate building blocks required in the renormalization process. The process generation is done via the same off-shell currents also used in numerical computations. The currents are evaluated analytically with FORM and further processed with SYMPY. The results are then available to REPT1L and are used in the renormalized model-file derivation. The red box indicates the analytic computations which uses the tool chain combining RECOLA2, FORM and SYMPY. After the renormalized model-file derivation, this tool chain and REPT1L are no longer needed. The blue box, i.e. RECOLA2 and model files, can be used as stand-alone versions (pure FORTRAN95) for numerical computations.

### 5.2.3 Computation of $R_2$ terms

In Section 4.1.2 we exemplified the computation of  $R_2$  which is inspired by the methods developed in Refs. [132, 133, 134]. REPT1L follows the same computation flow as for solving renormalization conditions as depicted in Fig. 5.2. For renormalizable theories it is possible to compute all  $R_2$  terms. To this end, REPT1L can generate the skeletons for all vertex functions of the theory that are potentially UV divergent according to power counting. FORM is used to construct each vertex function, replace tensor integrals by their pole parts and take the limit  $D \rightarrow 4$ . The finite parts are identified as Feynman rules associated to the original vertices, which are precisely the  $R_2$  terms. These steps are done in Python with the help of SYMPY.

The computation of tensor coefficients is performed in conventional dimensional regularization. Different regularizations will be supported in the future by exchanging the responsible FORM-procedure files.

In view of EFTs, the power counting can be disabled, and specific vertex functions can be selected. Further, the  $R_2$  extraction rules [132, 133, 134] have been extended to higher  $n$ -point functions and higher rank.<sup>5</sup> Finally, we remark that the computation of  $R_2$  can be run parallelized, which is done by default.

<sup>5</sup>3- and 4-point functions up to rank 6, 5- point functions up to rank 7 and 6-point functions up to rank 8.

## Validation methods

The validation of  $S$ -matrix elements is one of the most difficult and time-consuming issues in the calculation of processes in QFT. RECOLA2 did benefit from the parallel development with RECOLA which allowed to validate intermediate steps, finally guaranteeing the consistency with results tested at that time against independent approaches. At last, the automation and generality of RECOLA2 allowed to systematically validate all hard-coded elements in RECOLA, i.e. all the SM Feynman rules and BGR subroutines.

For BSM theories there are no other automated tools for EW corrections to compare with, if at all only individual calculations. For this reason, we decided to improve the reliability of RECOLA2 by supporting the BFM, which we introduce in Section 6.1 (partly taken from Ref. [52]). Alternatively, but less useful in practical calculations, we support the  $R_\xi$  gauge which is discussed in Section 6.2. The  $R_\xi$  gauge was used in App. C.1 to prove the gauge (in-)dependence (in that class of gauges) of specific  $S$ -matrix elements. Beyond that, the  $R_\xi$  gauge validated many aspects of RECOLA2 and REPT1L concerning high rank computations. Finally, in Section 6.3 further validation efforts are discussed.

### 6.1 Background-Field Method

The quantum realization of gauge theories requires to replace the concept of gauge invariance by the quantum analogue known as BRST invariance [76, 77, 78]. One of the reasons is the gauge-fixing procedure, being a necessity for a well-defined gauge-field propagator in perturbation theory, which breaks gauge, but not BRST invariance. Besides all the important consequences of BRST invariance, it implies non-linear symmetry transformations involving ghost fields in intermediate steps. Owing to the non-linearity, the resulting STI are less useful in practical calculations compared to the linear WI encountered in abelian theories. A quantum realization of gauge invariance is nevertheless possible within the BFM. The BFM is a powerful formulation for gauge theories which renders analytic calculations easier owing to a simple structure of the Feynman rules and additional symmetry relations. The method was originally derived by DeWitt in Refs. [135, 136] and has since then been used in many applications. The additional symmetry relation emerge for gauge theories in combination with a suited gauge-fixing term and imply the invariance of the theory under so-called Background-Field (BF) gauge invariance. This property is particularly useful for the calculations of  $\beta$  functions [137] in higher orders and is also of interest in beyond flat space-time quantum field theory. The BFM has been incorporated in REPT1L and RECOLA2 as an alternative way to calculate  $S$ -matrix elements,<sup>1</sup> and provides

<sup>1</sup> The construction of the  $S$ -matrix in the BFM requires special attention as has been shown in Ref. [138].

a powerful check of the consistency of the REPT1L/RECOLA tool-chain upon comparing to the conventional formulation. This feature is particularly useful for the validation of  $R_2$  terms where mistakes are difficult to spot. Besides the computational aspects, we use the BFM to formulate gauge-independent renormalization conditions in BSM models, presented in Section 7.3.<sup>2</sup> We stress that the BFM can be used as a complementary method in RECOLA2 and does not replace the usual formulation. Even though the use of the BFM in practical calculations is steered in precisely the same way as for model files in the conventional formulation, the internal machinery is different. In particular, the derivation of the Feynman rules and renormalization procedure requires special attention which is discussed in the following.

In Section 6.1.1 we give an introduction to the construction of the BFM action, following Ref. [140]. The application to THDM and HSESM is discussed in the Sections 6.1.2 and 6.1.3, starting with the definition of the fields, and followed by the construction of gauge-fixing functions and ghost terms. We make use of many ingredients of the SM BFM formulation [50] which are also valid in the THDM and HSESM. Finally, we conclude with subtleties concerning the renormalization in the BFM in Section 6.1.5.

### 6.1.1 The background-field effective action

The BF effective action  $\Gamma_{\text{BFM}}[\hat{\phi}]$ , as a functional of background fields  $\hat{\phi}$ , is constructed from an action  $S$  as follows. In the first step an auxiliary generating functional  $\tilde{Z}$  is defined in the presence of background fields  $\hat{\phi}$  via

$$\tilde{Z}[j; \hat{\phi}] := \int D[\phi] \exp\left(iS[\phi + \hat{\phi}] + i \int d^4x j(x)\phi(x)\right), \quad (6.1)$$

where  $j$  generically denotes the source of a quantum field  $\phi$ . The usual generating functional is recovered as  $Z[j] = \tilde{Z}[j; 0]$ . Following the standard computations for the effective action via Legendre transformation, denoting  $\Gamma$  and  $\tilde{\Gamma}$  as the effective actions corresponding to the generating functionals  $Z$  and  $\tilde{Z}$ , respectively, the original effective action  $\Gamma$  is related to  $\tilde{\Gamma}$  as

$$\tilde{\Gamma}[\bar{\phi}, \hat{\phi}] = \Gamma[\hat{\phi} + \bar{\phi}], \quad (6.2)$$

with the field  $\bar{\phi}$  being defined as

$$\bar{\phi}(j) = \left. \frac{\partial \log \tilde{Z}[j; \hat{\phi}]}{\partial j} \right|_{j=0}. \quad (6.3)$$

Therefore, the original effective action  $\Gamma$  can be computed using  $\tilde{\Gamma}[0, \hat{\phi}]$  instead, performing functional derivatives wrt background fields. The quantum fields exclusively appear in loops, whereas the background fields appear as external lines. Thus, the splitting of fields in (6.1) separates the classical solutions of the field equations, represented by background fields, from

---

<sup>2</sup>Note that the formulation of renormalization conditions in a definite gauge is controversial. Nevertheless, if done in the BFM, one benefits from gauge invariance and the fact that the BFM is viable beyond one-loop order (see e.g. Ref. [139]).

the excitation modes, represented by quantum fields. Finally, we define the **BF** effective action via  $\tilde{\Gamma}$ , requiring in addition gauge invariance under **BF** gauge transformations

$$\Gamma_{\text{BFM}}[\hat{\phi}] := \tilde{\Gamma}[\bar{\phi}, \hat{\phi}] \Big|_{\bar{\phi}=0} = \Gamma[\hat{\phi}], \quad \delta\Gamma_{\text{BFM}}[\hat{\phi}] = 0. \quad (6.4)$$

The requirement of **BF** gauge invariance severely restricts the structure of the gauge-fixing function as discussed in Section 6.1.3. Once a suited gauge-fixing function is found, the standard procedure for constructing a ghost term is performed as done in Section 6.1.4.

### 6.1.2 Background and quantum fields in extended Higgs sectors

The **BFM** splits fields into background and quantum fields and combines the new action with a special choice for the gauge-fixing function resulting in a manifest **BF** gauge invariance for the effective action on the quantum level. The Feynman rules are derived as usual, treating background and quantum fields on equal footing.<sup>3</sup> In principle, the splitting can be done for every field in the theory, however, as one is only interested in a **BF** gauge-invariant action, it is sufficient to shift fields which enter the gauge-fixing function. Thus, we perform

$$\begin{aligned} W^{a,\mu} &\rightarrow \underline{W}^{a,\mu} := W^{a,\mu} + \hat{W}^{a,\mu}, & B^\mu &\rightarrow \underline{B}^\mu := B^\mu + \hat{B}^\mu, \\ \Phi_i &\rightarrow \underline{\Phi}_i := \Phi_i + \hat{\Phi}_i, & S &\rightarrow \underline{S} := S + \hat{S}, \end{aligned} \quad (6.5)$$

where  $W^a$  ( $\hat{W}^a$ ) and  $B$  ( $\hat{B}$ ) are the **SM** quantum (background) gauge fields in the gauge eigenbasis with  $a = 1, 2, 3$ . The index  $i$  runs over all Higgs doublets  $\Phi_i$  in the theory under consideration and  $S$  is a singlet field, absent in the **THDM** or **SM**. The singlet field  $S$  does not appear explicitly in the gauge-fixing function [see (6.11)], but the inclusion of  $S$  in the splitting (6.5) is necessary due to the mixing with the neutral component of a Higgs doublet. The components for the background and quantum field doublets are defined as

$$\Phi_i = \begin{pmatrix} \phi_i^+ \\ \frac{1}{\sqrt{2}}(\rho_i + i\eta_i) \end{pmatrix}, \quad \hat{\Phi}_i = \begin{pmatrix} \hat{\phi}_i^+ \\ \frac{1}{\sqrt{2}}(v_i + \hat{\rho}_i + i\hat{\eta}_i) \end{pmatrix}. \quad (6.6)$$

### 6.1.3 Background-field gauge-invariant gauge-fixing function

Before dealing with the gauge-fixing term we demonstrate how **BF** gauge invariance is realized which is somewhat less obvious than the usual proofs of gauge invariance. The details discussed in the following are relevant if the reader is interested in understanding the **BRST** quantization in the **BFM**, in particular, the precise form of the gauge-fixing functions and ghost terms, otherwise skip to Eq. (6.11). We follow the arguments of Ref. [140] and extend them to the case with **SSB** focusing only on the **EW** sector.

The background fields are defined to transform in the same way as the fields in the conventional

<sup>3</sup>The **UFO** model files in the **BFM** were derived with **FEYNRULES**.

formulation, i.e. under representations of the **SM** gauge group in the following way

$$\delta\hat{W}_\mu = \partial_\mu\alpha^a - g \sum_{b,c=1}^3 \epsilon^{abc}\hat{W}_\mu^b\alpha^c, \quad \delta\hat{B}_\mu = \partial_\mu\beta, \quad \delta\hat{\Phi}_i = \frac{i}{2} \left( g \sum_{a=1}^3 \sigma^a\alpha^a - g'\sigma^0\beta \right) \hat{\Phi}_i, \quad (6.7)$$

with  $\sigma^a(\alpha^a)$  being the generators (gauge parameters) of  $SU(2)_w$  with structure constants  $\epsilon^{abc}$ , and  $\sigma^0(\beta)$  being the generator (gauge parameter) of the hypercharge, represented by a  $2 \times 2$  unit matrix. By performing a **BF** gauge transformation (6.7) on (6.1), gauge invariance is only manifest upon using additional gauge rotations as follows

$$\begin{aligned} \delta W_\mu^a &= -g\epsilon^{abc}\alpha^b W_\mu^c, & \delta j_\mu^a &= -g\epsilon^{abc}\alpha^b j_\mu^c, \\ \delta\Phi_i &= \frac{i}{2} \left( g \sum_{a=1}^3 \sigma^a\alpha^a - g'\sigma^0\beta \right) \Phi_i, & \delta j_i &= \frac{i}{2} \left( g \sum_{a=1}^3 \sigma^a\alpha^a - g'\sigma^0\beta \right) j_i, \end{aligned} \quad (6.8)$$

where  $j_\mu^a(j_i)$  represents the source to the  $W_\mu^a(\Phi_i)$  field. The field transformations of quantum fields are based on the freedom of choosing coordinates in the path integral, but the transformations for the sources  $\delta j_\mu^a, \delta j_i$  need to be included in the **BF** transformations in (6.7). It follows that source terms remain invariant

$$\delta(W_\mu^a j^{a,\mu}) = 0, \quad \delta(\Phi_i^\dagger j_i) = 0, \quad \delta(j_i^\dagger \Phi_i) = 0. \quad (6.9)$$

One observes that the **BF** gauge transformations (6.7) and the subsequent gauge rotations (6.8) act as uniform gauge transformation on shifted fields, e.g.

$$\delta(\Phi_i + \hat{\Phi}_i) \stackrel{(6.7),(6.8)}{\rightarrow} \frac{i}{2} \left( g \sum_{a=1}^3 \sigma^a\alpha^a - g'\sigma^0\beta \right) (\Phi_i + \hat{\Phi}_i). \quad (6.10)$$

From this we conclude the **BF** gauge invariance of the shifted action  $S[\phi + \hat{\phi}]$  because it was gauge-invariant prior to the field-shift by definition.

The gauge-fixing function is constructed in such a way to prevent mixings between the quantum gauge and quantum Goldstone bosons. This requirement can be realized in a family of gauge-fixing functions parametrized by one gauge parameter, similar to the  $R_\xi$  gauges in the conventional formulation. Since the  $R_\xi$  gauge in the **BFM** is not supported in **RECOLA**,<sup>4</sup> we restrict ourselves to the 't Hooft–Feynman gauge. The quantum gauge-fixing term has the traditional form. In the gauge eigenbasis it reads

$$\mathcal{L}_{\text{GF}} = -\frac{1}{2} \sum_{a=1}^3 (F_W^a)^2 - \frac{1}{2} F_B^2. \quad (6.11)$$

The standard ansatz for the gauge-fixing functions  $F \sim \partial^\mu A_\mu - igvG$  with  $A$  being a quantum gauge field,  $v$  the **vev** and  $G$  a Goldstone boson is not **BF** gauge invariant, but can be made so at the cost of non-linear gauge-fixing functions. To this end, the derivatives in the usual

<sup>4</sup>This is due to the necessity of having an  $R_\xi$  gauge photon propagator which is not supported. See Section 6.2 for more details.



gauge-fixing functions are augmented to covariant derivatives and the Higgs doublets are used to construct triplet and singlet states under  $SU(2)_W \times U(1)_Y$ . The resulting gauge-fixing functions are simple generalizations of the ones given in Ref. [50]

$$\begin{aligned} F_W^a &= \hat{D}^\mu W_\mu^a - i \frac{g}{2} \sum_i \left[ \hat{\Phi}_i^\dagger \sigma^a \Phi_i - \Phi_i^\dagger \sigma^a \hat{\Phi}_i \right], \\ F_B &= \partial^\mu B_\mu + i \frac{g'}{2} \sum_i \left[ \hat{\Phi}_i^\dagger \Phi_i - \Phi_i^\dagger \hat{\Phi}_i \right], \end{aligned} \quad (6.12)$$

with  $i$  running over the number of Higgs-doublets in the theory.<sup>5</sup> The gauge-fixing term (6.11) with gauge-fixing functions (6.12) is invariant under BF gauge transformations (6.7), (6.8). Notice that the covariant derivatives in (6.11) are defined with a pure BF gauge connection.

### 6.1.4 Construction of the ghost function

For the construction of the ghost term we follow the standard BRST quantization procedure, see e.g. Ref. [102]. In a first step the BRST transformation for physical fields and Goldstone boson fields are derived from the gauge transformations (6.7) by replacing the gauge parameters with

$$\alpha \rightarrow u_W, \quad \beta \rightarrow u_B, \quad (6.13)$$

where  $(\bar{u}_W^a) u_W^a$  and  $(\bar{u}_B) u_B$  are (anti-) ghost fields of the gauge eigenstates  $W^a$  and  $B$ . From the requirement of BRST invariance together with the precise structure of gauge-fixing term (6.11) the ghost Lagrangian can be constructed as

$$\mathcal{L}_{\text{ghost}} = - \sum_{a=1}^3 \bar{u}_W^a \delta_B F_W^a - \bar{u}_B \delta_B F_B. \quad (6.14)$$

After SSB the gauge fields are rotated into mass and charge eigenstates in the following way

$$\begin{aligned} W_\mu^1 &= \frac{W_\mu^- + W_\mu^+}{\sqrt{2}}, & W_\mu^2 &= \frac{W_\mu^- - W_\mu^+}{i\sqrt{2}}, & W_\mu^3 &= c_w Z_\mu - s_w A_\mu, & B_\mu &= s_w Z_\mu + c_w A_\mu, \\ u_W^1 &= \frac{u_W^- + u_W^+}{\sqrt{2}}, & u_W^2 &= \frac{u_W^- - u_W^+}{i\sqrt{2}}, & u_W^3 &= c_w u_Z - s_w u_A, & u_B &= s_w u_Z + c_w u_A. \end{aligned} \quad (6.15)$$

The BRST transformations are defined on quantum-fields, and are obtained by applying (6.13) to the corresponding gauge transformations (6.7) for quantum fields, with shifted gauge-field connections (6.5). Expressing the result in the gauge eigenbasis yields

$$\begin{aligned} \delta_B W_\mu^1 &= \underline{D}_\mu u_W^1 = \\ &= \frac{1}{\sqrt{2}} \partial_\mu (u_W^- + u_W^+) - \frac{ie}{\sqrt{2}} \left[ (u_W^- - u_W^+) \left( A_\mu - \frac{c_w}{s_w} Z_\mu \right) + \left( u_A - \frac{c_w}{s_w} u_Z \right) (W_\mu^+ - W_\mu^-) \right], \\ \delta_B W_\mu^2 &= \underline{D}_\mu u_W^2 = \end{aligned} \quad (6.16)$$

<sup>5</sup> $i = 1, 2$  for the THDM and  $i = 1$  for the SM and HSESM model.

$$\frac{i}{\sqrt{2}}\partial_\mu (u_W^+ - u_W^-) - \frac{e}{\sqrt{2}} \left[ (u_W^- + u_W^+) \left( \underline{A}_\mu - \frac{c_w}{s_w} \underline{Z}_\mu \right) - \left( u_A - \frac{c_w}{s_w} u_Z \right) (\underline{W}_\mu^+ + \underline{W}_\mu^-) \right], \quad (6.17)$$

$$\delta_B W_\mu^3 = \underline{D}_\mu u_W^3 = \partial_\mu (c_w u_Z - s_w u_A) - \frac{ie}{s_w} (u_W^- \underline{W}^+ - u_W^+ \underline{W}^-), \quad (6.18)$$

$$\delta_B B_\mu = \underline{D}_\mu u_B = \partial_\mu (c_w u_A + s_w u_Z). \quad (6.19)$$

Note that in contrast to the conventional formalism, the covariant derivatives entering the **BRST** transformations use the shifted gauge fields (6.5). For the Higgs doublets the **BRST** transformation rules can be defined at the level of components as follows

$$\delta_B \Phi_i := \begin{pmatrix} \delta_B \phi_i^+ \\ \frac{1}{\sqrt{2}} (\delta_B \rho_i + i \delta_B \eta_i) \end{pmatrix}, \quad (6.20)$$

with

$$\delta_B \phi_i^+ = \frac{ie}{2s_w} (i\eta_i + \rho_i + v_i) u_W^+ + \frac{ie(c_w^2 - s_w^2)}{2c_w s_w} \phi_i^+ u_Z - ie \phi_i^+ u_A, \quad (6.21)$$

$$\delta_B \rho_i = \frac{e}{2c_w s_w} \eta_i u_Z + \frac{ie}{2s_w} (\phi_i^+ u_W^- - \phi_i^- u_W^+), \quad (6.22)$$

$$\delta_B \eta_i = -\frac{e}{2c_w s_w} (\rho_i + v_i) u_Z + \frac{e}{2s_w} (\phi_i^+ u_W^- + \phi_i^- u_W^+). \quad (6.23)$$

The transformations for  $\delta_B \rho_i$  and  $\delta_B \eta_i$  are fixed by taking the real and imaginary parts of the **BRST** transformation of the lower doublet component, respectively. In this way, if the ghost term is formulated directly in the physical basis, as it is done in Ref. [50], the Lagrangian is guaranteed to be hermitian.

### 6.1.5 Renormalization and implementation details

The renormalization in the **BFM** follows the same procedure as described in Section 4.3, except that only background fields need to be renormalized. Moreover, the fully automated renormalization procedure as implemented in **REPT1L** (see Chapter 5) can be used within the **BFM**. This is made possible since **REPT1L** can distinguish between both types of fields by checking the field-type attribute. A field can be assigned to be a background and/or quantum field. In the conventional formalism, all fields play both roles and can thus appear in tree and loop amplitudes. In the presence of pure quantum fields, as it is the case in the **BFM**, the only contributing Feynman rules to tree and one-loop amplitudes are the ones with exactly none or two quantum fields.

Since we aim at the computation of  $S$ -matrix elements, an on-shell renormalization of physical fields is suited, and the conditions of Section 4.3.2 are employed for background fields. However, fixing the field renormalization constants of background fields via on-shell conditions breaks **BF** invariance and, as a consequence, some **BF WI** are not fulfilled. The reason is that **BF** gauge invariance requires e.g. a uniform renormalization of all covariant derivatives in the theory which is only possible if the field renormalization constants are not independent parameters but chosen accordingly [50]. The breaking of the **BF WI** does not pose a problem since this

additional symmetry is not mandatory for the renormalizability of the theory. Yet, one does not break the QED BF WI (4.105), which is valid also for EW theory in the BFM in contrast to the conventional formalism. Thus, requiring (4.105) yields the well-known one-loop relation in the BFM [50]

$$\delta Z_e = -\frac{\delta Z_A}{2}, \quad (6.24)$$

corresponding to the TL (Section 4.5.1).

Concerning the Fermi scheme introduced in Section 4.5.1 one cannot make use of the expression for  $\Delta r$  given in (4.109) which is valid for the conventional formulation in the 't Hooft–Feynman gauge, but not in the BFM since mixing and self-energies, or, in general, vertex functions differ by gauge-dependent terms in both formulations. Since the parameter  $\Delta r$  connects physical quantities it is necessarily gauge-independent, which implies that both formulations differ merely by a reshuffling of gauge-dependent terms between the self-energy and vertex parts. We have determined the difference in the vertex corrections between the BFM and conventional formulation in the 't Hooft–Feynman gauge, and, as expected, it cancels against the difference in the W self-energy. For a model-independent evaluation in the BFM, the result can be expressed in the same form as (4.109), but with a modified vertex correction<sup>6</sup>

$$\begin{aligned} \Delta r = & \frac{\Sigma_{WW}^{\text{1PI,BFM,T}}(0) - \Sigma_{WW}^{\text{1PI,BFM,T}}(\mu_W^2)}{\mu_W^2} + \frac{2}{c_w s_w} \frac{\Sigma_{AZ}^{\text{1PI,BFM,T}}(0)}{\mu_Z^2} + \frac{2\delta g}{g} \\ & + \frac{g^2}{16\pi^2} \left[ \frac{\log(c_w^2)}{s_w^2} \left( -\frac{1}{2} + 2s_w^2 \right) + 2 \right], \end{aligned} \quad (6.25)$$

which is valid only in the 't Hooft–Feynman gauge in the BFM.

Another subtlety concerns the renormalization within the CMS. REPT1L automatically renormalizes unstable particles in the CMS following the steps given in Section 4.4. The corresponding on-shell renormalization conditions require scalar integrals to be analytically continued to complex squared momenta. As we explained, this can be avoided by using an expansion around real momentum arguments,<sup>7</sup> which, however, gives rise to gauge-dependent terms of higher perturbative orders. Thus, comparing the BFM to the conventional formalism leads to somewhat different results for finite widths. The effect can be traced back to the difference of full self-energies in both formulations, e.g. the difference in the W self-energy is given by

$$\Sigma_{WW}^{\mu\nu,\text{BFM}}(p) - \Sigma_{WW}^{\mu\nu}(p) = \frac{g^2}{4\pi^2} (\mu_W^2 - p^2) g^{\mu\nu} [c_w^2 B_0(p^2, \mu_Z, \mu_W) + s_w^2 B_0(p^2, 0, \mu_W)], \quad (6.26)$$

with the conventions for scalar integrals given in App. A.1. The gauge dependence drops out in the mass renormalization constant, i.e.  $\delta\mu_W^2{}^{\text{BFM}} = \delta\mu_W^2$  in the CMS, because the self-energy is evaluated on the complex pole, i.e. for  $p^2 = \mu_W^2$ . However, performing an expansion of the self-

<sup>6</sup>Note that  $\Sigma_{AZ}^{\text{1PI,BFM,T}}(0)$  is zero in the BFM due to a Ward identity.

<sup>7</sup>The expansion breaks down for IR-singular contributions resulting from virtual gluons or photons. This can be corrected by including additional terms (see Ref. [97]), which is automatically handled in REPT1L as described in Section 4.4.2.

energy around the real mass  $M_W^2$  results in differences of the order of  $\mathcal{O}(\alpha^3)$ . For a comparison of both formulations it is useful to modify the expanded (exp) mass counterterm to match the conventional formalism in the following way

$$\begin{aligned} \delta\mu_{W,\text{exp}}^2{}^{\text{BFM}} &\rightarrow \delta\mu_{W,\text{exp}}^2 = \\ &= \delta\mu_{W,\text{exp}}^2{}^{\text{BFM}} - \frac{g^2}{4\pi^2} (M_W^2 - \mu_W^2)^2 [c_w^2 B'_0(M_W^2, \mu_Z, \mu_W) + s_w^2 B'_0(M_W^2, 0, \mu_W)], \end{aligned} \quad (6.27)$$

with  $B'_0$  being defined as the derivative of  $B_0$  with respect to  $p^2$ . Note that the difference is phenomenologically irrelevant.

## 6.2 $R_\xi$ gauge for massive vector bosons

The original motivation for the implementation of the  $R_\xi$  gauge in RECOLA2 was an alternative check of the gauge-parameter (in)dependence of  $S$ -matrix elements in combination with an  $\overline{\text{MS}}$  renormalization of the mixing angles as discussed in Section 4.2.3 (see also App. C.1). Beyond validation the  $R_\xi$  gauge is not very useful due to its additional computational cost at the one-loop level. Nevertheless, the implementation is valuable since the  $R_\xi$  gauge has validated, until then, untested aspects of REPT1L, most notably the capability of computations involving higher tensor ranks, both, in analytic as well as numerical calculations, thus proving the viability of REPT1L and RECOLA2 for more complicated theories.

In the following we describe the basic framework for the  $R_\xi$  gauge starting with the gauge-fixing function in Section 6.2.1. In Section 6.2.2 further details of the implementation are given, focusing on the numerator structure of the  $R_\xi$  gauge vector-boson propagators in one-loop BGR (3.27).

### 6.2.1 Gauge-fixing function

RECOLA2 supports  $R_\xi$  gauge propagators only for massive vector bosons. The restriction to the massive case comes from the fact that the photon  $R_\xi$  gauge propagator cannot be decomposed into single poles, but RECOLA2 only supports propagators with single poles and polynomial loop-momentum numerator structure. The use of the  $R_\xi$  gauge in RECOLA2 requires the Feynman rules to be derived in the  $R_\xi$  gauge with suited gauge-fixing functions. Starting from the generic gauge-fixing term defined as

$$\mathcal{L}_{\text{GF}} = -\frac{1}{\xi_W} C^+ C^- - \frac{1}{2\xi_Z} (C^Z)^2 - \frac{1}{2\xi_A} (C^A)^2, \quad (6.28)$$

a valid  $R_\xi$  gauge is given by the following gauge-fixing functions

$$C^A = \partial^\mu A_\mu, \quad C^Z = \partial^\mu Z_\mu - \xi_Z M_Z G_0, \quad C^\pm = \partial^\mu W_\mu^\pm \mp i\xi_W M_W G^\pm. \quad (6.29)$$

Here,  $\xi_A = 1$  is assumed and only listed in (6.28) for completeness. The  $R_\xi$  propagator for



The one-loop **BGR** requires to introduce a loop momentum  $q$  in propagator numerators as follows

$$\begin{aligned} \left( \text{diagram} \right)_{R_\xi} &= \text{diagram}_1 \Big|_{M_V} \left( -g^{\mu\nu} + \frac{(p+q)^\mu (p+q)^\nu}{M_V^2} \right) \\ &+ \text{diagram}_2 \Big|_{M_G} \left( -\frac{(p+q)^\mu (p+q)^\nu}{M_V^2} \right). \end{aligned} \quad (6.34)$$

The numerator structure needs to be combined with the vertex structure and ordered according to proper rank structure as explained in Section 3.4.

The automated renormalization and computation of rational terms presented in Chapter 5 can be used in the  $R_\xi$  gauge. Typically, we do not renormalize the gauge-fixing Lagrangian, i.e. we write it directly in terms of renormalized fields, which is sufficient to assure that all  $S$ -matrix elements are finite [75, 141]. REPT1L allows for alternative renormalization of the gauge-fixing term. Concerning the renormalization procedure, the only constraint is when employing the Fermi scheme where  $\Delta r$  (4.109) needs to be fixed to  $\xi_W = \xi_Z = 1$  since we have not determined the  $R_\xi$  gauge parameter dependence of the vertex and box corrections to the muon decay.

### 6.3 Automated testing suite

Since the release of RECOLA many further comparisons against independent approaches have been performed.<sup>9</sup> In order to prevent regression in the development of RECOLA2 an automated testing suite has been developed and integrated into REPT1L.<sup>10</sup> The starting point for each test is the tree-level **UFO** model file. For each test a minimal renormalization is performed and necessary rational terms are computed. The tests are defined for fixed phase-space points and compared to expected numerical results. All test are carried out in a fully automated way. In the current version, the following test cases are implemented:

**Pole approximation:** Various channels  $f\bar{f} \rightarrow V \rightarrow f\bar{f}$  with a resonant vector boson  $V$  are compared to validated results in RECOLA.

**Loop induced processes:** The loop-induced processes  $gg \rightarrow \gamma\gamma, hZ, WW, hh$  are validated against MADGRAPH5\_AMC@NLO.

**Off-shell  $t\bar{t}$  production in the SM:** We provide several tests for the off-shell production of  $t\bar{t}$  in the **SM** for the channels  $u\bar{u} \rightarrow e^+\nu_e b\mu^-\bar{\nu}_\mu\bar{b}$  and  $gg \rightarrow e^+\nu_e b\mu^-\nu_\mu\bar{b}$ . The **QCD** corrections are compared against MADGRAPH5\_AMC@NLO and RECOLA. The **EW** corrections are compared against RECOLA. Optionally, the tests for the full renormalized amplitudes can be run using the **BFM** in RECOLA2. These tests were performed together with M. Pellen.

**RG running of  $\alpha_s$ :** We test the running of  $\alpha_s$  to three different scales for  $t\bar{t}$  off-shell production in the channels  $u\bar{u} \rightarrow e^+\nu_e b\mu^-\bar{\nu}_\mu\bar{b}$  and  $gg \rightarrow e^+\nu_e b\mu^-\nu_\mu\bar{b}$ . The tests were performed together with M. Pellen.

<sup>9</sup>See Appendix B in Ref. [20] for a list of checks in RECOLA.

<sup>10</sup>Almost every aspect of REPT1L is tested thoroughly. More than 150 internal consistency tests, so-called unit tests, are implemented.

**Scalar 2-point functions in THDM:** All renormalized scalar two-point function of the extended Higgs-sector in the THDM are tested off-shell against an independent approach in QGRAF [142] and QGS, which an extension of GraphShot [143]. The tests were performed together with L. Jenniches.

$H_1 \rightarrow 4f$  **in the THDM:** This test compares results for Higgs decays into four fermions, which is closely related to the considered processes in Chapter 7, to an independent calculation [112] based on FEYNARTS/FORMCALC [15, 16] for various channels. The tests were performed together with L. Altenkamp.

**Anomalous TGC:** This test checks the anomalous CP-even and CP-odd triple gauge couplings (TGC) for the processes  $\bar{d}u \rightarrow \nu_e e^+ \gamma$ ,  $u\bar{u} \rightarrow W^+W^-$ ,  $u\bar{u} \rightarrow ZZ, \gamma Z$ ,  $\nu_e \bar{\nu}_e \rightarrow ZZ, \gamma Z$ . The tests are performed at NLO QCD, except for the neutrino-induced ones, which are performed at LO. The tests were compiled by M. Chiesa.

Besides the direct tests against independent calculations, REPT1L and RECOLA2 support several other consistency checks. For instance, during the renormalization procedure REPT1L explicitly checks that for massless particles the self-energy is proportional to the momentum squared  $p^2$ . For light particles, e.g. fermions in mass regularization, this has to hold in the massless limit such that indeed no mass counterterm is required. For the Fermi scheme (see Section 4.5.1) REPT1L verifies that  $\Delta r$  [Eq. (4.109)] is UV finite. In general, the UV finiteness of the theory can be verified numerically in RECOLA2 on a process by process approach at the phase-space level by varying the  $\mu_{UV}$  scale. This check also works in combination with  $\overline{\text{MS}}$  subtraction schemes, even though in this case amplitudes have an intrinsic scale dependence. To this end, we separate the scale dependence originating from the  $\overline{\text{MS}}$  subtraction, denoted as  $\mu_{\text{MS}}$ , from the UV one. The variation of the scale  $\mu_{\text{MS}}$  can be used to estimate missing higher-orders.

# Phenomenology in the HSESM and THDM

This chapter is based on Ref. [52]. We investigate two **BSM** Higgs-production processes at the **LHC**, namely Higgs production in association with a vector boson, usually referred to as Higgs strahlung, and Higgs production in association with two jets, known as Vector-Boson Fusion (**VBF**), in the **THDM** and **HSESM**. Those processes are particularly interesting for an extended Higgs sector, as they represent the next-to most dominant Higgs-production mechanisms at the **LHC**.

There has been enormous progress in higher-order calculations to Higgs strahlung and **VBF** in the **SM** and **BSM**. For Higgs strahlung the **QCD** corrections are known up to **NNLO** for inclusive [144, 145, 146] and differential [147, 148] cross sections. On-shell **EW** corrections were computed in Ref. [149] and followed by the off-shell calculation in Refs. [150, 151]. Higgs strahlung has also been investigated in the **THDM** with **QCD** [152] and **EW** [51] corrections. For **VBF**, the first one-loop **QCD** corrections were obtained in a structure-function approach [153] followed by the first two-loop prediction [154, 155] in the same framework. As for differential results, the first one-loop **QCD** and **EW** corrections were calculated in Ref. [156] and Refs. [157, 158], respectively. Since recently also the differential two-loop [159] and three-loop [160] **QCD** corrections are available. **VBF** has been interfaced to parton showers [161] and has been subject to studies for a 100 TeV collider [162]. In view of **BSM**, **VBF** has been studied in the **MSSM** [163]. Higgs strahlung and **VBF** are nowadays available in public codes, such as V2HV [164], MCFM [165], HAWK 2.0 [166] and VH@NNLO [167].

In Section 7.1 we give a brief description of the interface of RECOLA2 to HAWK 2.0, which has been used as Monte Carlo integrator. In Section 7.2 we fix the calculational setup and define the benchmark points, which were mainly taken from the Higgs Cross Section Working Group (**HXSWG**). For the numerical analysis we use different renormalization conditions for the mixing angles, which we introduce in Section 7.3. In Section 7.4 we present numerical results, discussing total cross sections in view of different renormalization schemes for light and heavy Higgs-boson production.

## 7.1 Interface to HAWK 2.0

In this section we describe the interface between HAWK 2.0 and RECOLA2 which allows for an automated computation of **NLO EW** and **QCD** corrections to observables in associated Higgs production with a vector boson and two jets. We start with the **LO** partonic channels and virtual



corrections and conclude with the computation of the real corrections. The implementation has been realized in a model-independent way, allowing in the future, apart from the two presented **BSM** models, for predictions in alternative models.

### 7.1.1 Process generation with RECOLA2

In the case of associated Higgs production with a vector boson, also known as Higgs strahlung, we consider processes with an intermediate vector boson decaying leptonically as

$$pp \rightarrow HV \rightarrow Hl^+l^- / Hl^\pm\nu / H\nu\nu. \quad (7.1)$$

Depending on the initial-state partons, the intermediate vector boson can be a  $Z$  or a  $W$  boson. For example for the signature  $pp \rightarrow HZ \rightarrow Hl^+l^-$ , neglecting the bottom contributions in the Parton Distribution Function (**PDF**), there are four different initial-state parton combinations:

$$u\bar{u}, \quad d\bar{d}, \quad c\bar{c}, \quad s\bar{s}. \quad (7.2)$$

Whenever possible, we optimize computations involving different quark generations. For instance, in (7.2) the processes involving the second generation are not computed explicitly, but the results for the first generation are employed instead. For the first generation of quarks the RECOLA2 library is used to generate the processes at tree and one-loop level.

The second process class under consideration is Higgs production in association with two hard jets

$$pp \rightarrow Hjj, \quad (7.3)$$

also known as **VBF**. There are plenty of partonic channels and, again, we exploit optimizations with respect to the different quark generations. For the **LO**, virtual **NLO EW**, virtual **NLO QCD**, real emission **EW**, and real emission **QCD** contributions RECOLA2 generates 32 partonic channels each, with the real kinematic channels corresponding to the Born kinematic ones, with an additional gluon or photon. For the gluon- and photon-induced channels RECOLA2 generates 20 channels each.

At the stage of the process definition the Higgs boson entering in (7.1) or (7.3) can be chosen freely<sup>1</sup> as long as it is supported by the RECOLA2 model file currently in use. For instance, in the case of the **THDM** the Higgs flavour can be set to  $H_1$ ,  $H_h$  or  $H_a$  (see Section 2.3), which is done in the HAWK 2.0 input file. In HAWK 2.0 the relevant parameters for process generation and computation are set by input files. This information is forwarded to RECOLA2, allowing to choose specific contributions. The selection works for individual corrections such as **QCD** or **EW** either virtual or real. For the results presented in this work we selected the pure **EW** corrections, including photon-induced corrections.

---

<sup>1</sup>Charged Higgs bosons are not supported by the HAWK 2.0 Monte Carlo. Pseudo-scalar Higgs-boson production is possible, but suppressed in the considered CP-conserving **THDM**.

### 7.1.2 Infrared divergences

The processes under consideration are not infrared safe and an IR subtraction scheme needs to be employed. We adhere to the Catani–Seymour dipole subtraction [168] which is used in HAWK 2.0 and employ mass regularization for soft and collinear divergences, i.e. a small photon mass and small fermion masses are used wherever needed. From the point of view of the interface, dealing with EW dipoles is a matter of replacing certain Born amplitudes with the ones computed by RECOLA2. As for the QCD dipoles one needs in general colour-correlated matrix elements. For processes with only two partons, as it is the case for Higgs strahlung, the colour correlation is diagonal due to colour conservation (see Eq. A1 [168]) and again no colour-correlated matrix elements are required. For VBF the internal construction of HAWK 2.0’s colour-correlated matrix elements has been replaced because intermediate building blocks, as used by HAWK 2.0, cannot be produced with RECOLA2. Instead, the colour-correlated matrix elements are computed directly with RECOLA2 and we use colour conservation to minimize the number of required computations. The dipoles are taken as implemented in HAWK 2.0. For the QCD dipoles consider Refs. [168, 169] and for EW dipoles see Refs. [170, 171].

## 7.2 Setup and benchmark points

### 7.2.1 Input parameters

For the numerical analysis in the two Higgs-boson production processes we use the following values for the SM input parameters [43]:

$$\begin{aligned} G_F &= 1.16638 \cdot 10^{-5} \text{ GeV}^{-2}, & m_t &= 173.21 \text{ GeV}, & M_h &= 125.09 \text{ GeV}, \\ M_W &= 80.385 \text{ GeV}, & \Gamma_W &= 2.0850 \text{ GeV}, & M_Z &= 91.1876 \text{ GeV}, & \Gamma_Z &= 2.4952 \text{ GeV}. \end{aligned} \quad (7.4)$$

For the THDM we present updated and new results for the benchmark points in Tables 7.1 and 7.2 as proposed by the HXSWG [172]. For the HSESM we compiled a list of benchmark points featuring different hierarchies and being compatible with the limits given in Refs. [56, 57].<sup>2</sup> The results include the SM-like and heavy Higgs-boson production for both models. The computation was carried out in the ’t Hooft–Feynman gauge both in the conventional formalism and in the BFM.

### 7.2.2 Cut setup

For the analysis of Higgs strahlung we consider the case of two charged muons in the final state,  $pp \rightarrow H\mu^+\mu^- + X$ . The muons are not recombined with collinear photons, and are assumed to be perfectly isolated, treated as bare muons as described in Ref. [150]. We use the cuts given in Ref. [173], i.e. we demand the muons to

- have transverse momentum  $p_{T,l} > 20 \text{ GeV}$  for  $l = \mu^+, \mu^-$ ,
- be central with rapidity  $|y_l| < 2.4$  for  $l = \mu^+, \mu^-$ ,

<sup>2</sup>Our conventions differ from those of Ref. [56]. We identify  $c_\alpha, t_\beta$  in Ref. [56] with  $-s_\alpha, 1/t_\beta$  in our conventions.

	$M_{H_h}$	$M_{H_a}$	$M_{H^\pm}$	$m_{12}$	$t_\beta$	$M_{\text{sb}}$
BP21A	200 GeV	500 GeV	200 GeV	135 GeV	1.5	198.7 GeV
BP21B	200 GeV	500 GeV	500 GeV	135 GeV	1.5	198.7 GeV
BP21C	400 GeV	225 GeV	225 GeV	0 GeV	1.5	0 GeV
BP21D	400 GeV	100 GeV	400 GeV	0 GeV	1.5	0 GeV
BP3A1	180 GeV	420 GeV	420 GeV	70.71 GeV	3	129.1 GeV

Table 7.1: **THDM** benchmark points in the alignment limit, i.e.  $s_{\alpha\beta} \rightarrow -1$ ,  $c_{\alpha\beta} \rightarrow 0$ , taken from Ref. [176]. The parameter  $M_{\text{sb}}$  depends on the other parameters and is given for convenience.

	$M_{H_h}$	$M_{H_a}$	$M_{H^\pm}$	$m_{12}$	$t_\beta$	$c_{\alpha\beta}$	$M_{\text{sb}}$
a-1	700 GeV	700 GeV	670 GeV	424.3 GeV	1.5	-0.0910	624.5 GeV
b-1	200 GeV	383 GeV	383 GeV	100 GeV	2.52	-0.0346	204.2 GeV
BP22A	500 GeV	500 GeV	500 GeV	187.08 GeV	7	0.28	500 GeV
BP3B1	200 GeV	420 GeV	420 GeV	77.78 GeV	3	0.3	142.0 GeV
BP3B2	200 GeV	420 GeV	420 GeV	77.78 GeV	3	0.5	142.0 GeV
BP43	263.7 GeV	6.3 GeV	308.3 GeV	52.32 GeV	1.9	0.14107	81.5 GeV
BP44	227.1 GeV	24.7 GeV	226.8 GeV	58.37 GeV	1.8	0.14107	89.6 GeV
BP45	210.2 GeV	63.06 GeV	333.5 GeV	69.2 GeV	2.4	0.71414	116.2 GeV

Table 7.2: **THDM** benchmark points outside the alignment limit taken from Ref. [177] (a-1, b-1) and Ref. [176]. The parameter  $M_{\text{sb}}$  depends on the other parameters and is given for convenience.

- have a pair invariant mass  $m_{\mu\mu}$  of  $75 \text{ GeV} < m_{\mu\mu} < 105 \text{ GeV}$ .

Further, we select boosted events with a

- transverse momentum  $p_{\text{T},\mu\mu} > 160 \text{ GeV}$ .

For VBF we employ the cuts as suggested by the HXSWG in Ref. [172], i.e. we require two hard jets  $j_i$ ,  $i = 1, 2$ , emerging from partons  $i$  with

- pseudo-rapidity  $|\eta_i| < 5$ .

The recombination is done in the anti- $k_T$  algorithm [174] with jet size  $D = 0.4$ . Further, events pass the cuts if the two hard jets have

- a transverse momentum  $p_{\text{T},j_i} > 19 \text{ GeV}$  each,
- a rapidity  $|y_{j_i}| < 5$  each,
- a rapidity difference  $|y_{j_1} - y_{j_2}| > 3$ ,
- an invariant mass  $M_{j_1j_2} > 130 \text{ GeV}$ .

We present the results for hadronic cross sections at the centre-of-mass energy of 13 TeV using the **NLO PDF** set NNPDF2.3 with **QED** corrections [175].

	$M_{H_h}/\text{GeV}$	$t_\beta$	$s_\alpha$
BP1	500	2.2	-0.979796
BP2	400	1.7	-0.96286
BP3	300	1.3	-0.950737
BP4	200	0.85	-0.932952
	$M_{H_1}/\text{GeV}$	$t_\beta$	$s_\alpha$
BP5	100	0.35	-0.35
BP6	50	0.2	-0.06

Table 7.3: HSESM benchmark points compiled from Ref. [178]. In the upper table typical scenarios are depicted with a heavy additional scalar Higgs boson. In the lower table inverted scenarios are listed with  $H_h$  identified as the SM Higgs boson and mass  $M_{H_h} = 125.09\text{ GeV}$ .

### 7.3 Renormalization conditions for mixing angles

The prime vertices of interest in the processes studied in Section 7.4 are the  $H_1VV$  and  $H_hVV$  vertices. Thus, the relevant one-loop corrections require to renormalize  $\alpha$  and  $\beta$  in the THDM and  $\alpha$ , but not  $\beta$ , in the HSESM. We present the counterterms for the mixing angles in an  $\overline{\text{MS}}$  scheme and two different on-shell schemes in the following:

$\overline{\text{MS}}$ : The mixing angles  $\alpha$ ,  $\beta$  are renormalized using  $\overline{\text{MS}}$  subtraction [51] for the vertices  $H_1 \rightarrow \tau^+\tau^-$ ,  $H_a \rightarrow \tau^+\tau^-$ , respectively, with  $\beta$  only being renormalized in the THDM. This is equivalent to using the identities

$$\begin{aligned}
 \delta\alpha &= \frac{\delta Z_{H_h H_1}^{\overline{\text{MS}}} - \delta Z_{H_1 H_h}^{\overline{\text{MS}}}}{4} = \frac{\Sigma_{H_h H_1}^{1\text{PI},\overline{\text{MS}}}(M_{H_h}^2) + \Sigma_{H_h H_1}^{1\text{PI},\overline{\text{MS}}}(M_{H_1}^2) + 2t_{H_1 H_h}^{\overline{\text{MS}}}}{2(M_{H_h}^2 - M_{H_1}^2)}, \\
 \delta\beta &= \frac{\delta Z_{G_0 H_a}^{\overline{\text{MS}}} - \delta Z_{H_a G_0}^{\overline{\text{MS}}}}{4} = -\frac{\Sigma_{H_a G_0}^{1\text{PI},\overline{\text{MS}}}(0) + \Sigma_{H_a G_0}^{1\text{PI},\overline{\text{MS}}}(M_{H_a}^2) + 2t_{H_a G_0}^{\overline{\text{MS}}}}{2M_{H_a}^2}
 \end{aligned} \tag{7.5}$$

with the relation for  $\delta\alpha$  being valid in the THDM and the HSESM and the one for  $\delta\beta$  only in the THDM. The origin of these relations can be traced back to the renormalizability of models in a minimal (symmetric) renormalization scheme. See Ref. [112] for the derivation of these and other UV-pole-part identities. The tadpole counterterms in (7.5) are treated in the *FJ Tadpole Scheme* Ref. [51] and using the renormalization condition (4.67) for tadpoles. Estimating the size of higher-order contributions via the usual scale variations has been improved via a partial resummation including the RG running of parameters.<sup>3</sup> For the THDM this requires to solve a coupled system of differential equations,

$$\begin{aligned}
 \frac{\partial}{\partial \log \mu^2} \alpha(\mu) &= f_\alpha(\alpha(\mu), \beta(\mu), M_{\text{sb}}(\mu)), \\
 \frac{\partial}{\partial \log \mu^2} \beta(\mu) &= f_\beta(\alpha(\mu), \beta(\mu), M_{\text{sb}}(\mu)),
 \end{aligned}$$

<sup>3</sup>In Ref. [112] the running of the mixing angles is investigated within various  $\overline{\text{MS}}$  and tadpole counterterm schemes in the THDM.

BP	$t_\beta(\mu_0/2)$	$c_{\alpha\beta}(\mu_0/2)$	$M_{\text{sb}}(\mu_0/2)/\text{GeV}$	$t_\beta(2\mu_0)$	$c_{\alpha\beta}(2\mu_0)$	$M_{\text{sb}}(2\mu_0)/\text{GeV}$
BP21A	1.41	-0.1166	192.3	1.54	0.0504	197.7
BP21B	1.16	-0.4163	199.7	1.51	0.0293	191.2
BP21C	1.40	-0.0029	0.0	1.64	0.0067	0.0
BP21D	1.37	-0.0017	0.0	1.68	-0.0119	0.0
BP3A1	2.34	-0.0681	121.6	3.53	0.1701	133.8
a1	0.86	-0.3801	614.1	1.78	-0.0202	638.5
b1	2.36	-0.1542	203.6	2.59	0.0116	203.3
BP22A	—	—	—	1.52	0.6538	274.5
BP3B1	3.15	0.1292	149.3	2.24	0.5972	123.8
BP3B2	4.17	0.2992	167.9	1.99	0.7809	119.3
BP43	1.76	0.0997	80.7	2.08	0.1906	82.8
BP44	1.66	0.1313	88.1	1.97	0.1511	91.5
BP45	2.29	0.6504	115.1	2.53	0.7666	117.5

Table 7.4: Running values for  $t_\beta$ ,  $c_{\alpha\beta}$  and  $M_{\text{sb}}$  in the THDM at the scales  $\mu_0/2$  and  $2\mu_0$ . The benchmark points are defined at the central scale  $\mu_0$  in Tables 7.1 and 7.2. The results for the alignment-limit scenarios are in the upper part of the table whereas the non-alignment scenarios are in the lower part. For BP22A the running  $\beta$  reaches  $\pi/2$  for a scale greater than  $\mu_0/2$ , thus,  $t_\beta$  becomes singular.

$$\frac{\partial}{\partial \log \mu^2} M_{\text{sb}}(\mu) = f_{M_{\text{sb}}}(\alpha(\mu), \beta(\mu), M_{\text{sb}}(\mu)). \quad (7.6)$$

The functions  $f_\alpha$ ,  $f_\beta$  and  $f_{M_{\text{sb}}}$  can be directly read off the pole parts of the corresponding counterterms. The counterterm  $\delta M_{\text{sb}}$  was fixed from the vertex  $H_h \rightarrow H^+ H^-$  in the  $\overline{\text{MS}}$  scheme. Note that  $\delta M_{\text{sb}}$  does not enter the considered processes at fixed one-loop order. For the HSESM we keep  $\beta$  fixed, assuming no scale dependence, resulting in a simple differential equation for  $\alpha$ ,

$$\frac{\partial}{\partial \log \mu^2} \alpha(\mu) = f_\alpha(\alpha(\mu)). \quad (7.7)$$

The (coupled) system has been solved to run the parameters from the reference scale  $\mu_0$  to  $\mu = \mu_0/2$  and  $\mu = 2\mu_0$ . The results are presented in Tables 7.4 and 7.5 for the benchmark points of Tables 7.1, 7.2, and 7.3 being defined at the typical scale of the process,  $\mu_0 = 2M_{H_1}$  if not stated otherwise.<sup>4</sup> The cross sections are evaluated at the scales  $\mu_0/2, \mu_0, 2\mu_0$ , using the running parameters of  $c_{\alpha\beta}$ ,  $t_\beta$ ,  $M_{\text{sb}}$  ( $s_\alpha$ ) at the corresponding scale as input parameters in the THDM (HSESM). The three different predictions for  $\sigma_{\text{NLO}}^{\text{EW}}$  normalized to the leading-order cross section  $\sigma_{\text{LO}}(\mu_0)$  at the central scale  $\mu_0$  and scale-dependent relative EW corrections are defined as

$$\delta_{\text{EW}}(\mu, \mu_0) := \frac{\sigma_{\text{NLO}}^{\text{EW}}(\mu) - \sigma_{\text{LO}}(\mu_0)}{\sigma_{\text{LO}}(\mu_0)}, \quad (7.8)$$

<sup>4</sup>Note that the running of parameters is independent of the scale at which they are defined.

BP	$s_\alpha(\mu_0/2)$	$s_\alpha(2\mu_0)$
BP1	-0.9802	-0.9794
BP2	-0.9646	-0.9612
BP3	-0.9557	-0.9455
BP4	-0.9367	-0.9293
BP5	-0.2780	-0.4463
BP6	-0.04647	-0.08194

Table 7.5: Running values for  $s_\alpha$  in the HSESM at the scales  $\mu_0/2$  and  $2\mu_0$ . The benchmark points are defined at the central scale  $\mu_0$  in Table 7.3.

such that

$$\sigma_{\text{NLO}}(\mu) = \left(1 + \delta_{\text{EW}}(\mu, \mu_0)\right) \sigma_{\text{LO}}(\mu_0). \quad (7.9)$$

Note that the tree-level matrix elements only depend on the scale through the running of parameters, whereas the one-loop matrix elements have an explicit scale dependence. As a shorthand notation for the relative corrections in the  $\overline{\text{MS}}$  scheme we use

$$\begin{aligned} \delta_{\text{EW}}^{\overline{\text{MS}}} &:= \delta_{\text{EW}}(\mu_0, \mu_0)_d^u, \\ u &:= \delta_{\text{EW}}(2\mu_0, \mu_0) - \delta_{\text{EW}}(\mu_0, \mu_0), \\ d &:= \delta_{\text{EW}}\left(\frac{\mu_0}{2}, \mu_0\right) - \delta_{\text{EW}}(\mu_0, \mu_0) \end{aligned} \quad (7.10)$$

with  $u$  and  $d$  being the upper and lower edges of the scale variation (see e.g. Table 7.6).

$p^*$ : The renormalized mixing angles  $\alpha$  and  $\beta$  are defined to diagonalize radiatively corrected mass matrices which implies a scale and momentum dependence for the mixing angles. The scale dependence can be eliminated by a special choice for the momentum  $p^2 = (p^*)^2$  at which the mixing two-point functions, and thus the running mixing angles, are evaluated. The original idea goes back to Ref. [179] (see also Ref. [180]) and has been applied to the HSESM in Ref. [178] and the THDM in Ref. [129]. In our conventions, the counterterms are defined as

$$\delta\alpha = \frac{\Sigma_{H_h H_1}^{\text{1PI, BFM}}\left(\frac{M_{H_h}^2 + M_{H_1}^2}{2}\right) + t_{H_1 H_h}}{M_{H_h}^2 - M_{H_1}^2}, \quad \delta\beta = -\frac{\Sigma_{H_a G_0}^{\text{1PI, BFM}}\left(\frac{M_{H_a}^2}{2}\right) + t_{H_a G_0}}{M_{H_a}^2}. \quad (7.11)$$

Note that for  $\delta\beta$  alternatively the mixing energy with the charged Higgs and Goldstone boson can be used. As the mixing energies are gauge-dependent an additional intrinsic prescription is required to fix the gauge-independent parts. We choose the BFM with quantum gauge parameter  $\xi_Q = 1$ , which corresponds to the gauge-fixing functions (6.11), (6.12). We remark that this is equivalent [181, 182] to the self-energy in the pinch technique [126, 127].

**BFM:** As an on-shell alternative to the  $p^*$  scheme, the authors of Ref. [129] propose to use the

on-shell scalar mixing energies defined within the pinch technique which has also been investigated in Ref. [183]. In our framework, this corresponds to

$$\begin{aligned}\delta\alpha &= \frac{\delta Z_{H_h H_1}^{\text{BFM}} - \delta Z_{H_1 H_h}^{\text{BFM}}}{4} = \frac{\Sigma_{H_h H_1}^{\text{1PI,BFM}}(M_{H_h}^2) + \Sigma_{H_1 H_h}^{\text{1PI,BFM}}(M_{H_1}^2) + 2t_{H_1 H_h}}{2(M_{H_h}^2 - M_{H_1}^2)}, \\ \delta\beta &= \frac{\delta Z_{G_0 H_a}^{\text{BFM}} - \delta Z_{H_a G_0}^{\text{BFM}}}{4} = -\frac{\Sigma_{H_a G_0}^{\text{1PI,BFM}}(0) + \Sigma_{H_a G_0}^{\text{1PI,BFM}}(M_{H_a}^2) + 2t_{H_a G_0}}{2M_{H_a}^2},\end{aligned}\quad (7.12)$$

with the mixing energies evaluated in the **BFM** with quantum gauge parameter  $\xi_Q = 1$ .

We note that the use of  $\overline{\text{MS}}$  schemes for the mixing angles in combination with alternative tadpole counterterm schemes can be made gauge-independent by including finite tadpole terms<sup>5</sup> which is equivalent to the use of the *FJ Tadpole Scheme*. As for the on-shell schemes in the 't Hooft–Feynman gauge any tadpole scheme can be used as tadpoles drop out [51], but for other gauges in the on-shell schemes one has to be careful due to a mismatch of the gauge prescription and the actual gauge-parameter choice (see Ref. [52]).

The results for total cross sections in the **BFM** renormalization scheme in Section 7.4 were not computed directly, but were obtained from the results in the  $p^*$  scheme using the following formulas, depending on the model (**THDM** or **HSESM**) and on the produced Higgs flavour ( $H_1$  or  $H_h$ ) as follows

$$\textbf{THDM } H_1: \delta_{\text{EW}}^{\text{BFM}} = \delta_{\text{EW}}^{p^*} - 2\frac{c_{\alpha\beta}}{s_{\alpha\beta}} (\delta\alpha^{p^*} - \delta\beta^{p^*} - \delta\alpha^{\text{BFM}} + \delta\beta^{\text{BFM}}),$$

$$\textbf{THDM } H_h: \delta_{\text{EW}}^{\text{BFM}} = \delta_{\text{EW}}^{p^*} + 2\frac{s_{\alpha\beta}}{c_{\alpha\beta}} (\delta\alpha^{p^*} - \delta\beta^{p^*} - \delta\alpha^{\text{BFM}} + \delta\beta^{\text{BFM}}),$$

$$\textbf{HSESM } H_1: \delta_{\text{EW}}^{\text{BFM}} = \delta_{\text{EW}}^{p^*} - 2\frac{c_\alpha}{s_\alpha} (\delta\alpha^{p^*} - \delta\alpha^{\text{BFM}}),$$

$$\textbf{HSESM } H_h: \delta_{\text{EW}}^{\text{BFM}} = \delta_{\text{EW}}^{p^*} + 2\frac{s_\alpha}{c_\alpha} (\delta\alpha^{p^*} - \delta\alpha^{\text{BFM}}).$$

Note that the formulas can be applied uniquely to the observables under consideration as these rely on the mixing-angle dependencies of the respective leading-order couplings.

## 7.4 Numerical results for total cross sections

In Table 7.6 we present results for the production of a **SM**-like Higgs boson in Higgs strahlung in the **THDM** in alignment scenarios. Non-alignment scenarios are given in Table 7.7. In Table 7.8 we provide the corresponding results for heavy Higgs-boson production in non-alignment scenarios. For the **HSESM** all considered scenarios are non-aligned. The results for light Higgs-boson production are given in Table 7.9, and the ones for heavy Higgs-boson production in Table 7.10. Note that for the benchmark points BP5 and BP6 with inverted hierarchy the heavy Higgs boson is **SM**-like with  $M_{H_h} = 125.09$  GeV. For the benchmark points in the **THDM** the light Higgs boson is always identified as the **SM** Higgs boson. Finally, in Table 7.11 results for **SM**-like and heavy Higgs-boson production in **VBF** are presented for the **THDM**. The **HSESM** predictions for **VBF** are given in Table 7.12.

<sup>5</sup>See Eq. (4.43) and the following ones in Ref. [112], Eq. (43) in Ref. [184], and Eq. (5.24) in Ref. [51].

BP	$\sigma_{\text{LO}}^{H_1}/\text{pb}$	$\delta_{\text{EW}}^{\overline{\text{MS}}}$	$\delta_{\text{EW}}^{p^*}$
BP21A	1.65	$-11.8^{+0.7\%}_{+2.3\%}$	$-11.8\%$
BP21B	1.65	$-13.0^{+1.2\%}_{-48\%}$	$-13.0\%$
BP21C	1.65	$-13.2^{-0.1\%}_{+0.1\%}$	$-13.2\%$
BP21D	1.65	$-13.6^{-0.2\%}_{+0.1\%}$	$-13.6\%$
BP3A1	1.65	$-13.3^{-6.4\%}_{+0.4\%}$	$-13.3\%$

Table 7.6: Relative NLO corrections  $\delta_{\text{EW}}$  to SM-like Higgs-boson production in Higgs strahlung  $pp \rightarrow H_1\mu^-\mu^+$  in alignment scenarios in the THDM. The results in the  $\overline{\text{MS}}$  scheme are given at the central scale  $\mu_0 = 2M_h = 250.18$  GeV with scale uncertainties estimated including the RG-running of parameters (7.10). Both on-shell schemes agree within the integration error, and only results in the  $p^*$  scheme are given. The SM EW correction is  $\delta_{\text{EW}} = -12.4\%$ .

BP	$\sigma_{\text{LO}}^{H_1}/\text{pb}$	$\delta_{\text{EW}}^{\overline{\text{MS}}}$	$\delta_{\text{EW}}^{p^*}$	$\delta_{\text{EW}}^{\text{BFM}}$
a-1	1.63	$-10.4^{-1.6\%}_{+40.0\%}$	$-12.6\%$	$-12.6\%$
b-1	1.64	$-12.9^{+0.5\%}_{+2.5\%}$	$-12.6\%$	$-12.6\%$
BP22A	1.52	$-40.5\%$	$-15.9\%$	$-15.9\%$
BP3B1	1.50	$-35.1^{-16.3\%}_{+29.7\%}$	$-13.4\%$	$-13.4\%$
BP3B2	1.23	$-66.6\%$	$-13.6\%$	$-13.6\%$
BP43	1.61	$-15.0^{-0.67\%}_{+1.2\%}$	$-12.6\%$	$-12.6\%$
BP44	1.61	$-11.2^{-3.4\%}$	$-12.6\%$	$-12.6\%$
BP45	0.806	$-31.3^{+4.3\%}_{-6.7\%}$	$-13.0\%$	$-13.0\%$

Table 7.7: Relative NLO corrections  $\delta_{\text{EW}}$  to SM-like Higgs-boson production in Higgs strahlung  $pp \rightarrow H_1\mu^-\mu^+$  in non-alignment scenarios in the THDM. The results in the  $\overline{\text{MS}}$  scheme are given at the central scale  $\mu_0 = 2M_h = 250.18$  GeV with scale uncertainties estimated including the RG-running of parameters (7.10). The scale uncertainties are large, and for some points (BP22A, BP3B2, BP44) the running is unstable and yields corrections beyond 100%, which is indicated as “-”.

BP	$\sigma_{\text{LO}}^{H_h}/\text{fb}$	$\delta_{\text{EW}}^{p^*}$	$\delta_{\text{EW}}^{\text{BFM}}$
BP22A	6.43	$-12.5\%$	$-12.9\%$
BP3B1	79.4	$-17.5\%$	$-17.4\%$
BP3B2	220.4	$-16.2\%$	$-16.1\%$
BP43	10.1	$-2.67\%$	$-2.74\%$
BP44	13.9	$-8.35\%$	$-8.39\%$
BP45	411.6	$-13.8\%$	$-13.8\%$

Table 7.8: Relative NLO corrections  $\delta_{\text{EW}}$  to heavy Higgs-boson  $H_h$  production in Higgs strahlung  $pp \rightarrow H_h\mu^-\mu^+$  in the THDM. No results for the  $\overline{\text{MS}}$  scheme are presented due to large scale uncertainties exceeding 100%.



BP	$\sigma_{\text{LO}}^{H_1}/\text{fb}$	$\delta_{\text{EW}}^{\overline{\text{MS}}}$	$\delta_{\text{EW}}^{p^*}$	$\delta_{\text{EW}}^{\text{BFM}}$
BP1	1580	-11.1%	-12.3%	-12.4%
BP2	1526	-10.5%	-12.2%	-12.3%
BP3	1486	-10.2%	-12.3%	-12.3%
BP4	1432	$-9.2^{+0.1}_{-0.3}\%$	-12.4%	-12.4%
BP5	242.0	-	-11.7%	-11.7%
BP6	9.4	$+1.65^{+11.1}_{-48.1}\%$	-8.86%	-10.4%

Table 7.9: Relative NLO corrections  $\delta_{\text{EW}}$  to light Higgs-boson  $H_1$  production in Higgs strahlung  $pp \rightarrow H_1 \mu^- \mu^+$  in the HSESM. The scale uncertainties in the  $\overline{\text{MS}}$  scheme are estimated including the RG-running of parameters (7.10). The central scale for BP1–4 is  $\mu_0 = 2M_h = 250.18 \text{ GeV}$ . For BP6 we set the scale to  $\mu_0 = 130 \text{ GeV}$ . For BP5 the  $\overline{\text{MS}}$  scheme is unstable. The scale uncertainties for BP1–3 are smaller than the given accuracy.

BP	$\sigma_{\text{LO}}^{H_h}/\text{fb}$	$\delta_{\text{EW}}^{\overline{\text{MS}}}$	$\delta_{\text{EW}}^{p^*}$	$\delta_{\text{EW}}^{\text{BFM}}$
BP1	3.28	$-53.7^{+0.7}_{-1.0}\%$	-20.3%	-20.5%
BP2	12.3	$-47.4^{+1.5}_{-1.7}\%$	-20.0%	-20.3%
BP3	36.0	$-40.8^{+0.4}_{-0.5}\%$	-16.8%	-16.9%
BP4	114.0	$-36.8^{+1.2}_{-1.3}\%$	-16.0%	-15.1%
BP5	1444	$-12.6^{+4.7}_{+0.0}\%$	-12.5%	-12.5%
BP6	1640	$-12.3^{+0.4}_{-0.1}\%$	-12.5%	-12.6%

Table 7.10: Relative NLO corrections  $\delta_{\text{EW}}$  to heavy Higgs-boson  $H_h$  production in Higgs strahlung  $pp \rightarrow H_h \mu^- \mu^+$  in the HSESM. The scale uncertainties in the  $\overline{\text{MS}}$  scheme are estimated including the RG-running of parameters (7.10). For the BP1–4 the central scales are 580 GeV, 480 GeV, 380 GeV, and 280 GeV, respectively. For BP5 and BP6 the central scale is  $\mu_0 = 2M_h = 250.18 \text{ GeV}$ .

BP	$\sigma_{\text{LO}}^{H_1}/\text{pb}$	$\delta_{\text{EW}}^{p*}$	$\delta_{\text{EW}}^{\text{BFM}}$
BP21A	2.20	-5.3%	-5.3%
a1	2.18	-5.9%	-5.9%
b1	2.19	-6.0%	-6.0%
BP22A	2.02	-9.6%	-9.6%
BP3B1	2.00	-7.3%	-7.3%
BP3B2	1.65	-7.8%	-7.8%
BP43	2.15	-6.1%	-6.1%
BP44	2.15	-6.0%	-6.0%
BP45	1.08	-6.4%	-6.4%
BP	$\sigma_{\text{LO}}^{H_h}/\text{fb}$	$\delta_{\text{EW}}^{p*}$	$\delta_{\text{EW}}^{\text{BFM}}$
BP22A	26.3	+1.5%	+1.1%
BP3B1	126.2	-6.1%	-6.0%
BP3B2	350.5	-5.6%	-5.5%
BP43	19.7	-8.4%	-8.5%
BP44	23.0	-3.5%	-4.6%
BP45	637.1	-5.6%	-5.6%

Table 7.11: Relative NLO corrections  $\delta_{\text{EW}}$  to Higgs-boson production in VBF  $pp \rightarrow H_1/H_{\text{hjj}}$  in the THDM. The SM-like Higgs production is in the upper table, indicated as  $\sigma_{\text{LO}}^{H_1}$  whereas the heavy one is the lower table, indicated as  $\sigma_{\text{LO}}^{H_h}$ . The SM EW correction to  $\sigma_{\text{LO}}^{H_1}$  is  $\delta_{\text{EW}} = -5.5\%$ .

BP	$\sigma_{\text{LO}}^{H_1}/\text{fb}$	$\delta_{\text{EW}}^{p*}$	$\delta_{\text{EW}}^{\text{BFM}}$
BP1	2108	-5.6%	-5.6%
BP2	2035	-5.6%	-5.7%
BP3	1984	-5.5%	-5.6%
BP4	1911	-5.6%	-5.6%
BP5	315.6	-5.7%	-5.7%
BP6	12.8	-3.8%	-5.3%
BP	$\sigma_{\text{LO}}^{H_h}/\text{fb}$	$\delta_{\text{EW}}^{p*}$	$\delta_{\text{EW}}^{\text{BFM}}$
BP3	79.2	-4.6%	-4.7%
BP4	181.7	-4.4%	-4.5%
BP5	1927	-5.6%	-5.6%
BP6	2188	-5.5%	-5.6%

Table 7.12: Relative NLO corrections  $\delta_{\text{EW}}$  to Higgs-boson production in VBF  $pp \rightarrow H_1/H_{\text{hjj}}$  in the HSESM. The light Higgs production is in the upper table, indicated as  $\sigma_{\text{LO}}^{H_1}$  whereas the heavy one is in the lower table, indicated as  $\sigma_{\text{LO}}^{H_h}$ .

## Discussion of the numerical results

In the following we compare cross sections in different renormalization schemes and models for Higgs-boson production in Higgs strahlung. For VBF the picture is similar and not discussed in detail. In particular, for the  $\overline{\text{MS}}$  scheme we collect some observations concerning large corrections.

### $\overline{\text{MS}}$ scheme

We start with the  $\overline{\text{MS}}$  scheme and SM-like Higgs production in the alignment limit of the THDM in Table 7.6. In a fixed-order calculation no scale dependence appears in the  $\overline{\text{MS}}$  scheme, because the relevant counterterms  $\delta Z_{H_h H_1}$ ,  $\delta\alpha$  and  $\delta\beta$  entering the vertices  $H_1 ZZ$  and  $H_1 WW$  are screened by the factor  $c_{\alpha\beta}/s_{\alpha\beta} = 0$  in the alignment limit. For the same reason, the on-shell schemes agree with the  $\overline{\text{MS}}$  scheme at the central value. Yet, with the running of parameters, a small scale dependence is visible. For BP21B the running is unstable towards smaller scales, signalling a potential problem. In non-alignment scenarios the  $\overline{\text{MS}}$  results for the THDM in Table 7.7 are almost all unstable and suffer from large scale dependencies. This suggests a breakdown of perturbativity in the  $\overline{\text{MS}}$  scheme for the THDM in the considered scenarios, which is also clearly visible in the running parameters for  $c_{\alpha\beta}$  and  $t_\beta$  in Table 7.4. For heavy Higgs-boson production in the THDM (Table 7.8) no predictions in the  $\overline{\text{MS}}$  scheme are presented as the non-perturbative behaviour is even more enhanced due to ratios  $s_{\alpha\beta}/c_{\alpha\beta}$  entering the predictions.

The situation for the  $\overline{\text{MS}}$  renormalization in the HSESM for light (Table 7.9) and heavy (Table 7.10) Higgs-boson production is clearly more stable. This is reflected in a reasonable running of the parameter  $s_\alpha$  in Table 7.5, except for BP5 and arguably for BP6. Due to the smaller running, we obtain reasonable results even for the heavy Higgs-boson production near the alignment limit, where potential problems coming from the mixing energy would be enhanced by  $s_\alpha/c_\alpha$ . Perturbativity breaks down in the  $\overline{\text{MS}}$  scheme for light Higgs-boson production in BP6 and in particular for almost degenerate neutral Higgs bosons in BP5. Further, one observes that the  $\overline{\text{MS}}$  scheme leads to larger deviations from the SM corrections, which, however, do not come with large scale uncertainties for the well-behaved benchmark points.

In the HSESM the main source for large corrections are the top-quark contributions to the neutral scalar mixing energy, which is not subtracted in the  $\overline{\text{MS}}$  scheme. This particular effect is enhanced for degenerate neutral Higgs bosons owing to the denominator structure in (7.5) which is not cancelled against the one coming from the on-shell off-diagonal field renormalization constants. Besides the top-quark contributions it is possible to induce moderate contributions coming from the Higgs potential by tuning  $\lambda_3$ . This requires, however, large  $M_{H_h}^2 - M_{H_1}^2$  with not too small  $s_\alpha$ , and it is not straightforward to tune the parameters in order to exceed the top-quark contribution without getting close to the non-perturbative limit  $|\lambda_i| \sim 4\pi$ . In the THDM, the reason for the large corrections in the  $\overline{\text{MS}}$  scheme is more difficult to grasp, especially because in view of our observables we have to deal with the renormalization of  $\beta$  which is known to cause difficulties in the MSSM [184].<sup>6</sup> The problem with  $\beta$  can be traced back to large

<sup>6</sup>Note that  $\beta$  in the HSESM suffers the same problems, but does not enter our fixed-order calculations and the observables we consider. For this reason  $\beta$  has been decoupled from the running of  $\alpha$  in the HSESM in order

contributions in the tadpoles. For  $\alpha$ , the largest contributions cannot be explained by tadpoles nor by the top-quark contribution in the neutral scalar mixing energy. Here, we observe that the large contributions to the neutral scalar mixing energy are mediated through the charged and pseudo-scalar Higgs boson, which, eventually, exceed all other contributions.

### On-shell schemes

For the considered on-shell schemes none of the observed problems of the  $\overline{\text{MS}}$  scheme is encountered because the large contributions in the mixing energy and the tadpoles are subtracted via  $\delta\alpha$  and  $\delta\beta$ , i.e. all terms involving the poles  $1/(M_{H_h}^2 - M_{H_1}^2)$  and  $1/M_{H_a}^2$  cancel in  $S$ -matrix elements. Further, in view of the size of the corrections the on-shell methods perform much better in the sense that the SM-like Higgs-boson production processes (see Tables 7.6, 7.7 for the THDM and Tables 7.9, 7.10 for the HSESM) yield corrections which are close to the SM correction. In heavy Higgs-boson production (see Table 7.8 for the THDM and Table 7.10 for the HSESM) the results for on-shell renormalization schemes remain stable even for aligned<sup>7</sup> or degenerate scenarios. The difference between the  $p^*$  and BFM schemes is tiny. It seems to us that the schemes are too similar for their difference to provide a qualitative estimate of higher orders. The difference between these schemes just results from the momentum dependence of the mixing energies, which turns out to be small and starts at the orders

$$\begin{aligned}\delta\alpha^{p^*} - \delta\alpha^{\text{BFM}} &= \mathcal{O}(M_{H_h}^2 - M_{H_1}^2), \\ \delta\beta^{p^*} - \delta\beta^{\text{BFM}} &= \mathcal{O}(M_{H_a}^2).\end{aligned}$$

Note also, that the large contributions in the scalar mixing energies were observed to have almost no momentum dependence. For VBF the computation has only been carried out in the on-shell schemes. For the THDM (Table 7.11) and HSESM (Table 7.12) the SM-like scenarios almost coincide with the SM predictions.

---

to avoid problems related to its renormalization.

<sup>7</sup>For heavy-Higgs production one expects large one-loop corrections in almost aligned scenarios (e.g. benchmark point b1) because in the exact alignment the LO vanishes. In that case the cross section should be computed including squared one-loop amplitudes, making the one-loop computation effectively a LO approximation.

## Conclusion and outlook

In the upcoming years precision studies of the [SM](#) will become more and more important for the progress in the field of high-energy physics. New tools are required which allow for a systematic analysis of all accessible observables at the [LHC](#) and future colliders. Future analyses need to be performed in the [SM](#), beyond the [SM](#), and in an effective-field-theory approach with high precision; in particular, one-loop [EW](#) corrections need to be included in all [BSM](#) scenarios. In this thesis, we have extended the tool [RECOLA](#), and developed its generalization [RECOLA2](#) as well as the new tool [REPT1L](#) which fulfil all the requirements to compute amplitudes in the [SM](#) and beyond at one-loop order, including [QCD](#) and [EW](#) corrections, in a fully automated way.

The [RECOLA2](#) algorithm operates in a purely numerical and fully recursive way, allowing for extreme computations which enable precise predictions based on realistic final states. Besides the recursion, the algorithm benefits from features like the partial colour factorization in the colour-flow representation, the use of helicity conservation and the identification of equal fermion loops. Furthermore, we support the (multi) pole approximation which is fully automated for factorizable corrections. The process-generation and process-computation phases are kept general for arbitrary theories, allowing the computation of any process in the underlying theory with limitations only due to internal memory and CPU power. On the model side, [RECOLA2](#) is currently limited to scalars, Dirac fermions and vector bosons, but in the near future Majorana fermions will be supported. [RECOLA2](#) can handle operators in effective-field-theory which has been tested for various anomalous couplings including [SM QCD](#) corrections. Much effort has gone into a user-friendly environment. For the users of [RECOLA2](#), in fact, no knowledge of the inner workings of the tools are required. [RECOLA2](#) can be used as a black box which makes it particularly suited for being interfaced to general purpose Monte Carlo programs.

Renormalized model files are generated automatically with the dedicated tool [REPT1L](#). Once the renormalization conditions for the model are established, [REPT1L](#) performs the renormalization, computes the  $R_2$  rational terms and builds the one-loop renormalized model files in the [RECOLA2](#) format. We support standard renormalization conditions as encountered in the literature as well as the possibility to implement custom ones. The computation of the rational terms is general and not restricted to specific models or renormalizable theories. [RECOLA2](#) and [REPT1L](#) have been tested against various independent approaches, yet, an automated validation system is desired since [RECOLA2](#) is acquiring a pioneering position. For this reason we introduced the Background-Field Method to extended Higgs sectors as a complementary method in [RECOLA2](#). We performed the renormalization in the Background-Field Method which is handled on equal footing with the usual formulation, serving as a powerful and automated validation method. Besides that, [RECOLA2](#) can be used in the  $R_\xi$  gauge or non-linear gauges.

All the automation mentioned so far does not help to solve actual problems encountered in the renormalization of specific models or parameters. Difficulties arise for the  $\overline{\text{MS}}$  renormalization of physical parameters which give rise to gauge dependencies in combination with standard tadpole renormalization schemes encountered in the literature. From a theoretic point of view the renormalization of tadpoles is not necessary, but in practical calculations it is desirable to avoid unnecessary computations of graphs with explicit tadpoles, if their contribution can be included indirectly by other means, e.g. via a suited renormalization. To render the  $\overline{\text{MS}}$  renormalization gauge independent, a consistent treatment of tadpoles is crucial. We proposed a generalization of the Fleischer and Jegerlehner tadpole scheme used in the **SM**. Further, we have examined the difference between popular tadpole counterterm schemes used in the literature and clarified their range of applicability. We showed in particular that an  $\overline{\text{MS}}$  renormalization of the mixing angles in the extended Higgs sector within popular schemes leads to gauge-dependent predictions. Our proposed extension of the *FJ Tadpole Scheme* can be straightforwardly applied to more general theories and has been incorporated in REPT1L. This opens the way for consistent renormalization prescriptions of theories with more complicated extended Higgs sectors.

Finally, we applied our new tools to study the **NLO EW** corrections to **VBF** and Higgs strahlung in the **THDM** and **HSESM**. We compared Higgs-production cross sections for different renormalization schemes of the mixing angles in both models. We analysed the scale dependence in an  $\overline{\text{MS}}$  scheme for the mixing angles, which has been improved including the RG running of parameters. We found unnaturally large corrections at one-loop order for the  $\overline{\text{MS}}$  scheme, while the considered on-shell schemes remain well-behaved. The difference between the  $\overline{\text{MS}}$  scheme and on-shell schemes could be traced back to large uncancelled contributions in the off-diagonal **LSZ** factors in the  $\overline{\text{MS}}$  scheme. This interesting observation should be investigated in more detail in the future, since a proper estimation of higher-order uncertainties, as it can be done based on scale variation in  $\overline{\text{MS}}$  schemes, is highly desirable. For the on-shell schemes, our results for the **EW** corrections to **SM**-like Higgs-boson production are almost not distinguishable from the corresponding **SM** corrections for all considered benchmark points. For the production of heavy Higgs bosons interesting shape-distortion effects for the **EW** corrections at the level of several percent are observed in the **THDM**. The considered simple models do by far not exhaust the range of applicability of RECOLA2 and REPT1L, and further models will be implemented in the future.

# Appendices





## A Tensor integrals

### A.1 Tensor-integral conventions

In this work we use dimensional regularization for all computations. We work on formally divergent integrals and perform an analytic continuation to  $D$  dimensions in the conventions of Ref. [84]. The formal expressions of four-dimensional  $N$ -point tensor integrals of rank  $P$  of the form

$$\tilde{T}_{\mu_1 \dots \mu_p}^N(p_1, \dots, p_{N-1}, m_0, \dots, m_{N-1}) = \int \frac{d^4 q}{(2\pi)^4} \frac{q_{\mu_1} \dots q_{\mu_p}}{D_0 D_1 \dots D_{N-1}}, \quad (\text{A.1})$$

with

$$D_i = (q + p_i)^2 - m_i^2 + i\epsilon, \quad i = 0, \dots, N-1, \quad p_0 = 0, \quad (\text{A.2})$$

are defined in  $D$  dimensions in the following way

$$\begin{aligned} \tilde{T}_{\mu_1 \dots \mu_p}^N(\dots) &= \frac{i}{16\pi^2} \mu^{D-4} T_{\mu_1 \dots \mu_p}^N(\dots), \\ T_{\mu_1 \dots \mu_p}^N(p_1, \dots, p_{N-1}, m_0, \dots, m_{N-1}) &= \frac{(2\pi\mu)^{4-D}}{i\pi^2} \int d^D q \frac{q_{\mu_1} \dots q_{\mu_p}}{D_0 D_1 \dots D_{N-1}}. \end{aligned} \quad (\text{A.3})$$

In particular, the scalar integrals  $A_0$  and  $B_0$  in  $D$  dimensions are defined as

$$A_0(m_0) = \frac{(2\pi\mu)^{4-D}}{i\pi^2} \int d^D q \frac{1}{q^2 - m_0^2 + i\epsilon}, \quad (\text{A.4})$$

$$B_0(p^2, m_0, m_1) = \frac{(2\pi\mu)^{4-D}}{i\pi^2} \int d^D q \frac{1}{q^2 - m_0^2 + i\epsilon} \frac{1}{(q+p)^2 - m_1^2 + i\epsilon}. \quad (\text{A.5})$$

When taking the limit  $D \rightarrow 4$ , a universal and divergent part in scalar integrals can be identified, given by

$$(4\pi)^{4-D} \frac{\Gamma(1+4-D)}{4-D} = \Delta + \mathcal{O}(4-D), \quad (\text{A.6})$$

with

$$\Delta = \frac{2}{4-D} - \gamma_E + \log(4\pi). \quad (\text{A.7})$$

In the  $\overline{\text{MS}}$  renormalization we subtract all of  $\Delta$ , i.e. including the finite terms.

### A.2 Selected PV reduction results

In this section we list the analytic results for the **PVR** as used in **REPT1L**. The Lorentz-covariant decomposition is defined in (4.12). The first one- and two-point decompositions for low rank read

$$A^{\mu\nu}(m_0) = g^{\mu\nu} A_{00}, \quad (\text{A.8})$$

$$A^{\mu\nu\rho\sigma}(m_0) = (g^{\mu\nu}g^{\rho\sigma} + g^{\mu\rho}g^{\nu\sigma} + g^{\mu\sigma}g^{\nu\rho}) A_{0000}(m_0) \quad (\text{A.9})$$

...

$$B^\mu(p, m_0, m_1) = p^\mu B_0(p^2, m_0, m_1), \quad (\text{A.10})$$

$$B^{\mu\nu}(p, m_0, m_1) = g^{\mu\nu} B_{00}(p^2, m_0, m_1) + p^\mu p^\nu B_{11}(p^2, m_0, m_1), \quad (\text{A.11})$$

$$B^{\mu\nu\rho}(p, m_0, m_1) = (g^{\mu\nu}p^\rho + g^{\mu\rho}p^\nu + g^{\nu\rho}p^\mu) B_{001}(p^2, m_0, m_1) + p^\mu p^\nu p^\rho B_{111}(p^2, m_0, m_1), \quad (\text{A.12})$$

...

Special attention has to be devoted when using the **PVR** in actual computations, since the **PVR** can break down for degenerate Gram determinants. For rank 5 and rank 6 the reduction for  $B_{111111}$  and  $B_{1111111}$  is not resolved. However, for these cases closed analytic results exist which can be used instead. The formulas can be obtained from recursion rules given in Ref. [80].

### 1-point

$$A_{00}(m_0) = \frac{m_0^2}{4} \left( A_0(m_0) + \frac{m_0^2}{2} \right), \quad (\text{A.13})$$

$$A_{0000}(m_0) = \frac{m_0^4}{24} \left( A_0(m_0) + m_0^2 \left( \frac{1}{2} + \frac{1}{3} \right) \right), \quad (\text{A.14})$$

$$A_{000000}(m_0) = \frac{m_0^6}{192} \left( A_0(m_0) + m_0^2 \left( \frac{1}{2} + \frac{1}{3} + \frac{1}{4} \right) \right). \quad (\text{A.15})$$

### 2-point rank 1

$$B_1(p^2, m_0, m_1) = \frac{1}{2p^2} (A_0(m_0) - A_0(m_1) + (m_1^2 - m_0^2 - p^2) B_0(p^2, m_0, m_1)). \quad (\text{A.16})$$

### 2-point rank 2

$$B_{00}(p^2, m_0, m_1) = \frac{1}{6} \left( A_0(m_1) + 2m_0^2 B_0(p^2, m_0, m_1) + (p^2 - m_1^2 + m_0^2) B_1(p^2, m_0, m_1) + m_0^2 + m_1^2 - \frac{p^2}{3} \right), \quad (\text{A.17})$$

$$B_{11}(p^2, m_0, m_1) = \frac{1}{6p^2} \left( 2A_0(m_1) - 2m_0^2 B_0(p^2, m_0, m_1) - 4(p^2 - m_1^2 + m_0^2) B_1(p^2, m_0, m_1) - m_0^2 - m_1^2 + \frac{p^2}{3} \right). \quad (\text{A.18})$$

### 2-point rank 3

$$B_{001}(p^2, m_0, m_1) = \frac{1}{8} \left( 2m_0^2 B_1(p^2, m_0, m_1) - A_0(m_1) + (p^2 - m_1^2 + m_0^2) B_{11}(p^2, m_0, m_1) - \frac{1}{6} (2m_0^2 + 4m_1^2 - p^2) \right), \quad (\text{A.19})$$

$$B_{111}(p^2, m_0, m_1) = -\frac{1}{2p^2} \left( m_0^2 B_1(p^2, m_0, m_1) + \frac{A_0(m_1)}{2} \right) + \frac{3}{2} (p^2 - m_1^2 + m_0^2) B_{11}(p^2, m_0, m_1) - \frac{1}{12} (2m_0^2 + 4m_1^2 - p^2). \quad (\text{A.20})$$

**2-point rank 4**

$$B_{0000}(p^2, m_0, m_1) = \frac{1}{10} \left( A_{00}(m_1) + 2m_0^2 B_{00}(p^2, m_0, m_1) + (p^2 - m_1^2 + m_0^2) B_{001}(p^2, m_0, m_1) + \frac{1}{60} (p^4 - 5p^2(m_0^2 + m_1^2) + 10(m_0^4 + m_0^2 m_1^2 + m_1^4)) \right), \quad (\text{A.21})$$

$$B_{0011}(p^2, m_0, m_1) = \frac{1}{10} \left( A_0(m_1) + 2m_0^2 B_{11}(p^2, m_0, m_1) + (p^2 - m_1^2 + m_0^2) B_{111}(p, m_1, m_2) - \frac{1}{30} (3p^2 - 5m_0^2 - 15m_1^2) \right), \quad (\text{A.22})$$

$$B_{1111}(p^2, m_0, m_1) = \frac{1}{p^4} \left( (p^2 + m_0^2 + m_1^2) A_0(m_1) + m_0^4 B_0(p^2, m_0, m_1) - 24B_{0000}(p^2 + m_0^2 + m_1^2) - 12p^2 B_{0011}(p^2, m_0, m_1) + \frac{5}{6} (m_0^4 + m_0^2 m_1^2 + m_1^4) - \frac{p^2}{12} (3m_0^2 - m_1^2 + 5p^2) \right). \quad (\text{A.23})$$

**2-point rank 5**

$$B_{00001}(p^2, m_0, m_1) = -\frac{1}{4} \left( A_{00}(m_1) + (p^2 - m_1^2 + m_0^2) B_{0011}(p^2, m_0, m_1) + 2p^2 B_{00111}(p^2, m_0, m_1) \right), \quad (\text{A.24})$$

$$B_{00111}(p^2, m_0, m_1) = -\frac{1}{8} \left( A(m_1) + (p^2 - m_1^2 + m_0^2) B_{1111}(p^2, m_0, m_1) + 2p^2 B_{11111}(p^2, m_0, m_1) \right). \quad (\text{A.25})$$

**2-point rank 6**

$$B_{000000}(p^2, m_0, m_1) = -\frac{1}{2} \left( -A_{0000}(m_1) + (p^2 - m_1^2 + m_0^2) B_{00001}(p^2, m_0, m_1) + 2p^2 B_{000011}(p^2, m_0, m_1) \right), \quad (\text{A.26})$$

$$B_{000011}(p^2, m_0, m_1) = -\frac{1}{6} \left( -A_{00}(m_1) + (p^2 - m_1^2 + m_0^2) B_{00111}(p^2, m_0, m_1) + 2p^2 B_{001111}(p^2, m_0, m_1) \right), \quad (\text{A.27})$$

$$B_{001111}(p^2, m_0, m_1) = -\frac{1}{10} \left( -A_0(m_1) + (p^2 - m_1^2 + m_0^2) B_{11111}(p^2, m_0, m_1) \right)$$

$$+ 2p^2 B_{111111} (p^2, m_0, m_1) \Big). \quad (\text{A.28})$$

## B The FJ Tadpole Scheme applied to the THDM and HSESM

In this appendix we list several results for tadpoles in the **THDM** which have been derived in Ref. [51]. We give corresponding results for **HSESM**.

The **THDM** and **HSESM** as presented in Section 2.3 contain two neutral Higgs bosons which both develop a **vev**, such that (4.15) becomes

$$\mathcal{L}_{H,B} (\rho_{1,B} + v_{1,B} + \Delta v_1, \rho_{2,B} + v_{2,B} + \Delta v_2; \dots). \quad (\text{B.29})$$

As in the **SM**, we use (4.18) to obtain  $\Delta v_1$  and  $\Delta v_2$  expressed by the  $L$ -loop tadpole counterterms, but instead of calculating the tadpoles in the generic basis, we define the **vevs** in terms of the tadpole counterterms associated to the physical Higgs fields  $H_1$  and  $H_h$ . Of course, the result does not depend on the choice of parametrization. In the **THDM** and **HSESM** the tadpole counterterms are defined as

$$\begin{aligned} t_{H_1} &= \Delta \mathcal{L}_{H_1} (\rho_{1,B} + v_{1,B} + \Delta v_1, \rho_{2,B} + v_{2,B} + \Delta v_2; \dots), \\ t_{H_h} &= \Delta \mathcal{L}_{H_h} (\rho_{1,B} + v_{1,B} + \Delta v_1, \rho_{2,B} + v_{2,B} + \Delta v_2; \dots). \end{aligned} \quad (\text{B.30})$$

At tree level, the tadpole counterterms  $t_{H_1}$  and  $t_{H_h}$  vanish, such that  $\Delta v_1 = \Delta v_2 = 0$ . This provides the conditions (2.28), (2.33) for the potential minimum at tree level, and the relations between the generic and the physical Higgs basis (2.30), (2.34) for bare quantities. Thus, the bare parameters in the symmetric basis are expressed by the bare parameters in the physical basis. Linearising (B.30) by using the expansion (4.27), one can solve for  $\Delta v_1^{(1)}$  and  $\Delta v_2^{(1)}$ . The results for  $\Delta v_1^{(1)}$  and  $\Delta v_2^{(1)}$  simplify after using the potential minimum conditions at lowest order and the relation between the parameters in the generic and physical basis.

Evaluating the linearised versions of (B.30) for bare physical parameters, one obtains the one-loop expressions

$$\begin{aligned} \Delta v_1^{(1)} &= \frac{t_{H_1}^{(1)} \sin \alpha}{M_{H_1}^2} - \frac{t_{H_h}^{(1)} \cos \alpha}{M_{H_h}^2}, \\ \Delta v_2^{(1)} &= -\frac{t_{H_1}^{(1)} \cos \alpha}{M_{H_1}^2} - \frac{t_{H_h}^{(1)} \sin \alpha}{M_{H_h}^2}. \end{aligned} \quad (\text{B.31})$$

Just as in the **SM**, tadpole counterterms arise from all terms in the Lagrangian that depend on the **vevs**. This results in tadpole counterterms to two- and three-point functions involving scalars and vector bosons as well as to fermionic two-point functions. Explicit graphs with tadpoles can be omitted upon fixing the tadpole counterterms according to (4.26). The results for the tadpoles  $T_{H_1}$  and  $T_{H_h}$  in the **THDM** and **HSESM** are listed in App. B.1.

## B.1 Results for tadpoles in the THDM

We give the results for the tadpoles  $t_{H_1}$  and  $t_{H_h}$  corresponding to the Higgs bosons  $H_1$  and  $H_h$  in the THDM, restricted to the Type II Yukawa interactions (see Section 2.3) with only the top quark being massive, in the  $R_\xi$  gauge defined in Section 6.2.1,

$$\begin{aligned}
 t_{H_1} = -T_{H_1} = & \frac{s_{\alpha\beta} g}{8\pi^2 M_W} \left\{ -3m_t^2 A_0(m_t) \right. \\
 & + \frac{M_{H_1}^2}{8} \left( A_0(\sqrt{\xi_Z} M_Z) + 2A_0(\sqrt{\xi_W} M_W) \right) + \frac{(D-1)}{4} (M_Z^2 A_0(M_Z) + 2M_W^2 A_0(M_W)) \\
 & + \frac{3}{8} (M_{H_1}^2 (1 + 2c_{\alpha\beta}^2) - 2c_{\alpha\beta}^2 M_{\text{sb}}^2) A_0(M_{H_1}) \\
 & + \frac{1}{8} \left( (1 - 2c_{\alpha\beta}^2) (M_{H_1}^2 + 2M_{H_h}^2) - 2M_{\text{sb}}^2 (1 - 3c_{\alpha\beta}^2) \right) A_0(M_{H_h}) \\
 & + \frac{1}{8} (2M_{H_a}^2 + M_{H_1}^2 - 2M_{\text{sb}}^2) A_0(M_{H_a}) + \frac{1}{4} (2M_{H^\pm}^2 + M_{H_1}^2 - 2M_{\text{sb}}^2) A_0(M_{H^\pm}) \left. \right\} \\
 & + \frac{c_{\alpha\beta} g}{8\pi^2 M_W t_\beta} \left\{ 3m_t^2 A_0(m_t) \right. \\
 & + \frac{t_\beta^2 - 1}{8} \left( 3c_{\alpha\beta}^2 (M_{H_1}^2 - M_{\text{sb}}^2) A_0(M_{H_1}) + s_{\alpha\beta}^2 (2M_{H_h}^2 + M_{H_1}^2 - 3M_{\text{sb}}^2) A_0(M_{H_h}) \right. \\
 & \left. \left. + (M_{H_1}^2 - M_{\text{sb}}^2) A_0(M_{H_a}) + 2(M_{H_1}^2 - M_{\text{sb}}^2) A_0(M_{H^\pm}) \right) \right\}, \tag{B.32}
 \end{aligned}$$

$$\begin{aligned}
 t_{H_h} = -T_{H_h} = & \frac{c_{\alpha\beta} g}{8\pi^2 M_W} \left\{ 3m_t^2 A_0(m_t) \right. \\
 & - \frac{M_{H_h}^2}{8} \left( A_0(\sqrt{\xi_Z} M_Z) + 2A_0(\sqrt{\xi_W} M_W) \right) - \frac{(D-1)}{4} (M_Z^2 A_0(M_Z) + 2M_W^2 A_0(M_W)) \\
 & - \frac{3}{8} (M_{H_h}^2 (1 + 2s_{\alpha\beta}^2) - 2s_{\alpha\beta}^2 M_{\text{sb}}^2) A_0(M_{H_h}) \\
 & - \frac{1}{8} \left( (1 - 2s_{\alpha\beta}^2) (M_{H_h}^2 + 2M_{H_1}^2) - 2M_{\text{sb}}^2 (1 - 3s_{\alpha\beta}^2) \right) A_0(M_{H_1}) \\
 & - \frac{1}{8} (2M_{H_a}^2 + M_{H_h}^2 - 2M_{\text{sb}}^2) A_0(M_{H_a}) - \frac{1}{4} (2M_{H^\pm}^2 + M_{H_h}^2 - 2M_{\text{sb}}^2) A_0(M_{H^\pm}) \left. \right\} \\
 & + \frac{s_{\alpha\beta} g}{8\pi^2 M_W t_\beta} \left\{ 3m_t^2 A_0(m_t) \right. \\
 & + \frac{t_\beta^2 - 1}{8} \left( 3s_{\alpha\beta}^2 (M_{H_h}^2 - M_{\text{sb}}^2) A_0(M_{H_h}) + c_{\alpha\beta}^2 (M_{H_h}^2 + 2M_{H_1}^2 - 3M_{\text{sb}}^2) A_0(M_{H_1}) \right. \\
 & \left. \left. + (M_{H_h}^2 - M_{\text{sb}}^2) A_0(M_{H_a}) + 2(M_{H_h}^2 - M_{\text{sb}}^2) A_0(M_{H^\pm}) \right) \right\}. \tag{B.33}
 \end{aligned}$$

The scalar integral  $A_0$  is defined in App. A.1. Note that by the transformation

$$s_{\alpha\beta} \rightarrow c_{\alpha\beta}, \quad c_{\alpha\beta} \rightarrow -s_{\alpha\beta}, \quad M_{H_1} \leftrightarrow M_{H_h} \quad (\text{B.34})$$

the tadpoles turn into each other in the following way

$$t_{H_1} \rightarrow -t_{H_h}, \quad t_{H_h} \rightarrow t_{H_1}. \quad (\text{B.35})$$

## B.2 Results for 2-point tadpole counterterms in the FJ Tadpole Scheme in the THDM

In this section, we list the tadpole counterterms for the two-point functions derived according to the definition (4.19). Using the abbreviations

$$t_s(a, b) = a t_\beta + b (1 - t_\beta^2), \quad (\text{B.36})$$

$$t_{\alpha\beta} = (s_{\alpha\beta} + c_{\alpha\beta} t_\beta) (c_{\alpha\beta} - s_{\alpha\beta} t_\beta), \quad (\text{B.37})$$

$$t_{f,1} = \frac{g}{2M_W} \left[ -\frac{t_{H_1}}{M_{H_1}^2} (s_{\alpha\beta} + t_\beta c_{\alpha\beta}) + \frac{t_{H_h}}{M_{H_h}^2} (c_{\alpha\beta} - s_{\alpha\beta} t_\beta) \right], \quad (\text{B.38})$$

$$t_{f,2} = \frac{g}{2M_W t_\beta} \left[ \frac{t_{H_1}}{M_{H_1}^2} (c_{\alpha\beta} - s_{\alpha\beta} t_\beta) + \frac{t_{H_h}}{M_{H_h}^2} (s_{\alpha\beta} + c_{\alpha\beta} t_\beta) \right], \quad (\text{B.39})$$

the expressions read:

$$\begin{aligned} t_{H_1 H_1} = & -t_{H_1} \frac{3g}{2M_W t_\beta} \left[ s_{\alpha\beta} t_{\alpha\beta} + t_s(2s_{\alpha\beta}, -c_{\alpha\beta}) \left( 1 - \frac{M_{\text{sb}}^2 c_{\alpha\beta}^2}{M_{H_1}^2} \right) \right] \\ & - t_{H_h} \frac{g c_{\alpha\beta}}{2M_W t_\beta} \left[ -\left( 1 + \frac{2M_{H_1}^2}{M_{H_h}^2} \right) t_{\alpha\beta} + \frac{M_{\text{sb}}^2}{M_{H_h}^2} t_s(2(c_{\alpha\beta}^2 - 2s_{\alpha\beta}^2), 3s_{\alpha\beta} c_{\alpha\beta}) \right], \end{aligned} \quad (\text{B.40})$$

$$\begin{aligned} t_{H_h H_h} = & -t_{H_h} \frac{3g}{2M_W t_\beta} \left[ c_{\alpha\beta} t_{\alpha\beta} - t_s(2c_{\alpha\beta}, s_{\alpha\beta}) \left( 1 - \frac{M_{\text{sb}}^2 s_{\alpha\beta}^2}{M_{H_h}^2} \right) \right] \\ & - t_{H_1} \frac{g s_{\alpha\beta}}{2M_W t_\beta} \left[ -\left( 1 + \frac{2M_{H_1}^2}{M_{H_h}^2} \right) t_{\alpha\beta} - \frac{M_{\text{sb}}^2}{M_{H_1}^2} t_s(2(s_{\alpha\beta}^2 - 2c_{\alpha\beta}^2), -3s_{\alpha\beta} c_{\alpha\beta}) \right], \end{aligned} \quad (\text{B.41})$$

$$\begin{aligned} t_{H_h H_1} = t_{H_1 H_h} = & \frac{g}{2M_W t_\beta} t_{H_1} c_{\alpha\beta} \left[ \left( 2 + \frac{M_{H_h}^2}{M_{H_1}^2} \right) t_{\alpha\beta} + \frac{M_{\text{sb}}^2}{M_{H_1}^2} t_s(2(2s_{\alpha\beta}^2 - c_{\alpha\beta}^2), -3s_{\alpha\beta} c_{\alpha\beta}) \right] \\ & + \frac{g}{2M_W t_\beta} t_{H_h} s_{\alpha\beta} \left[ \left( 2 + \frac{M_{H_1}^2}{M_{H_h}^2} \right) t_{\alpha\beta} - \frac{M_{\text{sb}}^2}{M_{H_h}^2} t_s(2(2c_{\alpha\beta}^2 - s_{\alpha\beta}^2), 3s_{\alpha\beta} c_{\alpha\beta}) \right], \end{aligned} \quad (\text{B.42})$$

$$\begin{aligned} t_{H_a H_a} = t_{H_1} \frac{g}{2M_W t_\beta} & \left[ \frac{M_{\text{sb}}^2}{M_{H_1}^2} t_s(2s_{\alpha\beta}, -c_{\alpha\beta}) - \frac{M_{H_a}^2}{M_{H_1}^2} 2s_{\alpha\beta} t_\beta - t_s(s_{\alpha\beta}, -c_{\alpha\beta}) \right] \\ & + t_{H_h} \frac{g}{2M_W t_\beta} \left[ -\frac{M_{\text{sb}}^2}{M_{H_h}^2} t_s(2c_{\alpha\beta}, s_{\alpha\beta}) + \frac{M_{H_a}^2}{M_{H_h}^2} 2c_{\alpha\beta} t_\beta + t_s(c_{\alpha\beta}, s_{\alpha\beta}) \right], \end{aligned} \quad (\text{B.43})$$

$$t_{H^\pm H^\mp} = t_{H_a H_a} (M_{H_a} \rightarrow M_{H^\pm}), \quad (\text{B.44})$$

$$t_{G_0 G_0} = t_{G^\pm G^\mp} = \frac{g}{2M_W} (-t_{H_1} s_{\alpha\beta} + t_{H_h} c_{\alpha\beta}), \quad (\text{B.45})$$

$$t_{G_0 H_a} = t_{H_a G_0} = t_{H_1} \frac{g c_{\alpha\beta}}{2M_W} \left( 1 - \frac{M_{H_a}^2}{M_{H_1}^2} \right) + t_{H_h} \frac{g s_{\alpha\beta}}{2M_W} \left( 1 - \frac{M_{H_a}^2}{M_{H_h}^2} \right), \quad (\text{B.46})$$

$$t_{G^\pm H^\mp} = t_{H^\pm G^\mp} = t_{G_0 H_a} (M_{H_a} \rightarrow M_{H^\pm}), \quad (\text{B.47})$$

$$t_{W^\pm W^\mp}^{\mu\nu} = g^{\mu\nu} g M_W \left( \frac{t_{H_1}}{M_{H_1}^2} s_{\alpha\beta} - \frac{t_{H_h}}{M_{H_h}^2} c_{\alpha\beta} \right), \quad (\text{B.48})$$

$$t_{ZZ}^{\mu\nu} = \frac{t_{W^\pm W^\mp}^{\mu\nu}}{c_w}, \quad (\text{B.49})$$

$$t_{W^\pm H^\mp}^\mu = i q^\mu \frac{g}{2} \left( \frac{t_{H_1}}{M_{H_1}^2} c_{\alpha\beta} + \frac{t_{H_h}}{M_{H_h}^2} s_{\alpha\beta} \right), \quad (\text{B.50})$$

$$t_{W^\pm G^\mp}^\mu = \pm q^\mu \frac{g}{2} \left( \frac{t_{H_1}}{M_{H_1}^2} s_{\alpha\beta} - \frac{t_{H_h}}{M_{H_h}^2} c_{\alpha\beta} \right), \quad (\text{B.51})$$

$$t_{ZH_a}^\mu = -i \frac{t_{W^\pm H^\mp}^\mu}{c_w}, \quad (\text{B.52})$$

$$t_{ZG_0}^\mu = -i \frac{t_{W^- G^+}^\mu}{c_w}, \quad (\text{B.53})$$

$$t_{ff} = \begin{cases} m_f t_{f,1} & \text{if } f \text{ couples to } \Phi_1 \text{ in (2.38)} \\ m_f t_{f,2} & \text{if } f \text{ couples to } \Phi_2 \text{ in (2.38)} \end{cases}, \quad (\text{B.54})$$

with  $q^\mu$  being the incoming momentum of the corresponding vector boson. The Feynman rules for the tadpole counterterms are obtained by multiplying the tadpole expression with the imaginary unit  $i$ .

### B.3 Results for tadpoles in the HSESM

We give the tadpoles  $t_{H_1}$  and  $t_{H_h}$  corresponding to the Higgs bosons  $H_1$  and  $H_h$  in the HSESM, with only the top quark being massive, in the 't Hooft–Feynman gauge,

$$\begin{aligned} t_{H_1} = -T_{H_1} = & \frac{g}{8\pi^2 M_W} \left\{ -3m_t^2 s_\alpha A_0(m_t) \right. \\ & + A_0(M_{H_h}) (M_{H_1}^2 + 2M_{H_h}^2) \frac{c_\alpha s_\alpha}{8t_\beta} (-s_\alpha + c_\alpha t_\beta) \\ & + A_0(M_{H_1}) M_{H_1}^2 \frac{3}{8t_\beta} (-c_\alpha^3 + s_\alpha^3 t_\beta) \\ & + A_0(M_W) \frac{s_\alpha}{4} (M_{H_1}^2 + 2(D-1)M_W^2) \\ & \left. + A_0(M_Z) \frac{s_\alpha}{8} (M_{H_1}^2 + 2(D-1)M_Z^2) \right\}, \end{aligned} \quad (\text{B.55})$$

$$\begin{aligned} t_{H_h} = -T_{H_h} = & \frac{g}{8\pi^2 M_W} \left\{ 3m_t^2 c_\alpha A_0(m_t) \right. \\ & \left. - A_0(M_{H_1}) (M_{H_h}^2 + 2M_{H_1}^2) \frac{c_\alpha s_\alpha}{8t_\beta} (c_\alpha + s_\alpha t_\beta) \right\} \end{aligned}$$

$$\begin{aligned}
& + A_0(M_{H_h}) M_{H_h}^2 \frac{3}{8t_\beta} (-s_\alpha^3 - c_\alpha^3 t_\beta) \\
& - A_0(M_W) \frac{c_\alpha}{4} (M_{H_h}^2 + 2(D-1)M_W^2) \\
& - A_0(M_Z) \frac{c_\alpha}{8} (M_{H_h}^2 + 2(D-1)M_Z^2) \Big\}. \tag{B.56}
\end{aligned}$$

The scalar integral  $A_0$  is defined in App. A.1. Note that by the transformation

$$s_\alpha \rightarrow c_\alpha, \quad c_\alpha \rightarrow -s_\alpha, \quad M_{H_1} \leftrightarrow M_{H_h} \tag{B.57}$$

the tadpoles turn into each other in the following way

$$t_{H_1} \rightarrow -t_{H_h}, \quad t_{H_h} \rightarrow t_{H_1}. \tag{B.58}$$

## C Alternative tadpole counterterm schemes

In this appendix give simple recipes for efficiently generating the tadpole counterterms in the different models and tadpole counterterm schemes at one-loop order. In Section C.1 we use the derived results to prove the gauge dependence of the  $S$ -matrix in the  $R_\xi$  gauge in popular tadpole counterterms for the  $\overline{\text{MS}}$  renormalization of the mixing angles defined in Section 4.6.1, Section 4.6.2. The following parts are taken from Ref. [51] and extended to the case of the HSESM.

We start from the tree-level Lagrangian (4.15) in the symmetric basis in terms of the theory-defining parameters where the fields have been shifted by independent parameters  $v_{i,B}$ . Then, we perform the shifts of the parameters as defined below. Thereafter, the **vevs**  $v_{i,B}$  are determined at leading order, and the bare physical basis is introduced by using the tree-level relations (2.28)–(2.30) for the THDM and (2.33), (2.34) for the HSESM. Finally, the bare parameters can be expressed in terms of renormalized parameters and counterterms according to e.g. (5.9).

The tadpole renormalization in the different schemes can be generated by shifting the corresponding bare parameters as follows:

### Scheme 1

A commonly used renormalization scheme for the SM was proposed in Ref. [84]. There, the bare physical masses are defined as the coefficients of the quadratic terms in the fields, and the tadpoles are the coefficients of the terms linear in the fields. For the SM the tadpole counterterms in Ref. [84] are obtained upon performing the shifts

$$\lambda_B \rightarrow \lambda_B + \frac{2t_h}{v_B^3}, \quad \mu_B^2 \rightarrow \mu_B^2 + \frac{3}{2} \frac{t_h}{v_B}. \tag{C.59}$$

Applying this definition to the THDM, we can construct the corresponding Lagrangian by a shift in the bare parameters as

$$\lambda_{1,B} \rightarrow \lambda_{1,B} - \frac{1}{v_1^3} (t_{H_1} \sin \alpha - t_{H_h} \cos \alpha),$$



$$\begin{aligned}
 \lambda_{2,B} &\rightarrow \lambda_{2,B} + \frac{1}{v_2^3} (t_{H_1} \cos \alpha + t_{H_h} \sin \alpha), \\
 \lambda_{3,B} &\rightarrow \lambda_{3,B} - \frac{2v_2^2}{v_1 v^4} (t_{H_1} \sin \alpha - t_{H_h} \cos \alpha) + \frac{2v_1^2}{v_2 v^4} (t_{H_1} \cos \alpha + t_{H_h} \sin \alpha), \\
 \lambda_{4,B} &\rightarrow \lambda_{4,B} + \frac{v_2^2}{v_1 v^4} (t_{H_1} \sin \alpha - t_{H_h} \cos \alpha) - \frac{v_1^2}{v_2 v^4} (t_{H_1} \cos \alpha + t_{H_h} \sin \alpha), \\
 \lambda_{5,B} &\rightarrow \lambda_{5,B} + \frac{v_2^2}{v_1 v^4} (t_{H_1} \sin \alpha - t_{H_h} \cos \alpha) - \frac{v_1^2}{v_2 v^4} (t_{H_1} \cos \alpha + t_{H_h} \sin \alpha), \\
 m_{1,B}^2 &\rightarrow m_{1,B}^2 + \frac{3}{2v_1} (t_{H_1} \sin \alpha - t_{H_h} \cos \alpha), \\
 m_{2,B}^2 &\rightarrow m_{2,B}^2 - \frac{3}{2v_2} (t_{H_1} \cos \alpha + t_{H_h} \sin \alpha).
 \end{aligned} \tag{C.60}$$

For the **HSESM** the rules read

$$\begin{aligned}
 \lambda_{1,B} &\rightarrow \lambda_{1,B} - \frac{1}{v^3} (t_{H_1} \sin \alpha - t_{H_h} \cos \alpha), \\
 \lambda_{2,B} &\rightarrow \lambda_{2,B} + \frac{1}{v_s^3} (t_{H_1} \cos \alpha + t_{H_h} \sin \alpha), \\
 \lambda_{3,B} &\rightarrow \lambda_{3,B}, \\
 m_{1,B}^2 &\rightarrow m_{1,B}^2 + \frac{3}{2v} (t_{H_1} \sin \alpha - t_{H_h} \cos \alpha), \\
 m_{2,B}^2 &\rightarrow m_{2,B}^2 - \frac{3}{2v_s} (t_{H_1} \cos \alpha + t_{H_h} \sin \alpha),
 \end{aligned} \tag{C.61}$$

which correspond to the ones in the **THDM** (C.60) by identifying the rule for  $\lambda_{3,B}$  with the rule for  $\lambda_{3,B} + \lambda_{4,B} + \lambda_{5,B}$ .

One can verify that the prescription (C.60) leads to the tadpole equations (B.30) in the **THDM** and **HSESM**. Note that in the alignment limit, the **SM** tadpoles (see App. A in Ref. [84]) are recovered.

## Scheme 2

In the  $\beta_h$  scheme of Ref. [85], the mass parameters in the Higgs potential are eliminated in favour of explicit tadpoles, while the quartic Higgs couplings  $\lambda_i$  are kept fixed. Thus, no tadpole counterterm contributions appear in the triple and quartic vertices between scalars, but the mass parameters of the Higgs potential and thus the two-point functions are shifted by tadpole counterterms. For the **SM** one obtains

$$\lambda_B \rightarrow \lambda_B, \quad \mu_B^2 \rightarrow \mu_B^2 + \frac{t_h}{v_B}. \tag{C.62}$$

For the **THDM** the rules read

$$\begin{aligned}
 \lambda_{i,B} &\rightarrow \lambda_{i,B}, \\
 m_{1,B}^2 &\rightarrow m_{1,B}^2 + \frac{(t_{H_1} \sin \alpha - t_{H_h} \cos \alpha)}{v_1}, \\
 m_{2,B}^2 &\rightarrow m_{2,B}^2 - \frac{(t_{H_1} \cos \alpha + t_{H_h} \sin \alpha)}{v_2}.
 \end{aligned} \tag{C.63}$$

For the **HSESM** the rules are the same with properly identified **vevs**

$$\begin{aligned}
\lambda_{i,B} &\rightarrow \lambda_{i,B}, \\
m_{1,B}^2 &\rightarrow m_{1,B}^2 + \frac{(t_{H_1} \sin \alpha - t_{H_h} \cos \alpha)}{v}, \\
m_{2,B}^2 &\rightarrow m_{2,B}^2 - \frac{(t_{H_1} \cos \alpha + t_{H_h} \sin \alpha)}{v_s}.
\end{aligned}
\tag{C.64}$$

For explicit computations, Scheme 2 is very convenient because tadpole counterterms appear only in two-point functions. This scheme is widely used, e.g. in the **THDM** [185, 186, 187, 188, 128] and in the **MSSM** [189, 184, 190]. In contrast, in Scheme 1 two-point functions do not receive tadpole counterterms due to the definition of the bare masses in that scheme.

### Scheme 3

As described in detail in Section 4.2.1, in the *FJ Tadpole Scheme*, the **vevs** are replaced by  $(v_{1,B} + \Delta v_1)$  and  $(v_{2,B} + \Delta v_2)$ , which in the **SM** corresponds to the following shift

$$v_B \rightarrow v_B - \frac{t_h}{M_h^2}.$$
(C.65)

For the **THDM** and **HSESM** the rules read

$$\begin{aligned}
v_{1,B} &\rightarrow v_{1,B} + \frac{t_{H_1} \sin \alpha}{M_{H_1}^2} - \frac{t_{H_h} \cos \alpha}{M_{H_h}^2}, \\
v_{2,B} &\rightarrow v_{2,B} - \frac{t_{H_1} \cos \alpha}{M_{H_1}^2} - \frac{t_{H_h} \sin \alpha}{M_{H_h}^2}.
\end{aligned}
\tag{C.66}$$

This prescription has to be applied to the full Lagrangian and is not restricted to the Higgs potential. Further, only after these shifts the **vevs** are fixed by minimizing the scalar potential.

We stress again, as we have shown in Section 4.2.2, that the bare parameters of the theory are shifted by (gauge-dependent) tadpole contributions in Schemes 1 and 2, as opposed to the prescription of the *FJ Tadpole Scheme* (C.66), where only the unphysical **vevs** receive a shift which can be understood as a suited field reparametrization.

## C.1 Gauge dependence of the mixing angle $\alpha$ in popular tadpole schemes

We study the tadpole-counterterm-scheme dependence of vertices in the **THDM** in the  $R_\xi$  gauge. We find that the  $\overline{\text{MS}}$  renormalization of  $\alpha$  defined in Section 4.6.1 combined with alternative tadpole counterterm schemes is responsible for the gauge dependence of the  $S$ -matrix, while it is gauge-independent in the *FJ Tadpole Scheme*. These results directly translate to the **HSESM**.

In the following we make use of the fact that a different tadpole counterterm scheme merely leads to different solutions for counterterms. Thus, the tadpole-counterterm-scheme dependence can be studied on the level of counterterms. We name the schemes as in the previous section, i.e. Scheme 1 for the scheme employed in Ref. [84] and Scheme 2 for the  $\beta_h$  scheme of Ref. [85].

The *FJ Tadpole Scheme* is referred to as Scheme 3. We generically label the difference in the schemes for a counterterm  $\delta c_i$  by

$$\Delta_i \delta c = \delta c_i - \delta c_3, \quad i = 1, 2, \quad (\text{C.67})$$

where the  $\Delta_i$  describe the difference of Scheme  $i$  with respect to the Scheme 3.

In the following we list the results for the counterterm parameters. Thereby, we make use of results for tadpoles listed in Apps. B.1 and B.2. As a first result, we note that the counterterms of couplings in the **SM** are not affected by the choice of the tadpole renormalization scheme, i.e.

$$\Delta_i \delta e = \Delta_i \delta c_w = 0, \quad i = 1, 2. \quad (\text{C.68})$$

However, the mass counterterms for all fermions and gauge-bosons change equally for  $i = 1, 2$  as

$$\begin{aligned} \Delta_i \delta M_V^2 &= \frac{g}{M_W} M_V^2 \left( \frac{t_{H_1}}{M_{H_1}^2} s_{\alpha\beta} - \frac{t_{H_h}}{M_{H_h}^2} c_{\alpha\beta} \right), \\ \Delta_i \delta m_f^d &= \frac{g}{2M_W} m_f^d \left( \frac{t_{H_1}}{M_{H_1}^2} (c_{\alpha\beta} t_\beta + s_{\alpha\beta}) + \frac{t_{H_h}}{M_{H_h}^2} (s_{\alpha\beta} t_\beta - c_{\alpha\beta}) \right), \\ \Delta_i \delta m_f^u &= \frac{g}{2M_W t_\beta} m_f^u \left( \frac{t_{H_1}}{M_{H_1}^2} (s_{\alpha\beta} t_\beta - c_{\alpha\beta}) - \frac{t_{H_h}}{M_{H_h}^2} (c_{\alpha\beta} t_\beta + s_{\alpha\beta}) \right), \\ \Delta_i \delta m_f^l &= \frac{g}{2M_W} m_f^l \left( \frac{t_{H_1}}{M_{H_1}^2} (c_{\alpha\beta} t_\beta + s_{\alpha\beta}) + \frac{t_{H_h}}{M_{H_h}^2} (s_{\alpha\beta} t_\beta - c_{\alpha\beta}) \right), \end{aligned} \quad (\text{C.69})$$

which is easily derived because neither in Scheme 1 nor in Scheme 2 there are tadpole contributions to two-point functions of fermions and gauge bosons. Therefore, the difference (C.69) is the full tadpole dependence of the two-point functions in the *FJ Tadpole Scheme*. The results for the scalar fields are more complicated and not given since most of them are not needed in the following discussion. For Scheme 1, the difference is again given by the full tadpole dependence in the *FJ Tadpole Scheme*, which can be found in App. B.1.

In the *FJ Tadpole Scheme*, the mass counterterms are gauge independent by definition, which we have verified in the  $R_\xi$  gauge. Consequently, the mass counterterms in Schemes 1 and 2 are gauge dependent, and their gauge dependence is given by the gauge dependence of the corresponding tadpole counterterms.

Next, we derive the tadpole-counterterm-scheme dependence for the mixing angles. Since they are renormalized in the  $\overline{\text{MS}}$  scheme, we only need to study their UV-divergent parts which are given by (4.123) and (4.120), holding in any of the presented tadpole counterterm schemes in the  $R_\xi$  gauge. For  $\beta$ , defined in Section 4.6.2, we obtain

$$\Delta_i \delta \beta^{\overline{\text{MS}}} = \Delta_i \frac{\delta Z_{G_0 H_a}^{\overline{\text{MS}}} - \delta Z_{H_a G_0}^{\overline{\text{MS}}}}{4} = -\frac{\Delta_i t_{G_0 H_a}^{\overline{\text{MS}}}}{M_{H_a}^2}, \quad i = 1, 2, \quad (\text{C.70})$$

In the first step we used (4.123). The second step can be derived by solving the renormalization

conditions for the relevant mixing energies

$$(p^2 - M_{H_a}^2) \frac{\delta Z_{H_a G_0}}{2} + p^2 \frac{\delta Z_{G_0 H_a}}{2} + t_{G_0 H_a} + \text{self-energy diagrams} \stackrel{!}{=} \text{finite}, \quad (\text{C.71})$$

where we omitted any explicit tadpoles because of the tadpole renormalization condition  $\hat{T}_i = 0$ . Since the self-energy contributions do not depend on the tadpole counterterm scheme, the scheme-dependent divergence of the tadpole counterterms has to cancel against the scheme-dependent divergence of the non-diagonal field renormalization constants, and for  $i = 1, 2$  we obtain

$$\Delta_i \left( (p^2 - M_{H_a}^2) \delta Z_{H_a G_0}^{\overline{\text{MS}}} + p^2 \delta Z_{G_0 H_a}^{\overline{\text{MS}}} + 2t_{G_0 H_a}^{\overline{\text{MS}}} \right) \stackrel{!}{=} 0, \quad (\text{C.72})$$

which implies

$$\Delta_i \delta Z_{H_a G_0}^{\overline{\text{MS}}} = 2 \frac{\Delta_i t_{G_0 H_a}^{\overline{\text{MS}}}}{M_{H_a}^2}, \quad \Delta_i \delta Z_{G_0 H_a}^{\overline{\text{MS}}} = -2 \frac{\Delta_i t_{G_0 H_a}^{\overline{\text{MS}}}}{M_{H_a}^2}. \quad (\text{C.73})$$

Therefore, the scheme dependence of  $\delta\beta^{\overline{\text{MS}}}$  is given by the scheme dependence of the tadpole contribution  $t_{G_0 H_a}$  of (C.70). The explicit results for  $t_{G_0 H_a}$  in the *FJ Tadpole Scheme* are listed in App. B.2, and those for Schemes 1 and 2 are given by

$$t_{G_0 H_a, 1} = t_{G_0 H_a, 2} = \frac{g}{2M_W} (t_{H_1} c_{\alpha\beta} + t_{H_h} s_{\alpha\beta}), \quad (\text{C.74})$$

and hence

$$\frac{\Delta_i t_{G_0 H_a}}{M_{H_a}^2} = \frac{g}{2M_W} \left( c_{\alpha\beta} \frac{t_{H_1}}{M_{H_1}^2} + s_{\alpha\beta} \frac{t_{H_h}}{M_{H_h}^2} \right), \quad i = 1, 2. \quad (\text{C.75})$$

While the change in  $\delta\beta^{\overline{\text{MS}}}$  at one-loop order is independent of the gauge parameters in the usual  $R_\xi$  gauge and in their generalizations to non-linear gauges, we show in App. B.1 that it is nevertheless already gauge dependent at the one-loop level in the **THDM**. This result applies to the **MSSM** and **HSESM**.

For the difference in the counterterms to the mixing angle  $\alpha$ , we obtain

$$\Delta_1 \delta\alpha^{\overline{\text{MS}}} = -\frac{\Delta_1 \delta Z_{H_1 H_h}^{\overline{\text{MS}}}}{2} = \frac{\Delta_1 t_{H_h H_1}^{\overline{\text{MS}}}}{M_{H_h}^2 - M_{H_1}^2} = -\frac{t_{H_h H_1}^{\overline{\text{MS}}}}{M_{H_h}^2 - M_{H_1}^2} \quad (\text{C.76})$$

and

$$\Delta_2 \delta\alpha^{\overline{\text{MS}}} = -\frac{\Delta_2 \delta Z_{H_1 H_h}^{\overline{\text{MS}}}}{2} = \frac{\Delta_2 t_{H_h H_1}^{\overline{\text{MS}}}}{M_{H_h}^2 - M_{H_1}^2} = -\frac{t_{H_h H_1}^{\overline{\text{MS}}} - t_{H_h H_1, 2}^{\overline{\text{MS}}}}{M_{H_h}^2 - M_{H_1}^2}, \quad (\text{C.77})$$



$$- (c_{\alpha\beta} - s_{\alpha\beta}t_\beta) \left( \Delta_i \frac{\delta Z_{H_h H_1}}{2} - \Delta_i \delta\alpha^{\overline{\text{MS}}} \right) \Big]. \quad (\text{C.81})$$

The terms can be split into two parts which are separately UV finite, thus allowing for a simple interpretation

$$\begin{aligned} \Delta_i \delta\beta^{\overline{\text{MS}}} + \frac{\Delta_i \delta m_\tau}{m_\tau} - \frac{\Delta_i \delta M_W}{M_W} &= \Delta_i \frac{\delta Z_{H_a G_0}^{\text{fin}}}{2}, \\ \Delta_i \frac{\delta Z_{H_h H_1}}{2} - \Delta_i \delta\alpha^{\overline{\text{MS}}} &= -\Delta_i \frac{\delta Z_{H_1 H_h}^{\text{fin}}}{2}, \end{aligned} \quad (\text{C.82})$$

where we used (C.69), (C.70), (C.76), and (C.77) and “fin” denotes the UV-finite part, i.e. the remnant after  $\overline{\text{MS}}$  subtraction. The final result reads

$$\Delta_i \text{---} \begin{array}{c} \tau^- \\ \circlearrowleft \\ H_1 \\ \circlearrowright \\ \tau^+ \end{array} = \text{---} \begin{array}{c} \tau^- \\ \bullet \\ H_1 \\ \bullet \\ \tau^+ \end{array} \times \Delta_i \frac{\delta Z_{H_a G_0}^{\text{fin}}}{2} - \text{---} \begin{array}{c} \tau^- \\ \bullet \\ H_h \\ \bullet \\ \tau^+ \end{array} \times \Delta_i \frac{\delta Z_{H_1 H_h}^{\text{fin}}}{2}, \quad (\text{C.83})$$

with

$$\begin{aligned} \Delta_1 \delta Z_{H_a G_0}^{\text{fin}} &= -2 \frac{t_{G_0 H_a}^{\text{fin}} - t_{G_0 H_a,1}^{\text{fin}}}{M_{H_a}^2}, & \Delta_2 \delta Z_{H_a G_0}^{\text{fin}} &= -2 \frac{t_{G_0 H_a}^{\text{fin}} - t_{G_0 H_a,2}^{\text{fin}}}{M_{H_a}^2}, \\ \Delta_1 \delta Z_{H_1 H_h}^{\text{fin}} &= 2 \frac{t_{H_h H_1}^{\text{fin}}}{M_{H_h}^2 - M_{H_1}^2}, & \Delta_2 \delta Z_{H_1 H_h}^{\text{fin}} &= 2 \frac{t_{H_h H_1}^{\text{fin}} - t_{H_h H_1,2}^{\text{fin}}}{M_{H_h}^2 - M_{H_1}^2}, \end{aligned} \quad (\text{C.84})$$

where  $t_{G_0 H_a}$  and  $t_{H_h H_1}$  are defined in App. B.2, and  $t_{G_0 H_a,1,2}$  and  $t_{H_h H_1,2}$  in (C.74) and (C.78), respectively. The first contribution in (C.83) appears owing to the differences in the definition of  $\beta$ , the second one is a consequence of the definition of  $\alpha$ . The *FJ Tadpole Scheme* yields gauge-independent predictions for the decay rate  $H_1 \rightarrow \tau^+ \tau^-$ , whereas in Schemes 1 and 2 the prediction is gauge dependent in the  $R_\xi$  gauge due to the second term in (C.83). This has been confirmed via explicit calculation of the  $S$ -matrix element in the  $R_\xi$  gauge.

At one-loop order, the results for the *FJ Tadpole Scheme* can be obtained from Schemes 1 and 2 via the mapping

$$\left( \delta\beta^{\overline{\text{MS}}} \right)_i \rightarrow \left( \delta\beta^{\overline{\text{MS}}} \right)_i - \Delta_i \frac{\delta Z_{H_a G_0}^{\text{fin}}}{2}, \quad \left( \delta\alpha^{\overline{\text{MS}}} \right)_i \rightarrow \left( \delta\alpha^{\overline{\text{MS}}} \right)_i - \Delta_i \frac{\delta Z_{H_1 H_h}^{\text{fin}}}{2}, \quad i = 1, 2. \quad (\text{C.85})$$

Note that the “Tadpole scheme” introduced in Ref. [184] for the renormalization of  $t_\beta$  in the **MSSM** is equivalent to the *FJ Tadpole Scheme* applied to the **MSSM** combined with  $\overline{\text{MS}}$  subtraction for  $t_\beta$ . Indeed for the **MSSM** the finite shift  $\delta t_\beta^{\text{fin}}$  defined in Eq. (43) of Ref. [184] corresponds exactly to the shift of  $(\delta\beta^{\overline{\text{MS}}})_2$  in Eq. (C.85), which translates the popular Scheme 2 to the *FJ Tadpole Scheme*.

### The $ZZH_h$ vertex

We derive the tadpole counterterm dependence of the  $ZZH_h$  vertex, obtaining formally analogous results as in the previous calculation. The following Feynman rules were used

$$\begin{array}{c} \text{---} H_h \end{array} \begin{array}{c} Z \\ \diagup \\ \bullet \\ \diagdown \\ Z \end{array} = \frac{ie c_{\alpha\beta} M_W}{s_w c_w c_w} g^{\mu\nu}, \quad \begin{array}{c} \text{---} H_1 \end{array} \begin{array}{c} Z \\ \diagup \\ \bullet \\ \diagdown \\ Z \end{array} = -\frac{ie s_{\alpha\beta} M_W}{s_w c_w c_w} g^{\mu\nu}. \quad (\text{C.86})$$

For this vertex an explicit tadpole counterterm needs to be taken into account, given by

$$\begin{array}{c} \text{---} H_h \end{array} \begin{array}{c} Z \\ \diagup \\ \times \\ \diagdown \\ Z \end{array} \supset t_{ZZH_h} = -\frac{ie^2}{2s_w^2 c_w^2} \frac{t_{H_h}}{M_{H_h}^2} g^{\mu\nu}. \quad (\text{C.87})$$

With the same line of arguments as before we obtain the difference of the renormalized vertex in different tadpole counterterm schemes as

$$\Delta_i \begin{array}{c} \text{---} H_h \end{array} \begin{array}{c} Z \\ \diagup \\ \textcircled{R} \\ \diagdown \\ Z \end{array} = \begin{array}{c} \text{---} H_1 \end{array} \begin{array}{c} Z \\ \diagup \\ \bullet \\ \diagdown \\ Z \end{array} \times \Delta_i \frac{-\delta Z_{H_a G_0}^{\text{fin}} + \delta Z_{H_1 H_h}^{\text{fin}}}{2}. \quad (\text{C.88})$$

The gauge independence of the renormalized  $ZZH_h$  vertex has been verified in the *FJ Tadpole Scheme* by explicit computation in the  $R_\xi$  gauge. Schemes 1 and 2 can be mapped to the *FJ Tadpole Scheme* via (C.85). Since the mapping (C.85) is gauge dependent, the renormalized  $ZZH_h$  vertex becomes gauge dependent in Schemes 1 and 2.

## C.2 Gauge dependence of the mixing angle $\beta$ in popular tadpole schemes

In the following we prove the gauge dependence of  $\delta\beta^{\overline{\text{MS}}}$  in popular tadpole counterterm schemes at the one-loop order by explicit calculation. Further, we show that in the *FJ Tadpole Scheme*  $\delta\beta^{\overline{\text{MS}}}$  is gauge independent.

In the *THDM* the apparent gauge independence of  $\delta\beta^{\overline{\text{MS}}}$  in the  $R_\xi$  gauge at the one-loop level can be understood as follows: Consider the linear combination of  $\Phi_1$  and  $\Phi_2$  that does not have a **vev**(see Section 2.3.1)

$$\cos\beta\Phi_2 - \sin\beta\Phi_1 = \begin{pmatrix} H^\pm \\ \frac{1}{\sqrt{2}}(\cos\beta v_2 - \sin\beta v_1 + H_1 c_{\alpha\beta} + H_h s_{\alpha\beta} + iH_a) \end{pmatrix}, \quad (\text{C.89})$$

with  $\cos\beta v_2 - \sin\beta v_1 = 0$ . Performing the shift in the **vevs** according to (B.30) and using (B.31), we obtain the tadpole corresponding to the neutral Higgs field  $\tilde{H} = H_1 c_{\alpha\beta} + H_h s_{\alpha\beta}$ ,

$$\sin\beta\Delta v_1 - \cos\beta\Delta v_2 = c_{\alpha\beta} \frac{t_{H_1}}{M_{H_1}^2} + s_{\alpha\beta} \frac{t_{H_h}}{M_{H_h}^2}, \quad (\text{C.90})$$

which enters the shift of  $\Delta_i \beta^{\overline{\text{MS}}}$  between the *FJ Tadpole Scheme* and the popular Schemes 1 and 2 found in (C.70) and (C.75). The Higgs field  $\tilde{H}$  does neither couple to two gauge bosons nor to two would-be Goldstone bosons, and, moreover, it does not enter the gauge fixing in the  $R_\xi$  gauge and thus does not couple to Faddeev–Popov ghost fields. Consequently, there are no gauge-dependent Feynman diagrams for the  $\tilde{H}$  tadpole at one-loop order and thus  $\Delta_i \delta \beta^{\overline{\text{MS}}}$  does not depend on the gauge-parameter in the  $R_\xi$  gauge. Since  $\delta \beta^{\overline{\text{MS}}}$  is gauge independent in the *FJ Tadpole Scheme*, this translates to Schemes 1 and 2. This argument can be generalized to non-linear  $R_\xi$  gauges at one-loop order.<sup>1</sup>

Nevertheless, it is possible to demonstrate the gauge dependence of  $\delta \beta^{\overline{\text{MS}}}$  in Schemes 1 and 2 at one-loop order in a suitably chosen gauge. Since  $\tilde{H}$  couples to one gauge boson or would-be Goldstone boson and  $H_a$ , we can generate a gauge-dependent contribution to its tadpole by allowing for mixing propagators induced by the gauge fixing. Here, we provide an appropriate gauge-fixing function and prove the gauge dependence of  $\delta \beta^{\overline{\text{MS}}}$  via two different approaches. In addition, we show that also in this class of gauges the gauge independence of  $\delta \beta^{\overline{\text{MS}}}$  is preserved in the *FJ Tadpole Scheme*.

The appropriate choice of the gauge-fixing function can be motivated as follows. From the point of view of the *FJ Tadpole Scheme* the gauge dependence appears in the Schemes 1 [Eq. (C.60)] or 2 [Eq. (C.63)] if it is possible to generate a gauge-dependent tadpole contribution of the form of (C.90). For a gauge-fixing function  $C$  linear in the gauge fields the infinitesimal variation of Green’s functions under a change in the gauge-fixing function,  $\Delta C$ , with respect to some parameter can be derived (see e.g. Section 2.5.4.4 of Ref. [102], Section 12.4 of Ref. [191], or Ref. [141]). For the one-point function of a field  $\varphi$  this reads

$$\begin{aligned} \delta_{\Delta C} \langle T\varphi(x) \rangle &:= \delta_{\Delta C} \left( \text{diagram with } \varphi \text{ at } x \text{ and } \mathbb{1} \text{ in a circle} \right) = \left( \text{diagram with } \varphi \text{ at } x \text{ and } \mathbb{1} \text{ in a circle, labeled } C+\Delta C \right) - \left( \text{diagram with } \varphi \text{ at } x \text{ and } \mathbb{1} \text{ in a circle, labeled } C \right) \\ &= i \int d^4y \left[ \text{diagram with } s\varphi \text{ at } x \text{ and } \bar{u}\Delta C \text{ at } y \text{ connected by a loop} \right], \end{aligned} \quad (\text{C.91})$$

where  $s\varphi$  represents the **BRST** transformation of the field  $\varphi$  at the space–time point  $x$  and  $\bar{u}$  is the anti-ghost field associated to the gauge-fixing function  $C$ , both at the space–time point  $y$ . For

$$\varphi = \tilde{H} = c_{\alpha\beta} H_1 + s_{\alpha\beta} H_h, \quad (\text{C.92})$$

the required **BRST** transformation in (C.91) reads

$$s\tilde{H} = \frac{e}{2s_w c_w} u^Z H_a + \frac{ie}{2s_w} (u^- H^+ - u^+ H^-). \quad (\text{C.93})$$

We note that  $s\tilde{H}$  does neither induce would-be Goldstone bosons nor vevs. Hence, one can easily

<sup>1</sup>Specifically, we verified the independence of  $\delta \beta^{\overline{\text{MS}}}$  of the gauge parameters for a non-linear gauge-fixing function  $C^Z = \partial_\mu Z_\mu - \xi_{G_0} M_Z G_0 (1 + \xi_{H_h} H_h)$  for general  $\xi_{G_0}$  and  $\xi_{H_h}$ .



read off the condition for a gauge dependence of (C.90). We modify the gauge-fixing function in (6.29) by setting  $\xi_W = \xi_A = \xi_Z = 1$  and adding a term proportional to  $H_a$  to  $C^Z$ ,

$$C^Z = \partial^\mu Z_\mu - M_Z G_0 - \xi_\beta M_{H_a} H_a, \quad (\text{C.94})$$

which is required to obtain non-vanishing contributions to (C.91). The resulting gauge-fixing function (C.94) in the  $\xi_\beta$  gauge looks simple, but gives rise to a non-diagonal propagator matrix (see App. C.3 for the Feynman rules). An infinitesimal change in the gauge-fixing function is obtained by performing an expansion for small  $\xi_\beta$ , i.e. we identify  $\Delta C$  with  $-\xi_\beta M_{H_a} H_a$ , defining

$$\delta_{\xi_\beta} X := \left. \frac{\partial}{\partial \xi_\beta} X \right|_{\xi_\beta=0} \xi_\beta. \quad (\text{C.95})$$

While we work only to leading order in  $\xi_\beta$ , an exact calculation is possible and straightforward in the gauge of (C.94). At one-loop order we find after Fourier transformation to momentum space

$$\text{F.T.} \int d^4 y \left[ x \text{---} \overset{u^Z}{\curvearrowright} \text{---} y \right]_{H_a} = \int \frac{d^4 q}{(2\pi)^4} \frac{i}{q^2 - M_Z^2} \frac{i}{q^2 - M_{H_a}^2}, \quad (\text{C.96})$$

and hence using (C.91)

$$\langle \tilde{H} \rangle_{\xi_\beta} := \text{F.T.} \delta_{\xi_\beta} \langle T \tilde{H}(x) \rangle = \text{F.T.} \left[ c_{\alpha\beta} \delta_{\xi_\beta} \overset{\textcircled{1}}{\downarrow} H_1 + s_{\alpha\beta} \delta_{\xi_\beta} \overset{\textcircled{1}}{\downarrow} H_h \right] \quad (\text{C.97})$$

$$= -\frac{ie\xi_\beta M_{H_a}}{2s_w c_w} \int \frac{d^4 q}{(2\pi)^4} \frac{i}{q^2 - M_Z^2} \frac{i}{q^2 - M_{H_a}^2}. \quad (\text{C.98})$$

Consequently, there is a non-zero gauge-dependent and UV-divergent contribution to the tadpole in (C.90), which proves the gauge dependence in the popular schemes, where tadpole contributions are absorbed in bare parameters. Note that this argument can be carried over to the supersymmetric case, where  $\langle \tilde{H} \rangle_{\xi_\beta}$  does not change if the same gauge is used. This result is used below to derive the  $\xi_\beta$  dependence of  $\delta\beta^{\overline{\text{MS}}}$  in Schemes 1 and 2 [see Eq. (C.115)].

We validate (C.98) in the THDM using an explicit Feynman-diagrammatic calculation of the tadpole  $\langle \tilde{H} \rangle$ . Inspecting the Feynman rules listed in App. C.3, we find three sources that can induce a linear  $\xi_\beta$  dependence of the tadpole  $\langle \tilde{H} \rangle$ . These are provided by the mixing propagators  $ZH_a$  and  $G_0H_a$  and the coupling of the neutral Higgs bosons  $H_1$  and  $H_h$  to Faddeev–Popov ghosts  $\bar{u}^Z$  and  $u^Z$ . For the  $\xi_\beta$ -dependent tadpole contributions corresponding to (C.97) in momentum space we obtain

$$\delta_{\xi_\beta} \overset{\textcircled{1}}{\downarrow} \varphi = Z \overset{\curvearrowright}{\downarrow} \varphi + G_0 \overset{\curvearrowright}{\downarrow} \varphi + \overset{\curvearrowright}{\downarrow} \varphi \quad \text{for } \varphi = H_1, H_h, \quad (\text{C.99})$$

and the sum of the contributions yields

$$\begin{aligned}
\delta_{\xi_\beta} \textcircled{1} H_1 &= -\frac{ie\xi_\beta M_{H_a} c_{\alpha\beta}}{2s_w c_w} \int \frac{d^4q}{(2\pi)^4} \frac{i}{q^2 - M_Z^2} \frac{i}{q^2 - M_{H_a}^2} = c_{\alpha\beta} \langle \tilde{H} \rangle_{\xi_\beta}, \\
\delta_{\xi_\beta} \textcircled{1} H_h &= -\frac{ie\xi_\beta M_{H_a} s_{\alpha\beta}}{2s_w c_w} \int \frac{d^4q}{(2\pi)^4} \frac{i}{q^2 - M_Z^2} \frac{i}{q^2 - M_{H_a}^2} = s_{\alpha\beta} \langle \tilde{H} \rangle_{\xi_\beta}.
\end{aligned} \tag{C.100}$$

Thus, we reproduce the result in (C.98).

Finally, we show explicitly that  $\delta\beta^{\overline{\text{MS}}}$  remains gauge independent in the *FJ Tadpole Scheme* at one-loop order, but depends explicitly on  $\xi_\beta$  in the gauge of (C.94) in Schemes 1 and 2. To this end, we derive the gauge dependence directly from the renormalized vertex function in (4.121), working only at leading order in  $\xi_\beta$ .

In the *FJ Tadpole Scheme* it is enough to verify that all counterterm parameters that enter the renormalization of  $\beta$  are gauge independent and that no gauge dependence is introduced by the bare vertex function in (4.121). The renormalization constant  $\delta Z_e$  is independent of  $\xi_\beta$  since no Higgs-boson couplings enter this quantity. For  $\delta M_W^2$  and  $\delta M_Z^2$ , the tadpole contributions to the  $WW$  and  $ZZ$  two-point functions are proportional to (see App. B.2)

$$s_{\alpha\beta} \frac{t_{H_1}}{M_{H_1}^2} - c_{\alpha\beta} \frac{t_{H_h}}{M_{H_h}^2}, \tag{C.101}$$

which is not sensitive to our choice of gauge-fixing function. The W-boson self-energy receives no other contributions linear in  $\xi_\beta$ . The linear  $\xi_\beta$ -dependent contribution induced in the Z-boson self-energy contributes only to its longitudinal part and does not influence  $\delta M_Z^2$ . This implies the  $\xi_\beta$  independence of  $\delta M_W^2$  and  $\delta M_Z^2$  which we have also verified via explicit calculation in the  $\xi_\beta$  gauge. For the vertex  $H_a \tau^+ \tau^-$  there is no  $\xi_\beta$ -dependent and at the same time UV-divergent term. This is consistent with the fact that there is no tadpole contribution to the bare vertex function which could cancel a would-be gauge dependence. For  $\delta Z_{G_0 H_a}$  and  $\delta m_\tau$  no such argument can be given, and a cancellation of  $\xi_\beta$ -dependent terms between self-energy diagrams and tadpoles takes place. We explicitly show this cancellation starting with  $\delta Z_{G_0 H_a}$ .

The terms linear in  $\xi_\beta$  contributing to the  $G_0 H_a$  mixing energy are given by<sup>2</sup>

$$\begin{aligned}
\delta_{\xi_\beta} \textcircled{1} G_0 H_a &= \text{---} \textcircled{1} \text{---} \\
&= \text{---} \textcircled{1} \text{---} + \text{---} \textcircled{1} \text{---} + \text{---} \textcircled{1} \text{---} + \text{---} \textcircled{1} \text{---} \\
&\quad + \text{---} \textcircled{1} \text{---} + \text{---} \textcircled{1} \text{---} + \text{---} \textcircled{1} \text{---} + \text{---} \textcircled{1} \text{---} \\
&\quad + \text{---} \textcircled{1} \text{---}.
\end{aligned} \tag{C.102}$$

Note that each diagram contains one mixing propagator. The diagrams involving a neutral

<sup>2</sup>In the alignment limit, the second line in (C.102) vanishes.

Higgs boson propagator and a mixing propagator of a pseudoscalar Higgs boson and a would-be Goldstone boson do not contribute to the  $\overline{\text{MS}}$  renormalization of  $\beta$  because they are UV finite. The other self-energy diagrams are UV divergent, and we obtain for the combined contributions to the  $G_0 H_a$  mixing energy

$$\sum_{\varphi=H_1, H_h} \text{---} \begin{array}{c} Z \\ \curvearrowright \\ \bullet \\ \curvearrowleft \\ H_a \\ \text{---} \\ \varphi \end{array} \text{---} = -\frac{ie}{2s_w M_W} \left[ s_{\alpha\beta}^2 M_{H_1}^2 + c_{\alpha\beta}^2 M_{H_h}^2 + 2M_{H_a}^2 - 2M_{\text{sb}}^2 \right. \\ \left. + c_{\alpha\beta} s_{\alpha\beta} \frac{1-t_\beta^2}{t_\beta} (M_{H_h}^2 - M_{H_1}^2) \right] \langle \tilde{H} \rangle_{\xi_\beta} + \text{UV-finite terms}, \quad (\text{C.103})$$

$$\sum_{\varphi=H_1, H_h} \text{---} \begin{array}{c} H_a \\ \curvearrowright \\ \bullet \\ \curvearrowleft \\ Z \\ \text{---} \\ \varphi \end{array} \text{---} = \frac{ie}{2s_w M_W} [M_{H_a}^2 - s_{\alpha\beta}^2 M_{H_h}^2 - c_{\alpha\beta}^2 M_{H_1}^2] \langle \tilde{H} \rangle_{\xi_\beta} + \text{UV-finite terms}, \quad (\text{C.104})$$

$$\text{---} \begin{array}{c} G_0 \\ \curvearrowright \\ \bullet \\ \curvearrowleft \\ H_a \\ \text{---} \end{array} \text{---} = \frac{ie}{2s_w M_W} \left[ M_{H_1}^2 + 2M_{H_h}^2 - 2M_{\text{sb}}^2 \right. \\ \left. + c_{\alpha\beta} \left( -c_{\alpha\beta} + s_{\alpha\beta} \frac{1-t_\beta^2}{t_\beta} \right) (M_{H_h}^2 - M_{H_1}^2) \right] \langle \tilde{H} \rangle_{\xi_\beta}, \quad (\text{C.105})$$

where for arriving at the (C.103) and (C.104) the numerator structure has been cancelled against one of the neutral Higgs-boson propagators. Adding all contributions leads to

$$\delta_{\xi_\beta} \text{---} \begin{array}{c} \textcircled{1} \\ \text{---} \\ G_0 \end{array} \text{---} \begin{array}{c} \text{---} \\ H_a \end{array} = -\frac{ie}{2s_w M_W} [M_{H_a}^2 - s_{\alpha\beta}^2 M_{H_h}^2 - c_{\alpha\beta}^2 M_{H_1}^2] \langle \tilde{H} \rangle_{\xi_\beta} + \text{UV-finite terms}, \quad (\text{C.106})$$

for the linear dependence of self-energy diagrams on  $\xi_\beta$ . The tadpole contributions to the  $G_0 H_a$  mixing energy are derived using the results in (C.100) leading to

$$\sum_{\varphi=H_1, H_h} \text{---} \begin{array}{c} \textcircled{1} \\ \delta_{\xi_\beta} \varphi \\ \text{---} \\ \bullet \end{array} \text{---} = \frac{ie}{2s_w M_W} [M_{H_a}^2 - s_{\alpha\beta}^2 M_{H_h}^2 - c_{\alpha\beta}^2 M_{H_1}^2] \langle \tilde{H} \rangle_{\xi_\beta}, \quad (\text{C.107})$$

which cancels against the  $\xi_\beta$  dependent terms in (C.106) contributing to the renormalization of  $\beta$ . Thus, we have proven that

$$\left( \delta_{\xi_\beta} \delta Z_{G_0 H_a}^{\overline{\text{MS}}} \right)_3 = 0. \quad (\text{C.108})$$

For the on-shell renormalization of  $\delta m_\tau$  we pursue the same strategy. The  $\xi_\beta$ -dependent contributions to the  $\tau$  self-energy are given by

$$\delta_{\xi_\beta} \begin{array}{c} \tau \\ \text{---} \\ \textcircled{1} \\ \text{---} \\ p \end{array} = \text{---} \begin{array}{c} Z \\ \curvearrowright \\ \bullet \\ \curvearrowleft \\ H_a \\ \text{---} \\ \tau \end{array} \text{---} + \text{---} \begin{array}{c} H_a \\ \curvearrowright \\ \bullet \\ \curvearrowleft \\ Z \\ \text{---} \\ \tau \end{array} \text{---} + \text{---} \begin{array}{c} G_0 \\ \curvearrowright \\ \bullet \\ \curvearrowleft \\ H_a \\ \text{---} \\ \tau \end{array} \text{---} + \text{---} \begin{array}{c} H_a \\ \curvearrowright \\ \bullet \\ \curvearrowleft \\ G_0 \\ \text{---} \\ \tau \end{array} \text{---}. \quad (\text{C.109})$$

Projecting the  $\tau$  self-energy onto a Dirac spinor, putting the momentum on shell, using the Dirac equation, and considering only the scalar and vector part that is relevant for the mass counterterm, we find

$$\delta_{\xi_\beta} \left[ \text{Diagram: } \tau \text{ line with momentum } p \text{ entering a circle labeled } 1 \text{, then } u(p) \text{ line} \right] \Big|_{p^2=m_\tau^2} = \frac{ie^2 t_\beta m_\tau \xi_\beta M_{H_a}}{4M_W s_w^2 c_w} u(p) \times \quad (\text{C.110})$$

$$\int \frac{d^4 q}{(2\pi)^4} \frac{i}{q^2 - M_Z^2} \frac{i}{q^2 - M_{H_a}^2} \frac{i}{(p+q)^2 - m_\tau^2} \left( (p+q)^2 - m_\tau^2 \right) \Big|_{p^2=m_\tau^2}$$

$$= - \frac{iem_\tau t_\beta}{2s_w M_W} \langle \tilde{H} \rangle_{\xi_\beta} u(p) \Big|_{p^2=m_\tau^2}. \quad (\text{C.111})$$

The tadpole contribution to the  $\tau$  self-energy is derived using the results in (C.100) leading to

$$\sum_{\varphi=H_1, H_h} \left[ \text{Diagram: } \tau \text{ line with momentum } p \text{ entering a circle labeled } 1 \text{, then } \delta_{\xi_\beta} \varphi \text{ line} \right] = \frac{iem_\tau t_\beta}{2s_w M_W} \langle \tilde{H} \rangle_{\xi_\beta}. \quad (\text{C.112})$$

The tadpole contribution in (C.112) cancels against the self-energy contribution in (C.111) and we conclude that  $\delta m_\tau$  is independent of  $\xi_\beta$  in on-shell renormalization,

$$(\delta_{\xi_\beta} \delta m_\tau)_3 = 0. \quad (\text{C.113})$$

Altogether, we have proven the gauge independence of  $\delta\beta^{\overline{\text{MS}}}$  in the  $\xi_\beta$  gauge in the *FJ Tadpole Scheme*,

$$\left( \delta_{\xi_\beta} \delta\beta^{\overline{\text{MS}}} \right)_3 = 0. \quad (\text{C.114})$$

Finally, we can give the precise  $\xi_\beta$  dependence of  $\delta\beta$  for Schemes 1 and 2 originating from the gauge dependence of the tadpoles in  $\delta m_\tau$  and  $\delta Z_{G_0 H_a}$ . Using (4.122) for the counterterm, the full  $\xi_\beta$  dependence is obtained as

$$(\delta_{\xi_\beta} \delta\beta^{\overline{\text{MS}}})_i = \frac{e}{2s_w M_W} \left[ 1 - \frac{s_{\alpha\beta}^2 M_{H_h}^2 + c_{\alpha\beta}^2 M_{H_1}^2}{M_{H_a}^2 (1 + t_\beta^2)} \right] \langle \tilde{H} \rangle_{\xi_\beta} \Big|_{\text{P.P.}}, \quad i = 1, 2, \quad (\text{C.115})$$

which is evidently nonzero.

### C.3 Feynman rules in the $\xi_\beta$ gauge

We list the Feynman rules used to derive the gauge dependence of  $\delta\beta^{\overline{\text{MS}}}$  in App. C.2. The gauge-fixing function (C.94) gives rise to mixing of propagators, which is required to actually observe the gauge dependence at one-loop order. The gauge-fixing Lagrangian includes the following mixing terms

$$\mathcal{L}_{\text{GF}} \supset \xi_\beta M_{H_a} (\partial_\mu Z^\mu + M_Z G_0) H_a. \quad (\text{C.116})$$

The corresponding 2-point vertex function in the basis  $(Z_\mu, G_0, H_a)$  reads

$$\Gamma = \begin{pmatrix} -(p^2 - M_Z^2) g^{\mu\nu} & 0 & i\xi_\beta M_{H_a} p^\mu \\ 0 & p^2 - M_Z^2 & \xi_\beta M_{H_a} M_Z \\ -i\xi_\beta M_{H_a} p^\mu & \xi_\beta M_{H_a} M_Z & p^2 - M_{H_a}^2 (1 + \xi_\beta^2) \end{pmatrix}. \quad (\text{C.117})$$

By inverting the vertex function to linear order in  $\xi_\beta$  we obtain the propagators as

$$\text{---} \overset{Z}{\text{~~~~~}} \text{---} = \frac{-ig^{\mu\nu}}{p^2 - M_Z^2} + \mathcal{O}(\xi_\beta^2), \quad (\text{C.118})$$

$$\text{---} \overset{G_0}{\text{-----}} \text{---} = \frac{i}{p^2 - M_Z^2} + \mathcal{O}(\xi_\beta^2), \quad (\text{C.119})$$

$$\text{---} \overset{H_a}{\text{-----}} \text{---} = \frac{i}{p^2 - M_{H_a}^2}, \quad (\text{C.120})$$

$$\text{---} \overset{Z}{\text{~~~~~}} \text{---} \overset{G_0}{\text{-----}} \text{---} = \mathcal{O}(\xi_\beta^2), \quad (\text{C.121})$$

$$\text{---} \overset{Z}{\text{~~~~~}} \text{---} \overset{H_a}{\text{-----}} \text{---} = -\xi_\beta M_{H_a} p^\mu \frac{i}{p^2 - M_Z^2} \frac{i}{p^2 - M_{H_a}^2}, \quad (\text{C.122})$$

$$\text{---} \overset{G_0}{\text{-----}} \text{---} \overset{H_a}{\text{-----}} \text{---} = i\xi_\beta M_{H_a} M_Z \frac{i}{p^2 - M_Z^2} \frac{i}{p^2 - M_{H_a}^2}, \quad (\text{C.123})$$

where the momentum flows from left to right. We identify mixing propagators by two particle labels. The Faddeev–Popov-ghost Lagrangian is derived by the standard methods which requires for the  $\xi_\beta$  gauge the BRST variation of  $H_a$ ,

$$sH_a = -\frac{e}{2s_w c_w} u^Z (c_{\alpha\beta} H_l + s_{\alpha\beta} H_h) + \frac{e}{2s_w} (u^+ H^- + u^- H^+). \quad (\text{C.124})$$

The additional contribution to the ghost Lagrangian involving  $\xi_\beta$  is then given by

$$\mathcal{L}_{\text{gh}} \supset \xi_\beta M_{H_a} \frac{e}{2s_w c_w} \bar{u}^Z u^Z (c_{\alpha\beta} H_l + s_{\alpha\beta} H_h), \quad (\text{C.125})$$

yielding the following gauge-dependent Feynman rules

$$\begin{array}{c} \bar{u}^Z \text{---} \bullet \text{---} \overset{H_h}{\text{---}} \\ \text{---} \bullet \text{---} \overset{H_l}{\text{---}} \\ \text{---} \bullet \text{---} \overset{u^Z}{\text{---}} \end{array} = \frac{ie s_{\alpha\beta}}{2s_w c_w} \xi_\beta M_{H_a}, \quad \begin{array}{c} \bar{u}^Z \text{---} \bullet \text{---} \overset{H_l}{\text{---}} \\ \text{---} \bullet \text{---} \overset{H_h}{\text{---}} \\ \text{---} \bullet \text{---} \overset{u^Z}{\text{---}} \end{array} = \frac{ie c_{\alpha\beta}}{2s_w c_w} \xi_\beta M_{H_a}. \quad (\text{C.126})$$

Finally, we list all other vertices needed in the calculation of App. C.2 with the convention that all particles and momenta are incoming:

$$\begin{array}{c} \overset{H_l}{\text{---}} \\ \text{---} \bullet \text{---} \overset{H_h}{\text{---}} \\ \text{---} \bullet \text{---} \overset{H_a}{\text{---}} \end{array} = \frac{ic_{\alpha\beta} e}{2M_W s_w} (M_{H_a}^2 - M_{H_l}^2), \quad \begin{array}{c} \overset{H_h}{\text{---}} \\ \text{---} \bullet \text{---} \overset{H_l}{\text{---}} \\ \text{---} \bullet \text{---} \overset{H_a}{\text{---}} \end{array} = \frac{is_{\alpha\beta} e}{2M_W s_w} (M_{H_a}^2 - M_{H_h}^2), \quad (\text{C.127})$$

$$\begin{array}{c}
\begin{array}{c}
\text{---} Z^\mu \text{---} \\
\bullet \\
\text{---} H_1 \text{---} \\
\text{---} H_a \text{---} \\
\bullet \\
\text{---} Z^\mu \text{---} \\
\text{---} H_1 \text{---} \\
\text{---} G_0 \text{---}
\end{array}
= \frac{c_{\alpha\beta} e}{2s_w c_w} (p_{H_a}^\mu - p_{H_1}^\mu),
\end{array}
\quad
\begin{array}{c}
\begin{array}{c}
\text{---} Z^\mu \text{---} \\
\bullet \\
\text{---} H_h \text{---} \\
\text{---} H_a \text{---} \\
\bullet \\
\text{---} Z^\mu \text{---} \\
\text{---} H_h \text{---} \\
\text{---} G_0 \text{---}
\end{array}
= \frac{s_{\alpha\beta} e}{2s_w c_w} (p_{H_a}^\mu - p_{H_h}^\mu),
\end{array}
\quad (C.128)$$

$$\begin{array}{c}
\begin{array}{c}
\text{---} Z^\mu \text{---} \\
\bullet \\
\text{---} H_a \text{---} \\
\text{---} H_1 \text{---} \\
\bullet \\
\text{---} Z^\mu \text{---} \\
\text{---} G_0 \text{---}
\end{array}
= -\frac{e s_{\alpha\beta}}{2s_w c_w} (p_{G_0}^\mu - p_{H_1}^\mu),
\end{array}
\quad
\begin{array}{c}
\begin{array}{c}
\text{---} Z^\mu \text{---} \\
\bullet \\
\text{---} H_h \text{---} \\
\text{---} H_a \text{---} \\
\bullet \\
\text{---} Z^\mu \text{---} \\
\text{---} G_0 \text{---}
\end{array}
= \frac{e c_{\alpha\beta}}{2s_w c_w} (p_{G_0}^\mu - p_{H_h}^\mu),
\end{array}
\quad (C.129)$$

$$\begin{array}{c}
\begin{array}{c}
\text{---} H_1 \text{---} \\
\bullet \\
\text{---} H_a \text{---} \\
\text{---} H_a \text{---} \\
\bullet \\
\text{---} H_h \text{---} \\
\text{---} H_a \text{---}
\end{array}
= \frac{ie}{2M_W s_w} \left( s_{\alpha\beta} (M_{H_1}^2 + 2M_{H_a}^2 - 2M_{sb}^2) - c_{\alpha\beta} \frac{1-t_\beta^2}{t_\beta} (M_{H_1}^2 - M_{sb}^2) \right),
\end{array}
\quad (C.130)$$

$$\begin{array}{c}
\begin{array}{c}
\text{---} H_a \text{---} \\
\bullet \\
\text{---} H_a \text{---} \\
\text{---} H_h \text{---} \\
\bullet \\
\text{---} H_a \text{---}
\end{array}
= \frac{ie}{2M_W s_w} \left( -c_{\alpha\beta} (M_{H_h}^2 + 2M_{H_a}^2 - 2M_{sb}^2) - s_{\alpha\beta} \frac{1-t_\beta^2}{t_\beta} (M_{H_h}^2 - M_{sb}^2) \right),
\end{array}
\quad (C.131)$$

$$\begin{array}{c}
\begin{array}{c}
\text{---} G_0 \text{---} \\
\bullet \\
\text{---} H_a \text{---} \\
\text{---} H_a \text{---}
\end{array}
= -\frac{ie^2}{2M_W^2 s_w^2} \left( (M_{H_1}^2 + 2M_{H_h}^2 - 2M_{sb}^2) - c_{\alpha\beta} \left( c_{\alpha\beta} - s_{\alpha\beta} \frac{1-t_\beta^2}{t_\beta} \right) (M_{H_h}^2 - M_{H_1}^2) \right).
\end{array}
\quad (C.132)$$

## D Two-loop Higgs-boson self-energy in the FJ Tadpole Scheme

The following is taken from Ref. [51]. In this appendix, we relate the renormalized two-loop self-energy of the Higgs boson in the SM in the two schemes based on  $\hat{T}_h = 0$  and  $\Delta v = 0$ . Analogously to (4.38) at one loop, we show that the two-loop tadpole contributions to the self-energy, which are generated by  $\Delta v$  in the scheme with  $\hat{T}_h = 0$ , reproduce the self-energy in the scheme with  $\Delta v = 0$ , where unrenormalized tadpoles are explicitly taken into account. The latter situation is given in (4.24) if the renormalized tadpoles are replaced by unrenormalized ones.

To start with, we note that the 1PI two-loop self-energy and tadpole contributions depend on the tadpole renormalization scheme, more precisely, they differ by  $\Delta v$ -dependent terms. Having performed the renormalization at one-loop, the 1PI two-loop self-energy diagrams in both schemes are related via

$$\begin{array}{c}
\text{---} \textcircled{2} \text{---} \Big|_{\hat{T}_h=0} = \text{---} \textcircled{2} \text{---} \Big|_{\Delta v=0} + \text{---} \textcircled{\times} \text{---},
\end{array}
\quad (D.133)$$

where the second diagram on the right-hand side schematically denotes all one-loop self-energy diagrams with an additional insertion of the one-loop two-point tadpole counterterm  $t_{hh}^{(1)}$ . Using the one-loop result (4.38) which relates  $t_{hh}^{(1)}$  with the bare one-loop tadpole  $t_h^{(1)}$ , this can be

written as

$$\begin{array}{c} \text{---} \circlearrowleft 2 \text{---} \end{array} \Big|_{\hat{T}_h=0} = \begin{array}{c} \text{---} \circlearrowleft 2 \text{---} \end{array} \Big|_{\Delta v=0} + \begin{array}{c} \circlearrowleft 1 \\ | \\ \text{---} \circlearrowleft 1 \text{---} \end{array}. \quad (\text{D.134})$$

Next, we consider the two-loop 1PI tadpole which fixes  $t_h^{(2)}$  in the scheme where  $\hat{T}_h = 0$ ,

$$-t_h^{(2)} = \begin{array}{c} \circlearrowleft 2 \\ | \\ \text{---} \end{array} \Big|_{\hat{T}_h=0} = \begin{array}{c} \circlearrowleft 2 \\ | \\ \text{---} \end{array} \Big|_{\Delta v=0} + \begin{array}{c} t_{hh}^{(1)} \\ \circlearrowleft \\ | \\ \text{---} \end{array} = \begin{array}{c} \circlearrowleft 2 \\ | \\ \text{---} \end{array} \Big|_{\Delta v=0} + \begin{array}{c} \circlearrowleft 1 \\ | \\ \text{---} \circlearrowleft 1 \end{array}. \quad (\text{D.135})$$

The first equality is the renormalization condition. In the second equality we separate the  $\Delta v$ -dependent terms, where the second diagram schematically represents all tadpole one-loop diagrams with an additional insertion of  $t_{hh}^{(1)}$ . In the third equality we use again the one-loop result (4.38). In the scheme where the tadpoles are renormalized according to  $\hat{T}_h = 0$  the renormalized two-loop self-energy can be expressed exclusively by 1PI contributions and is given by

$$\hat{\Sigma}_{hh}^{(2)}(q^2) \Big|_{\hat{T}_h=0} = \left[ \begin{array}{c} \text{---} \circlearrowleft 2 \text{---} \end{array} + \begin{array}{c} \text{---} \times \text{---} \end{array} \right] \Big|_{\hat{T}_h=0}. \quad (\text{D.136})$$

The *FJ Tadpole Scheme* for  $\hat{T}_h = 0$  includes tadpoles via the  $\Delta v$ -dependent counterterms. In addition to the  $\Delta v^{(1)}$ -dependent one-loop counterterms appearing in (D.133) and (D.135), the two-loop counterterm induces a further dependence on  $\Delta v^{(1)}$  and  $\Delta v^{(2)}$ . In the SM the additional two-loop tadpole counterterms are derived from (4.47), which can be written as

$$t_{hh} h_{\text{B}}^2 = \left( \lambda_{hhh,\text{B}} \Delta v + \frac{\lambda_{hhhh,\text{B}}}{2} (\Delta v)^2 \right) h_{\text{B}}^2 \quad (\text{D.137})$$

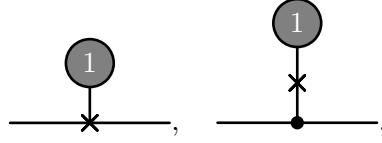
upon identifying  $\lambda_{hhh,\text{B}}$  and  $\lambda_{hhhh,\text{B}}$  as the bare triple and quartic Higgs-boson couplings. The dependence on the two-loop tadpole counterterm  $t_h^{(2)}$  originates from the term proportional to  $\lambda_{hhh,\text{B}} \Delta v^{(2)}$ . Using (4.45) and (D.135) the contribution of  $t_h^{(2)}$  can be written as

$$\begin{array}{c} \circlearrowleft 2 \\ | \\ \text{---} \end{array} \Big|_{\hat{T}_h=0} = \begin{array}{c} \circlearrowleft 2 \\ | \\ \text{---} \end{array} \Big|_{\Delta v=0} + \begin{array}{c} \circlearrowleft 1 \\ | \\ \text{---} \circlearrowleft 1 \end{array}. \quad (\text{D.138})$$

Next, we consider the quadratic 1PI one-loop tadpole contributions which are included in  $\Delta v^{(2)}$  and  $(\Delta v^{(1)})^2$  being proportional to  $\lambda_{hhh}$  and  $\lambda_{hhhh}$ , respectively. We identify the two contributions with

$$\begin{array}{c} \circlearrowleft 1 \\ | \\ \text{---} \circlearrowleft 1 \end{array}, \quad \begin{array}{c} \circlearrowleft 1 \\ | \\ \text{---} \circlearrowleft 1 \end{array}. \quad (\text{D.139})$$

The last two-loop tadpole counterterms result from products of the one-loop tadpole  $t_h^{(1)}$  with the counterterms to  $\lambda_{hhh}$ , the Higgs-boson mass [entering via (4.44)], and the Higgs-boson field-renormalization constant and can be represented as follows:


(D.140)

where in the counterterms  $\Delta v = 0$  is understood. Finally, we separate the  $\Delta v$  dependence from the renormalized two-loop self-energy (D.136). For the bare 1PI two-loop self-energy we use the result (D.134). The two-loop  $\Delta v$ -dependent counterterms are given by the sum of the diagrams in (D.138), (D.139), and (D.140). The result reads

$$\begin{aligned}
 \hat{\Sigma}_{hh}^{(2)}(q^2) \Big|_{\hat{T}_h=0} &= \left[ \text{---} \textcircled{2} \text{---} + \text{---} \times \text{---} \right]_{\hat{T}_h=0} \\
 &= \left[ \text{---} \textcircled{2_R} \text{---} + \text{---} \textcircled{2} \text{---} + \text{---} \textcircled{1} \text{---} + \text{---} \textcircled{1} \textcircled{1_R} \text{---} \right]_{\Delta v=0} \\
 &\quad + \text{---} \textcircled{1} \textcircled{1} \text{---} + \text{---} \textcircled{1} \textcircled{1} \text{---} \\
 &= \hat{\Sigma}_{hh}^{(2)}(q^2) \Big|_{\Delta v=0}.
 \end{aligned}
 \tag{D.141}$$

In the second equation we combine counterterms, evaluated for  $\Delta v = 0$ , and bare-loop topologies to renormalized objects. The result matches the renormalized two-loop self-energy in (4.24) when tadpoles are not renormalized, i.e. for  $\Delta v = 0$ .

## E Distributions for Higgs strahlung and VBF in Higgs-boson production

The following is based on Ref. [52]. We present distributions for the transverse momentum  $p_{T,H_h}$  and rapidity  $y_{H_h}$  of heavy Higgs bosons in Higgs strahlung and VBF. In addition, we show distributions in the rapidity  $y_{\mu^-}$  of the muon  $\mu^-$  in Higgs strahlung and in the rapidity  $y_{j_1}$  of the hardest jet  $j_1$  in VBF. We selected a typical subset of all benchmark points, namely the benchmark points BP3B1, BP43 and BP45 in the THDM and BP3 in the HSESM. All results are given in the  $p^*$  renormalization scheme for  $\alpha$  and  $\beta$ . We do not show any SM-like Higgs-production scenarios in the THDM or HSESM as no shape distortions are observed compared to the SM and basically only the normalization of the distributions is affected. Our results are thus consistent with the observation made in SM EFT matched to the full model for the HSESM and THDM in Ref. [192], where it is stated that for small mixing angles, near the alignment, new operators do not play a significant role.



BP	$\sigma_{\text{LO}}^h/\text{fb}$	$\delta_{\text{EW}}$
BP3B1	877	-13.7%
BP45	802	-13.7%
BP43	501	-13.5%
BP3	366	-13.7%
BP	$\sigma_{\text{LO}}^h/\text{fb}$	$\delta_{\text{EW}}$
BP3B1	1402	-4.0%
BP45	1324	-4.1%
BP43	991	-4.7%
BP3	823	-4.8%

Table .1: Relative NLO corrections  $\delta_{\text{EW}}$  to Higgs-boson production in Higgs strahlung  $pp \rightarrow H_1\mu^-\mu^+$  in the upper table and **VBF**  $pp \rightarrow H_1/H_hjj$  in the lower table in the **SM**. The Higgs-boson mass  $M_h$  is set to the heavy Higgs-boson mass  $M_{H_h}$  in the corresponding benchmark point.

The results for  $p_{\text{T},H_h}$  distributions in Higgs strahlung and **VBF** are shown in Fig. E.1 and Fig. E.2, respectively, the ones for  $y_{H_h}$  in Higgs strahlung and **VBF** in Fig. E.3 and Fig. E.4, and those for  $y_{\mu^-}$  and  $y_{j_1}$  in Fig. E.5 and Fig. E.6.<sup>3</sup> In the upper plots we show the LO and NLO EW differential cross section. In the lower plots the relative EW corrections  $\delta_{\text{EW}}$  are depicted. In order to isolate the genuine effects of the underlying model from the kinematic ones, we have computed the pure **SM** corrections with the **SM** Higgs-boson mass set to the heavy Higgs-boson mass  $M_{H_h}$  denoted as “SM” in the lower panels. The corresponding **SM** total EW cross sections are listed in Table .1.

In the following we focus on shape distortion effects relative to the **SM** results. Starting with the distributions in Higgs strahlung, we observe quite large effects in the  $p_{\text{T},H_h}$  distribution in Fig. E.1 for BP3B1 and BP43 in the **THDM**, small effects for BP3 in the **HSESM**, and no effect in BP45 in the **THDM**, which perfectly reproduces the **SM** result. The situation changes for the distributions in the rapidities  $y_{H_h}$  and  $y_{\mu^-}$  in Figs. E.3 and E.5. Here, the largest deviations from the **SM** are observed for BP43, where the relative EW corrections to the  $y_{H_h}$  distribution in the **THDM** are flatter than in the **SM**. For the  $y_{\mu^-}$  curve the opposite tendency is observed, i.e. the **SM** correction is flatter. For BP3B1, BP45, and BP3 shape distortions relative to the **SM** appear at large rapidities, which are less important due to low statistics in those regions. Switching to the distributions for **VBF** in Figs. E.2, E.4, and E.6, we observe a stronger trend towards **SM**-like results. The largest differences are observed for BP43 in the  $p_{\text{T},H_h}$  and  $y_{j_1}$  distributions. For BP3B1 the effects for the same distributions are smaller but significant. For BP3 the shape distortion in the  $p_{\text{T},H_h}$  distribution for **VBF** is not larger than the one for Higgs strahlung. In general in the considered benchmark points for the **HSESM** the effects in **VBF**, but also in Higgs strahlung, are tiny compared to the ones observed in the **THDM**.

<sup>3</sup>All rapidity distributions were symmetrized.

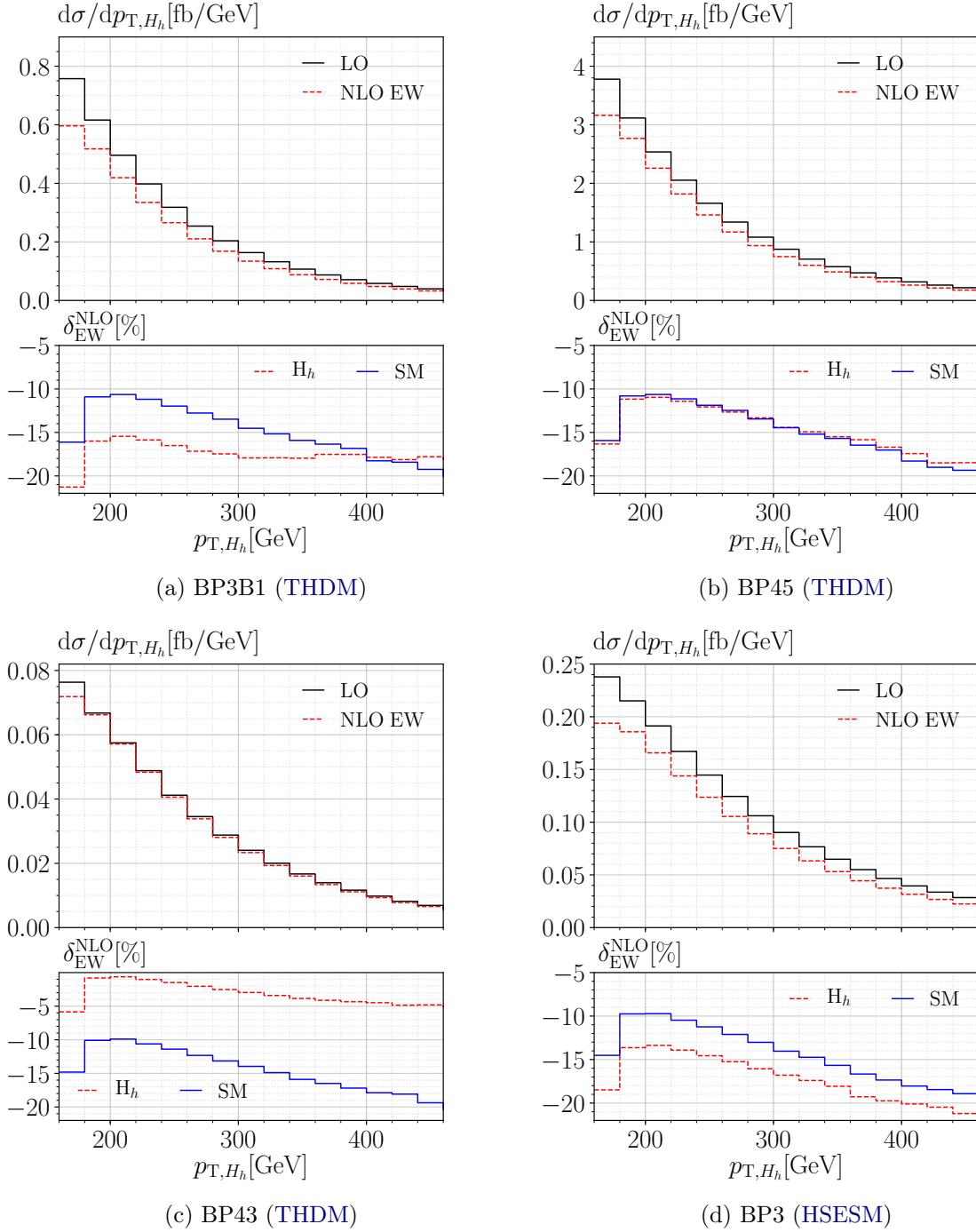


Figure E.1: Distributions in the transverse momentum of the Higgs boson  $p_{T,H_h}$  for heavy Higgs production in Higgs strahlung for the benchmark points BP3B1 in (a), BP45 in (b) and BP43 in (c) in the THDM, and BP3 in (d) in the HSESM.

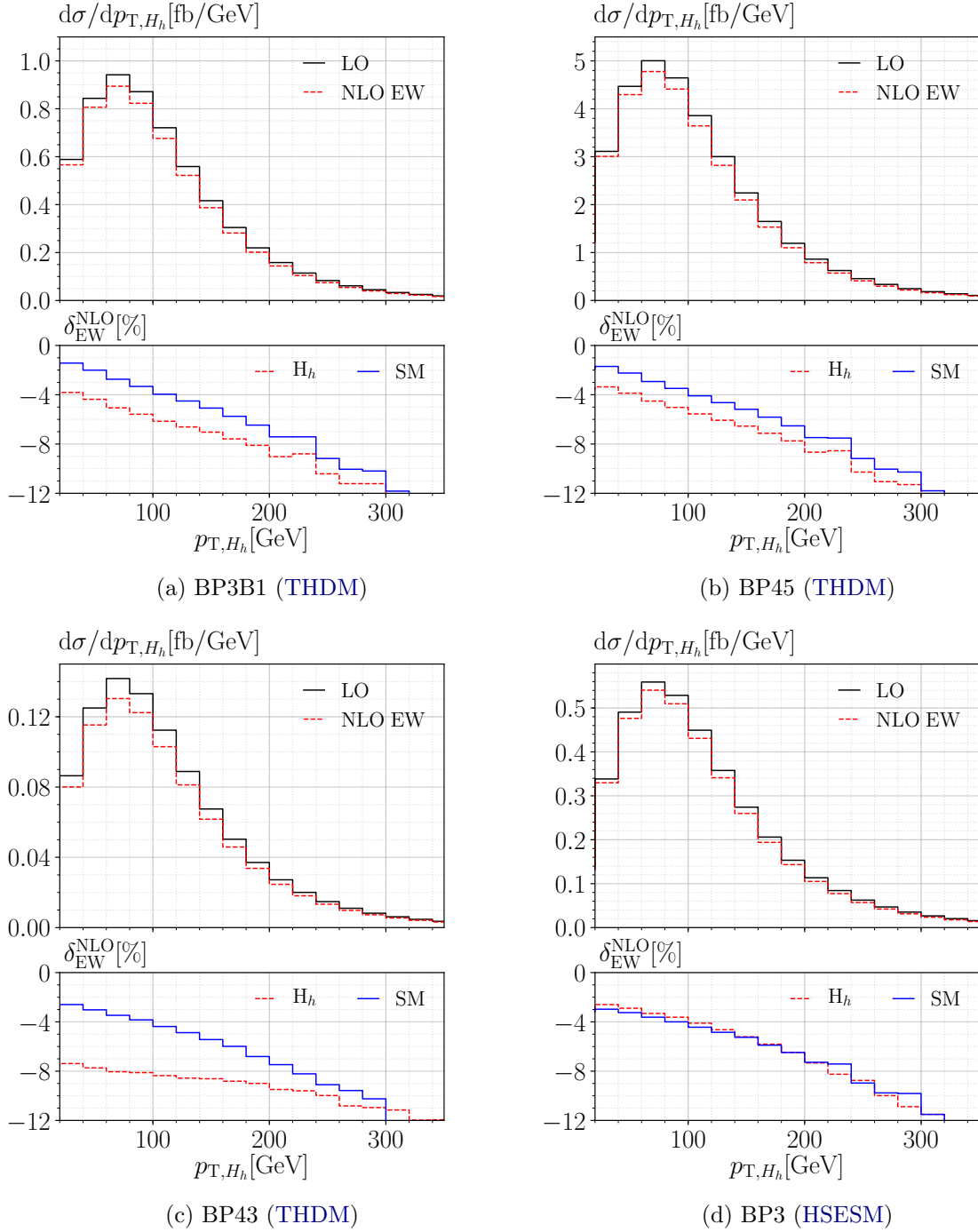
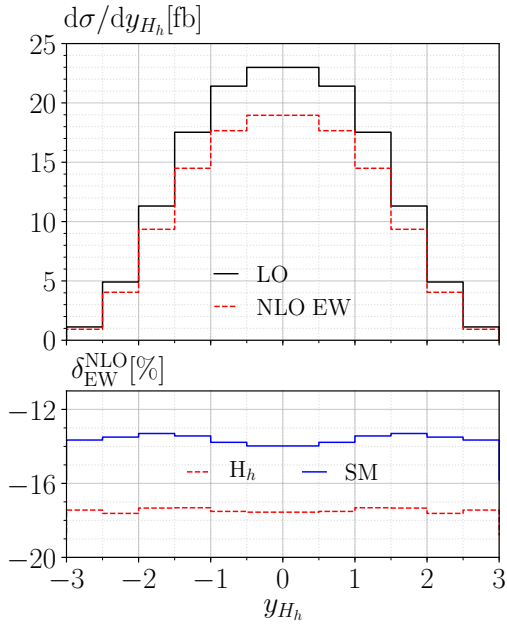
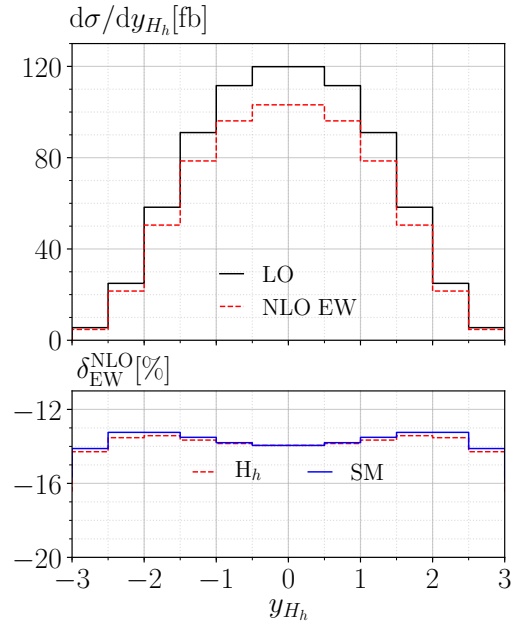


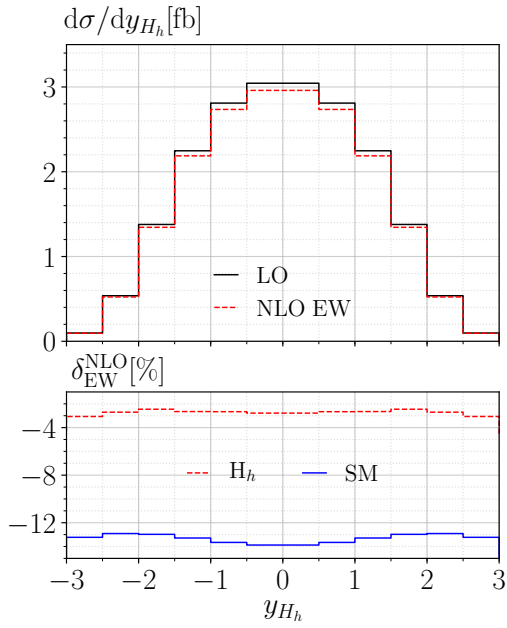
Figure E.2: Distributions in the transverse momentum of the Higgs boson  $p_{T,H_h}$  for heavy Higgs production in VBF for the benchmark points BP3B1 in (a), BP45 in (b) and BP43 in (c) in the THDM, and BP3 in (d) in the HSESM.



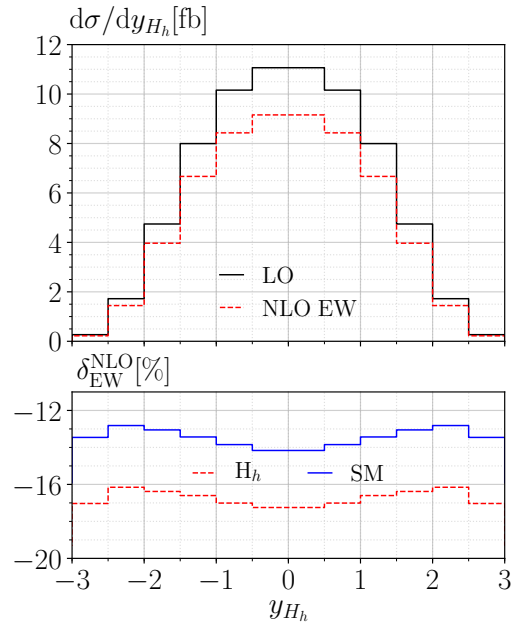
(a) BP3B1 (THDM)



(b) BP45 (THDM)



(c) BP43 (THDM)



(d) BP3 (HSESM)

Figure E.3: Distributions in the rapidity of the Higgs boson  $y_{H_h}$  for heavy Higgs production in Higgs strahlung for the benchmark points BP3B1 in (a), BP45 in (b) and BP43 in (c) in the THDM, and BP3 in (d) in the HSESM.

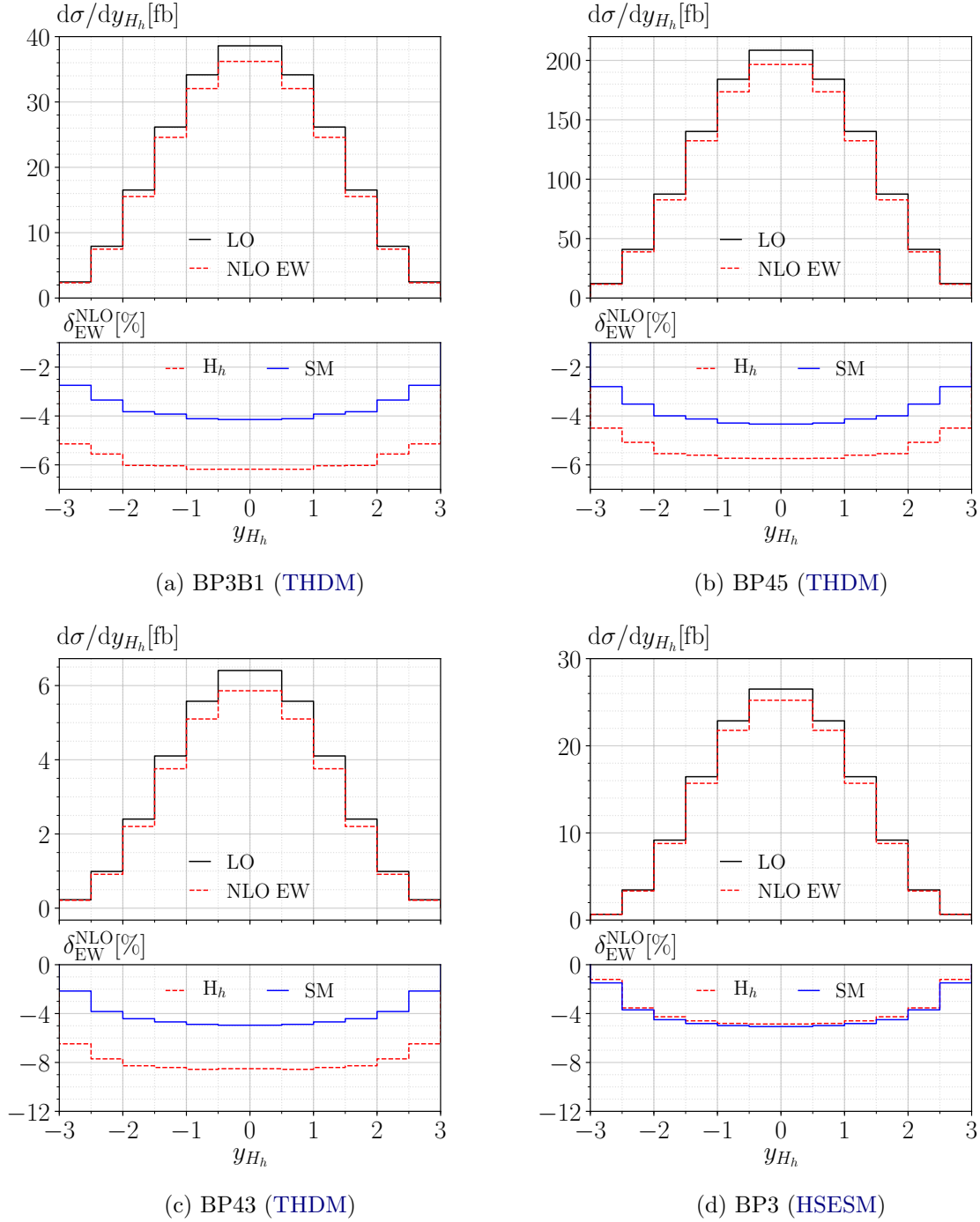
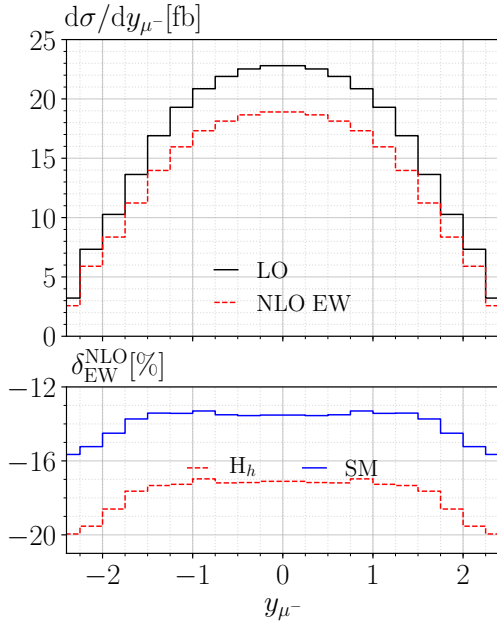
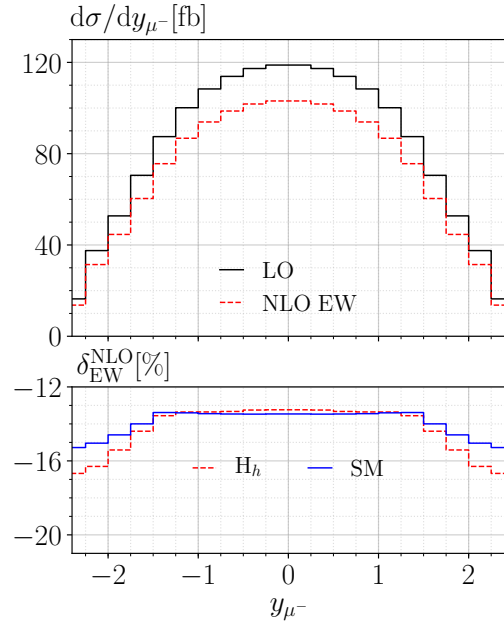


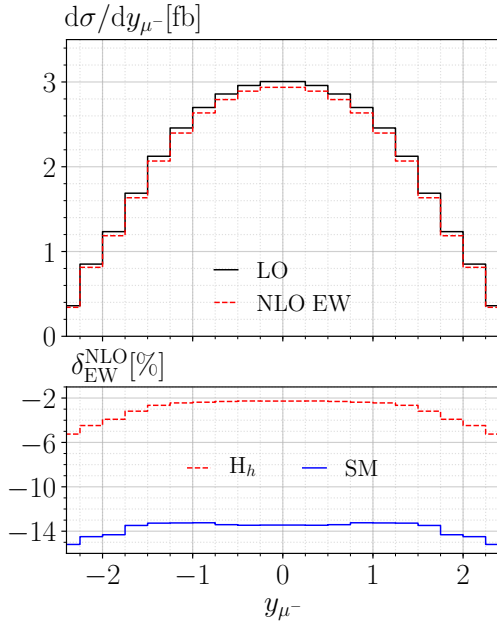
Figure E.4: Distributions in the rapidity of the Higgs boson  $y_{H_h}$  for heavy Higgs production in VBF for the benchmark points BP3B1 in (a), BP45 in (b) and BP43 in (c) in the THDM, and BP3 in (d) in the HSESM.



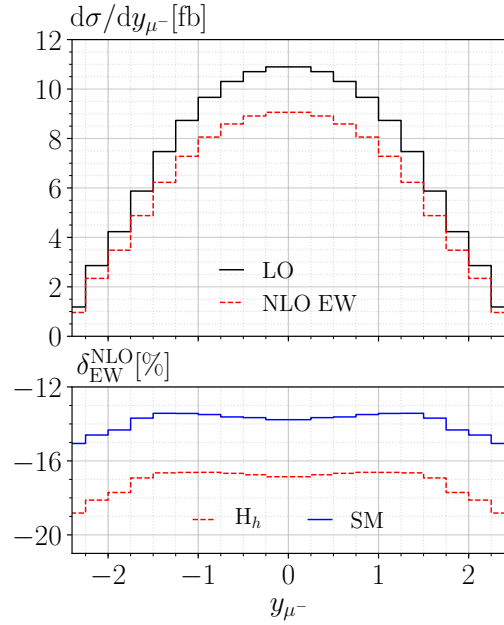
(a) BP3B1 (THDM)



(b) BP45 (THDM)



(c) BP43 (THDM)



(d) BP3 (HSESM)

Figure E.5: Distributions in the rapidity of the muon  $y_{\mu^-}$  for heavy Higgs production in Higgs strahlung for the benchmark points BP3B1 in (a), BP45 in (b) and BP43 in (c) in the THDM, and BP3 in (d) in the HSESM.

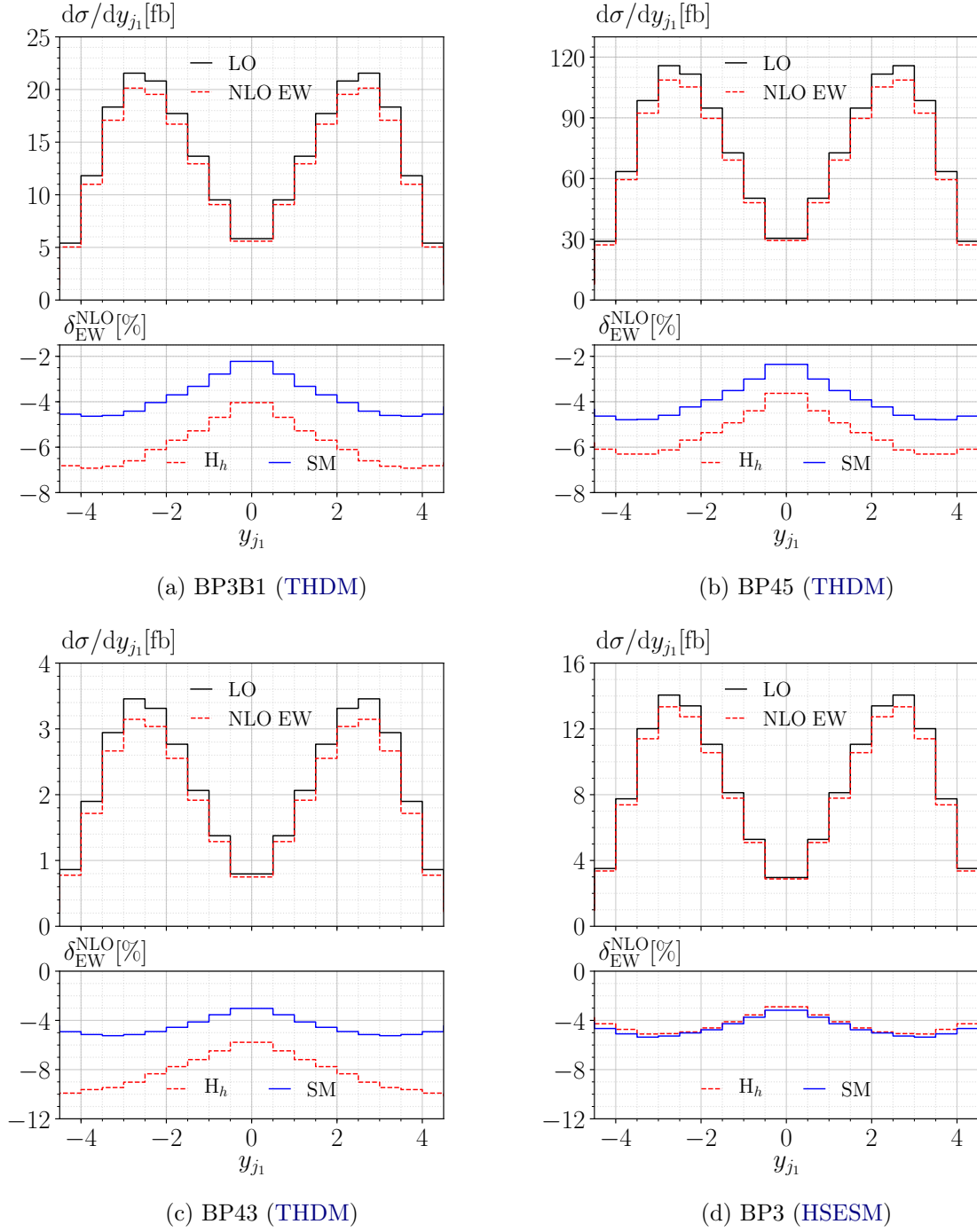


Figure E.6: Distributions in the rapidity of hardest jet  $y_{j_1}$  for heavy Higgs production in VBF for the benchmark points BP3B1 in (a), BP45 in (b) and BP43 in (c) in the THDM, and BP3 in (d) in the HSESM.





# Acronyms

<b>1PI</b>	one-particle irreducible	<b>BF</b>	Background-Field
<b>BRST</b>	Becchi, Rouet, Stora and Tyutin	<b>UFO</b>	Universal FeynRules Output
<b>LHC</b>	Large Hadron Collider	<b>rhs</b>	right-hand side
<b>CMS</b>	Complex-Mass Scheme	<b>Eq</b>	Equation
<b>CSE</b>	Common Subexpression Elimination	<b>SM</b>	Standard Model
<b>DREG</b>	dimensional regularization	<b>BSM</b>	Beyond Standard Model
<b>DRED</b>	dimensional reduction	<b>GR</b>	General Relativity
<b>PVR</b>	Passarino-Veltman Reduction	<b>BEH</b>	Brout-Englert-Higgs
<b>PDF</b>	Parton Distribution Function	<b>THDM</b>	Two-Higgs-Doublet Model
<b>dof</b>	degrees of freedom	<b>MSSM</b>	Minimal Supersymmetric Standard Model
<b>DS</b>	Dyson-Schwinger	<b>SUSY</b>	Supersymmetry
<b>LSZ</b>	Lehmann-Symanzik-Zimmermann	<b>LO</b>	leading order
<b>CKM</b>	Cabibbo Kobayashi Maskawa	<b>NLO</b>	next-to-leading order
<b>lhs</b>	left-hand side	<b>NNLO</b>	next-to-next-to-leading order
<b>MOM</b>	momentum subtraction	<b>HSESM</b>	Higgs-Singlet extension of the SM
<b>BGR</b>	Berends-Giele recursion	<b>SSB</b>	Spontaneous Symmetry Breaking
<b>QCD</b>	Quantum Chromodynamics	<b>STI</b>	Slavnov-Taylor Identities
<b>QED</b>	Quantum Electrodynamics	<b>WI</b>	Ward identity
<b>EW</b>	Electroweak	<b>VBF</b>	Vector-Boson Fusion
<b>QFT</b>	Quantum Field Theory	<b>HXSWG</b>	Higgs Cross Section Working Group
<b>EFT</b>	Effective Field Theory	<b>vev</b>	vacuum expectation value
<b>TGC</b>	triple gauge couplings	<b>wrt</b>	with respect to
<b>RGE</b>	renormalization group equations		
<b>TL</b>	Thomson-Limit		
<b>BFM</b>	Background-Field Method		

# List of Tables

2.1	Gauge-boson fields and associated gauge couplings in the SM. <b>8</b> stands for octet, <b>3</b> for triplet and <b>1</b> for singlet representations. The value in the parenthesis denotes the hypercharge. . . . .	8
2.2	Fermion-field representations of (2.3) in the SM. <b>3</b> stands for triplet, <b>2</b> for doublet and <b>1</b> for singlet representations. The value in the parenthesis denotes the hypercharge $Y$ . . . . .	9
2.3	SM Higgs doublet field representations. <b>2</b> stands for doublet and <b>1</b> for singlet representations. The value in the parenthesis denotes the hypercharge $Y$ . Since the Higgs doublet is chosen to be complex, it comes with 4 dof instead of 2. . . . .	10
2.4	Independent parameters in the gauge and mass eigenbasis of the THDM and HSESM. The EW gauge couplings need to be considered in order to properly identify the independent parameters in the mass eigenbasis after SSB. Note that there are no additional independent parameters, and we intentionally did not list vev or tadpole parameters. . . . .	15
3.1	Recursive computation of a 4-particle process using BGR ordered in increasing number of bits. The external currents are set to one, treating them as scalars. Note that the computation order in RECOLA2 is slightly different. . . . .	22
7.1	THDM benchmark points in the alignment limit, i.e. $s_{\alpha\beta} \rightarrow -1$ , $c_{\alpha\beta} \rightarrow 0$ , taken from Ref. [176]. The parameter $M_{\text{sb}}$ depends on the other parameters and is given for convenience. . . . .	87
7.2	THDM benchmark points outside the alignment limit taken from Ref. [177] (a-1, b-1) and Ref. [176]. The parameter $M_{\text{sb}}$ depends on the other parameters and is given for convenience. . . . .	87
7.3	HSESM benchmark points compiled from Ref. [178]. In the upper table typical scenarios are depicted with a heavy additional scalar Higgs boson. In the lower table inverted scenarios are listed with $H_h$ identified as the SM Higgs boson and mass $M_{H_h} = 125.09$ GeV. . . . .	88
7.4	Running values for $t_\beta$ , $c_{\alpha\beta}$ and $M_{\text{sb}}$ in the THDM at the scales $\mu_0/2$ and $2\mu_0$ . The benchmark points are defined at the central scale $\mu_0$ in Tables 7.1 and 7.2. The results for the alignment-limit scenarios are in the upper part of the table whereas the non-alignment scenarios are in the lower part. For BP22A the running $\beta$ reaches $\pi/2$ for a scale greater than $\mu_0/2$ , thus, $t_\beta$ becomes singular. . . . .	89
7.5	Running values for $s_\alpha$ in the HSESM at the scales $\mu_0/2$ and $2\mu_0$ . The benchmark points are defined at the central scale $\mu_0$ in Table 7.3. . . . .	90

7.6	Relative NLO corrections $\delta_{\text{EW}}$ to SM-like Higgs-boson production in Higgs strahlung $pp \rightarrow H_1\mu^-\mu^+$ in alignment scenarios in the THDM. The results in the $\overline{\text{MS}}$ scheme are given at the central scale $\mu_0 = 2M_h = 250.18 \text{ GeV}$ with scale uncertainties estimated including the RG-running of parameters (7.10). Both on-shell schemes agree within the integration error, and only results in the $p^*$ scheme are given. The SM EW correction is $\delta_{\text{EW}} = -12.4\%$ . . . . .	92
7.7	Relative NLO corrections $\delta_{\text{EW}}$ to SM-like Higgs-boson production in Higgs strahlung $pp \rightarrow H_1\mu^-\mu^+$ in non-alignment scenarios in the THDM. The results in the $\overline{\text{MS}}$ scheme are given at the central scale $\mu_0 = 2M_h = 250.18 \text{ GeV}$ with scale uncertainties estimated including the RG-running of parameters (7.10). The scale uncertainties are large, and for some points (BP22A, BP3B2, BP44) the running is unstable and yields corrections beyond 100%, which is indicated as “-” . . . . .	92
7.8	Relative NLO corrections $\delta_{\text{EW}}$ to heavy Higgs-boson $H_h$ production in Higgs strahlung $pp \rightarrow H_h\mu^-\mu^+$ in the THDM. No results for the $\overline{\text{MS}}$ scheme are presented due to large scale uncertainties exceeding 100%. . . . .	92
7.9	Relative NLO corrections $\delta_{\text{EW}}$ to light Higgs-boson $H_1$ production in Higgs strahlung $pp \rightarrow H_1\mu^-\mu^+$ in the HSESM. The scale uncertainties in the $\overline{\text{MS}}$ scheme are estimated including the RG-running of parameters (7.10). The central scale for BP1–4 is $\mu_0 = 2M_h = 250.18 \text{ GeV}$ . For BP6 we set the scale to $\mu_0 = 130 \text{ GeV}$ . For BP5 the $\overline{\text{MS}}$ scheme is unstable. The scale uncertainties for BP1–3 are smaller than the given accuracy. . . . .	93
7.10	Relative NLO corrections $\delta_{\text{EW}}$ to heavy Higgs-boson $H_h$ production in Higgs strahlung $pp \rightarrow H_h\mu^-\mu^+$ in the HSESM. The scale uncertainties in the $\overline{\text{MS}}$ scheme are estimated including the RG-running of parameters (7.10). For the BP1–4 the central scales are 580 GeV, 480 GeV, 380 GeV, and 280 GeV, respectively. For BP5 and BP6 the central scale is $\mu_0 = 2M_h = 250.18 \text{ GeV}$ . . . . .	93
7.11	Relative NLO corrections $\delta_{\text{EW}}$ to Higgs-boson production in VBF $pp \rightarrow H_1/H_hjj$ in the THDM. The SM-like Higgs production is in the upper table, indicated as $\sigma_{\text{LO}}^{H_1}$ whereas the heavy one is the lower table, indicated as $\sigma_{\text{LO}}^{H_h}$ . The SM EW correction to $\sigma_{\text{LO}}^{H_1}$ is $\delta_{\text{EW}} = -5.5\%$ . . . . .	94
7.12	Relative NLO corrections $\delta_{\text{EW}}$ to Higgs-boson production in VBF $pp \rightarrow H_1/H_hjj$ in the HSESM. The light Higgs production is in the upper table, indicated as $\sigma_{\text{LO}}^{H_1}$ whereas the heavy one is in the lower table, indicated as $\sigma_{\text{LO}}^{H_h}$ . . . . .	94
.1	Relative NLO corrections $\delta_{\text{EW}}$ to Higgs-boson production in Higgs strahlung $pp \rightarrow H_1\mu^-\mu^+$ in the upper table and VBF $pp \rightarrow H_1/H_hjj$ in the lower table in the SM. The Higgs-boson mass $M_h$ is set to the heavy Higgs-boson mass $M_{H_h}$ in the corresponding benchmark point. . . . .	125

Table

Page

# List of Figures

2.1	The particle content of the SM. The innermost region unifies strongly interacting particles. The next to innermost region describes the QED interactions with the photon. The outermost region represents the weak force mediated by the massive gauge bosons, which includes interactions with neutrinos. The Higgs boson interacts with all massive particles. <sup>4</sup> . . . . .	7
5.1	The RECOLA2 model file generation. UFO vertices are taken as input and each vertex is permuted and mapped to a suited BGR operator. Given a counterterm expansion (5.9), REPT1L can generate all counterterm vertices and include them in the BGR. Once the renormalization is done and the $R_2$ -terms are computed, the model file is derived once again, including solutions to counterterm parameters and $R_2$ terms. . . . .	67
5.2	The REPT1L–RECOLA2 tool chain. REPT1L can generate tree-level model files which can then be used in combination with the RECOLA2 library to generate building blocks required in the renormalization process. The process generation is done via the same off-shell currents also used in numerical computations. The currents are evaluated analytically with FORM and further processed with SYMPY. The results are then available to REPT1L and are used in the renormalized model-file derivation. The red box indicates the analytic computations which uses the tool chain combining RECOLA2, FORM and SYMPY. After the renormalized model-file derivation, this tool chain and REPT1L are no longer needed. The blue box, i.e. RECOLA2 and model files, can be used as stand-alone versions (pure FORTRAN95) for numerical computations. . . . .	72
E.1	Distributions in the transverse momentum of the Higgs boson $p_{T,H_h}$ for heavy Higgs production in Higgs strahlung for the benchmark points BP3B1 in (a), BP45 in (b) and BP43 in (c) in the THDM, and BP3 in (d) in the HSESM. . . .	126
E.2	Distributions in the transverse momentum of the Higgs boson $p_{T,H_h}$ for heavy Higgs production in VBF for the benchmark points BP3B1 in (a), BP45 in (b) and BP43 in (c) in the THDM, and BP3 in (d) in the HSESM. . . . .	127
E.3	Distributions in the rapidity of the Higgs boson $y_{H_h}$ for heavy Higgs production in Higgs strahlung for the benchmark points BP3B1 in (a), BP45 in (b) and BP43 in (c) in the THDM, and BP3 in (d) in the HSESM. . . . .	128
E.4	Distributions in the rapidity of the Higgs boson $y_{H_h}$ for heavy Higgs production in VBF for the benchmark points BP3B1 in (a), BP45 in (b) and BP43 in (c) in the THDM, and BP3 in (d) in the HSESM. . . . .	129

E.5 Distributions in the rapidity of the muon  $y_{\mu^-}$  for heavy Higgs production in Higgs strahlung for the benchmark points BP3B1 in (a), BP45 in (b) and BP43 in (c) in the THDM, and BP3 in (d) in the HSESM. . . . . 130

E.6 Distributions in the rapidity of hardest jet  $y_{j_1}$  for heavy Higgs production in VBF for the benchmark points BP3B1 in (a), BP45 in (b) and BP43 in (c) in the THDM, and BP3 in (d) in the HSESM. . . . . 131

**Figure** **Page**

# Bibliography

- [1] **CMS** Collaboration, S. Chatrchyan et al., *Observation of a new boson at a mass of 125 GeV with the CMS experiment at the LHC*, *Phys. Lett.* **B716** (2012) 30–61, [[arXiv:1207.7235](#)].
- [2] **ATLAS** Collaboration, G. Aad et al., *Observation of a new particle in the search for the Standard Model Higgs boson with the ATLAS detector at the LHC*, *Phys. Lett.* **B716** (2012) 1–29, [[arXiv:1207.7214](#)].
- [3] Z. Bern, L. J. Dixon, D. C. Dunbar, and D. A. Kosower, *Fusing gauge theory tree amplitudes into loop amplitudes*, *Nucl. Phys.* **B435** (1995) 59–101, [[hep-ph/9409265](#)].
- [4] R. Britto, F. Cachazo, and B. Feng, *Generalized unitarity and one-loop amplitudes in  $N=4$  super-Yang-Mills*, *Nucl. Phys.* **B725** (2005) 275–305, [[hep-th/0412103](#)].
- [5] G. Ossola, C. G. Papadopoulos, and R. Pittau, *Reducing full one-loop amplitudes to scalar integrals at the integrand level*, *Nucl. Phys.* **B763** (2007) 147–169, [[hep-ph/0609007](#)].
- [6] R. K. Ellis, W. T. Giele, and Z. Kunszt, *A Numerical Unitarity Formalism for Evaluating One-Loop Amplitudes*, *JHEP* **03** (2008) 003, [[arXiv:0708.2398](#)].
- [7] W. T. Giele, Z. Kunszt, and K. Melnikov, *Full one-loop amplitudes from tree amplitudes*, *JHEP* **04** (2008) 049, [[arXiv:0801.2237](#)].
- [8] R. K. Ellis, W. T. Giele, Z. Kunszt, and K. Melnikov, *Masses, fermions and generalized  $D$ -dimensional unitarity*, *Nucl. Phys.* **B822** (2009) 270–282, [[arXiv:0806.3467](#)].
- [9] V. Hirschi, et al., *Automation of one-loop QCD corrections*, *JHEP* **05** (2011) 044, [[arXiv:1103.0621](#)].
- [10] F. Cascioli, P. Maierhöfer, and S. Pozzorini, *Scattering Amplitudes with Open Loops*, *Phys. Rev. Lett.* **108** (2012) 111601, [[arXiv:1111.5206](#)].
- [11] S. Kallweit, J. M. Lindert, P. Maierhöfer, S. Pozzorini, and M. Schönherr, *NLO electroweak automation and precise predictions for  $W$ +multijet production at the LHC*, *JHEP* **04** (2015) 012, [[arXiv:1412.5157](#)].
- [12] J. Alwall, et al., *The automated computation of tree-level and next-to-leading order differential cross sections, and their matching to parton shower simulations*, *JHEP* **07** (2014) 079, [[arXiv:1405.0301](#)].
- [13] G. Cullen et al., *GoSam-2.0: a tool for automated one-loop calculations within the Standard Model and beyond*, *Eur. Phys. J.* **C74** (2014), no. 8 3001, [[arXiv:1404.7096](#)].

- [14] M. Chiesa, N. Greiner, and F. Tramontano, *Automation of electroweak corrections for LHC processes*, *J. Phys.* **G43** (2016), no. 1 013002, [[arXiv:1507.08579](#)].
- [15] T. Hahn, *Generating Feynman diagrams and amplitudes with FeynArts 3*, *Comput. Phys. Commun.* **140** (2001) 418–431, [[hep-ph/0012260](#)].
- [16] C. Groß, et al., *New Developments in FormCalc 8.4*, [arXiv:1407.0235](#).  
[PoSLL2014,035(2014)].
- [17] A. van Hameren, *Multi-gluon one-loop amplitudes using tensor integrals*, *JHEP* **0907** (2009) 088, [[arXiv:0905.1005](#)].
- [18] F. A. Berends and W. T. Giele, *Recursive Calculations for Processes with  $n$  Gluons*, *Nucl. Phys.* **B306** (1988) 759–808.
- [19] S. Actis, A. Denner, L. Hofer, A. Scharf, and S. Uccirati, *Recursive generation of one-loop amplitudes in the Standard Model*, *JHEP* **04** (2013) 037, [[arXiv:1211.6316](#)].
- [20] S. Actis, et al., *RECOLA: REcursive Computation of One-Loop Amplitudes*, *Comput. Phys. Commun.* **214** (2017) 140–173, [[arXiv:1605.01090](#)].
- [21] A. Denner, S. Dittmaier, and L. Hofer, *Collier: a fortran-based Complex One-Loop Library in Extended Regularizations*, *Comput. Phys. Commun.* **212** (2017) 220–238, [[arXiv:1604.06792](#)].
- [22] A. Denner, L. Hofer, A. Scharf, and S. Uccirati, *Electroweak corrections to  $Z + 2$  jets production at the LHC*, *PoS RADCOR2013* (2013) 019, [[arXiv:1311.5336](#)].
- [23] A. Denner, L. Hofer, A. Scharf, and S. Uccirati, *Electroweak corrections to lepton pair production in association with two hard jets at the LHC*, *JHEP* **01** (2015) 094, [[arXiv:1411.0916](#)].
- [24] B. Biedermann, A. Denner, S. Dittmaier, L. Hofer, and B. Jäger, *Electroweak corrections to  $pp \rightarrow \mu^+ \mu^- e^+ e^- + X$  at the LHC: a Higgs background study*, *Phys. Rev. Lett.* **116** (2016), no. 16 161803, [[arXiv:1601.07787](#)].
- [25] B. Biedermann, et al., *Next-to-leading-order electroweak corrections to  $pp \rightarrow W^+ W^- \rightarrow 4$  leptons at the LHC*, *JHEP* **06** (2016) 065, [[arXiv:1605.03419](#)].
- [26] B. Biedermann, A. Denner, S. Dittmaier, L. Hofer, and B. Jäger, *Next-to-leading-order electroweak corrections to the production of four charged leptons at the LHC*, *JHEP* **01** (2017) 033, [[arXiv:1611.05338](#)].
- [27] A. Denner, R. Feger, and A. Scharf, *Irreducible background and interference effects for Higgs-boson production in association with a top-quark pair*, *JHEP* **04** (2015) 008, [[arXiv:1412.5290](#)].

- [28] A. Denner and R. Feger, *NLO QCD corrections to off-shell top-antitop production with leptonic decays in association with a Higgs boson at the LHC*, *JHEP* **11** (2015) 209, [[arXiv:1506.07448](#)].
- [29] A. Denner and M. Pellen, *NLO electroweak corrections to off-shell top-antitop production with leptonic decays at the LHC*, *JHEP* **08** (2016) 155, [[arXiv:1607.05571](#)].
- [30] A. Denner, J.-N. Lang, M. Pellen, and S. Uccirati, *Higgs production in association with off-shell top-antitop pairs at NLO EW and QCD at the LHC*, *JHEP* **02** (2017) 053, [[arXiv:1612.07138](#)].
- [31] B. Biedermann, A. Denner, and M. Pellen, *Large electroweak corrections to vector-boson scattering at the Large Hadron Collider*, [arXiv:1611.02951](#).
- [32] T. Gleisberg, et al., *SHERPA 1. alpha: A Proof of concept version*, *JHEP* **02** (2004) 056, [[hep-ph/0311263](#)].
- [33] T. Gleisberg, et al., *Event generation with SHERPA 1.1*, *JHEP* **02** (2009) 007, [[arXiv:0811.4622](#)].
- [34] M. Moretti, T. Ohl, and J. Reuter, *O'Mega: An Optimizing matrix element generator*, [hep-ph/0102195](#).
- [35] W. Kilian, T. Ohl, and J. Reuter, *WHIZARD: Simulating Multi-Particle Processes at LHC and ILC*, *Eur. Phys. J.* **C71** (2011) 1742, [[arXiv:0708.4233](#)].
- [36] J. Reuter, B. Chokoufe Nejad, and C. Weiss, *NLO QCD Corrections to Off-shell  $t\bar{t}$  and  $t\bar{t}H$  at the ILC*, in *International Workshop on Future Linear Colliders 2016 (LCWS2016) Morioka, Iwate, Japan, December 5-9, 2016*, 2017. [arXiv:1703.05791](#).
- [37] A. Alloul, N. D. Christensen, C. Degrande, C. Duhr, and B. Fuks, *FeynRules 2.0 - A complete toolbox for tree-level phenomenology*, *Comput. Phys. Commun.* **185** (2014) 2250–2300, [[arXiv:1310.1921](#)].
- [38] F. Staub, *SARAH 4: A tool for (not only SUSY) model builders*, *Comput. Phys. Commun.* **185** (2014) 1773–1790, [[arXiv:1309.7223](#)].
- [39] C. Degrande, *Automatic evaluation of UV and R2 terms for beyond the Standard Model Lagrangians: a proof-of-principle*, *Comput. Phys. Commun.* **197** (2015) 239–262, [[arXiv:1406.3030](#)].
- [40] C. Degrande, et al., *UFO - The Universal FeynRules Output*, *Comput. Phys. Commun.* **183** (2012) 1201–1214, [[arXiv:1108.2040](#)].
- [41] **LIGO Scientific Collaboration and Virgo Collaboration** Collaboration, B. P. Abbott, et al., *Observation of gravitational waves from a binary black hole merger*, *Phys. Rev. Lett.* **116** (Feb, 2016) 061102.



- [42] G. Bertone, D. Hooper, and J. Silk, *Particle dark matter: Evidence, candidates and constraints*, *Phys. Rept.* **405** (2005) 279–390, [[hep-ph/0404175](#)].
- [43] **Particle Data Group** Collaboration, C. Patrignani et al., *Review of Particle Physics*, *Chin. Phys.* **C40** (2016), no. 10 100001.
- [44] G. C. Dorsch, S. J. Huber, T. Konstandin, and J. M. No, *A Second Higgs Doublet in the Early Universe: Baryogenesis and Gravitational Waves*, [arXiv:1611.05874](#).
- [45] M. E. Peskin and T. Takeuchi, *Estimation of oblique electroweak corrections*, *Phys. Rev.* **D46** (1992) 381–409.
- [46] W. Grimus, L. Lavoura, O. M. Ogreid, and P. Osland, *A Precision constraint on multi-Higgs-doublet models*, *J. Phys.* **G35** (2008) 075001, [[arXiv:0711.4022](#)].
- [47] P. Bechtle, O. Brein, S. Heinemeyer, G. Weiglein, and K. E. Williams, *HiggsBounds: Confronting Arbitrary Higgs Sectors with Exclusion Bounds from LEP and the Tevatron*, *Comput. Phys. Commun.* **181** (2010) 138–167, [[arXiv:0811.4169](#)].
- [48] P. Bechtle, S. Heinemeyer, O. Stål, T. Stefaniak, and G. Weiglein, *HiggsSignals: Confronting arbitrary Higgs sectors with measurements at the Tevatron and the LHC*, *Eur. Phys. J.* **C74** (2014), no. 2 2711, [[arXiv:1305.1933](#)].
- [49] D. Eriksson, J. Rathsmann, and O. Stal, *2HDMC: Two-Higgs-Doublet Model Calculator Physics and Manual*, *Comput. Phys. Commun.* **181** (2010) 189–205, [[arXiv:0902.0851](#)].
- [50] A. Denner, G. Weiglein, and S. Dittmaier, *Application of the background field method to the electroweak standard model*, *Nucl. Phys.* **B440** (1995) 95–128, [[hep-ph/9410338](#)].
- [51] A. Denner, L. Jenniches, J.-N. Lang, and C. Sturm, *Gauge-independent  $\overline{MS}$  renormalization in the 2HDM*, *JHEP* **09** (2016) 115, [[arXiv:1607.07352](#)].
- [52] A. Denner, J.-N. Lang, and S. Uccirati, *NLO electroweak corrections in extended Higgs Sectors with RECOLA2*, [arXiv:1705.06053](#).
- [53] J. F. Gunion and H. E. Haber, *The CP conserving Two-Higgs-Doublet Model: the approach to the decoupling limit*, *Phys. Rev.* **D67** (2003) 075019, [[hep-ph/0207010](#)].
- [54] G. C. Branco, et al., *Theory and phenomenology of Two-Higgs-Doublet Models*, *Phys. Rept.* **516** (2012) 1–102, [[arXiv:1106.0034](#)].
- [55] G. M. Pruna and T. Robens, *Higgs singlet extension parameter space in the light of the LHC discovery*, *Phys. Rev.* **D88** (2013), no. 11 115012, [[arXiv:1303.1150](#)].
- [56] T. Robens and T. Stefaniak, *Status of the Higgs Singlet Extension of the Standard Model after LHC Run 1*, *Eur. Phys. J.* **C75** (2015) 104, [[arXiv:1501.02234](#)].
- [57] T. Robens and T. Stefaniak, *LHC Benchmark Scenarios for the Real Higgs Singlet Extension of the Standard Model*, *Eur. Phys. J.* **C76** (2016), no. 5 268, [[arXiv:1601.07880](#)].

- [58] G. Chalons, D. Lopez-Val, T. Robens, and T. Stefaniak, *The Higgs singlet extension at LHC Run 2*, in *Proceedings, 38th International Conference on High Energy Physics (ICHEP 2016): Chicago, IL, USA, August 3-10, 2016*, 2016. [arXiv:1611.03007](#).
- [59] R. M. Schabinger and J. D. Wells, *A Minimal spontaneously broken hidden sector and its impact on Higgs boson physics at the large hadron collider*, *Phys. Rev.* **D72** (2005) 093007, [[hep-ph/0509209](#)].
- [60] B. Patt and F. Wilczek, *Higgs-field portal into hidden sectors*, [hep-ph/0605188](#).
- [61] M. Bowen, Y. Cui, and J. D. Wells, *Narrow trans-TeV Higgs bosons and  $H \rightarrow hh$  decays: Two LHC search paths for a hidden sector Higgs boson*, *JHEP* **03** (2007) 036, [[hep-ph/0701035](#)].
- [62] S. L. Glashow and S. Weinberg, *Natural Conservation Laws for Neutral Currents*, *Phys. Rev.* **D15** (1977) 1958.
- [63] E. A. Paschos, *Diagonal Neutral Currents*, *Phys. Rev.* **D15** (1977) 1966.
- [64] F. J. Dyson, *The S matrix in quantum electrodynamics*, *Phys. Rev.* **75** (1949) 1736–1755.
- [65] J. S. Schwinger, *On the Green's functions of quantized fields. 1.*, *Proc. Nat. Acad. Sci.* **37** (1951) 452–455.
- [66] J. S. Schwinger, *On the Green's functions of quantized fields. 2.*, *Proc. Nat. Acad. Sci.* **37** (1951) 455–459.
- [67] A. Kanaki and C. G. Papadopoulos, *HELAC: A Package to compute electroweak helicity amplitudes*, *Comput. Phys. Commun.* **132** (2000) 306–315, [[hep-ph/0002082](#)].
- [68] C. Hartmann and M. Trott, *On one-loop corrections in the standard model effective field theory; the  $\Gamma(h \rightarrow \gamma\gamma)$  case*, *JHEP* **07** (2015) 151, [[arXiv:1505.02646](#)].
- [69] M. Ghezzi, R. Gomez-Ambrosio, G. Passarino, and S. Uccirati, *NLO Higgs effective field theory and  $\kappa$ -framework*, *JHEP* **07** (2015) 175, [[arXiv:1505.03706](#)].
- [70] F. Caravaglios and M. Moretti, *An algorithm to compute Born scattering amplitudes without Feynman graphs*, *Phys. Lett.* **B358** (1995) 332–338, [[hep-ph/9507237](#)].
- [71] J. Polchinski, *Renormalization and Effective Lagrangians*, *Nucl. Phys.* **B231** (1984) 269–295.
- [72] C. Degrande, et al., *Monte Carlo tools for studies of non-standard electroweak gauge boson interactions in multi-boson processes: A Snowmass White Paper*, in *Proceedings, 2013 Community Summer Study on the Future of U.S. Particle Physics: Snowmass on the Mississippi (CSS2013): Minneapolis, MN, USA, July 29-August 6, 2013*, 2013. [arXiv:1309.7890](#).

- [73] C. Degrande, et al., *Effective Field Theory: A Modern Approach to Anomalous Couplings*, *Annals Phys.* **335** (2013) 21–32, [[arXiv:1205.4231](#)].
- [74] C. Englert, et al., *Precision Measurements of Higgs Couplings: Implications for New Physics Scales*, *J. Phys.* **G41** (2014) 113001, [[arXiv:1403.7191](#)].
- [75] G. 't Hooft and M. J. G. Veltman, *Regularization and renormalization of gauge fields*, *Nucl. Phys.* **B44** (1972) 189–213.
- [76] C. Becchi, A. Rouet, and R. Stora, *The Abelian Higgs-Kibble Model. Unitarity of the S Operator*, *Phys. Lett.* **B52** (1974) 344–346.
- [77] C. Becchi, A. Rouet, and R. Stora, *Renormalization of the Abelian Higgs-Kibble Model*, *Commun. Math. Phys.* **42** (1975) 127–162.
- [78] I. V. Tyutin, *Gauge Invariance in Field Theory and Statistical Physics in Operator Formalism*, [arXiv:0812.0580](#).
- [79] W. Siegel, *Supersymmetric Dimensional Regularization via Dimensional Reduction*, *Phys. Lett.* **B84** (1979) 193–196.
- [80] A. Denner and S. Dittmaier, *Reduction schemes for one-loop tensor integrals*, *Nucl. Phys.* **B734** (2006) 62–115, [[hep-ph/0509141](#)].
- [81] G. Sulyok, *UV-divergent parts of the Passarino-Veltmann functions in dimensional regularisation*, [hep-ph/0609282](#).
- [82] F. Jegerlehner, *Facts of life with gamma(5)*, *Eur. Phys. J.* **C18** (2001) 673–679, [[hep-th/0005255](#)].
- [83] J. Fleischer and F. Jegerlehner, *Radiative corrections to Higgs decays in the extended Weinberg-Salam Model*, *Phys. Rev.* **D23** (1981) 2001–2026.
- [84] A. Denner, *Techniques for calculation of electroweak radiative corrections at the one-loop level and results for W physics at LEP-200*, *Fortsch. Phys.* **41** (1993) 307–420, [[arXiv:0709.1075](#)].
- [85] S. Actis, A. Ferroglia, M. Passera, and G. Passarino, *Two-loop renormalization in the Standard Model. Part I: Prolegomena*, *Nucl. Phys.* **B777** (2007) 1–34, [[hep-ph/0612122](#)].
- [86] B. A. Kniehl, C. P. Palisoc, and A. Sirlin, *Higgs-boson production and decay close to thresholds*, *Nucl. Phys.* **B591** (2000) 296–310, [[hep-ph/0007002](#)].
- [87] O. Piguet and K. Sibold, *Gauge Independence in Ordinary Yang-Mills Theories*, *Nucl. Phys.* **B253** (1985) 517–540.
- [88] A. Bredenstein, A. Denner, S. Dittmaier, and S. Pozzorini, *NLO QCD corrections to t anti-t b anti-b production at the LHC: 1. Quark-antiquark annihilation*, *JHEP* **08** (2008) 108, [[arXiv:0807.1248](#)].

- [89] M. J. G. Veltman, *Unitarity and causality in a renormalizable field theory with unstable particles*, *Physica* **29** (1963) 186–207.
- [90] R. G. Stuart, *Gauge invariance, analyticity and physical observables at the  $Z0$  resonance*, *Phys. Lett.* **B262** (1991) 113–119.
- [91] A. Aeppli, G. J. van Oldenborgh, and D. Wyler, *Unstable particles in one loop calculations*, *Nucl. Phys.* **B428** (1994) 126–146, [[hep-ph/9312212](#)].
- [92] S. Dittmaier, A. Huss, and C. Schwinn, *Mixed QCD-electroweak  $O(\alpha_s\alpha)$  corrections to Drell-Yan processes in the resonance region: pole approximation and non-factorizable corrections*, *Nucl. Phys.* **B885** (2014) 318–372, [[arXiv:1403.3216](#)].
- [93] R. G. Stuart, *General renormalization of the gauge invariant perturbation expansion near the  $Z0$  resonance*, *Phys. Lett.* **B272** (1991) 353–358.
- [94] A. Sirlin, *Theoretical considerations concerning the  $Z0$  mass*, *Phys. Rev. Lett.* **67** (1991) 2127–2130.
- [95] A. Sirlin, *Observations concerning mass renormalization in the electroweak theory*, *Phys. Lett.* **B267** (1991) 240–242.
- [96] A. Denner, S. Dittmaier, M. Roth, and D. Wackeroth, *Predictions for all processes  $e^+e^- \rightarrow 4$  fermions  $+\gamma$* , *Nucl.Phys.* **B560** (1999) 33–65, [[hep-ph/9904472](#)].
- [97] A. Denner, S. Dittmaier, M. Roth, and L. Wieders, *Electroweak corrections to charged-current  $e^+e^- \rightarrow 4$  fermion processes: Technical details and further results*, *Nucl.Phys.* **B724** (2005) 247–294, [[hep-ph/0505042](#)].
- [98] A. Denner and S. Dittmaier, *The Complex-mass scheme for perturbative calculations with unstable particles*, *Nucl.Phys.Proc.Suppl.* **160** (2006) 22–26, [[hep-ph/0605312](#)].
- [99] S. Actis and G. Passarino, *Two-Loop Renormalization in the Standard Model Part III: Renormalization Equations and their Solutions*, *Nucl. Phys.* **B777** (2007) 100–156, [[hep-ph/0612124](#)].
- [100] S. Actis, G. Passarino, C. Sturm, and S. Uccirati, *Two-Loop Threshold Singularities, Unstable Particles and Complex Masses*, *Phys. Lett.* **B669** (2008) 62–68, [[arXiv:0809.1302](#)].
- [101] A. Denner and J.-N. Lang, *The Complex-Mass Scheme and Unitarity in perturbative Quantum Field Theory*, *Eur. Phys. J.* **C75** (2015), no. 8 377, [[arXiv:1406.6280](#)].
- [102] M. Böhm, A. Denner, and H. Joos, *Gauge theories of the strong and electroweak interaction*. Teubner, Stuttgart, 2001.
- [103] A. Denner, S. Dittmaier, M. Roth, and D. Wackeroth, *Electroweak radiative corrections to  $e^+e^- \rightarrow WW \rightarrow 4$  fermions in double pole approximation: The RACOONWW approach*, *Nucl. Phys.* **B587** (2000) 67–117, [[hep-ph/0006307](#)].

- [104] S. Dittmaier and M. Kramer, 1, *Electroweak radiative corrections to  $W$  boson production at hadron colliders*, *Phys. Rev.* **D65** (2002) 073007, [[hep-ph/0109062](#)].
- [105] A. Sirlin, *Radiative corrections in the  $SU(2)_L \times U(1)$  theory: A simple renormalization framework*, *Phys. Rev.* **D22** (1980) 971–981.
- [106] W. J. Marciano and A. Sirlin, *Radiative corrections to neutrino induced neutral-current phenomena in the  $SU(2)_L \times U(1)$  theory*, *Phys. Rev.* **D22** (1980) 2695. [Erratum: *Phys. Rev.* **D31**,213(1985)].
- [107] A. Sirlin and W. J. Marciano, *Radiative corrections to  $\nu_\mu + N \rightarrow \mu^- + X$  and their effect on the determination of  $\rho^2$  and  $\sin^2 \theta_W$* , *Nucl. Phys.* **B189** (1981) 442–460.
- [108] T. Appelquist and J. Carazzone, *Infrared Singularities and Massive Fields*, *Phys. Rev.* **D11** (1975) 2856.
- [109] J. Collins, *Foundations of perturbative QCD*. Cambridge University Press, 2013.
- [110] K. G. Chetyrkin, B. A. Kniehl, and M. Steinhauser, *Strong-Coupling Constant at Three Loops in Momentum Subtraction Scheme*, *Nucl. Phys.* **B814** (2009) 231–245, [[arXiv:0812.1337](#)].
- [111] M. Krause, M. Muhlleitner, R. Santos, and H. Ziesche, *2HDM Higgs-to-Higgs Decays at Next-to-Leading Order*, *Phys. Rev.* **D95** (2017) 075019, [[arXiv:1609.04185](#)].
- [112] L. Altenkamp, S. Dittmaier, and H. Rzehak, *Renormalization schemes for the Two-Higgs-Doublet Model and applications to  $h \rightarrow WW/ZZ \rightarrow 4\text{fermions}$* , [[arXiv:1704.02645](#)].
- [113] A. Denner and T. Sack, *Renormalization of the Quark Mixing Matrix*, *Nucl. Phys.* **B347** (1990) 203–216.
- [114] B. A. Kniehl and A. Pilaftsis, *Mixing renormalization in Majorana neutrino theories*, *Nucl. Phys.* **B474** (1996) 286–308, [[hep-ph/9601390](#)].
- [115] P. Gambino, P. A. Grassi, and F. Madricardo, *Fermion mixing renormalization and gauge invariance*, *Phys. Lett.* **B454** (1999) 98–104, [[hep-ph/9811470](#)].
- [116] A. Barroso, L. Brucher, and R. Santos, *Renormalization of the Cabibbo-Kobayashi-Maskawa matrix*, *Phys. Rev.* **D62** (2000) 096003, [[hep-ph/0004136](#)].
- [117] K. P. O. Diener and B. A. Kniehl, *On mass shell renormalization of fermion mixing matrices*, *Nucl. Phys.* **B617** (2001) 291–307, [[hep-ph/0109110](#)].
- [118] D. Espriu, J. Manzano, and P. Talavera, *Flavor mixing, gauge invariance and wave function renormalization*, *Phys. Rev.* **D66** (2002) 076002, [[hep-ph/0204085](#)].
- [119] A. Pilaftsis, *Gauge and scheme dependence of mixing matrix renormalization*, *Phys. Rev.* **D65** (2002) 115013, [[hep-ph/0203210](#)].

- [120] A. Broncano, M. B. Gavela, and E. E. Jenkins, *Renormalization of lepton mixing for Majorana neutrinos*, *Nucl. Phys.* **B705** (2005) 269–295, [[hep-ph/0406019](#)].
- [121] A. Denner, E. Kraus, and M. Roth, *Physical renormalization condition for the quark mixing matrix*, *Phys. Rev.* **D70** (2004) 033002, [[hep-ph/0402130](#)].
- [122] B. A. Kniehl and A. Sirlin, *Simple On-Shell Renormalization Framework for the Cabibbo-Kobayashi-Maskawa Matrix*, *Phys. Rev.* **D74** (2006) 116003, [[hep-th/0612033](#)].
- [123] B. A. Kniehl and A. Sirlin, *Simple Approach to Renormalize the Cabibbo-Kobayashi-Maskawa Matrix*, *Phys. Rev. Lett.* **97** (2006) 221801, [[hep-ph/0608306](#)].
- [124] A. A. Almasy, B. A. Kniehl, and A. Sirlin, *On-shell renormalization of the mixing matrices in Majorana neutrino theories*, *Nucl. Phys.* **B818** (2009) 115–134, [[arXiv:0902.3793](#)].
- [125] Y. Yamada, *Gauge dependence of the on-shell renormalized mixing matrices*, *Phys. Rev.* **D64** (2001) 036008, [[hep-ph/0103046](#)].
- [126] J. M. Cornwall, *Dynamical mass generation in continuum QCD*, *Phys. Rev.* **D26** (1982) 1453.
- [127] J. M. Cornwall and J. Papavassiliou, *Gauge-invariant three gluon vertex in QCD*, *Phys. Rev.* **D40** (1989) 3474.
- [128] S. Kanemura, M. Kikuchi, and K. Yagyu, *Fingerprinting the extended Higgs sector using one-loop corrected Higgs boson couplings and future precision measurements*, *Nucl. Phys.* **B896** (2015) 80–137, [[arXiv:1502.07716](#)].
- [129] M. Krause, R. Lorenz, M. Muhlleitner, R. Santos, and H. Ziesche, *Gauge-independent Renormalization of the 2-Higgs-Doublet Model*, *JHEP* **09** (2016) 143, [[arXiv:1605.04853](#)].
- [130] J. A. M. Vermaseren, *New features of FORM*, [math-ph/0010025](#).
- [131] A. Meurer, et al., *Sympy: symbolic computing in python*, *PeerJ Computer Science* **3** (Jan., 2017) e103.
- [132] G. Ossola, C. G. Papadopoulos, and R. Pittau, *On the Rational Terms of the one-loop amplitudes*, *JHEP* **05** (2008) 004, [[arXiv:0802.1876](#)].
- [133] P. Draggiotis, M. V. Garzelli, C. G. Papadopoulos, and R. Pittau, *Feynman Rules for the Rational Part of the QCD 1-loop amplitudes*, *JHEP* **04** (2009) 072, [[arXiv:0903.0356](#)].
- [134] M. V. Garzelli, I. Malamos, and R. Pittau, *Feynman rules for the rational part of the Electroweak 1-loop amplitudes*, *JHEP* **01** (2010) 040, [[arXiv:0910.3130](#)]. [Erratum: *JHEP*10 (2010) 097].



- [135] B. S. DeWitt, *Theory of radiative corrections for non-abelian gauge fields*, *Phys. Rev. Lett.* **12** (1964) 742–746.
- [136] B. S. DeWitt, *Quantum Theory of Gravity. 2. The Manifestly Covariant Theory*, *Phys. Rev.* **162** (1967) 1195–1239.
- [137] J. P. Bornsen and A. E. M. van de Ven, *Three loop Yang-Mills beta function via the covariant background field method*, *Nucl. Phys.* **B657** (2003) 257–303, [[hep-th/0211246](#)].
- [138] L. F. Abbott, M. T. Grisaru, and R. K. Schaefer, *The Background Field Method and the S Matrix*, *Nucl. Phys.* **B229** (1983) 372–380.
- [139] L. F. Abbott, *The Background Field Method Beyond One Loop*, *Nucl. Phys.* **B185** (1981) 189–203.
- [140] L. F. Abbott, *Introduction to the Background Field Method*, *Acta Phys. Polon.* **B13** (1982) 33.
- [141] B. W. Lee and J. Zinn-Justin, *Spontaneously broken gauge symmetries. 4. General gauge formulation*, *Phys. Rev.* **D7** (1973) 1049–1056.
- [142] P. Nogueira, *Automatic Feynman graph generation*, *J. Comput. Phys.* **105** (1993) 279–289.
- [143] S. Actis, A. Ferroglia, G. Passarino, M. Passera, Ch. Sturm and S. Uccirati, *GraphShot, a Form package for automatic generation and manipulation of one- and two-loop Feynman diagrams*, unpublished.
- [144] R. Hamberg, W. L. van Neerven, and T. Matsuura, *A complete calculation of the order  $\alpha_s^2$  correction to the Drell-Yan K factor*, *Nucl. Phys.* **B359** (1991) 343–405. [Erratum: *Nucl. Phys.*B644,403(2002)].
- [145] O. Brein, A. Djouadi, and R. Harlander, *NNLO QCD corrections to the Higgs-strahlung processes at hadron colliders*, *Phys. Lett.* **B579** (2004) 149–156, [[hep-ph/0307206](#)].
- [146] O. Brein, R. Harlander, M. Wiesemann, and T. Zirke, *Top-quark mediated effects in hadronic Higgs strahlung*, *Eur. Phys. J.* **C72** (2012) 1868, [[arXiv:1111.0761](#)].
- [147] G. Ferrera, M. Grazzini, and F. Tramontano, *Associated WH production at hadron colliders: a fully exclusive QCD calculation at NNLO*, *Phys. Rev. Lett.* **107** (2011) 152003, [[arXiv:1107.1164](#)].
- [148] G. Ferrera, M. Grazzini, and F. Tramontano, *Associated ZH production at hadron colliders: the fully differential NNLO QCD calculation*, *Phys. Lett.* **B740** (2015) 51–55, [[arXiv:1407.4747](#)].
- [149] M. L. Ciccolini, S. Dittmaier, and M. Krämer, *Electroweak radiative corrections to associated WH and ZH production at hadron colliders*, *Phys. Rev.* **D68** (2003) 073003, [[hep-ph/0306234](#)].

- [150] A. Denner, S. Dittmaier, S. Kallweit, and A. Mück, *Electroweak corrections to Higgs-strahlung off  $W/Z$  bosons at the Tevatron and the LHC with HAWK*, *JHEP* **03** (2012) 075, [[arXiv:1112.5142](#)].
- [151] F. Granata, J. M. Lindert, C. Oleari, and S. Pozzorini, *NLO QCD+EW predictions for  $HV$  and  $HV+jet$  production including parton-shower effects*, [arXiv:1706.03522](#).
- [152] R. V. Harlander, S. Liebler, and T. Zirke, *Higgs strahlung at the Large Hadron Collider in the 2-Higgs-Doublet Model*, *JHEP* **02** (2014) 023, [[arXiv:1307.8122](#)].
- [153] T. Han, G. Valencia, and S. Willenbrock, *Structure function approach to vector boson scattering in  $p p$  collisions*, *Phys. Rev. Lett.* **69** (1992) 3274–3277, [[hep-ph/9206246](#)].
- [154] P. Bolzoni, F. Maltoni, S.-O. Moch, and M. Zaro, *Higgs production via vector-boson fusion at NNLO in QCD*, *Phys. Rev. Lett.* **105** (2010) 011801, [[arXiv:1003.4451](#)].
- [155] P. Bolzoni, F. Maltoni, S.-O. Moch, and M. Zaro, *Vector boson fusion at NNLO in QCD: SM Higgs and beyond*, *Phys. Rev.* **D85** (2012) 035002, [[arXiv:1109.3717](#)].
- [156] T. Figy, C. Oleari, and D. Zeppenfeld, *Next-to-leading order jet distributions for Higgs boson production via weak boson fusion*, *Phys. Rev.* **D68** (2003) 073005, [[hep-ph/0306109](#)].
- [157] M. Ciccolini, A. Denner, and S. Dittmaier, *Electroweak and QCD corrections to Higgs production via vector-boson fusion at the LHC*, *Phys. Rev.* **D77** (2008) 013002, [[arXiv:0710.4749](#)].
- [158] M. Ciccolini, A. Denner, and S. Dittmaier, *Strong and electroweak corrections to the production of Higgs + 2jets via weak interactions at the LHC*, *Phys. Rev. Lett.* **99** (2007) 161803, [[arXiv:0707.0381](#)].
- [159] M. Cacciari, F. A. Dreyer, A. Karlberg, G. P. Salam, and G. Zanderighi, *Fully Differential Vector-Boson-Fusion Higgs Production at Next-to-Next-to-Leading Order*, *Phys. Rev. Lett.* **115** (2015), no. 8 082002, [[arXiv:1506.02660](#)].
- [160] F. A. Dreyer and A. Karlberg, *Vector-Boson Fusion Higgs Production at Three Loops in QCD*, *Phys. Rev. Lett.* **117** (2016), no. 7 072001, [[arXiv:1606.00840](#)].
- [161] M. Rauch and S. Plätzer, *Parton-shower Effects in Vector-Boson-Fusion Processes*, *PoS DIS2016* (2016) 076, [[arXiv:1607.00159](#)].
- [162] D. Goncalves, T. Plehn, and J. M. Thompson, *Weak Boson Fusion at 100 TeV*, [arXiv:1702.05098](#).
- [163] T. Figy, S. Palmer, and G. Weiglein, *Higgs Production via Weak Boson Fusion in the Standard Model and the MSSM*, *JHEP* **02** (2012) 105, [[arXiv:1012.4789](#)].
- [164] M. Spira, *V2HV*, <http://tiger.web.psi.ch/proglist.html>.



- [165] J. Campbell, K. Ellis, and C. Williams, *MCFM—Monte Carlo for FeMtobarn processes*, <http://mcfm.fnal.gov/>.
- [166] A. Denner, S. Dittmaier, S. Kallweit, and A. Mück, *HAWK 2.0: A Monte Carlo program for Higgs production in vector-boson fusion and Higgs strahlung at hadron colliders*, *Comput. Phys. Commun.* **195** (2015) 161–171, [[arXiv:1412.5390](https://arxiv.org/abs/1412.5390)].
- [167] O. Brein, R. V. Harlander, and T. J. E. Zirke, *vh@nnlo - Higgs strahlung at hadron colliders*, *Comput. Phys. Commun.* **184** (2013) 998–1003, [[arXiv:1210.5347](https://arxiv.org/abs/1210.5347)].
- [168] S. Catani and M. H. Seymour, *A General algorithm for calculating jet cross-sections in NLO QCD*, *Nucl. Phys.* **B485** (1997) 291–419, [[hep-ph/9605323](https://arxiv.org/abs/hep-ph/9605323)]. [Erratum: *Nucl. Phys.* **B510** (1998) 503].
- [169] S. Catani, S. Dittmaier, M. H. Seymour, and Z. Trocsanyi, *The Dipole formalism for next-to-leading order QCD calculations with massive partons*, *Nucl. Phys.* **B627** (2002) 189–265, [[hep-ph/0201036](https://arxiv.org/abs/hep-ph/0201036)].
- [170] S. Dittmaier, *A General approach to photon radiation off fermions*, *Nucl. Phys.* **B565** (2000) 69–122, [[hep-ph/9904440](https://arxiv.org/abs/hep-ph/9904440)].
- [171] S. Dittmaier, A. Kabelschacht, and T. Kasprzik, *Polarized QED splittings of massive fermions and dipole subtraction for non-collinear-safe observables*, *Nucl. Phys.* **B800** (2008) 146–189, [[arXiv:0802.1405](https://arxiv.org/abs/0802.1405)].
- [172] **LHC Higgs Cross Section Working Group** Collaboration, D. de Florian et al., *Handbook of LHC Higgs Cross Sections: 4. Deciphering the Nature of the Higgs Sector*, [arXiv:1610.07922](https://arxiv.org/abs/1610.07922).
- [173] **CMS** Collaboration, S. Chatrchyan et al., *Search for the Standard Model Higgs boson produced in association with a W or a Z boson and decaying to bottom quarks*, *Phys. Rev.* **D89** (2014), no. 1 012003, [[arXiv:1310.3687](https://arxiv.org/abs/1310.3687)].
- [174] M. Cacciari, G. P. Salam, and G. Soyez, *The Anti- $k(t)$  jet clustering algorithm*, *JHEP* **04** (2008) 063, [[arXiv:0802.1189](https://arxiv.org/abs/0802.1189)].
- [175] **NNPDF** Collaboration, R. D. Ball, et al., *Parton distributions with QED corrections*, *Nucl. Phys.* **B877** (2013) 290–320, [[arXiv:1308.0598](https://arxiv.org/abs/1308.0598)].
- [176] **LHC Higgs Cross Section Working Group** Collaboration, I. Low et al., “Beyond the Standard Model Predictions.” <http://cds.cern.ch/record/2150772/files/>. Accessed: 2016-06-29.
- [177] J. Baglio, O. Eberhardt, U. Nierste, and M. Wiebusch, *Benchmarks for Higgs pair production and heavy Higgs searches in the Two-Higgs-Doublet Model of type II*, *Phys. Rev.* **D90** (2014), no. 1 015008, [[arXiv:1403.1264](https://arxiv.org/abs/1403.1264)].

- [178] F. Bojarski, G. Chalons, D. Lopez-Val, and T. Robens, *Heavy to light Higgs boson decays at NLO in the Singlet Extension of the Standard Model*, *JHEP* **02** (2016) 147, [[arXiv:1511.08120](#)].
- [179] J. R. Espinosa and I. Navarro, *Scale independent mixing angles*, *Phys. Rev.* **D66** (2002) 016004, [[hep-ph/0109126](#)].
- [180] J. R. Espinosa and Y. Yamada, *Scale independent and gauge independent mixing angles for scalar particles*, *Phys. Rev.* **D67** (2003) 036003, [[hep-ph/0207351](#)].
- [181] A. Denner, G. Weiglein, and S. Dittmaier, *Gauge invariance of green functions: Background field method versus pinch technique*, *Phys. Lett.* **B333** (1994) 420–426, [[hep-ph/9406204](#)].
- [182] D. Binosi, *Electroweak pinch technique to all orders*, *J. Phys.* **G30** (2004) 1021–1064, [[hep-ph/0401182](#)].
- [183] S. Kanemura, M. Kikuchi, K. Sakurai, and K. Yagyu, *Gauge invariant one-loop corrections to Higgs boson couplings in non-minimal Higgs models*, [arXiv:1705.05399](#).
- [184] A. Freitas and D. Stöckinger, *Gauge dependence and renormalization of  $\tan\beta$  in the MSSM*, *Phys. Rev.* **D66** (2002) 095014, [[hep-ph/0205281](#)].
- [185] R. Santos and A. Barroso, *On the renormalization of Two-Higgs-Doublet Models*, *Phys. Rev.* **D56** (1997) 5366–5385, [[hep-ph/9701257](#)].
- [186] S. Kanemura, Y. Okada, E. Senaha, and C. P. Yuan, *Higgs coupling constants as a probe of new physics*, *Phys. Rev.* **D70** (2004) 115002, [[hep-ph/0408364](#)].
- [187] D. Lopez-Val and J. Sola, *Neutral Higgs-pair production at linear colliders within the general 2HDM: quantum effects and triple Higgs boson self-interactions*, *Phys. Rev.* **D81** (2010) 033003, [[arXiv:0908.2898](#)].
- [188] D. Lopez-Val and J. Sola,  *$\Delta r$  in the Two-Higgs-Doublet Model at full one loop level – and beyond*, *Eur. Phys. J.* **C73** (2013) 2393, [[arXiv:1211.0311](#)].
- [189] D. Pierce and A. Papadopoulos, *Radiative corrections to the Higgs boson decay rate  $\Gamma(H \rightarrow ZZ)$  in the minimal supersymmetric model*, *Phys. Rev.* **D47** (1993) 222–231, [[hep-ph/9206257](#)].
- [190] N. Baro, F. Boudjema, and A. Semenov, *Automatised full one-loop renormalisation of the MSSM. I. The Higgs sector, the issue of  $\tan\beta$  and gauge invariance*, *Phys. Rev.* **D78** (2008) 115003, [[arXiv:0807.4668](#)].
- [191] J. C. Collins, *Renormalization*. Cambridge Monographs on Mathematical Physics. Cambridge University Press, Cambridge, 1986.
- [192] J. Brehmer, A. Freitas, D. Lopez-Val, and T. Plehn, *Pushing Higgs Effective Theory to its Limits*, *Phys. Rev.* **D93** (2016), no. 7 075014, [[arXiv:1510.03443](#)].

# Danksagung

An dieser Stelle möchte ich mich bei allen bedanken, die mich auf meinem Weg begleitet haben.

Ich bin meinem Betreuer Ansgar Denner zutiefst dankbar, dass ich meine Dissertation über ein derart spannendes und anspruchsvolles Thema anfertigen durfte. Darüberhinaus danke ich ihm für seine außergewöhnlich gute und persönliche Betreuung, sowie für das Aufzeigen weiterer Möglichkeiten innerhalb, sowie außerhalb des Projekts.

Mein Dank gilt der gesamten Arbeitsgruppe: Lars Hofer, für das Vermächtnis des Fußball Clubs, Andreas Scharf, für die Diskussionen über Linux, objektorientierte Programmierung, und dem bekannt machen mit dem Himmlischen Fastenbiers, Benedikt Biedermann, für die enge Zusammenarbeit und dem Austausch über Physik und Musik (sein Gepfeife im Gang wird mir in guter Erinnerung bleiben), Christian Pasold, dafür dass er mich als Büro Kollegen ertragen hat, Robert Feger, für seine professionelle Hilfe bei jeglichen technischen Fragen, Sandro Uccirati, für die Zusammenarbeit am RECOLA Projekt, und dass er sich hat überreden lassen Recola mit GIT zu verwalten, was mein Leben deutlich erträglicher gemacht hat. Weiterhin danke ich Laura Jenniches und Christian Sturm für die produktive Zusammenarbeit. Mein besonderer Dank gilt Mathieu Pellen, der mich durch seine positive Einstellung besonders motivieren konnte. Es hat mich sehr gefreut mit ihm zusammen arbeiten zu dürfen.

Daneben bedanke ich mich bei weiteren Personen am Lehrstuhl, voran Thomas Garratt, für den täglichen Geschichts- und Politikunterricht, Manuel Krauss und Christoph Uhlemann, für die Aufnahme in die 11 Uhr Gruppe, Christoph Gross, für die Initiierung des Film Clubs, und schließlich Brigitte Wehner, dafür, dass sie mir alle bürokratischen Aufgaben abgenommen und ein fast sorgenloses Doktoranden Dasein ermöglicht hat.

Ich danke der Studienstiftung für die finanzielle Unterstützung und für die Vernetzung mit anderen Doktoranden.

Ich danke Ulrich Müller, Guilherme Stein, Florian Amann und Bijan Chokoufé für die schöne Zeit, die wir mit Physik, aber auch jenseits der Physik verbracht haben. Weiterhin bedanke ich mich bei Moritz Pentecker und Manuel Daubner für die jahrelange Freundschaft, und für den Kontakt zur Außenwelt.

Zuletzt und allen voran danke ich meinen Eltern und meiner Schwester, für deren konstante und uneingeschränkte Unterstützung, Geduld und Verständnis, über all die Jahre hinweg. Mir fehlen die Worte.